IDENTIFICATION AND CHARACTERIZATION OF A NOVEL, CONSERVED METALLO-β-LACTAMASE REGULATOR OF DOPAMINE AND GLUTAMATE SIGNALING

By

James Andrew Hardaway III

Dissertation

Submitted to the Faculty of the

Graduate School of Vanderbilt University

in partial fulfillment of the requirements

of the degree of

DOCTOR OF PHILOSOPHY

in

Neuroscience

December, 2013

Nashville, Tennessee

Approved:

Randy D. Blakely, Ph.D.

David M. Miller, Ph.D.

Aurelio Galli, Ph.D.

Heidi E. Hamm, Ph.D.

Daniel L. Chase, Ph.D.

For Abby, family, and friends.

ACKNOWLEDGEMENTS

The efforts that I present here were not accomplished in a vacuum. I have been fortunate to be trained in one of the nation's premiere graduate programs in Neuroscience. I would like to thank Dr. Mark Wallace for his vision and superior leadership in leading this program during my time at Vanderbilt. Likewise, Dr. Doug McMahon has an important force in overseeing the quality of my training over the past several years. I would also like to thank the administrative and program staff of the Vanderbilt Brain Institute(VBI) including Mary Early-Zald, Mary Michael-Woolman, Shirin Pulous, Roz Johnson and Denise Malone. This work and my experience would not have been possible without you.

Several important mentors have enriched my scientific experiences over the years. Dr. Utpal Dave gave me my first chance at rigorous scientific experimentation as a Research Assistant. Dr. Aurelio Galli has been a source of moral and intellectual support for the duration of my graduate work and imparted important career advice that I will not forget. Dr. David Miller has been an exemplar of collegiality in an increasingly competitive scientific climate. He and his lab helped me become a better geneticist and experimentalist on a daily basis. Lastly, I would like to acknowledge the vision and training provided by Dr. Randy Blakely. His enthusiasm for discovery and unfailing optimism are a model that I strive for. This work supported by grants from the National Institute on Drug Abuse (NIDA) and National Institute for Mental Health (NIMH).

TABLE OF CONTENTS

Page

List of Tables

List of Figures

List of Abbreviations

3MT	3-methoxytyrosine
5HT	5-hydroxytryptamine (Serotonin)
5HTP	5-hydroxytryptophan
6-OHDA	6-hydroxydopamine
AADS	Aromatic Acid Decarboxylase
ACH	Acetycholine
ADE	Anterior Deirid
ADHD	Attention Deficit Hyperactivity Disorder
AMPH	Amphetamine
AMY	Amygdala
ATP	Adenosine Triphosphate
BNST	Bed Nucleus of Stria Terminalis
BSR	Basal Slowing Response
cAMP	Cyclic Adenonosine Monophosphate
CARIBN	Calcium Ratiometric Imaging of Behaving Nematodes
CEF	Ceftriaxone
CEP	Cephalic Neuron
COMT	Catechol O-methyltransferase
CNS	Central Nervous System
DA	Dopamine
DAT	Dopamine Transporter
DCX	Doublecortin

DG	Dentate Gyrus
DOPA	3,4-dihydroxyphenylalanine
DOPAC	3.4-dihydroxyphenylacetic acid
DPC	Dorsal Peduncular Cortex
DRN	Dorsal Raphe Nuclei
DS	Dorsal Striatum
EMS	ethylmethanesulfonate
ENU	N-ethyl-N-nitrosourea
EPI	Epinephrine
ESR	Enhanced Slowing Response
FIF	Formaldehyde-Induced-Flourescence
FSCV	Fast Scan Cyclic Voltammetry
GABA	Gamma-aminobutyric Acid
GIRK	G-protein Inwardly Rectifying Potassium
GFAP	Glial Fibrillary Acidic Protein
GFP	Green Fluorescent Protein
GLU	Glutamic Acid (Glutamate)
GLT	Glutamate Transporter
GS	Glutamine Synthetase
GST	Glutathione S-transferase
HIPP	Hippocampus
HPLC	High Performance Liquid Chromotography
HRP	Horseradish Peroxidase

HVA	Homovanillic Acid
IMI	Imipramine
iPSC	Inhibitory Post Synaptic Current
L-DOPA	L-dihydroxyphenylalanine
LC	Liquid Chromotography
LCN	Lateral Cerebellar Nucleus
LS	Lateral Septal Nucleus
MALDI	Matrix Associated Laser Desorption Ionization
MAO	Monoamine Oxidase
MHb	Medial Habenula
MRC	Mechanoreceptive Current
NAC	N-acetylcysteine
NCBI	National Center for Biotechnology Information
NAc	Nucleus Accumbens
NE	Norepinephrine
NET	Norepinephrine Transporter
NGM	Nematode Growth Medium
ORF	Open Reading Frame
OSTs	ORF Sequence Tags
PCR	Polymerase Chain Reaction
PD	Parkinson’s Disease
PFC	Prefrontal Cortex
RT-PCR	Reverse Transcriptase Polymerase Chain Reaction

sEPSC	Spontaneous Excitatory Postsynaptic Currents
SGZ	Subgranular Zone
SNc	Substantia Nigra Pars Compacta
SNP	Single Nucleotide Polymorphism
SSRI	Serotonin Selective Reuptake Inhibitor
SVZ	Subventricular Zone
Swip	Swimming Induced Paralysis
TB	Trapezoidal Body
TH	Tyrosine Hydroxylase
vGLUT	Vesicular Glutamate Transporter
vMAT	Vesicular Monoamine Transporter
VTA	Ventral Tegmental Area

Chapter I

DOPAMINERGIC NEUROTRANSMISSION IN THE CENTRAL NERVOUS SYSTEM

IDENTIFICATION OF DOPAMINE AS A NEUROTRANSMITTER

The chemical 3-hydroxytyramine or dopamine (DA) was first identified in the rabbit brain by Carlsson and colleagues (A Carlsson, LINDQVIST, MAGNUSSON, & WALDECK, 1958). Although techniques currently in use did not allow for the discrimination of DA from other catecholamines like norepinephrine (NE) or epinephrine (EPI), they adapted ion exchange chromatography, paper chromatography, and fluorometric techniques to identify endogenous DA in several tissues including the brain (A Carlsson, 1959). As Carlsson had previously observed for NE and 5-hydroxytryptophan (5HT), injection of rabbits with the chemical reserpine significantly reduced the amount of DA they isolated from the brain. Conversely, they found that preinjection of 3,4-dihydroxyphenylalanine (DOPA) increased the amount of DA they detected. These studies established that DA was present in the brain and that its levels are attenuated by the chemical reserpine and enhanced by DOPA.

DA's role as a neurotransmitter took more time to elucidate. Work by the German physiologist Otto Loewi and others on acetylcholine (ACH) in frog preparations established several criteria that a chemical must possess to be classified as a neurotransmitter: 1) It must be present in the presynaptic neuron, 2) The substance must be released from this cell following electrical stimulation,

3) Specific receptors for the compound must be present on the postsynaptic end, and 4) There must exist a mechanism for the cessation of signaling by that chemical (Purves, 2008). Carlsson and Fuxe, amongst others, used their new DA-labeling techniques to carry out studies in multiple species and demonstrated that DA was present in large cell bodies in the midbrain and at terminal fibers in the caudate nucleus and putamen (Andén et al., 1964; A Carlsson, DAHLSTROEM, Fuxe, & LINDQVIST, 1965; A Carlsson, FALCK, Fuxe, & Hillarp, 1964; A Carlsson, FALCK, Hillarp, & TORP, 1962; Dahlström & Fuxe, 1964). These studies established that DA is located in the presynaptic regions of the synapse.

Measurement of DA's release in response to electrical stimulation required the development of new technologies and experimental preparations. Though early physiological studies of neurons in the caudate nucleus in response to iontophoretic pulses of DA and stimulation of DA-containing neurons in the substantia nigra suggested that DA was released onto these neurons, direct measurement of DA itself was still lacking (Connor, 1968, 1970). The development of new brain perfusion techniques in combination with stimulation of certain brain regions allowed Portig *et al*. to stimulate midbrain DA neurons and collect ventricular perfusate around the caudate nucleus of a cat (Portig, Sharman, & Vogt, 1968; Portig & Vogt, 1969). Using previously established paper chromatographic methods, the authors determined that stimulation of the substantia nigra could trigger the release of DA into caudate nucleus perfusate. One of the most definitive studies of DA's coupling to

electrical stimulation used radiolabeled DA generated by treatment of rat brain slices with radiolabeled DOPA. Using brain slice superfusion, the authors demonstrated that [H^3] DOPA was taken up into catecholamine nerve terminals, and that radiolabeled DA product could then be detected in superfusates collected from these brain slices (Ng, Chase, Colburn, & Kopin, 1971). Moreover, they found that pretreatment of these brain slices with the neurotoxin 6-hydroxydopamine (6-OHDA) significantly blunted the amount of electrically evoked DA release. The development of liquid chromatography (LC) and electrochemical detection of DA helped usher in a new era of understanding how this putative neurotransmitter is released within distinct CNS nuclei. These studies rely on the oxidative potential of DA in response to a positive voltage, whereby DA will lose two electrons to form dopamine o-quinone. The current generated by this oxidation is directly proportional to the concentration of DA, and the voltage potential at which DA oxidizes provides a useful "signature" for DA relative to other biogenic amines or DA metabolites. Plotsky *et al.* used high performance LC (HPLC) coupled with electrochemical detection to measure the release of endogenous DA from rat brain slices treated with *d*-amphetamine (AMPH) or with chronic electrical stimulation (Plotsky, Wightman, Chey, & Adams, 1977). Later, this method was expanded to include the characterization of DA metabolites and in an intact rat brain (Ewing, Bigelow, & Wightman, 1983; Wightman, Strope, Plotsky, & Adams, 1978; Wightman, Strope, Plotsky, & Adams, 2004). Together, these studies using multiple preparations and

methodologies support the contention that DA is released in response to electrical stimulation.

With the development of radiolabeled compounds, including DA and antipsychotic drugs, researchers used these drugs to ask whether DA receptor sites might be present in the brain. In 1975, two studies were published using similar approaches that demonstrated that DA could bind specifically in membrane fractions isolated from the rat brain (Burt, Enna, Creese, & Snyder, 1975; P Seeman, Chau-Wong, Tedesco, & Wong, 1975). Furthermore, Seeman and colleagues demonstrated that the known antipsychotic drug haloperidol also had saturable and specific binding to similar dopamine receptor sites. In later studies, Seeman *et al*. expanded these studies to include other mammals including human tissue, thereby confirming the existence of a putative plasma membrane receptor for DA in the human brain (P Seeman, Chau-Wong, Tedesco, & Wong, 1976).

Though previous pharmacological approaches had established that certain compounds could act similarly to DA and elicit physiological responses, a more mechanistic explanation of how DA signals at postsynaptic dopamine receptors were facilitated by the development of molecular cloning strategies and *in vitro* molecular pharmacology. Over the course of several years, several groups isolated human and rodent DA receptors cDNAs and described their genomic positions (Bunzow et al., 1988; Giros et al., 1989; Monsma, McVittie, Gerfen, Mahan, & Sibley, 1989; Sokoloff, Giros, Martres, Bouthenet, & Schwartz, 1990; Sunahara et al., 1991; Sunahara et al., 1990; Van Tol et al., 1991; Zhou et

al., 1990). Together, these studies suggest that there exist five dopamine receptors, D1-D5, in mammals that can be broadly classified into two categories depending on their effects on the production of the second messenger cAMP: D1-like receptors whose stimulation results in an increase in cAMP and D2-like receptors that reduce the amount of cAMP when activated by ligand.

Around the same time that DA was being described as a neurotransmitter, researchers were already describing the chemical mechanisms necessary for its inactivation. Axelrod and others had discovered an enzyme from rat liver that modifies EPI and subsequently isolated an inhibitor of EPI o-methylation (J AXELROD, 1957; Julius Axelrod & Laroche, 1959). This enzyme, later known as catechol o-methyltransferase (COMT) was shown to be an enzyme that metabolizes DA (Kopin, 1985). As DA's role as a neurotransmitter followed after EPI and NE, it was not until Rutledge and Jonason discovered that exogenous DA injected into rat brain increased the production of the deaminated DA metabolites 3,4 dihydroxyphenylacetic acid (DOPAC) and homovanillic acid (HVA) (Rutledge & Jonason, 1967). Furthermore, inhibition of a molecule called monoamine oxidase (MAO) could increase the production of another DA metabolite 3-methoxytyrosine (3MT), DA, and its modified derivative NE. Together, these studies established that there exist metabolic mechanisms that alter the amount of DA available in the CNS.

While researchers were elucidating the existence of DA metabolism, other groups were describing alternative mechanisms of neurotransmitter clearance via the phenomenon of sodium-dependent transport. Coyle and Snyder

observed the localization of catecholamine uptake, including DA, to a synaptosomal fraction containing reconstituted nerve terminals (Coyle & Snyder, 1969b) and that antiparkinsonian drugs had the effect of inhibiting DA uptake in the rat striatum (Coyle & Snyder, 1969a). Further work by Snyder and others demonstrated sodium-dependent uptake of glutamic acid (GLU), glycine, and gamma-aminobutyric acid (GABA)(Bennett, Logan, & Snyder, 1972; Logan & Snyder, 1971). Similar to the DA receptor phenomenon, the precise mechanism of high-affinity sodium dependent transport was unclear until the advent of molecular cloning strategies (Blakely, Robinson, & Amara, 1988). Using these and related approaches, several groups reported the identification and characterization of mammalian cDNAs that exhibited high affinity DA transport (Giros et al., 1992; Kilty, Lorang, & Amara, 1991; Shimada et al., 1991). These studies established the role of the DA transporter (DAT) in the inactivation of DA signaling.

ANATOMICAL DISTRIBUTION OF DOPAMINE NEURON CELL BODIES AND PROJECTIONS

Localization of Dopamine Neurons

In the CNS, DA is produced within a group of neurons located in two midbrain nuclei: the substantia nigra pars compacta (SNc) and the ventral tegmental area (VTA). Additionally, there exists a smaller group of neurons in the arcuate nucleus of the hypothalamus that also produce DA. These neurons are labeled through a number of histochemical and molecular biological approaches

including the production of a naturally occurring black pigment called melanin or by immunohistochemical staining for DA-specific genes like tyrosine hydroxylase (TH) or DAT (Ciliax et al., 1995; Hornykiewicz, 1966; Kitahama et al., 1990).

Dopamine Neuron Projections

The SNc DA neurons are located more lateral and dorsal and send the majority of their projections to the dorsal striatum (DS) that together make up the nigro-striatal pathway (Roeper, 2013). The VTA DA neurons are located more medial and ventral to the SNc and send their projections to the forebrain where they innervate a number of targets through two primary projections: 1) the mesolimbic pathway that innervates the ventral striatum or nucleus accumbens (NAc), the amygdala (AMY), limbic cortex, and hippocampus (HIPP) and 2) the mesocortical pathway that sends dopamine-releasing terminals to the prefrontal cortex (PFC) and the insular cortex (Figure 1). The DA neurons in the arcuate nucleus only send their axons to the median eminence and make up the tuberoinfundibular pathway (Zhaoliang Hu, Cooper, Crockett, & Zhou, 2004).

Dopamine Neuron Efferents

Midbrain DA neurons receive inputs from a number of targets throughout the brain. Using injection of a retrograde horseradish peroxidase (HRP) tracer, Phillipson showed that the VTA receives a number of inputs from areas like the PFC, Nac,

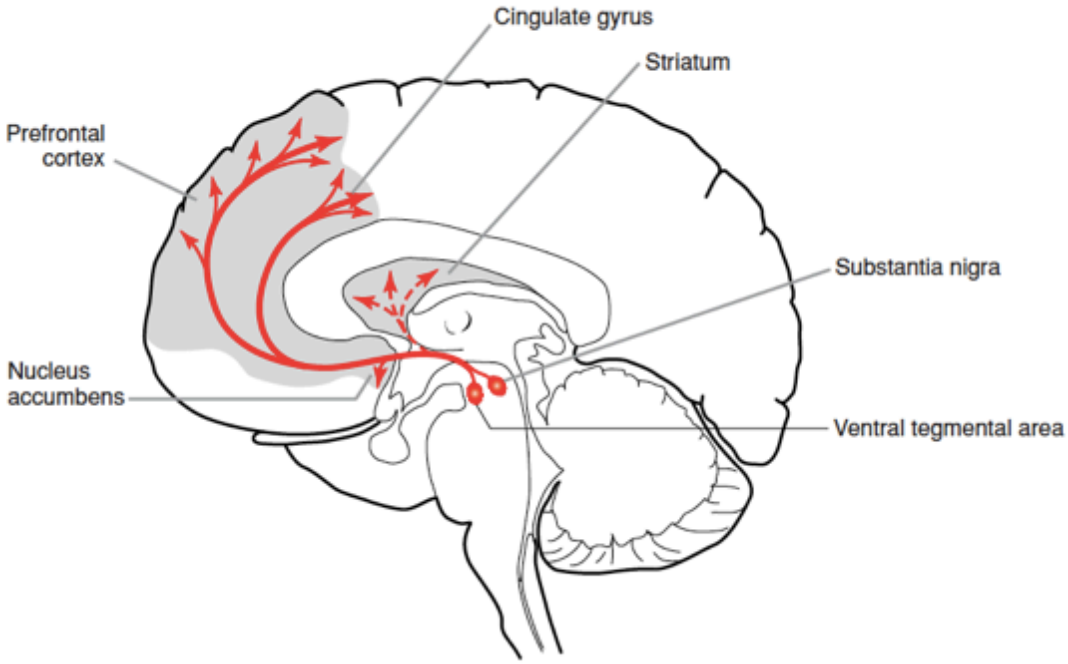

Figure 1 – Primary DA projection systems in the human brain. The substantia nigra send dopaminergic axons to the dorsal striatum in the nigro-striatal pathway, whereas the Ventral Tegmental Area sends its projections to the Nucleus Accumbens and Prefrontal Cortex. Figure from (Steven E Hyman, Malenka, & Nestler, 2006)

bed nucleus of stria terminalis (BNST), AMY, medial and lateral preoptic areas, multiple hypothalamic nuclei, superior colliculus, dorsal raphe nuclei (DRN), the parabrachial nucleus, and the locus coeruleus (Phillipson, 1979). Using a similar approach, Bunney and Aghajanian amongst others determined that the SNc receives inputs from the DS, the globus pallidus, the central nucleus of the AMY, and the DRN (Bunney & Aghajanian, 1976). More modern methods using a modified pseudo rabies virus have expanded on previous techniques to identify the afferent inputs to genetically defined neuronal subtypes (Osakada et al., 2011). The VTA and the SNc also contain numerous GABAergic neurons and the local injection of tracers into these nuclei does not distinguish between these and neighboring DA neurons. Recently, Watabe-Uchida *et al.* in a technical tour *de force* used pseudo rabies virus to fully map the afferents to both SN and VTA DA neurons (Watabe-Uchida, Zhu, Ogawa, Vamanrao, & Uchida, 2012). They validated the retrogradely labeled nuclei seen by previous groups and quantified the relative densities of each of the projections. Though a few overlapping areas were labeled that project to both the SNc and the VTA like the central AMY and the paraventricular nucleus, the DA neurons in these two areas have non-overlapping and heterogenous inputs. The VTA, in particular, receives a dense projection from the lateral hypothalamus, BNST, and reciprocal projection from the Nac core and shell.

SYNAPTIC COMPONENTS OF DOPAMINE SIGNALING

Dopamine Biosynthesis

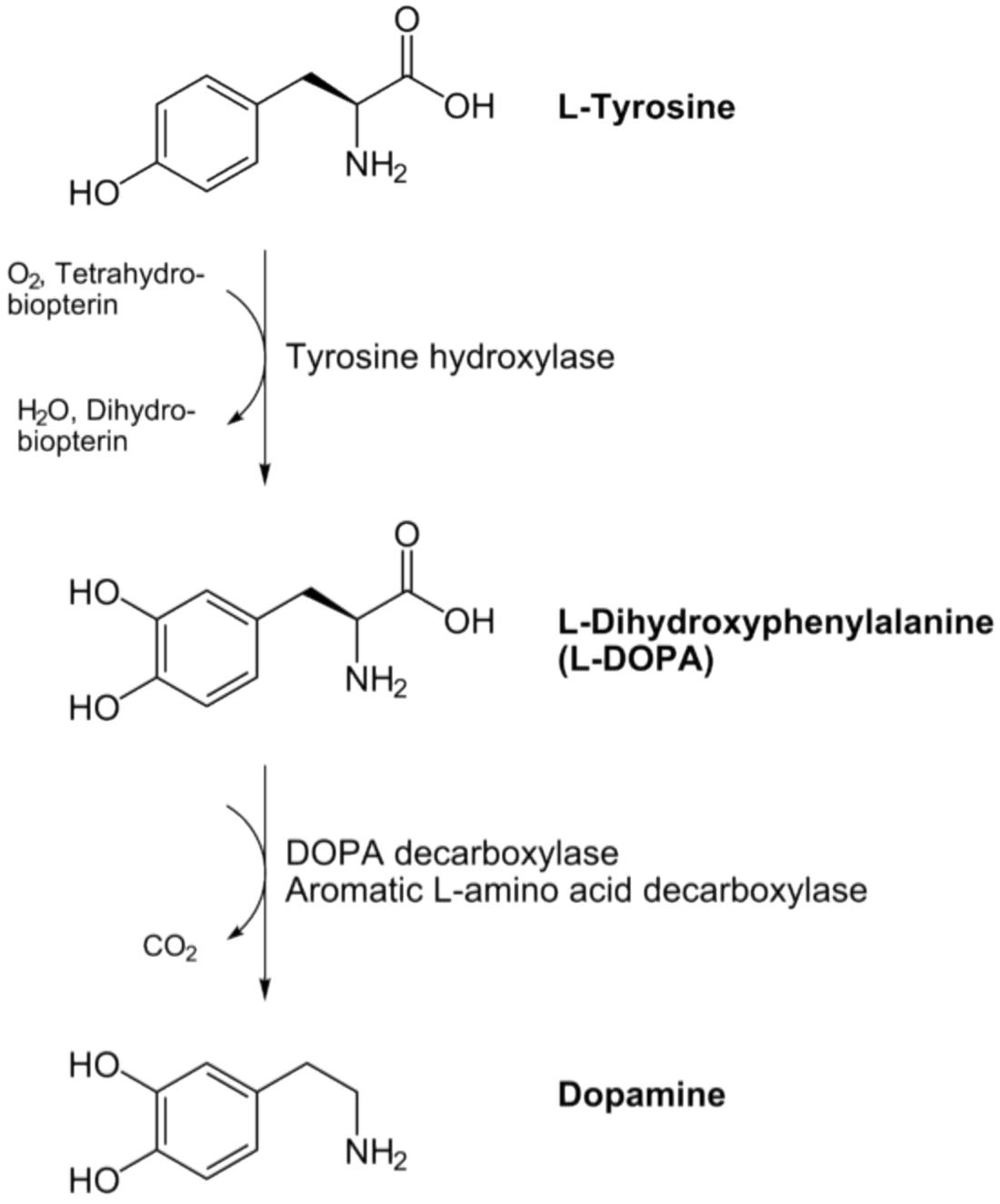

Figure 2 – Dopamine Biosynthetic Pathway. Image freely available at Wikimedia Commons.

DA is synthesized from its amino acid precursor tyrosine. The first step, shown to be the rate limiting step in the production of DA, involves the hydroxylation of tyrosine at the 3rd carbon via the actions of TH (NAGATSU, 1991; NAGATSU, LEVITT, & UDENFRIEND, 1964) to form L-dihydroxyphenylalanine (L-DOPA)(Figure 2). The actions of TH are required for the production of this catechol group that is typical of all catecholamines including EPI and NE. A carboxyl group is removed from L-DOPA via the actions of aromatic acid decarboxylase (AADC) to form 3,4-dihydroxyphenylethylamine or DA (NAGATSU, 1991).

Vesicular Packaging of Dopamine

Although DA is synthesized in the cytosol, it must be packaged into synaptic vesicles to allow for the electrically evoked release of this neurotransmitter into the synapse. Early studies in the adrenal glands demonstrated that catecholamines could be transported into chromaffin granules and that this process was enhanced by addition of adenosine triphosphate (ATP) and inhibited by application of the antihypertensive drug reserpine (KIRSHNER, 1962). Later studies demonstrated that similar transport processes exist for other biogenic amines, GABA, and GLU (Liu & Edwards, 1997). The molecular basis for this granular transport, however, was unclear until the cloning of two different cDNAs that transport biogenic amines (Erickson, Eiden, & Hoffman, 1992; Liu et al., 1992). Topological analysis of these cDNA clones demonstrated that vMAT2 encodes a twelve transmembrane domain containing protein with

cytosolic N and C termini. Extensive characterization of these two molecules, later named vesicular monoamine transporter 1 and 2 (vMAT1 and vMAT2), revealed that vMAT2 has a much higher affinity for biogenic amine substrates and that vMAT2 is the predominant transporter expressed in the midbrain containing DA, 5HT, and NE neurons (Peter et al., 1995). Immunoelectron microscopic analysis of vMAT in the nucleus of the solitary tract demonstrated that vMAT2 is localized to synaptic vesicles (SVs) and dense core vesicles (DCVs)(Nirenberg, Liu, Peter, Edwards, & Pickel, 1995). Thus, vMAT2 is expressed in DA neurons at synaptic vesicles and transports DA via an ATP and reserpine-sensitive process.

Dopamine Release

Having described the coupling of DA release to electrical stimulation, studies of DA release in different brain regions using methods such as brain slice superfusion, *in vivo* microdialysis, and fast scan cyclic voltammetry (FSCV) in combination with chemical, electrical, or optogenetic stimulation of midbrain DA neurons have established that excitation of DA neurons results in the release of DA at its targets. Furthermore electrophysiological recordings of midbrain DA neurons *in vivo* or in *ex vivo* brain slice preparations, have demonstrated that DA neurons have tonic pacemaker activity or exhibit burst firing patterns (Deister, Teagarden, Wilson, & Paladini, 2009; GOTO, OTANI, & GRACE, 2007). Work by John Williams among others have established that these patterns of burst firing are under the control of DA itself and that vesicular DA release onto DA neuron

cell bodies triggers an inhibitory post synaptic current (iPSC) that is blocked by a dopamine D2 receptor antagonists (Paladini, Robinson, Morikawa, Williams, & Palmiter, 2003) (Beckstead, Grandy, Wickman, & Williams, 2004; Usiello et al., 2000). These studies establish that DA is released in response to stimulation and that it exerts a local network feedback mechanism through activation of a D2 autoreceptor that controls the excitability of these neurons.

Reuptake

Following the isolation of a mammalian DAT cDNAs, researchers began to investigate the function of DAT *in vitro* and *in vivo*. Topological analysis of the DAT protein sequences demonstrated that, like vMAT, this protein has twelve predicted transmembrane domains with cytosolic N and C-termini (Shimada, et al., 1991). In the initial isolation of the DAT cDNA from a rat brain, Kilty and colleagues determined that treatment of HeLa cells expressing rat DAT cDNA with exogenous DA results in saturable high affinity DA uptake into these cells (Kilty, et al., 1991). The authors demonstrated that this uptake was antagonized by treatment with several compounds including the psychoactive drug cocaine. To determine the localization of the DAT *in vivo*, Ciliax *et al*. generated antibodies against different peptides within the DAT and performed immunohistochemistry on rat brain sections. They determined that the DAT was expressed in the SNc and the VTA and the terminal fields of the nigrostriatal, mesolimbic, and mesocortical pathways and that this innervation was lost by 6-OHDA pretreatment (Ciliax, et al., 1995). The localization of the DAT *in vivo* and

its *in vitro* characterization suggested that the DAT might have an important role in the clearance of DA *in vivo*. To determine how the DAT functions *in vivo,* Giros *et al*. used emerging genetic targeting strategies to disrupt the function of the endogenous DAT in a mouse (Giros, Jaber, Jones, Wightman, & Caron, 1996). Using FSCV, the authors determined that mutation of the DAT resulted in a loss of DA clearance and an insensitivity to amphetamine (AMPH) induced efflux in the striatum. Furthermore, loss of the DAT resulted in a spontaneous locomotor hyperactivity and changes in postsynaptic DA receptor expression. These studies established that the DAT represents the primary mechanism of DA clearance in the brain through sodium and chloride dependent uptake.

Metabolism

As in DA biosynthesis, our understanding of DA metabolism was greatly enhanced by studies EPI and NE metabolism in multiple preparations. DA undergoes two primary chemical modifications during its metabolism by two distinct pathways (Kopin, 1985). One of these pathways involves the deamination of DA by monoamine oxidase (MAOA) (left side of Figure 3) to form 3,4 dihyroxylphenylacetic acid (DOPAC). The other pathway involves the transfer of a methyl group to the 3' carbon via the actions of the magnesium-dependent cytosolic catechol o-methyltransferase (COMT) to form 3-methoxytyramine (3MT). These two metabolic precursors can then

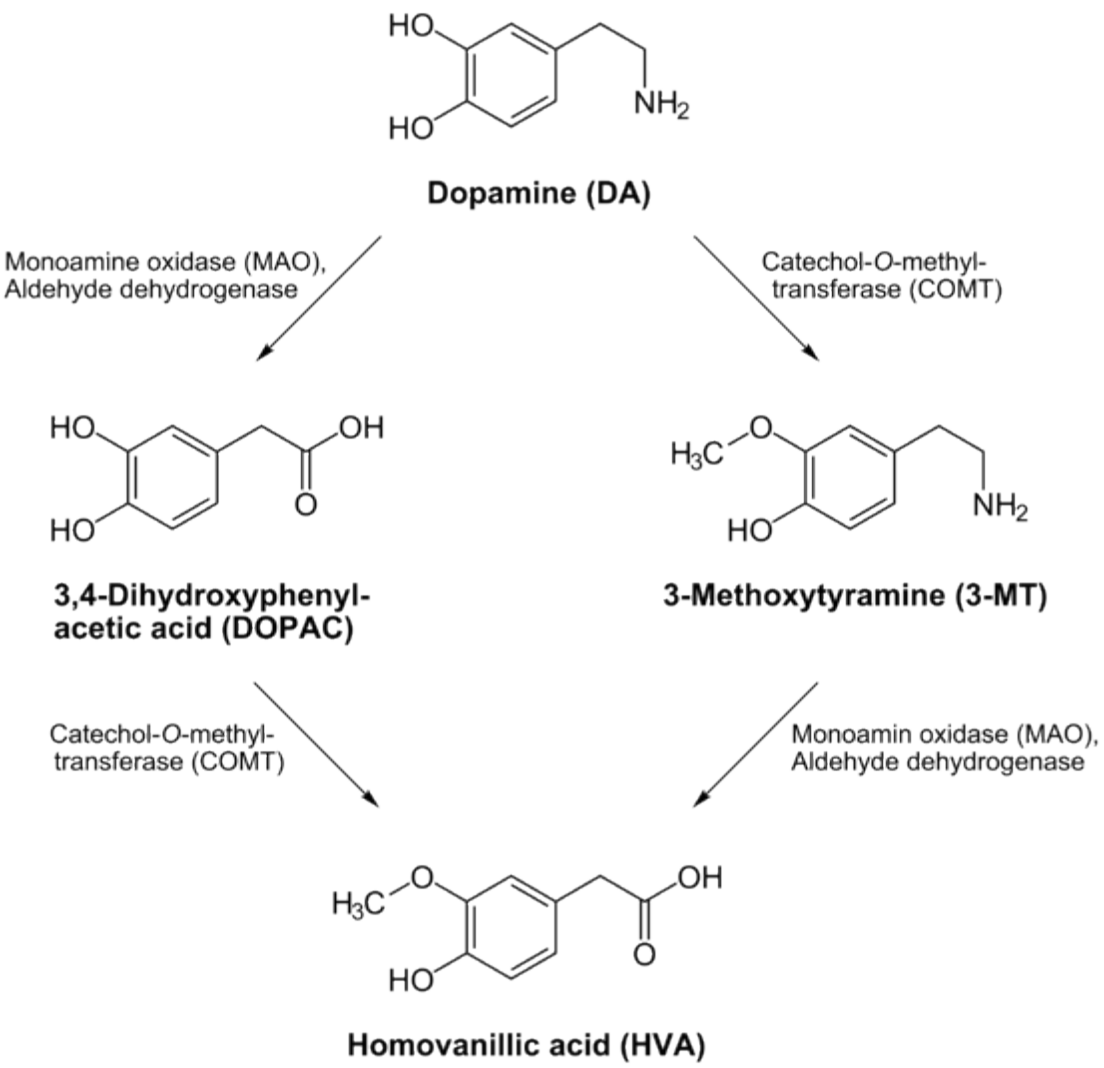

Figure 3 – Dopamine Metabolic Pathways. Schematic publically available on Wikimedia Commons.

be modified by the opposite pathway to form the final metabolite homovanillic acid (HVA). In areas rich in DA content, the relative amount of each of these metabolites and their ratio can be used to gauge the turnover of synaptic DA. These metabolites circulate through the body and are eventually excreted in the urine.

Chapter II

THE *C. elegans* DOPAMINERGIC NERVOUS SYSTEM

Anatomy of Dopamine Neurons in *C. elegans*

Like mammals, the nematode *Caenhorhabditis elegans* has a repertoire of DA neurons with stereotypical morphology and network connections. The DA neurons were initially described through a catecholamine cross-linking approach known as formaldehyde-induced-fluorescence (FIF) that generates a green fluorescent color in areas containing catecholamine (Jonsson, Einarsson, Fuxe, & Hallman, 1975). As nematodes have subsequently been shown not to contain NE, this approach remains a valid one to determine specific genetic contributions to DA signaling in the worm. In an elegant anatomical study, Sulston *et al*. used FIF to characterize the position and morphology of DA neurons in the worm (Sulston, Dew, & Brenner, 1975). In the hermaphrodite, there exist two bilaterally symmetric pairs in the nerve ring between the anterior and posterior bulb of the pharynx that, in comparison with existing electron microscopic reconstructions at the time, he determined these four neurons to be cephalic neurons (CEP). These neurons had the most dense DA-containing varicosities, could be detected at early embryonic stages, and send a process to the cephalic sensilla at the tip of the worm proboscis. More posteriorly, Sulston noted a pair of neurons that send a dorsal and ventral anterior process that contain a moderate density of FIF+ varicosities. The dorsal projection terminates at the deirid pore, thus they determined these two neurons to be deirid neurons

(ADE). Sulston also noted FIF+ lateral cells on the left and right side that he suspected to be deirid sensory neurons. These cells sent processes ventrally and harbored varicosities that extended anteriorly along a process close to the ventral nerve cord. Sulston also looked at the more rare *C. elegans* males and noted the presence of an additional three FIF+ pairs in the rays of the male tail. Therefore in total *C. elegans* harbor at least three DA neuron subgroups with a total of eight neurons in hermaphrodites and there exist an additional six neurons in male-specific structures (Figure 4). Around 25 years later, the cloning and molecular characterization of DA neuron specific genes and the use of green fluorescent protein (GFP) promoter fusions to these genes independently validated Sulston's seminal work on describing *C. elegans* DA neuron anatomy.

Molecular Regulation of Dopamine Signaling

In Sulston's initial work describing DA neuron anatomy, he also performed a small scale forward genetic screen using a chemical mutagen and identified mutants that had altered FIF (Sulston, et al., 1975). He named these six mutants *cat* mutants for catecholamine deficient. In so doing, he provided a foundation for the initial work to clone DA neuron signaling genes in *C. elegans*. Two of these mutants, *cat-1* and *cat-2*, had dramatically reduced FIF and DA levels as measured by alumina-based chromatography.

Duerr and colleagues were the first to clone one of these genes when they demonstrated that *cat-1* encodes the reserpine-sensitive homolog of mammalian vMAT2 (Duerr et al., 1999). They demonstrated that *cat-1* was

expressed in similar neurons as observed by Sulston, was localized to synaptic vesicles, and can transport biogenic amines including both DA and 5HT *in vitro*. Additionally, *cat-1* loss results in alterations in specific worm behaviors including locomotion, and that some of these phenotypes could be rescued by expression of human vMAT2.

Lints *et al.* was the first to take advantage of the development of the use of GFP promoter fusions in *C. elegans* to describe the genetic mechanisms of developmental patterning of dopamine in the male sensory rays (Chalfie, Tu, Euskirchen, Ward, & Prasher, 1994; R. Lints & S. W. Emmons, 1999). They determined the precise locus for the mutation in Sulston's original isolate, rescued FIF in this strain with transgenic expression of the wildtype locus, and generated several strains expressing a *cat-2*:GFP transgene that allowed them to visualize the DA neurons. They determined that this gene bears 50% protein sequence homology to TH in *Drosophila* and rat and that the pattern of GFP expression in their transgenic animals overlaps with that of FIF. They therefore determined that *cat-2* encodes the worm TH homolog.

In addition to mutagenesis screens, targeted expression cloning strategies have enhanced our understanding of the molecular mechanisms of *C. elegans* DA signaling. Prior to the genetic identification of *cat-1* and *cat-2*, Jayanthi and colleagues used a homology-based oligonucleotide plaque hybridization approach to screen a worm cDNA library for sequences that likely represent the *C. elegans* DAT homolog. They isolated several cDNA clones of T23G5.5, expressed these clones in heterologous cell lines, and used molecular

pharmacological techniques to determine if this gene can transport DA and how it responds to known dopamine transporter inhibitors (Jayanthi et al., 1998). They determined that T23G5.5 preferentially transports DA, is highly homologous to the human norepinephrine transporter (NET), and that DAT and known NET antagonists inhibit the transport activity of T23G5.5. The authors concluded that T23G5.5, later named *dat-1*, encodes the gene necessary for DA clearance in *C. elegans*. *In vivo* relevance of *dat-1* actions became apparent when Nass *et al*. created a strain expressing a *dat-1*:GFP transgene. As in the *cat-2*:GFP strain and in Sulston's FIF labeling, the *dat-1*:GFP transgene is expressed specifically in *C. elegans* DA neurons (Figure 4). Using this approach, the authors demonstrated a striking level of DA neuron labeling, and multiple labs now use this promoter as a way to express a gene of interest specifically in DA neurons (Cao, Gelwix, Caldwell, & Caldwell, 2005; Flames & Hobert, 2009; Hamamichi et al., 2008). Using this reporter, the authors determined that *dat-1* was required for the transport and subsequent toxicity of 6-OHDA such that brief treatment with 6-OHDA could cause specific degeneration of DA neurons and that this toxicity was lost in animals with a genetic lesion in their endogenous *dat-1* locus. These studies established that *dat-1* functions *in vivo* to transport DAT substrates.

cat-2/TH was the first gene to be identified within the DA biosynthetic pathway, but further clues to genes required for this process were still available from Sulston's original screen. *cat-4* encodes an enzyme, GTP cyclohydrolase, that catalyzes the biosynthesis of tetrahydrobiopterin, a cofactor necessary

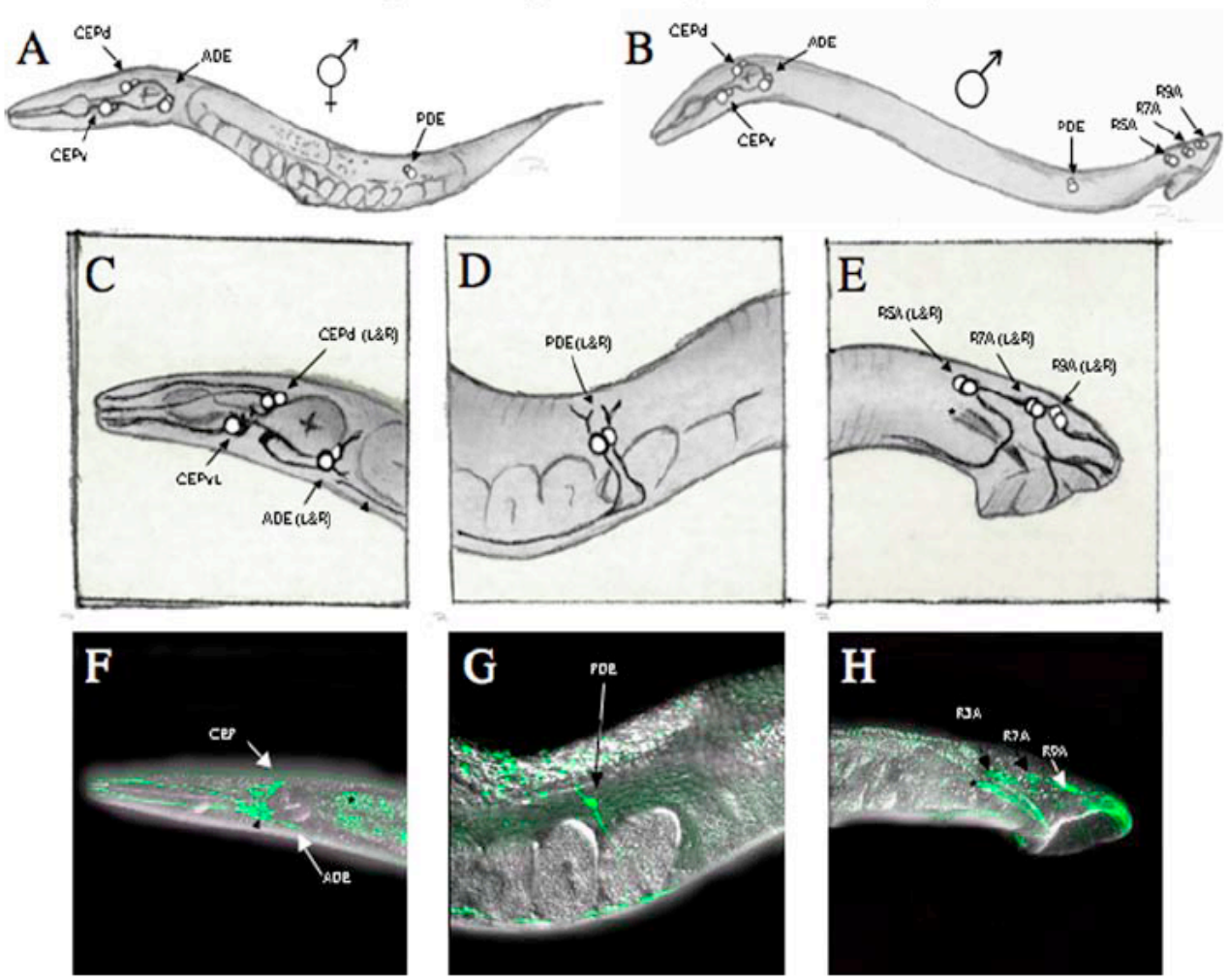

Figure 4 – Anatomy of the *C. elegans* dopamine system. A. Cartoon illustration of the DA neuron cell locations in the *C. elegans* hermaphrodite. B. Cartoon illustration of the DA neuron cell locations in the *C. elegans* male. C. Enlarged view of anteriorly positioned DA neurons. D. Enlarged view of the PDE neurons. E. Enlarged view of the male tail DA neurons R5A, R7A, and R9A pairs. F. Enlarged view of a worm expressing $p_{dat\text{-}1}$:GFP demonstrating expression in CEP and ADE neurons. G. Enlarged view of a worm expressing $p_{dat\text{-}1}$:GFP demonstrating expression in PDE neurons. H. Enlarged view of a worm expressing $p_{dat\text{-}1}$:GFP demonstrating expression in the ray neurons. DIC is overlaid. Figure taken from (Paul W McDonald, Jessen, Field, & Blakely, 2006).

for the decarboxylation of L-DOPA and 5-hydroxytryptophan (5HTP) by AADC, which was later identified as *bas-1* in the worm (Hare & Loer, 2004; Sawin, Ranganathan, & Horvitz, 2000). Together with the previous characterization of *cat-2*, there now existed a fuller picture of DA biosynthesis in the worm. Furthermore, with the description of *cat-1, cat-2,* and *dat-1*, many of the critical presynaptic genes necessary for presynaptic maintenance of DA signaling had been cloned.

Following the publication of the first draft of the human genome and the already published draft of the *C. elegans* genome sequence, researchers began using bioinformatic approaches to identify DA receptors in the worm. By using sequence similarity of predicted proteins in *C. elegans* against known protein sequences of mammalian DA receptors, Suo *et al*. cloned and characterized the first *C. elegans* DA receptors, *dop-1* and *dop-2* (Suo, Sasagawa, & Ishiura, 2002, 2003). Suo *et al.* found that the amino acid sequence of *dop-1* was 43% identical to the human D1 receptor and that this receptor had a high affinity for dopamine using radioactive ligand displacement assays. For *dop-2* they used similar molecular pharmacological approaches in heterologous systems to demonstrate that the *dop-2* receptor has a 44% protein sequence similarity to mammalian D2 receptors, exhibits a high affinity for DA relative to other biogenic amines, demonstrated that its activation reduces the production of cAMP, and used a GFP promoter fusion strain to demonstrate that *dop-2* is expressed in many neurons of the nerve ring, but is also expressed presynaptically in DA

neurons. Thus *dop-2* likely functions as a $G_{\alpha o}$-coupled D2-like receptor and represents a putative autoreceptor in the worm.

Chase *et al.* characterized the identity of another postsynaptic dopamine receptor (Chase, Pepper, & Koelle, 2004). Similar to Suo and colleagues, they used sequence similarity to the human D2 receptor to identify the existence of eighteen different putative receptors in *C. elegans*. After RT-PCR of the T14E8.3 cDNA, they determined that the *dop-3* receptor has 50% protein sequence similarity to the human D2 receptor. Using strains expressing GFP promoter fusion transgenes of *dop-3* and the previously cloned *dop-1*, they determined that both of these receptors were expressed in postsynaptic areas of the worm motor circuit including body wall muscle (*dop-3* only), cholinergic neurons (*dop-1* and *dop-3*), and GABAergic neurons (*dop-3* only). Interestingly, the expression of *dop-1* and *dop-3* overlap in the mechanosensitive PVD touch neuron (Smith et al., 2010).

Lastly, Sugiura and colleagues validated the cloning of *dop-3* and identified a novel DA receptor that they named *dop-4*. Using bioinformatic approaches, they determined that *dop-4* functions as a D1-like receptor to increase the production of cAMP and is expressed in neuronal cells like the ASG, ASL, PQR, and CAN neurons and non-neuronal cell types like the vulva, rectal epithelial cells, and Ray 8 of the male tail (Sugiura et al., 2005).

In summary, the *C. elegans* genome contains four known and characterized DA receptors: *dop-1, dop-2, dop-3*, and *dop-4*. *dop-1* and *dop-4*,

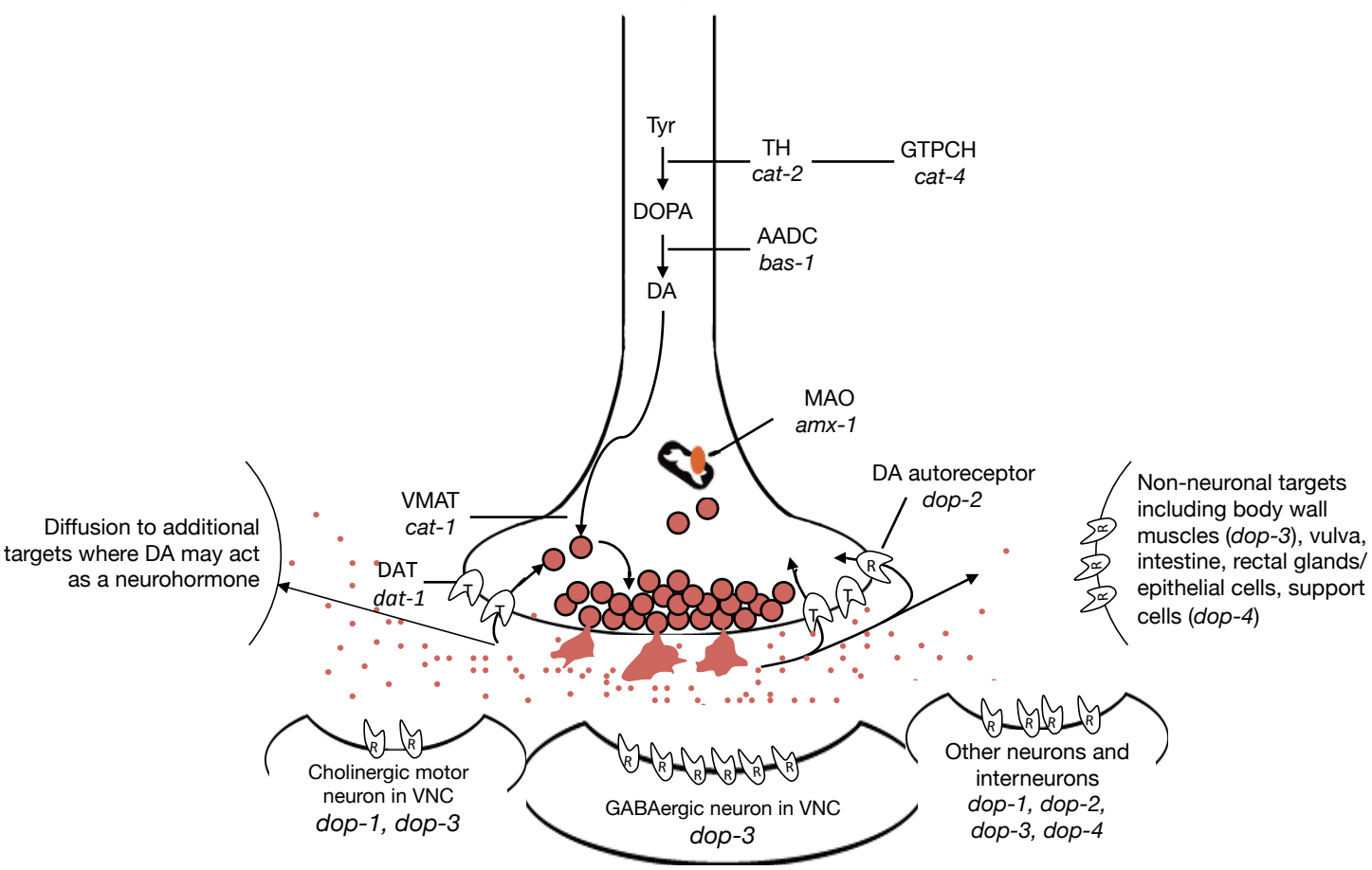

Figure 5 – Dopamine Signaling Genes in *C. elegans*. Cartoon diagram of the DA synapse in *C. elegans* illustrating pre and postsynaptic signaling genes. Schematic adapted from (R Nass & Blakely, 2003).

based on the characterization of their function in human cell lines, are likely D1-like receptors, whereas *dop-2* and *dop-3* are D2-like. These receptors are expressed in a variety of neuronal and non-neuronal tissues that suggests that they function to regulate multiple aspects of *C. elegans* physiology and behavior.

Dopamine Regulation of Locomotion in *C. elegans*

Our understanding of the *C. elegans* DA signaling network has been enriched by study of several behaviors that are altered by reduction or elevation of DA signaling such as egg-laying, defecation, habituation to touch, learning, and locomotion (reviewed in (Paul W McDonald, et al., 2006) and (Chase, 2007)). Rather than reviewing DA's role in modulating each of these behaviors, I will concentrate the following review solely on DA's role in modulating locomotory states in *C. elegans*.

Early research on 5HT and the biogenic trace amine, octopamine, indicated that these neurotransmitters could inhibit locomotion, but no such role for DA had been described (Horvitz, Chalfie, Trent, Sulston, & Evans, 1982). Schafer and Kenyon demonstrated that both biogenic amines could inhibit *C. elegans* locomotion, that worms could adapt to this paralysis over time, and that the calcium channel *unc-2* was required for adaptation to either compound (Schafer & Kenyon, 1995). Though these studies clearly established that exogenous DA could inhibit the vigor of worm locomotion, the role of endogenous DA during ethologically relevant behavior was still unknown.

Sawin and colleagues made one of the most important observations about DA's role in modulating locomotory behavior (Sawin, et al., 2000). They discovered that worms slow their locomotory rate in response to a lawn of bacteria, a phenotype they dubbed the basal slowing response (BSR). Furthermore, they noticed that worms previously starved displayed a more exaggerated slowing response that they conveniently named the enhanced slowing response (ESR). The authors determined that the previously described *cat-2* mutant had a defective BSR but intact ESR, whereas *bas-1* and *cat-4* mutants had defective BSR and ESR. As *bas-1* and *cat-4* mutants ought to harbor alterations in both DA and 5HT and the *cat-2* mutant only disrupts DA signaling, the authors concluded that endogenous DA mediates the BSR, while the ESR requires endogenous 5HT. Using exogenous DA and 5HT preincubation, they demonstrated that DA and 5HT restoration was sufficient for BSR and ESR. In the process they also replicated Schafer's previous findings that exogenous DA and 5HT could inhibit *C. elegans* locomotion. Consistent with their genetic experiments, they performed laser ablations of the DA neurons in full and in combinations and determined that the DA neurons function redundantly to mediate the BSR, but that ablation of the CEP neurons generated a dramatic reduction in the BSR. Lastly, they sought to determine the sensory mechanism by which the worm generates the BSR. As the anatomy of the DA neurons suggested that they might be mechanosensitive and a lawn of bacteria might trigger mechanical stimulation of the DA neuron dendrites, they found that wildtype animals also display BSR in response to a matrix of glass beads.

Importantly, as in the food-dependent BSR, *cat-2* animals or DA neuron laser ablated animals had a defective BSR to glass beads. The latter experiment suggested that mechanical stimulation alone was sufficient to trigger DA-mediated behavioral responses and hinted that mechanical stimulation of DA neurons might trigger their excitation and release of DA into the extrasynaptic space though methods for monitoring DA neuron excitability *in vivo* were not available at the time. These studies were a critical first step in elucidating DA's role in regulating locomotion in the worm, but a more mechanistic explanation of how DA acts postsynaptically was still lacking.

The pace of understanding DA's role in modulating locomotion matched that of the cloning of dopamine receptors and as new mutant alleles of these genes became available (Chase, et al., 2004). Chase *et al*., following the cloning of *dop-3*, isolated several new mutant alleles in *dop-1*, *dop-2*, and *dop-3*. As Sawin and colleagues had already established an assay to measure contributions of endogenous DA signaling, the authors screened these alleles using the BSR assay. Importantly, they discovered that loss of the *dop-3* receptor resulted in a complete loss of the BSR and that transgenic restoration of wildtype *dop-3* could restore BSR. Thus *dop-3* was required for a locomotory phenotype modulated by endogenous DA. As in Schafer *et al*., they demonstrated that exogenous DA was effective at promoting paralysis, but that mutations in *dop-3* resulted in resistance (Schafer & Kenyon, 1995). They used the sensitivity to exogenous DA, cell specific restoration of *dop-1* and *dop-3* in the GABAergic and cholinergic motor neurons, and a forward genetic screen for

DA-resistant mutants to paint a complete picture of the postsynaptic mechanism of dopamine signaling. *dop-1* functions through the G-protein *egl-30* and its downstream effector phospholipase Cβ *egl-8,* whereas *dop-3* functions through the G protein *goa-1* and its downstream effector *dgk-1*. These two pathways function antagonistically to promote normal BSR and exogenous DA-induced paralysis.

Identification of the Swimming Induced Paralysis Phenotype

The previous studies established the critical pre- and postsynaptic components of the DA signaling network, but researchers had not yet exploited the full potential of the model to augment our understanding the entire genetic network that is critical for maintenance of DA signaling. *C*. *elegans* has long been used in forward genetic mutagenesis screens to reveal novel, conserved genes for particular behavioral or physiological processes (Brenner, 1974). To carry out such a screen, we required a novel, quick, robust phenotype mediated by endogenous DA. In an effort to eventually carry out a screen for novel regulators of *dat-1*, we analyzed the locomotory behavior of a newly acquired deletion allele of *dat-1*. Unfortunately, in assays of normal movement on plates, the *dat-1* strain resembled the wildtype strain. In other words, DA clearance through *dat-1* did not dramatically impact crawling behavior. In an independent line of research for the presynaptic choline transporter, *cho-1*, we found that this strain had deficits in sustained swimming behavior that were revealed by growing this strain on a low choline producing bacteria (Matthies, Fleming, Wilkes, & Blakely,

2006). As previous studies had described DA's role in locomotion, we hypothesized that *dat-1*'s contributions to this process might be revealed in an alternative locomotory context. McDonald, Hardie and colleagues discovered that loss of *dat-1* results in a rapid all-or-none paralysis after a few minutes of swimming. Whereas wildtype animals will swim at a sustained rate after 10 minutes, loss of *dat-1* results in complete paralysis of each worm assayed during the same time frame (P. W McDonald et al., 2007). They then demonstrated that this phenotype, Swimming Induced Paralysis (Swip), was completely rescued by a loss of either TH/*cat-2* or the D2/*dop-3* receptor, or partially rescued by pretreatment with the vMAT2 inhibitor reserpine. As in Sulston's original FIF experiments, reserpine pretreatment of the *dat-1* strain resulted in a dramatic suppression of the Swip phenotype (Sulston, et al., 1975). Importantly as in Chase *et al.,* the authors transgenically restored *dat-1* and rescued the Swip phenotype, thereby demonstrating that loss of *dat-1* function was required for the Swip phenotype.

With the robust Swip phenotype and an acute rescuing agent (reserpine) in hand, I therefore set out to identify novel presynaptic regulators of DA signaling using forward genetics.

Specific Aims

Aim #1 – Perform a forward genetic screen for novel regulators of DA signaling using the *dat-1*-like Swip phenotype.

Aim #2 – Validate the dopaminergic phenotypes of the isolated mutation strains and the design of the screen by characterization of novel *dat-1* alleles.

Aim #3 – Map, identify and characterize a novel gene containing mutations in one or more of the isolated Swip strains.

CHAPTER III

A FORWARD GENETICS SCREEN FOR NOVEL REGULATORS OF DOPAMINE SIGNALING IN *C. ELEGANS*[1]

INTRODUCTION

The catecholamine dopamine (DA) is a phylogenetically conserved neurotransmitter that in vertebrates, including humans, regulates motor and cognitive behavior. Altered DA signaling contributes to multiple brain disorders including Parkinson's Disease (PD), dystonia, attention-deficit hyperactivity disorder (ADHD), schizophrenia and addiction (A. Carlsson, 1993; Kurian et al., 2011; Michelle S Mazei-Robison, Couch, Shelton, Stein, & Blakely, 2005; P. Seeman, 2010). DA signaling is achieved through both presynaptic and postsynaptic mechanisms that have been studied largely using biochemical, pharmacological and reverse genetic approaches. These studies have uncovered and characterized many fundamental components that control DA signaling, such as the genes that provide for DA synthesis, release, reuptake and response. The powerful, modulatory control exerted by DA over both cognitive and motor behavior and the incomplete understanding of the determinants of risk for DA-associated brain disorders suggest that a broader array of genes exist that controls DA signaling. Identification of these genes may benefit therefore from unbiased approaches, such as those afforded by forward genetic screens.

---

[1] Adapted from Hardaway and Hardie *et al. Genes, Genomes, and Genetics*. 2012

Among the most critical of known determinants of DA signaling, one molecule, the presynaptic DA transporter (DAT, *SLC6A3*), has special roles in controlling access of pre- and post-synaptic DA receptors to DA, in recycling DA into presynaptic terminals after release, and in maintaining levels of DA needed for sustained release (Giros, et al., 1996; Torres, Gainetdinov, & Caron, 2003). Knockout of DAT through homologous recombination in mice demonstrates an obligate role for the transporter in AMPH and cocaine-induced hyperlocomotion, as well as DA release and clearance (Giros, et al., 1996). Conversely, mice overexpressing DAT display reduced extracellular DA levels and heightened sensitivity to AMPH (Salahpour et al., 2008). These studies also demonstrate that genetic manipulation of DAT in mice leads to changes in the expression of genes that encode pre- and postsynaptic DA receptors and neuropeptides, underscoring the importance of DAT as a key regulator of a broad DA signaling network (Giros, et al., 1996). Following the cloning of DAT cDNAs (Brüss, Wieland, & Bönisch, 1999; Giros, et al., 1992; Jayanthi, et al., 1998; Kilty, et al., 1991; Shimada, et al., 1991), many have explored the impact of DAT mutations using heterologous expression models *in vitro* (Schmitt & Reith, 2010), though, as yet, the significance of many of these findings *in vivo* is unknown. Recently, we and others have identified rare, functionally penetrant, mutations in DAT in subjects with ADHD and juvenile dystonia (Kurian et al., 2009; M. S Mazei-Robison et al., 2008), compelling a better understanding of the impact of DAT mutations and altered DAT regulatory mechanisms *in vivo*.

Forward genetic strategies that rely on DAT-dependent phenotypes provide a path to the identification of key DAT structural elements as well as the elucidation of novel regulators of DA signaling. Although such methods overcome the bias of studies focused on known genes and pathways (Mohn, Yao, & Caron, 2004), they are typically quite difficult to implement in mammals, due to the time and cost associated with animal breeding, mutation mapping and functional characterization *in vivo*. The nematode *Caenorhabditis elegans* has long been used in forward genetic screens (Brenner, 1974), including identification of genes supporting DA signaling (Allen, Maher, Wani, Betts, & Chase, 2011; Chase, et al., 2004; Sawin, et al., 2000; Schafer & Kenyon, 1995; Sulston, et al., 1975; Wani et al., 2012). These and homology based approaches have revealed *C. elegans* orthologs of mammalian genes required for DA biosynthesis, TH/*cat-2* (R. Lints & S. Emmons, 1999), GTP cyclohydrolase/*cat-4* (Loer & Kenyon, 1993), and AADC/*bas*-1 (Bamford et al., 2004), the vMAT/*cat-1* (Duerr, et al., 1999), genes involved in DA response including the D1 and D2 type DA receptors *dop-1/2/3/4* (Chase, et al., 2004; Sugiura, et al., 2005; Suo, Ishiura, & Van Tol, 2004; Suo, et al., 2003), and the presynaptic DA transporter/*dat-1* (Jayanthi, et al., 1998). In a previous study, we demonstrated that worms lacking functional DAT-1 (*dat-1(ok157)*) demonstrate a robust, DA-dependent phenotype when placed in water, termed Swimming-induced paralysis (Swip), a behavior that is dependent on activation of the postsynaptic, D2-like receptor DOP-3 (P. W McDonald, et al., 2007). Here, we describe our efforts to capitalize on the Swip phenotype to capture modulators of

endogenous DA signaling using forward genetic approaches. Lines derived from this effort are subjected to conventional biochemical and pharmacological methods, as well as to a novel analytical platform that can more finely dissect features of disrupted motor function. We describe the isolation of multiple, independent mutant lines, including two (*vt21* and *vt22*) that possess novel alleles of DAT-1. Disrupted expression and trafficking of the *vt21* mutant provides the first demonstration of functional relevance *in vivo* of a highly conserved, structural feature of SLC6 transporters. Two additional lines, *vt25* and *vt29,* lack *dat-1* mutations, map to different genomic loci, and sustain distinct components of DA signaling.

MATERIALS AND METHODS

C. elegans Strains, Husbandry, and Genotyping

C. elegans strains were cultured on bacterial lawns of OP50 and maintained at 12 to 20°C using standard methods (Brenner, 1974) unless otherwise noted. The wild-type strain is N2 Bristol. The *dat-1(ok157)III* strain was a gift of J. Duerr and J. Rand (Oklahoma Medical Research Foundation, Oklahoma City), and is a complete loss of function mutation that eliminates the majority of the DAT-1 coding sequence. BY200 and BY250 are stable integrants (Richard Nass, Hall, Miller, & Blakely, 2002) that expresses the transcriptional fusion $P_{dat\text{-}1}$::GFP (pRB490) on an N2 background. BY250 (*vtIs7*) was used for imaging DA neuron morphology of cloned and outcrossed *swip* lines and for 6-OHDA experiments. A line producing a loss of function disruption of DOP-3 (*dop-3(vs106)X*) was

obtained from the *Caenorhabditis* Genetics Center (University of Minnesota, Minneapolis) and *cat-2(tm2261)* from Shohei Mitani at the National Bioresource Project at the Tokyo Women's Medical University. *C. elegans* genomic DNA was isolated as described previously (Richard Nass et al., 2005) and used at a concentration of 1ng/μL to genotype lines by polymerase chain reaction (PCR). For all crosses, either males were generated using the method originally described by Sulston and Hodgkin (Hodgkin, 2005), or alleles were crossed to males of publically available strains containing integrated fluorescent transgenes that mark distinct nematode structures. After 24 hours of mating, hermaphrodites were separated onto individual plates and considered successful if ~50% of the progeny from an individual hermaphrodite are males and/or if the F1 progeny contained the fluorescent transgene from the male parent. For generation of the *dat-1(ok157);vt29* strain, markers of LGIII and LGX were used, and the double mutant genotype was confirmed by re-segregation of the two genes and confirmation with PCR genotyping of *ok157* and SWIP testing for *vt29*. Generation of *vt25,dat-1(ok157)* will require recombination of the two alleles after identification of the *vt25* functional variant and will be presented in a later report.

C. elegans Assay for Swimming-Induced Paralysis (Swip)

In both batch and automated analyses, we generated synchronous populations of these strains by hypochlorite treatment and harvesting arrested L1 animals. Early-mid stage L4 animals were identified by characteristic morphology and

used for behavior as N2 animals show some stochastic Swip and quiescence bouts during the last larval molt. For automated analysis, single L4 hermaphrodites were placed in 20μL water in a single well of a Pyrex Spot Plate (Fisher catalog number 13-748B), and 10 minute movies (uncompressed AVI format) of their swimming behavior were created and analyzed as described previously (Matthies, et al., 2006; P. W McDonald, et al., 2007), with slight modifications. We processed thrashing data using an in-house movement processing program (Worm Tracker, available on request) that fits a 5-point spine to the worm in each frame. The 5-point spines consist of 4 segments and 3 "joints". In Worm Tracker, a spine is specified by the x and y positions of the spine center, the rotation of the spine with respect to the vertical axis, and finally the angles of the 3 joints. The spine positions are fit using a particle filter and motion detection. The Worm Tracker software processes a video and records the position of the fitted spine for each frame. A MATLAB script reads the exported files and computes the frequency of swimming using Fast Fourier Transform and by counting frames between angular extrema. This script then produces a data file that provides the frequency of motion of a given worm over time. These individual files are then grouped by genotype into a large data matrix and an accompanying annotation file made for each of the animals to be analyzed. These two files are then used as the input for a custom script written in the free publically available statistical program R. The program (SwimR, available upon request) smoothens individual data traces using a specified moving window and identifies any outliers in the sample file using a modified z

score calculation (Iglewicz & Hoaglin, 1993). SwimR then generates several output text and PDF files including a scatter plot of average frequency vs. time, a heat map of the samples ordered by strength of paralysis and a histogram of the binned frequency data. For paralyzers, the script calculates the latency to paralyze and several parameters that define the ability of individual animals to revert from paralysis to regular thrashing activity, including reversion probability (total time in reversion/total time after paralysis), time to 1st reversion, average reversion duration and reversion strength (area under the curve during all reversion events). The user can set parameters related to paralysis. We defined paralyzed animals in our studies as those animals that fall below 20% of their maximal thrashing value and stay below this threshold for at least 20 seconds. Revertants are defined as those animals that, after paralyzing, re-cross a threshold equivalent to 50% of their maximum thrashing rate for any length of time. For batch analysis, 10-20 worms were visually scored in a single well of the Pyrex Spot Plate. Worms displaying Swip after a 10 minute assay period were counted and in some cases isolated by hand for further tests. For reserpine treatments, worms from each line were first synchronized by hypochlorite treatment and L1 larvae are grown on OP50 plates containing 0.6mM reserpine. After ~48 hours of reserpine or vehicle treatment, the population Swip analysis was repeated on groups of L4 animals from each line.

Exogenous DA Sensitivity Assay

Assays were performed as described in (Chase, et al., 2004), except that L4

animals were used in lieu of young adults, as this stage is most relevant to the DAT-1-dependent Swip phenotype. Briefly 10 L4 animals were transferred to 1.7% agar plates containing 2 mM glacial acetic acid and various concentrations of DA, incubated for 20 minutes and then scored as paralyzed or moving. Animals were defined as moving if they were able to propagate a body bend through a minimum or maximum amplitude. All concentrations of DA were utilized on the same day.

C. elegans Mutagenesis Screen

Standard methods for a non-clonal, F2 screen were performed as originally described (Brenner, 1974) and were used on wild-type hermaphrodite worms carrying a DAT-1 promoter-driven GFP transgene (BY200)(Richard Nass, et al., 2002). A semi-synchronous population of healthy, well-fed late L4 animals was exposed to either 47 mM ethylmethanesulfonate (EMS) or 0.5mM N-ethyl-N-nitrosourea (ENU) at room temperature for 4 hrs in a chemical fume hood. After 24 hours of recovery, 30 gravid adult worms were placed on each of 8 10cm OP50 plates and allowed to lay ~50 eggs each (the F1s) before being discarded. After reaching adulthood and laying 20-30 eggs each for a total of 1000-1500 developing F2 animals per plate, the F1 animals were discarded. When F2 animals reached the L4 stage, they were batch screened for the Swip phenotype by rinsing off the plate and analyzing 50-100 animals per well as described above. We tracked the source plate of each F2 so that only one stable mutant line was kept for each plate of the mutant F1s. After 10 min, animals that exhibit

Swip were replated and allowed to recover. Swip-positive animals that recovered normal movement on solid media were cloned and retested in Swip assays to establish phenotype stability. Only lines where at least 50% of the animals displayed Swip on retest were saved for a test of reserpine reversal of Swip, as described above. In later rounds of screening this convention was increased to 80% to improve recovery of stable lines. Stable lines that demonstrated a significant rescue of Swip after reserpine treatment were kept for further analysis. All recovered lines passing the reserpine test were outcrossed to the N2 strain a minimum of three times before further analysis. After each outcross, lines were re-homozygosed and re-tested for stable Swip on separate days with multiple parental founders before proceeding to the next cross. All lines recovered from the screen were sequenced with sense and anti-sense primers that span all DAT-1 exons and includes 1 kb upstream of the transcription start site as well as 50 bp downstream of the translational stop codon) using Big Dye Terminator Cycle Sequencing Mix (ABI, Foster City, CA, USA). PCR products were sequenced on an ABI 3730xl DNA Analyzer (DNA Sequencing Core Facility, Vanderbilt Division of Medicine).

SNP Mapping

Mapping of mutant loci was performed as described previously (Davis et al., 2005). Briefly stable outcrossed *swip* strains were crossed to the CB4856 strain. For bulk segregant analysis, lysates from both Swip-positive and Swip-negative, F2 populations were generated and used as the input for genome-wide, 96 well

PCR. N2 animals were not used as a control in these efforts as we found nonspecific N2 Bristol islands in both the Swip-positive and Swip-negative F2s on the left arm of LGI. The bulk segregant protocol was used to identify linkage groups that can serve for fine mapping with experiments replicated at least twice with separate populations to demonstrate consistent linkage. For fine interval mapping, individual Swip-positive F2s were cloned and their F3 progeny were tested for a stable Swip phenotype. *Swip* mutations were considered homozygous if the F3 population demonstrated Swip comparable to the original strain. Populations were manually scored in at least 4-5 assays using 40-50 worms. DNA from individual clones was then used as the input for PCR of individual intervals to ascertain a specific Bristol island on the mapped linkage group.

Creation of plasmids and transgenic animals

Plasmids: P_{dat-1}:GFP::DAT-1(Carvelli, McDonald, Blakely, & DeFelice, 2004) (Carvelli, et al., 2004) and P_{dat-1}::GFP (Richard Nass, et al., 2002) have been described previously. The following plasmids were created to examine DAT-1 mutations in heterologous mammalian expression systems: pRB1026 (DAT-1(G460D) in pcDNA3); pRB1027 (DAT-1(W283*) in pcDNA3); pRB1028 (N-terminally HA-tagged DAT-1(G460D) in pcDNA3); and pRB1029 (N-terminally HA-tagged DAT-1 (W283*) in pcDNA3) were developed to examine the DAT-1 mutations Swip2 (G460D) and Swip3 (W283*). pRB1030 (DAT-1(G460D) in pRB491) and pRB1031 (DAT-1(W283*) in pRB491) were created to evaluate the

DAT-1 mutations *vt21* (G460D) and *vt22* (W283*) alleles in *C. elegans in vivo.* Lines shown in Fig. 6 are *ex21*, *ex62* and *ex65* for DAT-1, *vt21*, and *vt22.* All mutations were created using the Quick Change XL site-directed mutagenesis kit (Stratagene, La Jolla, CA, USA). *Transgenic animals:* Fully sequenced constructs (90 ng/μl) were coinjected with the lin-15 rescuing plasmid pJM23 (40 ng/μl) into *dat-1(ok157);lin-15(n765ts)* animals using methods described previously (Jin, Jorgensen, Hartwieg, & Horvitz, 1999). *vtIs18* is an outcrossed integrant of *ex21* which expresses a P_{dat-1}:GFP::DAT-1, rescues the *dat-1* strain, and maps to LGV.

Mammalian Cell Culture and Western Blot Analysis

Methods for western blot analysis and surface biotinylation of the *C. elegans* DAT-1 expressed in COS-7 have been described elsewhere (Carvelli, et al., 2004; Richard Nass, et al., 2005). Briefly, COS-7 cells were plated and allowed to attach for 24 hours prior to transfection. Cells were transfected with 250ng of either HA-tagged DAT-1 cDNA (pRB606, (Jayanthi, et al., 1998), HA-tagged DAT-1(G460D) cDNA (*vt21*, pRB1028), HA-tagged DAT-1(W283*) cDNA (*vt22*, pRB1029), or an empty vector (pcDNA3, Invitrogen, Carlsbad, CA) using TransIT-LT1 (Mirus, Madison, WI) as the transfection vehicle. At 48 hrs post-transfection, cells were harvested as previously described and equal amounts of sample protein were resolved on a 4-20% TRIS SDS-Page Ready Gel (Bio-Rad Cat# 161-1105) followed by transfer overnight to an Immobilon-P PVDF

membrane (Millipore Cat# IPVH00010). Membranes were blocked for 1 hr in PBS containing 0.5% TWEEN20 and 5% instant nonfat dried milk. After blocking, the membranes were incubated with a rat monoclonal anti-HA-peroxidase labeled antibody [High Affinity (3F10), Roche Diagnostics] at a 1:2000 dilution for 1 hr at room temperature. After washing, blots were developed with Western Lightening chemiluminescense reagents (Perkin Elmer) and exposed to High Performance Chemiluminescence film (Amersham, Piscataway, NJ, USA). To analyze surface expression, cells were biotinylated with sulfosuccinimidyl-2-(biotinamido)ethyl-1,3-dithiopropionate-(sulfo-NHS-SS-Biotin) (1.0 mg/mL; Pierce, Rockford, IL, USA) and following detergent extraction, samples were incubated with Streptavidin beads and eluted for SDS-PAGE analysis as previously described (Richard Nass, et al., 2005).

In vivo GFP imaging

In vivo imaging of DAT-GFP fusion protein expression and distribution was performed as previously described (P. W McDonald, et al., 2007). Briefly, a series of 1.2μm image planes was obtained using a Zeiss LSM 510, creating a "Z stack". Because of differences in GFP expression, different laser settings were used for imaging of the head neurons (CEP and ADE) and PDE neurons. Higher laser settings are also used to detect the GFP tagged *vt22* DAT variant. Z stacks were used to create 3D reconstructions of images as noted in the Figure Legends. Image stacks containing either cell body or synaptic regions were thresholded, rank filtered and pseudocolored using Metamorph (Molecular

Devices, Sunnyvale, CA). Final images of either CEPs and ADEs or PDEs were processed using identical brightness and contrast values.

HPLC measurement of DA levels

Synchronized L4 worms were washed in water, pelleted, frozen and then sonicated in buffer containing EDTA as previously described (Benedetto, Au, Avila, Milatovic, & Aschner, 2010). Protein content was measured by a BCA assay (Pierce) using 10 μl of the lysate. 5 ng/ml isoproterenol was added to the remaining sample, which was then applied to an alumina column to extract DA. Eluted samples were then analyzed by HPLC using a Waters 717+ autosampler and an Antec Decade II electrochemical detector (oxidation: 0.5V). Reverse phase HPLC was performed using a Phenomenex Nucleosil (5u, 100A) C18 column (150 x 4.60 mm) with a mobile phase of 89.5% 0.1M TCA, 0.1 M sodium acetate, 1mM EDTA and 10.5% methanol (pH 3.8) at a rate of 0.6ml/min, with data acquired by Millennium 32 software.

6-OHDA Toxicity Assay

DA neuron sensitivity to 6-OHDA was assessed as described previously (P. W McDonald, et al., 2007; Richard Nass, et al., 2005; Richard Nass, et al., 2002). Briefly, strains containing the *vtIs7* (p_{dat-1}:GFP) transgene were grown on NA22 media containing plates seeded with 8P bacteria (8P/NA22) and synchronized at the L1 stage by hypochlorite treatment. Animals were plated onto 10 cm 8P/NA22 plates for 1 day at 20°C until they reached the L2-L3 stage. Worms

were then washed off the plate and incubated with 2, 5 or 10 mM ascorbic acid +/- 10, 25, or 50 mM 6-OHDA, respectively, for 1 hr on a covered Nutator. Worms were then pelleted and re-plated onto 8P/NA22 plates without removal of the 6-OHDA and incubated for 3 days at 20°C until the worms reached adulthood. Degeneration of CEP neuron dendrites was scored blind on a 4 point scale (where 4 = all dendrites intact and 0 = complete loss of dendrites). For scoring, 100-200 worms were placed on a freshly prepared 2% agarose pad and immobilized using 225 mM 2,3 butanedione monoxime (Sigma-Aldrich) and 2.5 mM levamisole (Sigma-Aldrich) in 10 mM Na HEPES. Fifty worms were scored per slide in triplicate for each strain assayed.

RESULTS

Forward genetic screen for reserpine-sensitive Swip phenotype

An artificial increase in extrasynaptic DA produced by incubation of nematodes with exogenous DA leads to increased activation of inhibitory DA receptors expressed on cholinergic motor neurons (Chase, et al., 2004), decreasing the release of ACH from these neurons (Allen, et al., 2011), resulting in paralysis. Our previous studies demonstrated that *dat-1(ok157)* worms display a paralytic phenotype in water in the absence of exogenous DA that we named Swimming Induced Paralysis or Swip (P. W McDonald, et al., 2007). The Swip phenotype exhibited by *dat-1* animals is absent in *cat-2*/TH;*dat-1* double mutants and can be rescued by pretreatment of animals with the *cat-1*/vMAT inhibitor reserpine, a reagent that depletes vesicular DA stores (P. W McDonald, et al., 2007).

Importantly, *dat-1*;*dop-3* animals (Sugiura, et al., 2005) also lack Swip behavior, establishing Swip as a phenotype that can derive from hyperdopaminergic signaling. As schematized in Figure 6A, we hypothesize that incubation of worms in water (but not in isotonic medium-J. A. Hardaway and R. D. Blakely, personal communication) evokes DA release that in wild type animals is limited in action by DAT-1. In *dat-1* animals, DA cannot be recaptured and spills over to extrasynaptic sites, where it can activate DOP-3 on motor neurons, decreasing cholinergic, neuromuscular signaling (Allen, et al., 2011), producing Swip.

Since the Swip assay is a simple, rapid, and highly reproducible method for detecting genetic contributions to endogenous DA signaling, we implemented Swip in a forward genetic screen, using multiple, secondary tests to eliminate non-specific mutants. Screening was performed over four independent rounds of screening using EMS and ENU as mutagens. We performed one round of screening using ENU and only recovered one stable mutant line(*vt25)*, so EMS was used as the mutagen in subsequent studies. As outlined in Figure 6B, L4 BY200 (P_{dat-1}::GFP) animals were mutagenized with EMS, and their F2 progeny batch were tested for Swip. Animals exhibiting Swip were individually cloned and their progeny (F3s) were tested to determine Swip penetrance, scored as the percent of animals of a clonal population exhibiting Swip. Animals that failed to move normally on plates, and thus where Swip might reflect mutation of genes required for movement more generally (e.g. *unc* mutations), were eliminated. As a tertiary screen, we tested animals for Swip reversal after incubation with

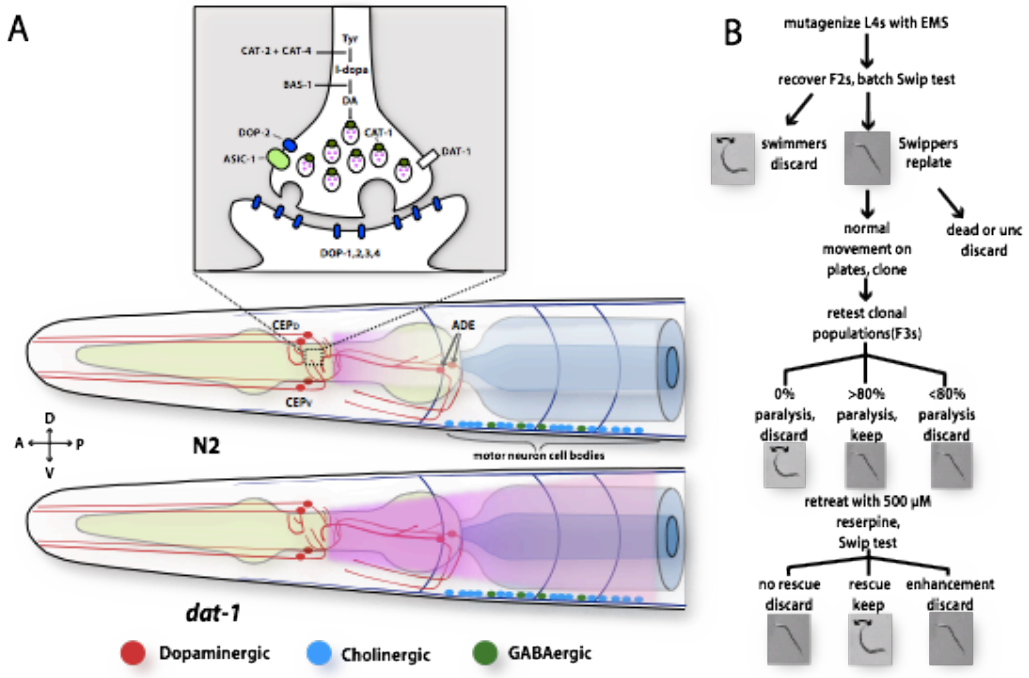

Figure 6 – Generation of reserpine-sensitive Swip establishes a phenotype for forward genetic identification of modulators limiting hyperdopaminergic signaling. A, *C. elegans* hermaphrodites contain eight DA neurons: four CEPs, two ADEs and two PDEs (not shown). These neurons release DA that can act humorally on the motor circuit through stimulation of the DA receptors DOP-1 and DOP-3 that are coexpressed in cholinergic motor neurons. [Inset: illustration of presynaptic DA terminals with gene products responsible for DA synthesis (CAT-2, CAT-4, BAS-1), packaging (CAT-1), release (DOP-2, acid-sensing ion channel 1 – ASIC-1) and inactivation(DAT-1)]. In DAT-1 deficient animals, the release of endogenous DA leads to a much larger increase in extrasynaptic DA, leading to hyperactivation of DOP-3 DA receptors and paralysis. B, Design of Swip-based forward genetic screen. We treat synchronized L4 animals with EMS, allowed animals to self-fertilize and isolate F1s. F2s are Swip tested in batch and paralyzing animals are cloned. Animals that do not display grossly normal movement on standard solid medium are eliminated, F3s are generated and then re-tested to insure transmission of Swip. Clones that demonstrate at least 80% paralysis (our pilot efforts used >50% but yielded poor stable transmission) are grown on 0.6 mM reserpine to deplete vesicular DA stores and tested for rescue of Swip. Clones that are rescued by reserpine pretreatment are given *vt* mutation designations and their progeny are used in all subsequent experiments.

reserpine (P. W McDonald, et al., 2007). Since Swip in the *dat-1* strain is fully penetrant, lines that exhibited ≥80% paralysis were pretreated with 0.6 mM reserpine, and animals were retested for Swip. In early rounds 1-3 which screened a lower number of haploid genomes, we used 50% as our convention, but this was later increased to 80% to maximize the chance that we would recover primary lines that could be stablely outcrossed. From this reserpine tertiary analysis, we identified mutants that were either unaffected, rescued or, surprisingly, enhanced by reserpine treatment. To date we have sampled ~10,000 mutant haploid genomes, and have isolated 25 primary mutant lines (*vt20-vt44)* that demonstrate a stable Swip phenotype and can be rescued by reserpine pretreatment. Of these 25, we found that 12 lines maintain their phenotype after 3X outcrossing, of which 10 lines are consistently rescued by reserpine pretreatment (Figure 7A). Flaherty *et al.* performed another round of clonal screening of 1,000 haploid genomes at Eckerd College, but it is unknown which of these primary lines are stable and are suitable for future characterization. They are currently being outcrossed. In this study, we report our genetic, biochemical and behavioral analysis on four of these lines: *vt21*, *vt22*, *vt25,* and *vt29*.

In order to demonstrate that *vt21, vt22, vt25* and *vt29* possess normal DA neuron morphology, we examined their CEP, ADE and PDE neurons via expression of a transcriptional reporter (Figure 8) and found that cell bodies and processes appear unaltered relative to N2 animals. These findings are consistent

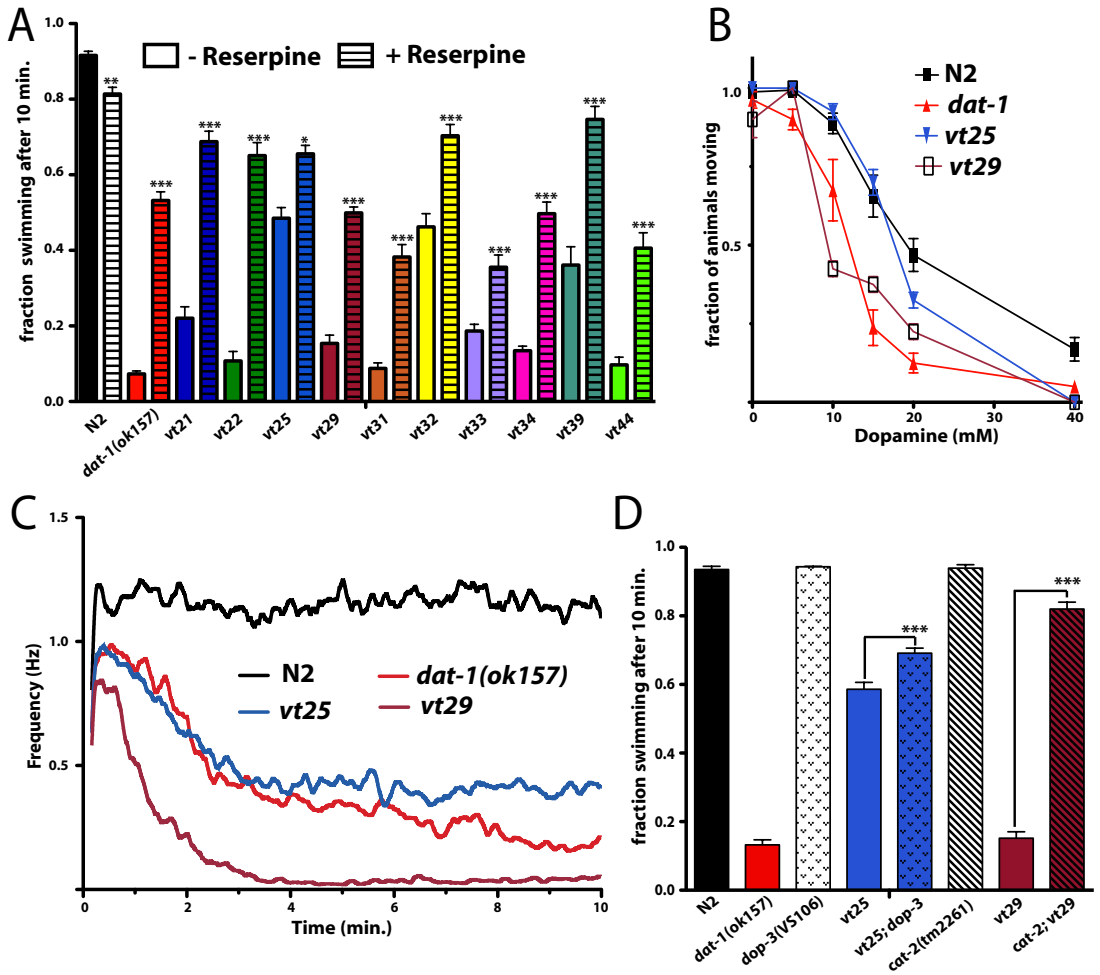

Figure 7 – *vt25* and *vt29* demonstrate alterations in DA-dependent locomotory behaviors. A. After a screen of ~10,000 haploid genomes, twenty-five *vt* mutant lines were outcrossed, of which ten were found to maintain their reserpine sensitivity. Populations of at least 10 worms were assayed in a single well and after 10 minutes, with animals scored as # animals swimming/total animals. Each bar represents at least 20 assays performed over several experimental days by multiple, blinded experimenters. Drug treatment effects were analyzed using an unpaired Student's t test comparing against basal Swip activity for that line, where * = $p < 0.05$, ** = $p < 0.01$ and *** = $P<0.001$ and error bars represent SEM. B. *Dat-1* and *vt29* display enhanced sensitivity to exogenous DA on a solid substrate, whereas *vt25* maintains an N2-like DA dose response. For these assays, 10 L4 stage worms were placed on plates containing increasing concentrations of exogenous DA, incubated for 20 min and then scored for 10 sec as paralyzed or moving. Dose-response curves were compared using two-way ANOVA with Bonferroni posttests comparing mutants to N2, where *dat-1* + *vt29* were all found to be significantly different from N2 with a $P<0.001$ at 15 + 20 mM DA. Data derive from at least 8 tests per strain per concentration. Error bars represent SEM. C. *vt25* demonstrates a higher average frequency of swimming at later time points as compared to *dat-1* animals, whereas *vt29* paralyzes faster. Individual animals were recorded using a video capture system and then analyzed with customed-designed Thrasher software that assigns multiple linear elements projecting from the worm centroid. The position of these linear elements are tracked and converted off-line to

Figure 7(cont'd) – movement frequency as a function of time. Batch conversions are generated, providing mean values and SEM along moving averages. Error bars are not shown in these plots for simplicity. Average thrashing plots were analyzed using two-way ANOVA with Bonferroni's multiple comparison analysis. *vt25* and *vt29* swimming frequencies were found to be significantly reduced from N2 after 58 sec and 39 sec, respectively. Although we observed no overall significant difference in these assays in comparing *dat-1(ok157)* and *vt25,* the thrashing frequency of *vt29* was found to be significantly reduced from *dat-1(ok157)* between 52 sec and 2 min 25 sec. D. *Swip* behavior of *vt25* and *vt29* is dependent on DOP-3 and CAT-2, respectively. The figure represents the mean swimming behavior as measured by manual scoring. Data derive from observations from > 24 trials for each strain. For *vt25; dop-3(vs106)* and *cat-2(tm2261); vt29*, the *vt* genotypes were confirmed via an independent complementation test. Data were analyzed using one-way ANOVA with multiple Bonferroni posttests where *** = $P<0.001$ and error bars represent SEM.

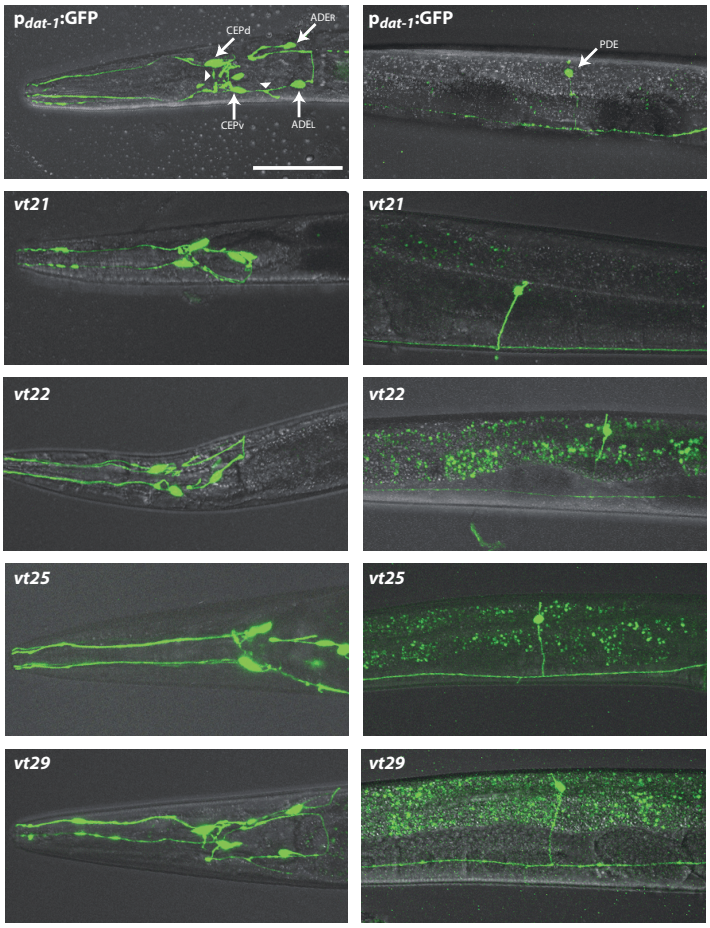

Figure 8 - ***Swip*** **mutants possess normal DA neuron morphology**. The left panels show that CEP and ADE neurons and processes are intact in all strains, possessing visibly normal dendrites(arrows) and terminals(arrowheads). On the right, PDE neurons and projections are shown for each strain, where a normal morphology is also evident. For all strains used, fully outcrossed *vt21, vt22,* vt25 *and vt29* were crossed onto a strain bearing an integrated p_{dat-1}:GFP transgene(BY250, *vtIs7*). *Swip* mutant genotypes were confirmed by Swip behavioral tests as the *vtIs7* line shows no paralysis on its own. Anterior is left in all images shown. Scale bar is equal to 50 uM.

with our hypothesis that Swip is a hyperdopaminergic phenotype that is unlikely to derive from gross alterations in DA neuron circuitry.

Isolation of novel *dat-1* null mutations

If our Swip screen is both specific and robust with respect to recovery of genes that control DA signaling, it should recover animals with *dat-1* alleles, as well as novel mutants. To assess this issue, we first crossed *vt21, vt22, vt25* and *vt29* with *dat-1(ok157)*, performing Swip complementation tests on their F1 progeny. From these experiments we found that N2 can complement *dat-1* and each of the mutant strains (Figure 9A) and that *vt25* and *vt29* both complement *dat-1*(Figure 9B) and one another (data not shown), indicating that *vt25* and *vt29* likely do not derive from mutations in *dat-1*. Likewise, these studies indicate that a single copy of *dat*-1 is happlosuficient to generate normal swimming behavior. In contrast,, *vt21* and *vt22* fail to fully complement Swip when crossed to *dat-1(ok157)*(Figure 9B). Likewise, when we crossed *vt21* and *vt22,* we observed a failure to complement (data not shown), indicating that they are likely alleles of the same gene, that most likely is *dat-1*.

To test this hypothesis, we overexpressed GFP-tagged DAT-1(P_{dat-1}::GFP:DAT-1) in *vt21* and *vt22* and tested for Swip in lines verified to express GFP in DA neurons. As previously demonstrated for the DAT-1 deletion allele *dat-1(ok157)* (P. W McDonald, et al., 2007), transgenic expression of GFP:DAT-1 rescued the Swip in *vt21* and *vt22* (Figure 10A), suggesting that these mutants reduce DAT activity. Whereas sequencing of the genomic DAT-1 locus

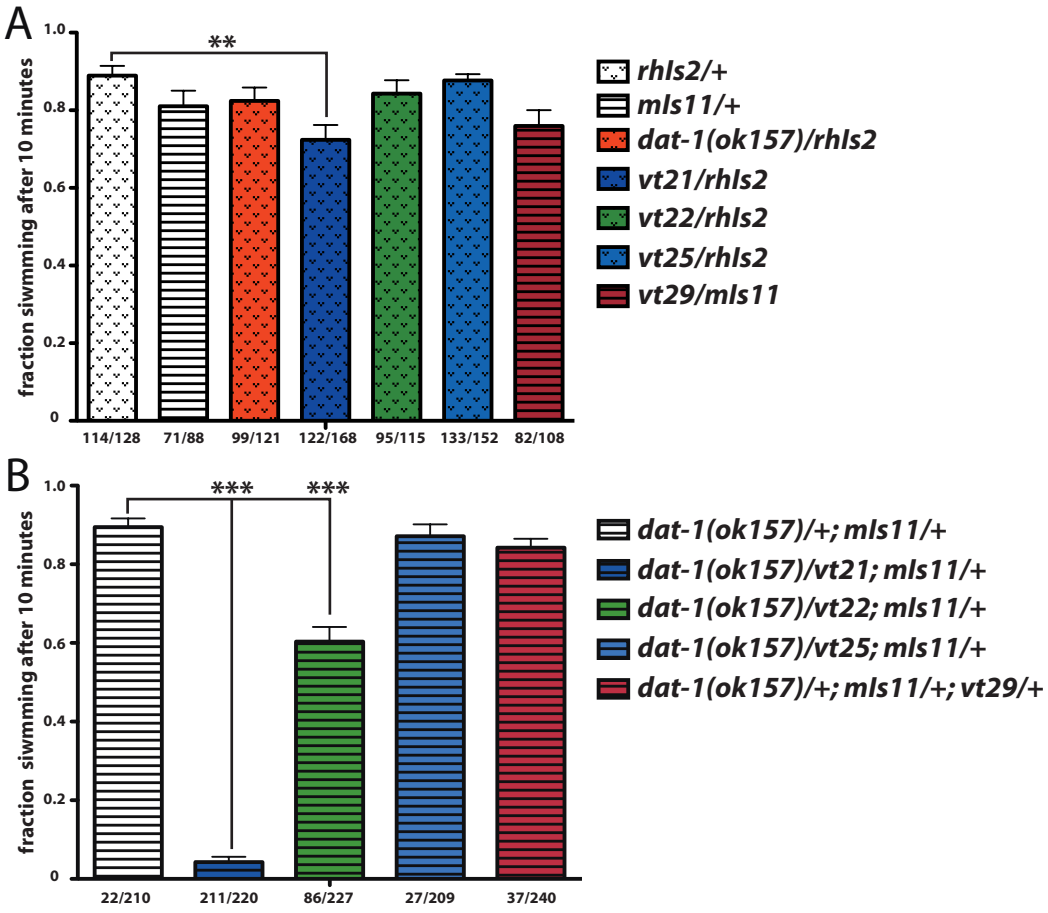

Figure 9 – Complementation assays of *swip* strains to N2 and *dat-1.* A, *swip* mutant heterozygotes are fully rescued in their Swip behavior. *vt21/rhls2* does show a significant reduction from control levels, but Swip is greatly suppressed from that seen in homozygotes (see Fig. 2). Lines containing integrated fluorescent transgenes were crossed to fully outcrossed *swip* hermaphrodites and fluorescent cross progeny were tested for Swip. These balancer lines display normal swimming behavior on their own. Data were analyzed using one-way ANOVA with selected Bonferroni post-tests comparing to controls bearing a single copy fluorescent transgene. Fractions below the bars represent # paralyzed/# assayed. B, *vt21* and *vt22* fail to complement *dat-1*, whereas *vt25* and *vt29* suppress Swip to control levels. *Dat-1(ok157)* males bearing a fluorescent transgene *in trans* were crossed to fully outcrossed *swip* mutants and fluorescent cross progeny were tested for Swip. Data were analyzed as in A.

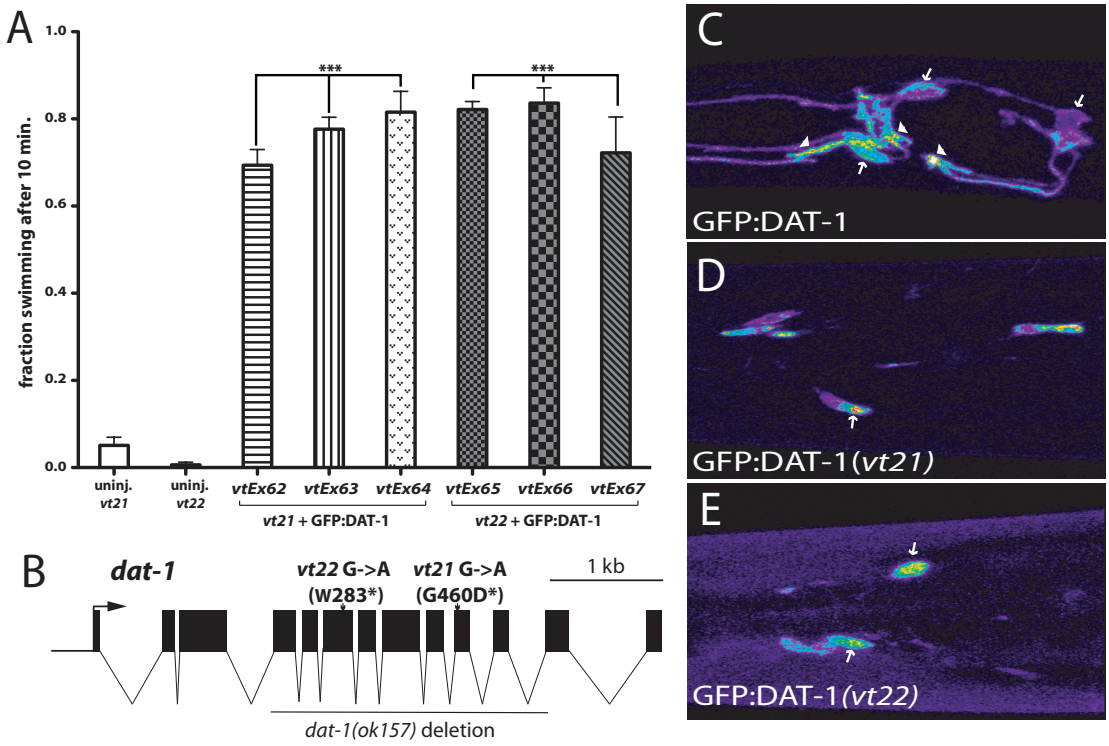

Figure 10 – Isolation of novel *dat-1* mutants. A. GFP:DAT-1 rescues swimming behavior of *vt21* and *vt22* animals. *vt21;lin-15(n765ts)* and *vt22;lin-15(n765ts)* were coinjected with GFP:DAT-1(pRB491) and lin-15(pJM23) and separate transgenic lines were manually scored for paralysis in water. Data are derived from $\geq$10 trials for each line. Data were analyzed using one-way ANOVA with selected Bonferroni post tests - *** = P<0.001. B. Gene structure of *dat-1* and position of mutant nucleotides in *vt21* and *vt22* as verified by DNA sequencing. Also illustrated is the *dat-1(ok157)* allele that derives from a 1.8 kb deletion encompassing exons 4-11 of *dat-1*. In *vt22,* a G->A transition at nucleotide 1687(from ATG start) results in the conversion of tryptophan (T) to a premature stop codon (*). In *vt21*, a G->A transition at nucleotide 2395 results in the conversion of a highly conserved glycine (G) to aspartic acid (D). C-E, Expression and trafficking deficits of *vt21* and *vt22* alleles of *dat-1*. Animals injected with $p_{dat\text{-}1}$*::*GFP:DAT-1 I display readily detectible expression and localization to CEP and ADE soma (white arrows) and terminals (white triangles) whereas mutant transporters (D and E) are much more weakly expressed and restricted in localization to DA neuron cell bodies. L4 animals were anesthetized and Z-stacks of CEP/ADE neurons were acquired and flattened to generate images of GFP:DAT-1 expression *in vivo*. Each image is representative of three separate transgenic lines that produced equivalent results.

in *vt25* and *vt29* yielded sequence identical to that found in N2 animals, *vt21* and *vt22* were found to bear single base-pair substitutions predicted to impact the DAT-1 coding sequence (Figure 10B). The DAT-1 gene contains thirteen exons that encode a 615 amino-acid protein with twelve transmembrane I domains and intracellular N and C-termini (Jayanthi, et al., 1998). *vt21* bears a G->A substitution at the beginning of exon 10 that results in the conversion of a highly conserved glycine residue to aspartic acid (G460D). G460 (conserved in hDAT) is predicted to lie in the small extracellular hairpin turn between TMs 9 and 10 (Figure 11A). *Vt22* possesses a G->A substitution in the middle of exon 6 that results in a stop codon at amino acid 283, as opposed to a tryptophan (W283*).

To examine the deleterious impact of the DAT-1 mutations identified in *vt21* and *vt22* lines, we implemented a previously described heterologous expression protocol (Richard Nass, et al., 2005). Our assay of [^{3}H]DA transport activity in COS-7 cells revealed that both *dat-1(vt21)* and *dat-1(vt22)* display significantly reduced DA uptake relative to that displayed by WT HA:DAT-1 (Figure 11C). Whereas *dat-1(vt22)* produced no significant [^{3}H]DA uptake above nontransfected cells, *dat-1(vt21)* exhibited low, but detectible, transport activity (Figure 11C). Analysis of total and cell-surface protein extracts demonstrated that *dat-1(vt21)* and *dat-1(vt22)* exhibit reduced cell surface expression levels and a premature truncation product respectively relative to WT DAT-1(Figure 11D). Furthermore, whereas GFP:DAT-1 expression rescued the Swip of *dat-1(*ok157)(Figure 11E), neither GFP:DAT-1(G460D) nor GFP:DAT-1(W283stop) rescued Swip. Confocal analysis of wildtype GFP:DAT-1 expression in CEP

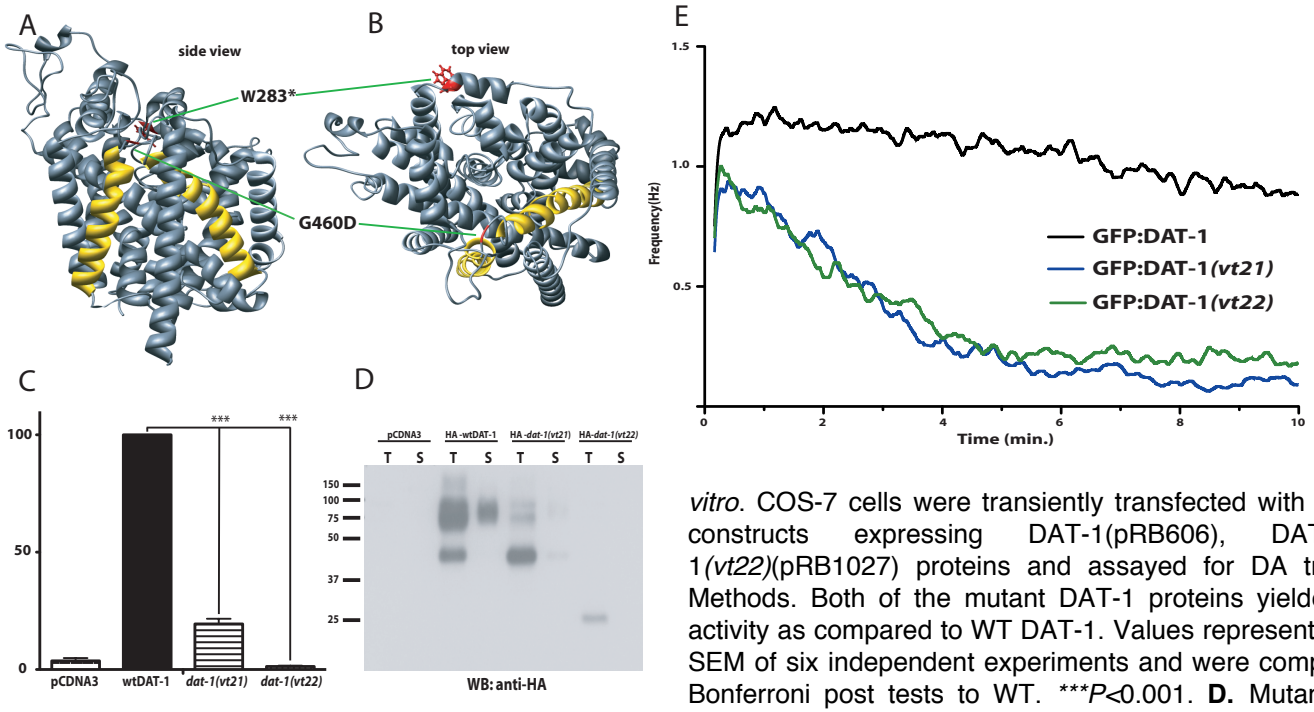

Figure 11 – Modeling and functional analyses of *dat-1* mutations. A and **B.** Positions of *vt21* and *vt22* mutations on DAT-1 protein, as predicted from the solved crystal structure of the bacterial leucine transporter ($LeuT_{Aa}$). Mutant residues are shown in red and TMs 9 and 10 adjoining the *vt22* mutation are colored in yellow. **A** – side view, **B** – extracellular view. **C**. *Vt21* and *vt22* (*dat-1(vt21)* and *dat-1(vt22*), respectively) exhibit reduced DA transport activity *in vitro*. COS-7 cells were transiently transfected with either empty vector (pcDNA3), or constructs expressing DAT-1(pRB606), DAT-1*(vt21)*(pRB1026) or DAT-1*(vt22)*(pRB1027) proteins and assayed for DA transport activity as described in Methods. Both of the mutant DAT-1 proteins yielded significantly reduced transport activity as compared to WT DAT-1. Values represent the mean % DA uptake of WT +/- SEM of six independent experiments and were compared using one-way ANOVA with Bonferroni post tests to WT. ****P*<0.001. **D.** Mutant DAT-1 proteins display altered levels and trafficking of transporter protein. Total and surface protein expression of HA-tagged DAT-1(pRB491), DAT-1*(vt21)*(pRB1028) and DAT-1*(vt22)*(pRB1029) were determined by western blot analysis, as described in Methods. Wildtype DAT-1 expression is evident as an immature species of ~45 kDa and a mature, glycosylated band at ~ 80 kDa, with the 80 kDa species detected in surface fractions. DAT-1*(vt21)* expression is detected as both an immature and a full length species, with a higher relative abundance of the immature species. Little to no expression of these species is detected in surface fractions. No full length product is evident in the total or surface lysates from DAT-1*(vt22)* transfected cells with only a short ~25 kDa fragment evident, consistent with the site of the nonsense mutation. Image presented is representative of 4 independent experiments with equivalent results. **E.** *vt21* and *vt22* mutations, engineered into GFP:DAT-1 expression constructs, fail to rescue Swip behavior of *dat-1(ok157);lin-15(n765ts)* animals. In contrast, expression of GFP:DAT-1 fully rescues Swip. Behavior plotted of animals expressing GFP:DAT-1(wt) is the average of four independent transgenic lines. Data from *vt21* and *vt22* mutant GFP:DAT-1 lines derives from at least 20 animals, with three lines scored for each test. Traces were compared using two-way ANOVA and multiple Bonferroni posttests where swimming behavior of GFP:DAT-1 fusions bearing *vt21* and *vt22* mutations was significantly reduced from WT ($p<0.001$ for all values along the running average after the first minute of swimming). The behavior of the two mutants was not significantly different from each other.

neurons revealed moderate levels of transporter expression in DA cell bodies (Figure 10C, white arrows), low levels in dendrites and axons and high expression in presynaptic terminals (white arrowheads). In contrast, GFP:DAT-1(G460D) demonstrated robust CEP cell body expression but failed to label CEP processes and terminals (Figure 10D). Animals expressing GFP:DAT-1(W283stop) demonstrated lower levels of GFP signal than was observed in GFP:DAT-1 or GFP:DAT-1(G460D), with all labeling confined to CEP cell bodies (Figure 10E).Together, these findings provide *in vitro* and *in vivo* support for the determinants of Swip in the *vt21* and *vt22* lines as derived from *dat-1* alleles. Since we did not observe mutations in DAT-1 in *vt25* and *vt29,* we further mapped the sites of these mutations as described in Methods. We found that *vt25* maps to LGIII whereas *vt29* maps to LGX (Figure 12). Likewise, we did not observe mutations in *dat*-1 for *vt31, vt32, vt33, vt34, vt39,* vt42 and *vt44.* These mutations were mapped to other positions in regions not containing known Daergic regions, and will require further study to identify the molecular lesion that is required for Swip. In the process of mapping, we made an important observation that the left arm of LGI is prone to non-specific N2 Bristol linkage. This non-specific linkage point increased the difficulty of fine mapping the interval for Swip mutants that mapped to LGI such as *vt31*, *vt34,* and *vt39*. No genes known to impact DA signaling lie in the region mapped in *vt25*. The *vt29* region harbors the *dop-4* gene. Sequencing of this gene in *vt29* animals revealed no mutations, indicating that the altered DA signaling of *vt29* is produced through a

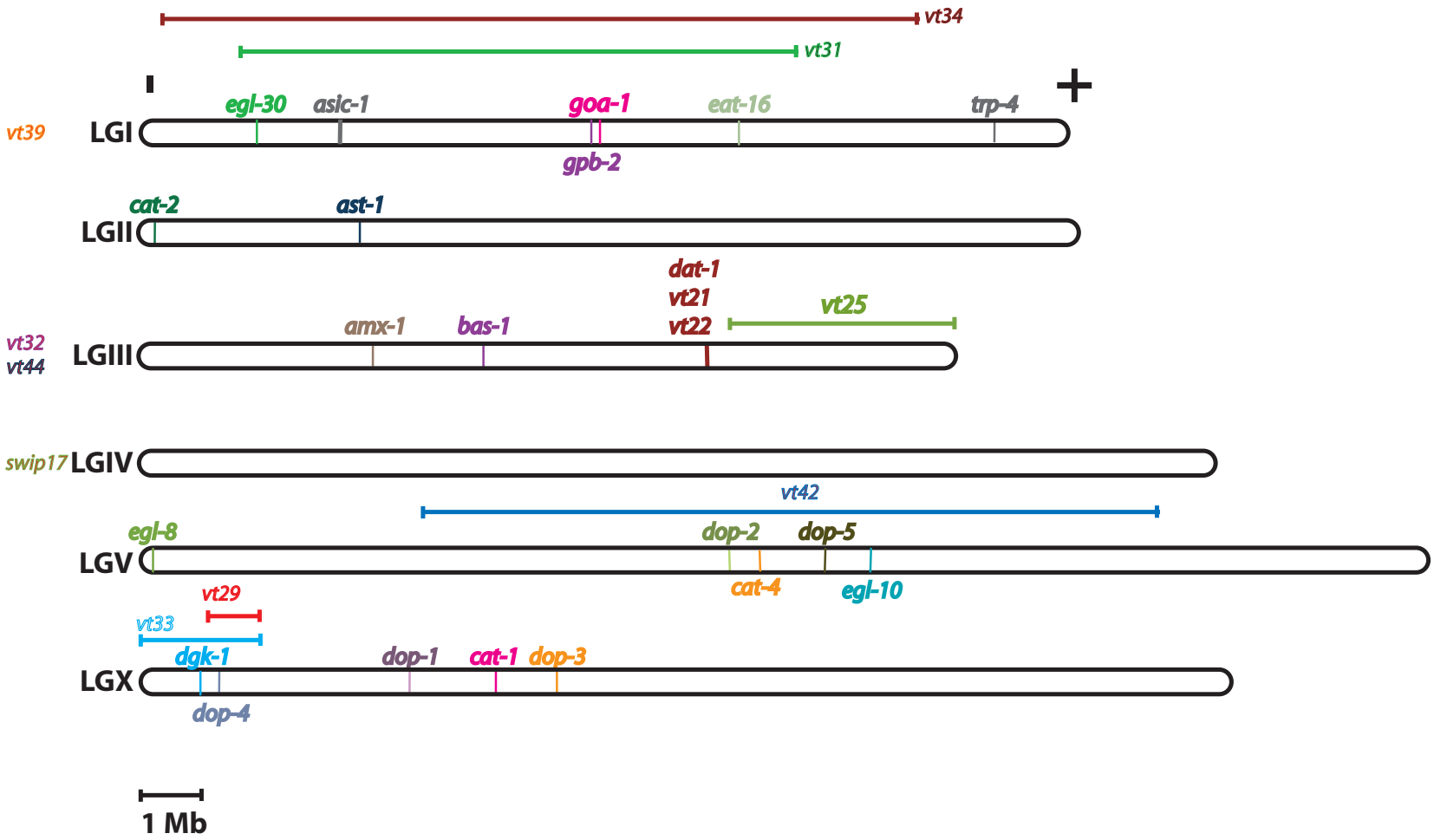

Figure 12 – Genomic Positions of all stable mutants that exhibit reserpine-sensitive Swip. *vt21, vt22, vt25, vt29, vt31, vt32, vt33, vt34, vt39, vt42,* and *vt44* were mapped by cross to the CB4856 strain and areas of N2 Bristol enrichment were determined in bulk and clonally by PCR of SNP-containing regions across all six chromosomes and restriction digest with DraI.

novel mechanism. These findings confirm that *vt25* and *vt29* do not harbor Swip-causing *dat-1* alleles, nor do they involve mutations in the same gene.

vt25 and *vt29* exhibit *dat-1*-like locomotive behaviors but distinct sensitivities to exogenous DA

To determine the similarity of *vt25* and *vt29* behavior to that of *dat-1*, we conducted a series of DA signaling dependent locomotor tests. We also assayed *dat-1(vt21)* and *dat-1(vt22)* in parallel to explore whether this test might reveal *dat-1* allele-specific effects. Using an automated assay of swimming behavior (Matthies, et al., 2006; P. W McDonald, et al., 2007), we found that *vt25* lacked a fully penetrant Swip phenotype, as evident by its ~50% paralysis in manual scoring (Figure 7A) and an average ~0.5 Hz thrashing frequency by our final assay time point (10 min) under automated recording (Figure 7C). In contrast, *vt29* displayed fully penetrant Swip, yielding ~100% paralysis in manual scoring assays (Figure 7A), and an even more rapid rate of paralysis than *dat-1* (Figure 7C and Table 1). In these and further assays, we determined that *dat-1(vt21)* and *dat-1(vt22)* behave similar to the *dat-1(ok157)* strain (Figure 13 and Table 1).

The Swip of *dat-1* animals requires the function of the $G\alpha_o$-coupled DA receptor DOP-3 (Allen, et al., 2011; Chase, et al., 2004; P. W McDonald, et al., 2007) that is expressed by body wall muscle and ventral cord motor neurons. As with *dat-1(ok157)* animals, *dat-1(vt21)* and *dat-1(vt22)* paralysis was completely suppressed in a cross to *dop-3* (Figure 13). *Vt25* paralysis was modestly, but significantly rescued by *dop-3* (Figure 7D). We could not examine rescue of *vt29*

with *dop-3* as they both map to the same chromosome. Therefore we crossed this line to a line deficient in the rate-limiting enzyme in DA biosynthesis, tyrosine hydroxylase *(cat-2*), as *cat-2* suppresses the Swip of *dat-1(ok157)* (MCDONALD et al. 2007). As with *dat-1* alleles, we found that *cat-2* completely suppressed the paralysis behavior of *vt29* (Figure 7D).

The application of exogenous DA to worms on solid substrate induces motor slowing and paralysis (Schafer & Kenyon, 1995). We found that *dat-1* animals transferred to plates containing increasing amounts of DA displayed a two-fold increase in DA sensitivity when compared to N2 animals (Figure 7B and Figure 13D), possibly reflecting a lack of DAT-1 dependent clearance of exogenous DA once the catecholamine permeates the cuticle. *Vt29* displayed sensitivity to exogenous DA like that of *dat-1* (Figure 7B). In contrast, *vt25* exhibited a DA dose-response more similar to N2 (Figure 7B). We also tested the response to exogenous DA for *vt31, vt32, vt33,* and *vt34*. Like *vt29*, *vt33* shows displays an enhanced sensitivity to intermediate doses of exogenous DA (Figure 14). More experiments will be necessary to make definitive conclusions about *vt31, vt32*, and *vt34*. Preliminarily, we observed that *vt31* and *vt34* display paralytic responses to exogenous DA that resemble N2 (Figure 14), while *vt32* displayed a reduced sensitivity to exogenous DA.

Automated analysis of Swip behavior reveals a differential impact on thrashing behavior for *vt25* and *vt29*. In order to probe more precisely quantify the thrashing behavior of our swip mutants, we developed software tools (SwimR, see Appendix A, Hardaway and Wang *et al*) that can provide

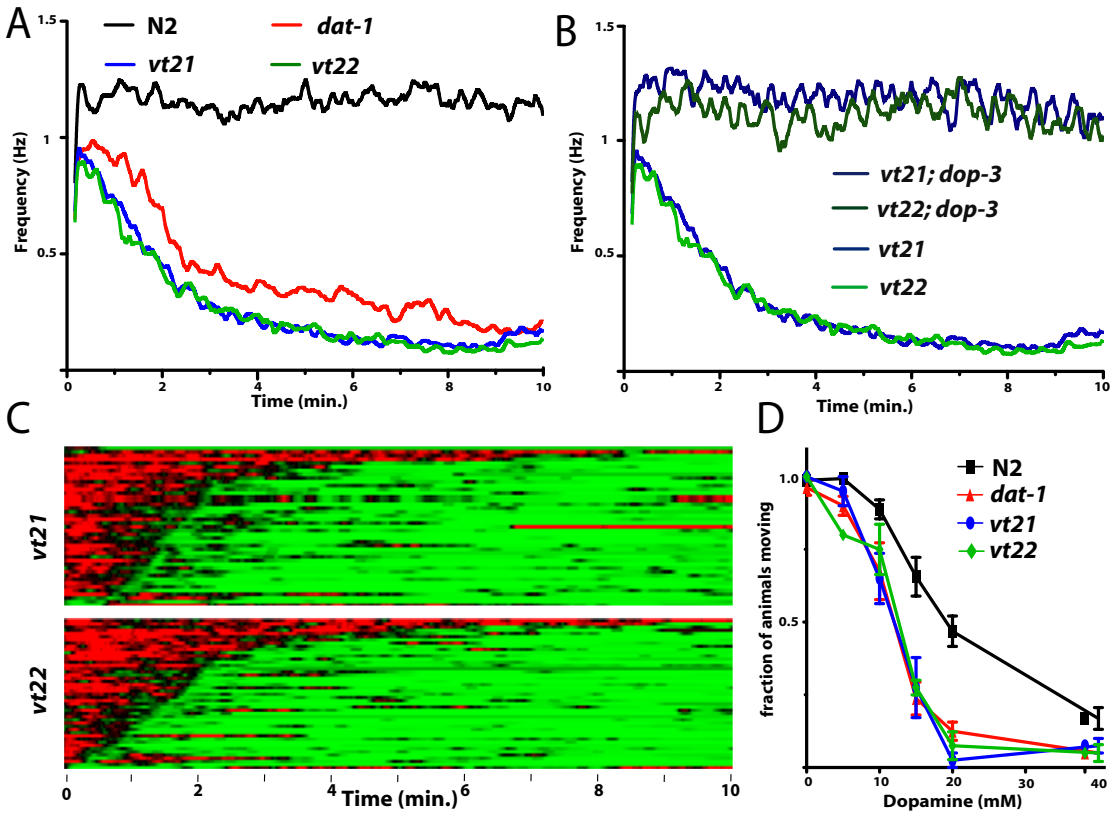

Figure 13 – Behavioral Analyses of the *dat-1(vt21)* and *dat-1(vt22)* strains. A. *Vt21* and *vt22* mimic the *dat-1* Swip phenotype as measured by automated thrashing analysis. Individual animals were recorded using a video capture system and then analyzed with customed-designed Thrasher software that assigns multiple linear elements projecting from the worm centroid. The position of these linear elements are tracked and converted off-line to movement frequency as a function of time. Batch conversions are generated, providing mean values and SEM along moving averages. Error bars are not shown in these plots for simplicity. *Dat-1(ok157)*, *vt21* and *vt22* were found to be significantly different from N2 using two-way ANOVA with Bonferroni posttests of mutants to N2, with each mutant possessing a $P<0.001$ after the one minute mark. B. Mutation of the postsynaptic receptor DOP-3 fully rescues the paralysis phenotype of *vt21* and *vt22*. Analyses were performed as described in B, where *vt21* and *vt22* were both found to be significantly different from the double mutants *vt21;dop-3(vs106)* and *vt22;dop-3(vs106)* with $P< 0.001$ after 1 minute. C. Heat map representations of *dat-1(vt21)* and *dat-1(vt22)* swimming traces. Analyses were performed as described in Figure 4. D. *vt21* and *vt22* display enhanced sensitivity to exogenous DA when tested on solid medium, as compared to N2, but are indistinguishable from *dat-1*. For these assays, 10 L4 stage worms were placed on plates containing increasing concentrations of exogenous DA, incubated for 20 min and then scored for 10 sec as paralyzed or moving. Dose-response curves were compared using two-way ANOVA with Bonferroni posttests comparing mutants to N2, in which *dat-1*, *vt21* + *vt22* were all found to be significantly different from N2, with a $P<0.001$ at 15 and 20 mM DA. Data derive from at least 4 tests per strain per DA concentration. Error bars represent SEM. Exogenous DA dose response profiles and data analysis were performed as described in the Methods and in Figure 3..

for a more detailed kinetic analysis of individual animals that may reveal patterns of behavior not readily detected in population averages (Table 1). For visualization, our software plots each animal's swimming behavior horizontally (Figure 15A), assigning a color code that ranges from red (high frequency) to green (low frequency) for each time block, and that orders the animals within each genotype so that more rapid paralyzers are displayed at the bottom and slower paralyzers (or relatively constant swimmers) are displayed at the top. These analyses revealed several significant differences between the mutants. All mutants recovered in the screen demonstrated significantly reduced maximal thrashing frequencies in water, with *vt29* being the most impacted, and accompanied by a greater percentage of animals displaying lower thrashing frequency values (Figure 17). With respect to paralysis, *vt25* animals again resembled *dat-1*, whereas *vt29* differed from these lines with a significantly reduced latency to paralyze. Although by definition, all lines paralyze in water, our single worm analyses revealed that *dat-1* and *vt25* lines feature a significant number of animals that revert back to relatively normal swimming behavior that we tabulated as reversion incidence (# revertants/# paralyzers)) and reversion probability (time in reversion/time after paralysis). *Vt29* demonstrated a significantly reduced reversion incidence from other lines (and *dat-1*), which can be readily detected in both the heat map plots and in selected individual thrashing traces (Figure 15B). When animals that did revert were analyzed separately, we found that the reversion frequency (# of events/animal), time to first reversion, and the average reversion event length did not differ among all

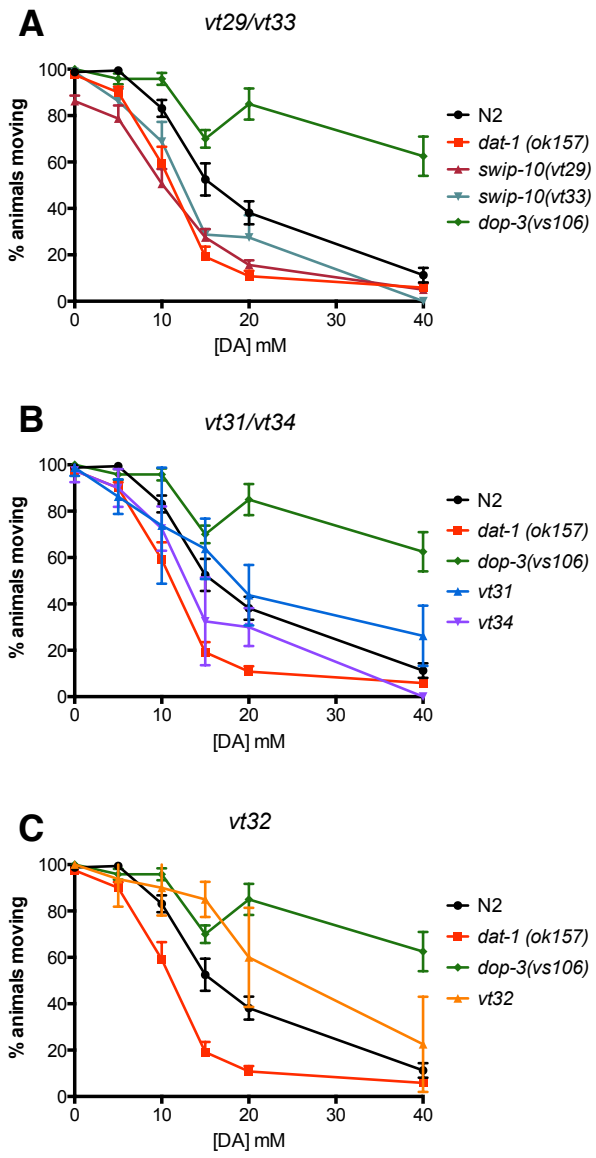

Figure 14 – Exogenous DA responses of *vt29, vt31, vt32, vt33,* and *vt34*. Experiments were performed as previously described**.** For all experiments, dose-response curves were compared using two-way ANOVA with Bonferroni posttests comparing all strains. Data derive from at least 4 tests per strain per DA concentration. Error bars represent SEM. **A.** *dat-1* was significantly different from N2 with a $P<0.001$ at 10, 15 and 20 mM DA. *vt29* was significantly different from N2 with a $P<0.05$ at 5, 10, 15, and 20 mM DA. **B.** *vt31* and *vt34* are not significantly different from N2 at any dose. **C.** *vt32* displays a reduced sensitivity to exogenous DA with significant reductions at 15 and 20 mM DA.

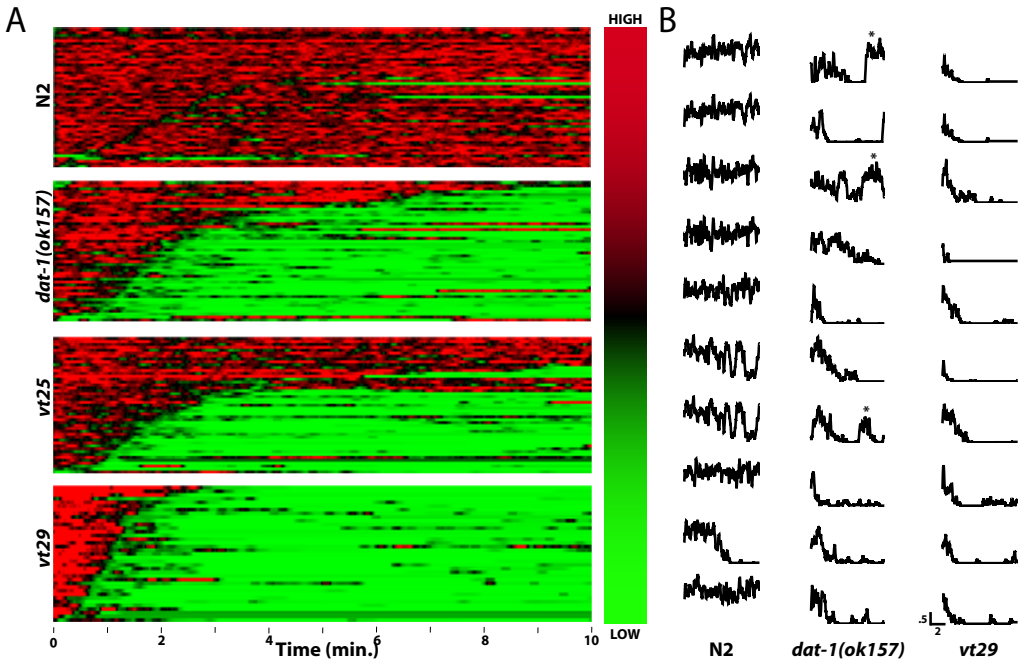

Figure 15 - *vt25* and *vt29* display distinct paralytic attributes. A. Heat map analysis for N2, *dat-1(ok157)*, *vt25* and *vt29* animals, generated using SwimR software as described in Methods. Individual swimming frequencies as a function of time, color coded as shown by the vertical bar on the right, are stacked with the fastest animals to initiate paralysis for each genotype placed on the bottom. B. Individual traces of N2, *dat-1* and *vt29* behavior illustrate that a proportion of *dat-1* animals demonstrate spontaneous reversal of paralysis (reversals marked with *), behavior that is rarely seen with *vt29* animals. Traces shown reflect individual traces from the full data set used for heat map generation, selected using a random number generator. Full quantitative analysis of reversal behavior elements is provided in Table 1. Scale bar for fraction swimming and time in sec is shown below *vt29* plots.

mutant strains (Table 1). These analyses suggest that differences exist in the functional impact of *dat-1*, *vt25* and *vt29* mutations prompting a further investigation of the differential behavior of these lines.

Evaluation of *vt25* and *vt29* sensitivity to osmolarity

Previously, we demonstrated that the *dat-1* Swip phenotype is highly dependent on the osmolarity of the swimming medium (Hardaway *et al.*, personal communication to WBG), with a near complete loss of Swip when these animals are subjected to aqueous solutions buffered to 300 mOsm with sucrose, or in M9 We used manual scoring of the fraction of animals paralyzed at 10 min to assay swimming behavior of N2, *dat-1, vt25,* and *vt29* as a function of medium osmolarity. N2 animals, as expected, maintained a relatively constant swimming rate regardless of osmolarity (Figure 16A), whereas *dat-1* animals displayed the expected loss of paralysis with increasing osmolarity. *Vt29* animals exhibited a virtually identical sensitivity to osmolarity as *dat-1*, except a slight, yet significantly increased paralysis at higher osmolarities. Remarkably, *vt25* animals displayed a lack of sensitivity to the osmolarity of solutions used in swimming assays. Although only minimal paralysis of *dat-1* and *vt29* animals was detected in M9 medium using hand scoring, automated analyses revealed that both *dat-1* and *vt29* exhibited reduced average rates of movement (Figure 16B). At a single-worm level, several parameters distinguished *dat-1* and *vt29* in M9 medium (Figure 16C-F, Table 1). V*t29* animals did not reach the same maximal swimming frequency as *dat-1* animals in M9, and unlike water, *dat-1* maximal rates were

	Maximal Frequency (Hz)	**Latency to Paralyze (sec)**	**Reversion Incidence¶**	**Reversion Frequency (events/ animal)**	**Reversion Probability‡**	**Time to 1st Reversion (sec)**	**Average Reversion Event Length (sec)**
***N2* (n = 52)**	1.76 +/- 0.01	N/A	N/A	N/A	N/A	N/A	N/A
***dat-1(ok157)* (48)**	1.45 +/- 0.04†*	174 +/- 17.5	0.25	3.22 +/- 0.571	0.031+/- 0.006	145 +/- 35.8	5.77 +/- 1.4
***dat-1(vt21)* (43)**	1.28 +/- 0.04*	130 +/- 14.4	0.365	1.76 +/- 0.302	0.015 +/-0.003	185 +/- 32.3	4.02 +/- 0.93
***dat-1(vt22) (*47)**	1.24 +/- 0.04***	131 +/- 14.5	0.391	2.00 +/- 0.271	0.020 +/- 0.004	112 +/- 17.7	4.54 +/- 0.93
***vt25* (47)**	1.28 +/- 0.04*	178 +/- 21.8	0.267	3.50 +/- 0.620	0.032 +/- 0.01	183 +/- 67.1	4.22 +/- 0.88
***vt29* (37)**	1.13 +/- 0.04***	81.2 +/- 6.05***	0.0540§*	2.50 +/- 0.500	0.018 +/- 0.007	146 +/- 108	3.59 +/- 0.69
***vtIs18* (42)**	1.64 +/- 0.02†^{ns}	N/A	N/A	N/A	N/A	N/A	N/A
***vt25; vtIs18* (38)**	1.45 +/- 0.03	337 +/- 61.9*	0.333	N/A	N/A	N/A	N/A
***vt29; vtIs18* (44)**	1.45 +/- 0.02	165 +/- 22.4	0.294	3.90 +/- 0.706	0.051 +/- 0.019	107 +/- 30.7	4.43 +/- 1.14
M9							
N2 (53)	1.76 +/- 0.01	N/A	N/A	N/A	N/A	N/A	N/A
***dat-1(ok157)* (56)**	1.66 +/- 0.02	166. +/- 34.1	0.810§$^{\#\#\#}$	5.06 +/- 0.774	0.052 +/- 0.014	110 +/- 11.7	4.18 +/- 1.10
***vt29* (53)**	1.29 +/- 0.03****	298 +/- 24.5	0.640§$^{\#\#}$	4.19 +/- 0.647	0.040 +/- 0.008	171 +/- 25.7	4.20 +/- 0.76

Table 1 – Kinetic Attributes of Swip-harboring strains in water and M9.

‡ Reversion Probability = total time spent in reversion/ total time after paralysis onset

¶ Reversion Incidence = fraction of animals that reverse from paralysis

Asterisks(*) indicate a significant difference to *dat-1(ok157)* as determined by one-way ANOVA with Bonferroni's multiple comparision test where * = $p < 0.05$, ** = $p < 0.01$, and *** = $p < 0.001$. Numeral signs(#) indicate a comparison within the same genotype between water and M9.

† comparison to N2(ns = not significant)

§ Chi-square test

N/A = not applicable(no comparisons were made to N2 for paralytic features as the N2 strain does not paralyze significantly)

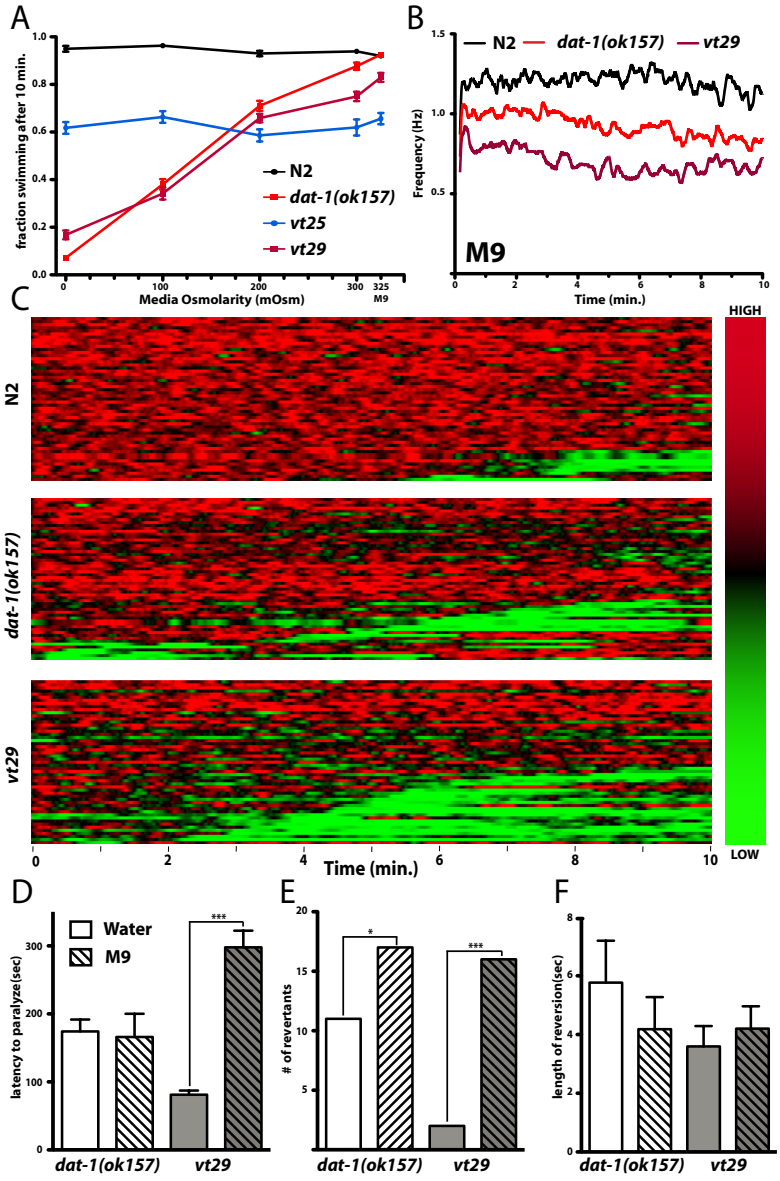

Figure 16 - Swip in *dat-1, vt25* and *vt29* are variably suppressed at high buffer osmolarities. A. The Swip penetrance of *dat-1* and *vt29* is reduced by increasing the osmolarity of the swimming medium, whereas *vt25* displays no sensitivity to changes in osmolarity. Manual Swip assays were performed as described previously with water supplemented with sucrose to produce 100, 200 + 300 mOsm. M9 was used as a high osmolarity control and was experimentally determined to be ~325 mOsm. Data were analyzed using two-way ANOVA, with the goal of evaluating a genotype X molarity interaction. Significant interactions were found for *dat-1* ($P<0.0001$) and *vt29* ($P<0.0001$)), whereas *vt25* displayed a non-significant interaction ($P=0.2385$). Bonferroni post hoc comparisons of each genotype at each osmolarity were performed to assess the ability of each buffer to suppress Swip. B. *vt29* bears an enhanced Swip penetrance in M9 as measured via automated thrashing analysis. Individual traces of N2, *dat-1* and *vt29* were acquired as described previously except M9 was used in lieu of water. Data were analyzed using two-way ANOVA with Bonferroni posttests along the running averages. The thrashing frequency of *vt29* was significantly reduced from *dat-1* from 3 min 14 sec – 3 min 17 sec and 4 min 37 sec to 4 min 39 sec and *dat-1* significantly reduced from N2 from 5 min 42 sec to 5 min 45 sec and 8 min 50 sec to 8 min 52 sec. C. Heat map analysis using SwimR software for N2, *dat-1(ok157)* and *vt29* animals in

Figure 16(cont'd) – (325 mOsm).

not significantly different from N2 (Table 1). In M9, *vt29* animals exhibited a significantly greater latency to paralyze than *dat-1* animals (Table 1 and Figure 16D), opposite to their relative sensitivities in water. Both *dat-1* and *vt29* lines demonstrated an increase in the number of revertants in M9 as compared to water (Figure 16E) without changing the length of reversion events (Figure 16F), though this effect was greatest in *vt29* animals. Therefore, *vt29* are more likely to paralyze in M9 than *dat-1*, but as a population reach paralysis more slowly and are more likely to reverse from paralysis than when assayed in water.

Suppression of Swip in *vt25* and *vt29* with DAT overexpression

Although we did not detect mutations at the DAT-1 locus in *vt25* and *vt29*, these mutations may still impact DA clearance, either through a functional impact on DAT-1 at DA terminals, or through changes in the somatic export of DAT-1 protein. To assess this issue, we crossed *vt25* and *vt29* onto a line containing an integrated $p_{dat\text{-}1}$::GFP:DAT-1 transgene and monitored swimming behavior. Overexpression of GFP:DAT-1 restored swimming behavior of *vt25* (Figure 19A) to near wildtype levels. Single worm analyses (Figure 19B + C) demonstrated that, although Swip is largely rescued when overexpressing DAT on the *vt25* background, short paralytic bouts are still evident. GFP:DAT-1 overexpression only modestly suppressed *vt29*. Automated analyses revealed that the partial suppression of *vt29* by overexpression of GFP:DAT-1 does not derive from an increased reversion probability or latency to paralyze (Table 1), but rather

appears to result from a reduction in Swip penetrance, with a reduced fraction of animals swimming at or near the rates observed with *vt29* alone (Figure 19A compared to Figure 15C). To examine whether the findings from the rescue experiments with p_{dat-1}::GFP:DAT-1 reflect a failure to synthesize or traffic the transporter, we examined the impact of *vt25* and *vt29* backgrounds on the localization of GFP:DAT-1 to the soma, dendrites, axons and presynaptic terminals of CEP, ADE and PDE neurons. We could detect no changes in the pattern of GFP:DAT-1 localization with the *vt25* and *vt29* strains, comparing animals with GFP:DAT-1 expressed on an otherwise wildtype background to (Figure 18).

vt25, vt29 and *dat-1* have reduced tissue DA content

One reason for *vt29* to possess a stronger, DA-dependent Swip phenotype than *dat-1(ok157)* would be for *vt29* to store excess DA in synaptic vesicles that, upon release, could produce higher levels of extrasynaptic DA than seen with wildtype DA levels and a loss of DAT-1 mediated DA clearance. To investigate this issue, we measured DA levels in *vt25* and *vt29* animals in parallel with assays of N2, *dat-1(ok157)* and *cat-2(tm2261)* lines. As expected, *cat-2(tm2261)* displayed a highly significant reduction in DA levels compared to N2 (Figure 19D). *Dat-1* DA levels were also reduced, in keeping with findings of reduced tissue DA content in DAT knockout mice believed to derive from a need to recycle extracellular DA to maintain vesicular stores (Giros, et al., 1996). Interestingly, both *vt25* and *vt29* also displayed reduced DA levels, suggesting that, analogous to *dat-1*, *vt25* and

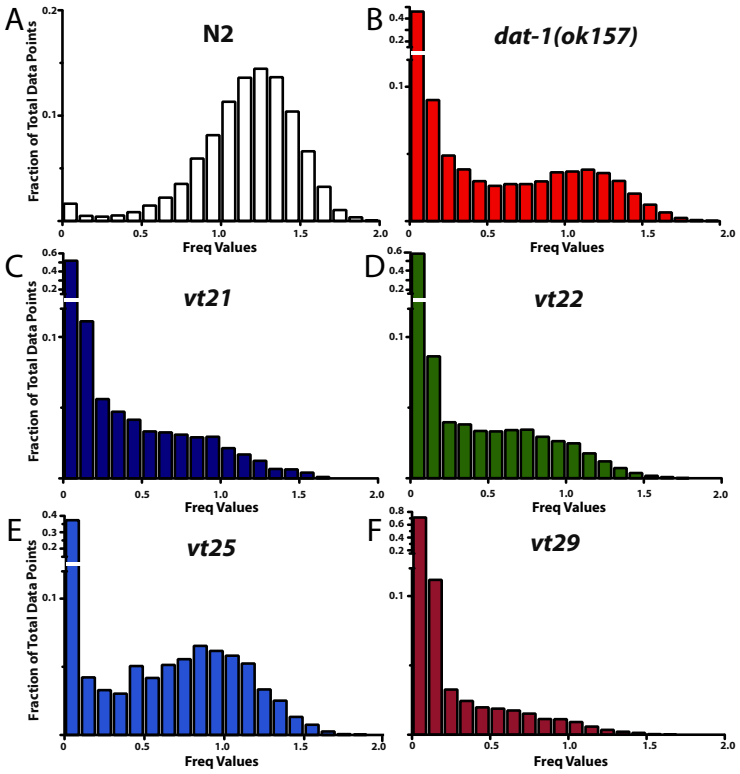

Figure 17 - Histogram of automated thrashing behavior in N2, *dat-1(ok157)* and *swip* lines generated by SwimR software. For all plots (A-F), the total # of data points for all animals within a genotype were grouped into successive 0.1 Hz bins and plotted as the fraction of the total # of data points. In the *swip* mutants (C-F), the y-axis and first column are broken in order to visualize the patterns of lower frequency bins.

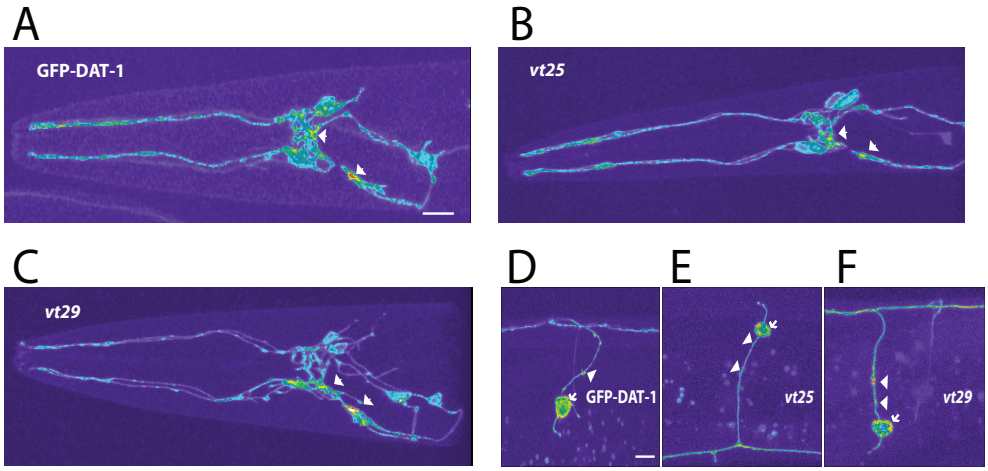

Figure 18 - *vt25* and *vt29* do not alter GFP-DAT somatic export: Expression pattern of p_{dat-1}::GFP:DAT-1(*vtIs18)* in the head(CEP and ADE neurons, A,B + C) and posterior(PDE, D,E + F) in WT, *vt25* and *vt29* were analyzed by confocal microscopy. The expression pattern of GFP:DAT-1 is not altered on the *vt25* or *vt29* backgrounds, with diffuse expression in DA neuron cell bodies(arrows) and punctate expression visible at terminal regions (arrowheads). Scale bar equal 10 uM.

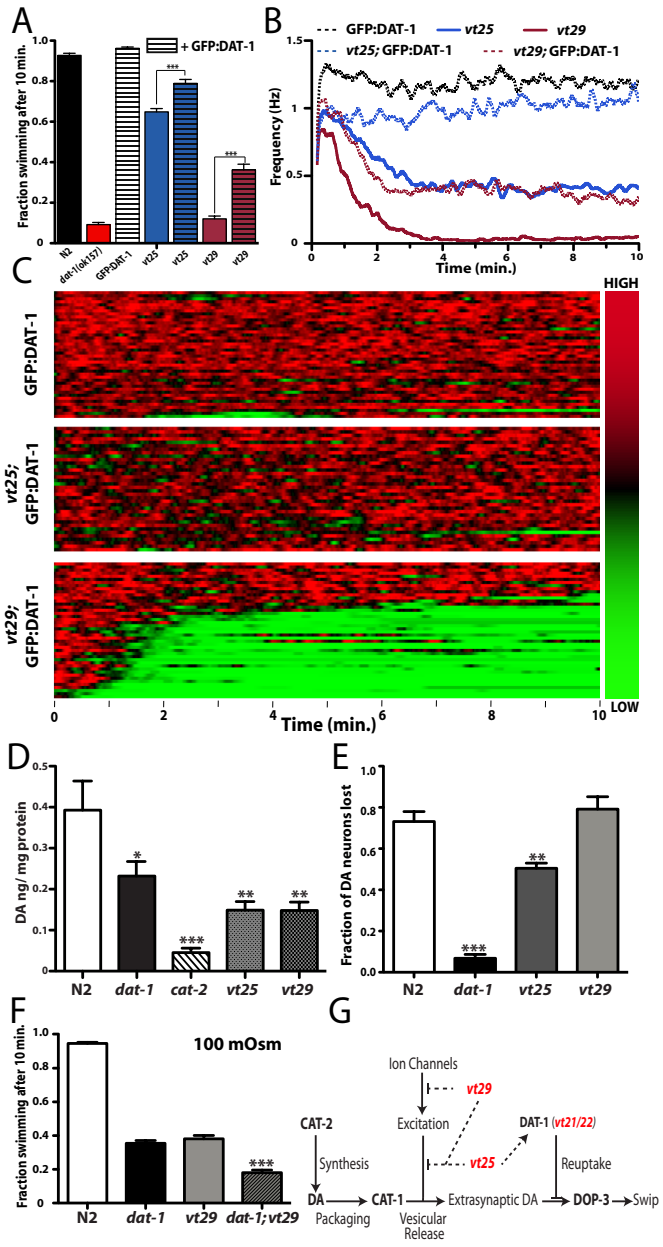

Figure 19 - Behavioral analysis of GFP-DAT overexpression, biochemical analysis and neurotoxic profiles of *vt25* and *vt29*. **A**, p_{dat-1}::GFP:DAT-1 transgene suppresses Swip behavior of *vt25* and *vt29* lines. A line containing an integrated functional p_{dat-1}:: GFP-DAT-1 (*vtIs18*) transgene was crossed onto *vt25* or *vt29*. Lines were tested manually over at least three experimental days with > 72 trials tested for each strain. Data were analyzed using a one-way ANOVA with multiple Bonferroni posttests. *** = $P< 0.001$ **B**, Automated thrashing analysis of *vt25* and *vt29*, generated as previously described, demonstrate rescue of Swip in cross to p_{dat-1}: GFP-DAT-1 (*vtIs18*). **C**, Heat map representations of *vt25; vtIs18* demonstrate that whereas the overexpression of GFP:DAT-1 fully rescues the paralysis of *vt25* (compare Fig XA), with transient bouts of paralysis evident, while *vt29; vtIs18* animals demonstrate a reduction in Swip penetrance relative to *vt29* (compare Fig 4A) and are not fully rescued. **D.** Analysis of DA levels in *vt25* and *vt29*. *dat-1(ok157), cat-2(tm2261), vt25* and *vt29* lines all contain significantly reduced DA levels as compared to N2. For each strain, DA was extracted from synchronized L4 populations and measured using high performance liquid chromatography as described in Methods. Data were analyzed using a one-way ANOVA with Dunnett's multiple comparison. *, **, *** indicate a significant reduction from N2 where $P< 0.05$, 0.01 and 0.001 respectively. Error bars represent SEM and derive from >7 experiments for each strain. **E.** DA neurons in N2 are highly sensitive to treatment with the neurotoxin 6-OHDA, which requires the presence of DAT-1. *vt29* is fully sensitive to 6-OHDA treatment, whereas *vt25* is partially resistant. Treatments were performed as described in the methods. Data were analyzed using a one-way ANOVA with multiple Bonferroni posttests where ** and *** indicate a significant reduction from N2 where $P < 0.01$ and $P < 0.001$ respectively. **F.** *dat-1(ok157); vt29* demonstrates an enhanced Swip penetrance relative to *dat-1(ok157)* and *vt29* alone at an intermediate osmolarity (100 mOsm). Lines were tested manually over at least three experimental days with > 48 trials for each strain. Data were analyzed using one-way ANOVA with multiple Bonferonni posttests. *dat-1(ok157); vt29* was found to be significantly reduced from either mutant line alone. **G.** Model for differential contributions of *swip-6(vt25)* and *swip-10(vt29)* to Swip. *Vt21/vt22* impact DAT activity directly through mutation of DAT-1 and loss of function. *swip-10* is hypothesized to function in a pathway parallel and upstream of DAT-1 activity, whereas *swip-6* acts to constrain both extracellular DA release and re-uptake.

vt29 animals produce a hyperdopaminergic phenotype that precludes the maintenance of normal presynaptic DA levels.

vt25 and vt29 demonstrate differential protection against 6-OHDA neurotoxicity *in vivo*

The reduction in DA levels in *vt25* and *vt29*, in the context of a hyperdopaminergic phenotype, raised the possibility that the mutations harbored by these lines produces a loss of DAT-1 loss function that might be masked by other effects, and thus not detected via the methods we had employed to this point. Our lab previously demonstrated that treatment of worms with 6-hydroxydopamine (6-OHDA) results in a necrotic loss of DA neurons, and that this process requires transport of the compound by presynaptic DAT-1 to produce neural degeneration (Richard Nass, et al., 2002). This phenotype presented us with an opportunity to more directly examine the function of DAT-1 in *vt25* and *vt29* lines *in vivo*. Consistent with our published studies, we observed degeneration of DA neurons in N2, but not *dat-1* animals, after an acute (1hr) treatment with 6-OHDA (Figure 19E). 6-OHDA was significantly less effective in lesioning DA neurons in *vt25* animals compared to N2, suggesting that the gene responsible for Swip in this line normally plays a role in modulating DAT-1 activity. In contrast, *vt29* demonstrated full sensitivity to the toxin, consistent with the mutation in this line impacting a process parallel to DAT-1 in constraining DA signaling.

Dat-1 and *vt29* exhibit additivity for Swip when assayed under hypotonic conditions

With evidence that *vt29* impacts DA signaling in a DAT-1-independent pathway, we returned to our assessment of Swip behavior under hypotonic conditions, examining paralysis at an intermediate osmolarity using single and double mutant lines. At a medium osmolarity of 100 mOsm, we observed a significant increase in Swip in the *dat-1;vt29* double mutant, as compared to the Swip penetrance of *dat-1* or *vt29* alone (Figure 19F) and consistent with the mutation harbored by *vt29* impacting a pathway parallel to that impacted by *dat-1* (Figure 19G).

DISCUSSION

The *C. elegans* gene T23G5.5 (DAT-1) was the first invertebrate SLC6 family member to be cloned and characterized, revealing structural and functional characteristics similar to those of vertebrate catecholamine transporters (Jayanthi, et al., 1998). *In vitro* heterologous expression studies revealed DAT-1 to exhibit substrate specificity for DA over other catecholamines, and to be antagonized by imipramine, amphetamine and cocaine. Subsequent *in vivo* efforts (Richard Nass, et al., 2002) demonstrated that a 700bp DNA element immediately upstream of the DAT-1 transcription start site confers expression of GFP in all *C. elegans* DA neurons (CEP, ADE, PDE in the hermaphrodite). Nass and coworkers capitalized on the visibility of DA neurons in living nematodes to

monitor neurotoxin (6-OHDA)-induced DA neuron degeneration and demonstrate the dependence of cell death on toxin accumulation by DAT-1.

The discovery of a DAT-1 dependent phenotype provided an initial opportunity to implement forward genetic approaches for the identification of 6-OHDA toxicity suppressors (R Nass & Blakely, 2003; Richard Nass, et al., 2005). As the basis for this screen derives from sensitivity to an exogenous agent, the utility of the 6-OHDA screen for the elucidation of molecules regulating endogenous, DAT-1 dependent DA synaptic events is limited. Therefore, we sought to identify behavioral alterations arising from compromised, endogenous DA signaling, as revealed in studies of a genetic loss of DAT-1. Although loss of DAT in mice produces a dramatic motor phenotype (Giros, et al., 1996), and exogenous DA can paralyze worms (Chase, et al., 2004; Sawin, et al., 2000; Schafer & Kenyon, 1995), deletion of a large portion of the *C. elegans* DAT-1 gene fails to induce an overt motor phenotype on solid substrate. DA neurons in the worm are mechanosensitive (Sawin, et al., 2000), and thus we reasoned that insufficient physical stimulation is present under normal culture conditions to elicit sufficient DA release, thereby reducing the sensitivity of measures focused on a *dat-1* mutation. Wild type worms placed in water thrash rapidly for 20 minutes or longer, and we considered whether this more vigorous mode of motion might trigger more elevated DA release. Indeed, when we placed *dat-1(ok157)* animals in water, we discovered that these animals swim briefly at normal rates and then paralyze – a phenotype we termed Swip (P. W McDonald, et al., 2007). Swip in *dat-1* animals requires the biosynthesis of endogenous DA, packaging of DA into

synaptic vesicles, and activation of the DOP-3/Gα_o pathway (P. W McDonald, et al., 2007). The current study confirms that Swip can be used to screen for molecular alterations that impact DAT-dependent DA clearance.

In our initial screen, many of the lines we identified, when retested in a subsequent generation, demonstrated incomplete penetrance of the Swip phenotype, and, thus we chose to save only those clones where at least 80% of animals in subsequent generations exhibited Swip. The current report represents an analysis of ~10,000 haploid genomes, where we uncovered ten stable lines originating from mutations in at least three distinct genes, as determined through direct sequencing, rescue experiments, mapping, and complementation analyses. Visualization of GFP-labeled DA neurons on the mutant backgrounds verified that gross morphological deficits of DA neurons do not account for the Swip phenotype of the lines presented in the current report. Our design also reduced the probability that mutations recovered would arise in shared elements of neurotransmitter release machinery or determinants of cholinergic and GABAergic signaling, as these lines would be predicted to exhibit locomotor dysfunction on solid substrate. Evidence that the lines recovered in our screen 1) display *cat-2* and/or *dop-3* reversal, 2) can be rescued by the presynaptically-directed vMAT/*cat-1* inhibitor reserpine, 3) include two novel *dat-1* alleles, 4) produce changes in DA levels (for *vt25* and *vt29*) and 5) (for *vt25*) reduces 6-OHDA sensitivity lead us to infer that the approach we have used provides for a preferential identification of presynaptically acting genes. Of course, we cannot rule out that our design and subsequent tests could recover mutants acting

postsynaptically, though it seems more likely that a screen to identify suppressors of *dat-1* mediated Swip would be more useful in recovering such animals(Wani, et al., 2012). Finally, although we chose not pursue them, we also identified multiple lines that exhibited *enhanced* Swip following reserpine treatment, which could reflect an influence of octopamine, tyramine or serotonin, as these neurotransmitters can also modulate motor activity and their vesicular packaging by CAT-1 should also be reserpine-sensitive(Alkema, Hunter-Ensor, Ringstad, & Horvitz, 2005; Duerr, et al., 1999).

Two of the lines recovered in our screen harbor point mutations in the coding region of DAT-1. *Vt22* bears a nonsense mutation, predicted to truncate the DAT-1 protein at Trp283, whereas *vt21* possesses a missense mutation predicted to generate a nonconservative substitution of Gly for Asp at amino acid 460. All eukaryotic SLC6 family members possess a Gly residue at this position, though ours is the first study to demonstrate a functional significance of this site *in vivo*. Importantly, our studies of *vt21* and *vt22* provide critical proof of concept that a Swip-based, forward genetic screen can target genes critical for the regulation of DA signaling.

In addition to the isolation of new *dat-1* alleles, we present a functional characterization of two additional stable lines exhibiting Swip, *vt25* and *vt29.* These two lines share reserpine-sensitive Swip with *dat-1(ok157*), *dat-1(vt21)* and *dat-1(vt22),* and like these mutants, their Swip is suppressed by *dop-3* or *cat-2* mutations. Complementation analyses and mapping of the mutant genes harbored by *vt25* and *vt29* revealed that they bear mutations in two independent

loci that do not overlap or contain mutations in known regulators of DA signaling and thus likely represent novel genetic components of DA signaling.

In parallel with *dat-1(vt21)* and *dat-1(vt22)*, we assayed the response of *vt25* and *vt29* to increasing doses of exogenous DA. Relative to N2, all *dat-1* mutants, as well as *vt29*, exhibited a statistically significant, two-fold increase in sensitivity to exogenous DA on solid substrate. In contrast, *vt25* demonstrated a more N2-like response to DA, our first indication that these genes support DA signaling via separate pathways. The molecular mechanisms supporting a hypersensitivity to exogenous DA are yet to be determined, though in the case of the *dat-1* mutants, a plausible basis is a reduced requirement for exogenous DA to achieve DOP-3 activation in animals that cannot capitalize on the DA clearance activity provided by DAT-1. This mechanism has some support from the demonstration that DAT-1 can accumulate other exogenous substrates, such as the dopaminergic toxin 6-OHDA (Richard Nass, et al., 2005). A second possibility is that, in DAT-1 deficient animals, chronically elevated levels of extrasynaptic DA may lead to a desensitization of a DA autoreceptor that may normally act to suppress DA release via a negative-feedback mechanism. In mammals, the D2 receptor serves both to suppress DA neuron firing and to reduce DA release (Beckstead, et al., 2004; Bello et al., 2011; Schmitz, Schmauss, & Sulzer, 2002; Usiello, et al., 2000). Although such a mechanism has not been defined in nematodes, a D2-like DA receptor DOP-2 is also expressed by *C. elegans* DA neurons (Suo, et al., 2003). By inference, desensitization of presynaptic DOP-2 produced by constitutively elevated

extracellular DA could result in enhanced DA release that synergizes with exogenous DA, thereby reducing the amount of DA needed on plates needed to produce immobility. Studies are needed that utilize lines with DA neuron-specific elimination of DOP-2 to test this possibility. Such animals would also be useful in testing whether mutants recovered in our screen produce their hyperdopaminergic phenotype by suppressing DOP-2 mediated, inhibitory control of DA neuron excitability and/or DA release.

As our studies progressed, we recognized that our automated movement analysis software (SwimR) could be augmented to provide a much more detailed analysis of activity patterns than is reported in standard thrashing assays. To accomplish this goal, we developed a new suite of analytical tools that would allow for an unbiased assessment of the behavior of animals, both as individuals and across a population. Although the essential patterns among the strains we assayed were consistent, finer aspects of their swimming behavior were now observable. One such novel observation concerns the finding that a significant fraction of *dat-1* animals spontaneously recovered from paralysis for short intervals (termed here “reversals”). Since we observe these reversals in the context of a hyper-dopaminergic phenotype, it is possible that excess postsynaptic DA signaling produces reversals in the course of moving between two distinct behavioral states. In this regard, Vidal-Gadea and colleagues demonstrated that DA is necessary and sufficient for *C. elegans* transit from swimming to crawling (Vidal-Gadea et al., 2011). Whereas the Swip of *dat-1* animals is dependent solely on DOP-3, the swim-crawl transition requires DOP-1

and DOP-4 (Vidal-Gadea, et al., 2011). Alternatively, reversals may derive from recruitment of other circuits that stimulate movement and that become evident when DOP-3 receptors are desensitized. Regardless, the relative presence of Swip revertants amongst our mutant strains suggests that these reversions can be triggered or unmasked by specific genetic perturbations in DA signaling. Specifically, we found that *vt29* exhibits a significantly reduced reversion incidence from *dat-1* and *vt25*. Multiple automated tracking systems for *C. elegans* swimming have been developed (Buckingham & Sattelle, 2008; Fang-Yen et al., 2010; Ghosh & Emmons, 2008, 2010; Pierce-Shimomura et al., 2008). Our system and its associated analytical tools (Hardaway *et al*, *manuscript under review*) has been designed to detect multiple parameters of swimming behavior and subtle fluctuations between mobile and immobile states.

Our automated thrashing analysis of *vt25* and *vt29* revealed striking differences between them, and with *dat-1*. Using SwimR, we observed that fewer *vt25* animals fail to paralyze than *dat-1*, and that *vt29* has a shorter latency to paralyze and a lower incidence of Swip reversion from the *dat-1* strain. Reversion analysis also revealed that incidence of reversion is more sensitive to genotype than reversion frequency (# of reversals/animal), time to first reversion, or average reversion event length. These findings reveal that *vt29* differs from *dat-1* and *vt25* in its threshold for reversion, and that behavior during reversion, as well as transition back to a paralytic state, is determined by independent factors. Based on additional functional data discussed below, we propose that the biological mechanism impacted by *vt29* may determine overall sensitivity to the

physical environment encountered in the Swip assay, whereas *vt25*, like *dat-1*, impacts mechanisms more directly supporting DA inactivation.

The kinetic differences in Swip behavior observed for *vt25* and *vt29* raised the question as to whether the strength of Swip in these lines is maintained under conditions in which Swip is suppressed in the *dat-1* strain. Previous study of the environmental dependence of the *dat-1* Swip phenotype revealed that an increase in the osmolarity of the swimming media significantly suppresses the Swip phenotype (Hardaway *et al.* – personal communication/WBG). In this study, we were able to replicate that finding using both manual assays and automated thrashing analysis. Remarkably, *vt25* maintained its Swip behavior across all osmolarities, whereas *vt29* swimming behavior, like *dat-1*, was recovered as the osmolarity of the medium approached that of M9. We also assayed the behavior of the *dat-1; vt29* double mutant across these osmolarities and observed an increase in Swip penetrance at intermediate osmolarities. These findings suggest that *dat-1* and *vt29* act in parallel, independent pathways that can sum to produce an additive paralytic response at intermediate osmolarities. Although both the *dat-1* and *vt29* strain demonstrated recovery of swimming in the isotonic buffer M9, our automated analysis demonstrated that, nonetheless, *dat-1* behavior could be differentiated from *vt29* in that the latter line maintains a stronger Swip phenotype even in media of high osmolarity. It is commonplace to use salt-buffered solutions in the study of neurotransmitter regulation of swimming, despite the fact that the organism normally resides in an environment with variable ionic content. Together, these studies demonstrate that the

attribution of genes to DA signaling pathways, as well as their epistasis, will benefit from the use of osmotic profiling.

To investigate the potential pathways in which *vt25* and *vt29* reside, we assayed their Swip phenotypes in the context of DAT-1 transgenic overexpression, This transgene fully rescues the *dat-1* mutant (P. W McDonald, et al., 2007), and almost completely restored the swimming behavior of *vt25,* though short transient bouts were still evident. In contrast, *vt29* swimming behavior was only partially restored by DAT-1 overexpression. Since the *vt25* strain displays a weaker phenotype, the relative magnitude of suppression between *vt25* and *vt29* is roughly equivalent, and suggests that overexpression of DAT can partially restore disruptions in multiple pathways regulating DA homeostasis. Manipulation of multiple DAT-interacting proteins have been implicated in the folding, trafficking, stability and activity of the transporter including PICK1 (Torres et al., 2001), Hic-5 (Carneiro et al., 2002), syntaxin1A (K.-H. Lee, Kim, Kim, & Lee, 2004), RACK1 (K.-H. Lee, et al., 2004), α-synuclein (F. J. Lee, Liu, Pristupa, & Niznik, 2001), synaptogyrin-3 (Egaña et al., 2009) and the D2 dopamine receptor (F. J. S. Lee et al., 2007), though the significance of these interactions *in vivo* has not been studied. Mutation of the *C. elegans* orthologs (where they exist) of these genes is unlikely to contribute to the phenotypes of *vt25* and *vt29* based on their absence from mapped loci. Additionally, since we observed no difference in the somatic export of GFP:DAT-1, we doubt they produce Swip through alterations in transporter trafficking to the synapse. This is particularly evident with *vt29* animals that retained the full 6-

OHDA sensitivity exhibited by N2. However, *vt25* displayed a more moderate 6-OHDA sensitivity and thus part of its actions may involve local, synaptic DAT-1 trafficking to the plasma membrane or control of transporter activity.

Finally, as *vt25* or *vt29* display a hyperdopaminergic signaling phenotype, release of enhanced, synthesized, or stored DA could explain their phenotypes. However, when we measured the DA content of these lines by HPLC, we found that, as with *dat-1*, both exhibited a significant *decrease* in DA levels, though not as reduced as the *cat-2* mutant that actually fails to Swip. Measurement of synaptic DA *in vivo* in *C. elegans* is not currently feasible. Interestingly, however, DAT KO mice demonstrate tonically elevated synaptic DA, accompanied by a reduction in tissue DA (Giros, et al., 1996), which these investigators ascribed to a failure to replenish resting vesicular stores via recapture of synaptic DA. Although, as noted above, a contribution of *vt25* to DAT trafficking or activity could result in reduced DA levels, multiple lines of evidence do not support such a role for *vt29*. Rather we hypothesize that the gene mutated in *vt29* causes excess DA release that cannot be restored through the normal pathways of DA synthesis and recapture. A reasonable hypothesis for the phenotype of the *vt29* mutant (and to a lesser degree *vt25*), and one that now can be targeted in future studies, is that the *vt29* gene normally exerts suppression of DA neuron excitability and/or DA vesicular release (Figure 19G). Efforts are underway to identify the sites of the molecular lesions borne by *vt25* and *vt29* animals. The conservation of components of DA signaling throughout phylogeny suggests that our efforts in this regard may identify molecules whose intensive study can

provide insights into brain disorders involving compromised DA signaling, as well as the development of novel therapeutics.

Chapter IV

IDENTIFICATION OF *swip-10* in *C. ELEGANS*

INTRODUCTION

In our previous study, we identified a number of mutant strains that demonstrate a reserpine-sensitive hyperdopaminergic phenotype. We demonstrated that one of these mutants, *vt29* maps to a distinct genomic locus from *dat-1*, has a normal neurotoxic response to DAT-dependent 6-OHDA, and functions in parallel with *dat-1* to trigger Swip. In this study, I aim to determine the site of the molecular lesion in *vt29*.

MATERIALS AND METHODS

C. elegans strains, husbandry, and genotyping

C. elegans strains were cultured on bacterial lawns of OP50 and maintained at 12 to 20°C using standard methods (Brenner, 1974) unless otherwise noted. The wild-type strain is N2 Bristol.

The following strains were used in this study:

BY810 *swip-10(vt29)* - G->A substitution 3289 bp downstream of start site

BY828 *swip-10(vt33)* - G->A substitution 3243 bp downstream of start site

BY1010 *swip-10(tm5915)* - 339 bp deletion (bp 31-370 from start) generated by Shohei Mitani

The following lines were acquired from the Caenhorhabditis Genetics Center (U. Minnesota), the National Bioresource Project, or the noted lab by request:

cat-2(tm2261)

LX703 *dop-3(vs106)*

RM2702 *dat-1(ok157)*

Genetic Crosses

Crosses were performed using publically available integrated fluorescent reporter strains to mark chromosomes *in trans*. Single worm PCR were performed to confirm the presence of the indicated mutation. For all deletions, we used a three primer multiplex strategy that produces PCR amplicons with 100-200 bp difference between N2 and mutant. This was highly effective in eliminating preferential amplification of a lower molecular weight species. In all cases, a synthetic heterozygous control was utilized to ensure that heterozygous clones could be identified within that experiment. All PCR reactions were performed with Platinum PCR Supermix (Life Technologies).

The following strains were generated by cross:

BY957 *cat-2(tm2261); swip-10(vt29)*

PCR Genotyping of *cat-2(tm2261)* was performed using the following primers:

5’ sense – ctccaacaactgaacgacgaagg

3’ antisense – atttctcgtagacagccttccacg

inner antisense – agcagctctgccgagtgaattaa

swip-10(vt29) was determined by Sanger sequencing of PCR amplicons generated using the following primers:

Sense – ccagAACGATACGATGAACC(Sequencing primer)

Antisense – GCAACCATAGCGCCTTCTAG

BY873 *cat-2(tm2261); swip-10(vt33)*

swip-10(vt33) was determined by Sanger sequencing of PCR amplicons generated using the same primer set for *swip-10(vt29)*.

BY1034 *cat-2(tm2261); swip-10(tm5915)*

PCR genotyping of *swip-10(tm5915)* was performed using the following primers:

5' sense – GGAAAACACTCGTTCTCTCACCAATTG

3' antisense – TGTATCATACTTGCAAGTTGCTCATAGTC

inner antisense – GCAAACATTCCCCCTTGACTTATCATT

BY1030 *swip-10(tm5915) dop-3(vs106)* – The two alleles were crossed and recombinant progeny were identified via PCR.

PCR genotyping of *dop-3(vs106)* was performed using the following primers:

5' sense – tcaagaagtgggagacggaacgaa

3' antisense – gacctggcaatgtctgggtagaaa

inner antisense – gtggtgttgtccagccaacattct

C. elegans Assay for Swip

In both batch and single worm analyses, we generated synchronous populations of these strains by hypochlorite treatment and harvesting arrested L1 animals.

Early-mid stage L4 animals were identified by characteristic morphology and used for behavior as N2 animals show some stochastic Swip and quiescence bouts during the last larval molt. For automated analysis, single L4 hermaphrodites were placed in 20μL water or drug in a single well of a Pyrex Spot Plate (Fisher catalog number 13-748B), and 10 minute movies (uncompressed AVI format) of their swimming behavior were created and analyzed as described previously (Hardaway and Wang *et al.)*. For testing responses to *dat-1* blockade, Imipramine HCl(Sigma) was dissolved in MilliQ water at 10 mM and serially diluted to the indicated dose. Assays with N-acetyl cysteine were performed by dissolving NAC (Sigma) at 100 mM in MilliQ water and serially diluting the drug to the indicated dose.

Preparation of gDNA for Whole Genome Sequencing

gDNA was isolated as in Sarin *et al.*{Sarin, 2008 #233} Briefly, BY200 (parental strain), *vt25, vt29, vt31, vt32, vt33* and *vt34* worms were harvested from a 10 cM 8p/NA22 plate by rinsing with M9. After a brief pre-clearing wash with M9, the worms were rocked in M9 for 2-3 hours to allow them to clear ingested bacteria. Worms were washed with M9 and then pelleted for DNA extraction. Prior to extraction the worm pellet was incubated at -80 degrees for 1 hour to o/n. gDNA was extracted from the worm pellet using a Qiagen Gentra Puregene kit as described by the manufacturer and a post-hoc phenol/chloroform extraction, RNAse A digestion, and additional phenol/chloroform digestion. The quality of

the gDNA was confirmed on a 2% agarose gel prior to submitting the samples for Illumina sequencing (Vanderbilt Genome Technology Core).

Whole Genome Sequencing

Sequencing libraries were generated from gDNA as described in Sarin *et al.* Each sample was assigned a unique barcode so that samples could be pooled onto several flow cells of an Illumina Genome Analyzer Iix for sequencing as single-end 76mers. Sequence reads were filtered for quality and offloaded in a Fastq format for subsequent analysis. Sequence data were analyzed in MaqGene (Bigelow, Doitsidou, Sarin, & Hobert, 2009) and a text file containing mutations against the reference sequence (WS180) were extracted. We then compared these mutant strain lists against the parental strain (BY200) to identify mutagen-induced SNPs. For *vt29* and *vt33*, we compared the SNPs on LGX to identify the mutant sites on F53B1.6.

***swip-10* rescue experiments**

A full length 4.3 Kb genomic fragment from -738 to 3569 downstream of the ATG start site was amplified and injected at 20 ng/µl onto *swip-10(vt29)* and *swip-10(vt33)* with $p_{unc-122}$:GFP to generate *vtEx74-75* and *vtEx76-78* respectively.

Bioinformatic Analysis

Homologs of *swip-10* were identified using online databases at the National Center for Biotechnology Information (NCBI), most notably AceView. Multiple sequence alignments were performed in the MegAlign plugin of DNAStar.

Secondary Structure Prediction for *swip-10*

The predicted and molecularly determined protein sequences for *swip-10* were input into two independent secondary structure prediction programs – PredictProtein (https://www.predictprotein.org/) and XtalPred (http://ffas.burnham.org/XtalPred-cgi/xtal.pl). Both of these programs predict structural features and potential post-translational modifications of the input sequence based on hydrophilicity and known sequence motifs from other proteins.

Cloning of the *swip-10* cDNA

Total RNA was harvested from asynchronous N2 animals and first strand cDNA was generated using Superscript III First-Strand Synthesis System (Invitrogen-Carlsbad,CA). We amplified a 1.6 kB PCR product using the following primers: ATGCTTTTTCATTTTCTAATCGCTA(S) and TTAACATTTCAAAGCTTTCTT(A). This fragment was TA cloned into PCR8/GW/TOPO for further manipulations.

RESULTS

***vt29*/*vt33* Complementation Analysis**

In our previous study we identified several reserpine sensitive mutants and mapped the genomic locus of the Swip-causing mutation. In these analyses we determined that *vt29* and *vt33*, while isolated in separate rounds of screening, both harbor mutations that map to the negative end of LGX (see Figure 12 in Chapter III). To determine if *vt29* and *vt33* are different alleles of the same gene, we crossed them together and performed Swip on their F_1 cross progeny. We determined that *vt29* and *vt33* are complemented by the corresponding wildtype allele, but fail to complement when crossed together (Figure 20). Thus *vt29* and *vt33* likely harbor mutations in a shared gene and these mutations display an a recessive pattern of inheritance.

Identification of F53B1.6

To determine the exact site of the molecular lesion in *vt29* and *vt33*, we performed whole genome sequencing on these mutants in parallel with the parental strain used for mutagenesis (Flibotte et al., 2010; Hardaway et al., 2012; Sarin, Prabhu, O'meara, Pe'er, & Hobert, 2008). We mapped the sequence reads to a reference genome, excluded SNPs present in the parental strain, compared SNPs with our previously mapped locus on LGX, and identified shared SNPs present in both *vt29* and *vt33*. We identified one gene, F53B1.6, which harbors a mutation in both *vt29* and *vt33.* To determine if F53B1.6 is the Swip-causing mutation, we used two parallel approaches. We obtained a deletion in F53B1.6 (*tm5915*) and determined that it displays a highly penetrant Swip phenotype comparable to *vt29* and *vt33* (Figure 21).

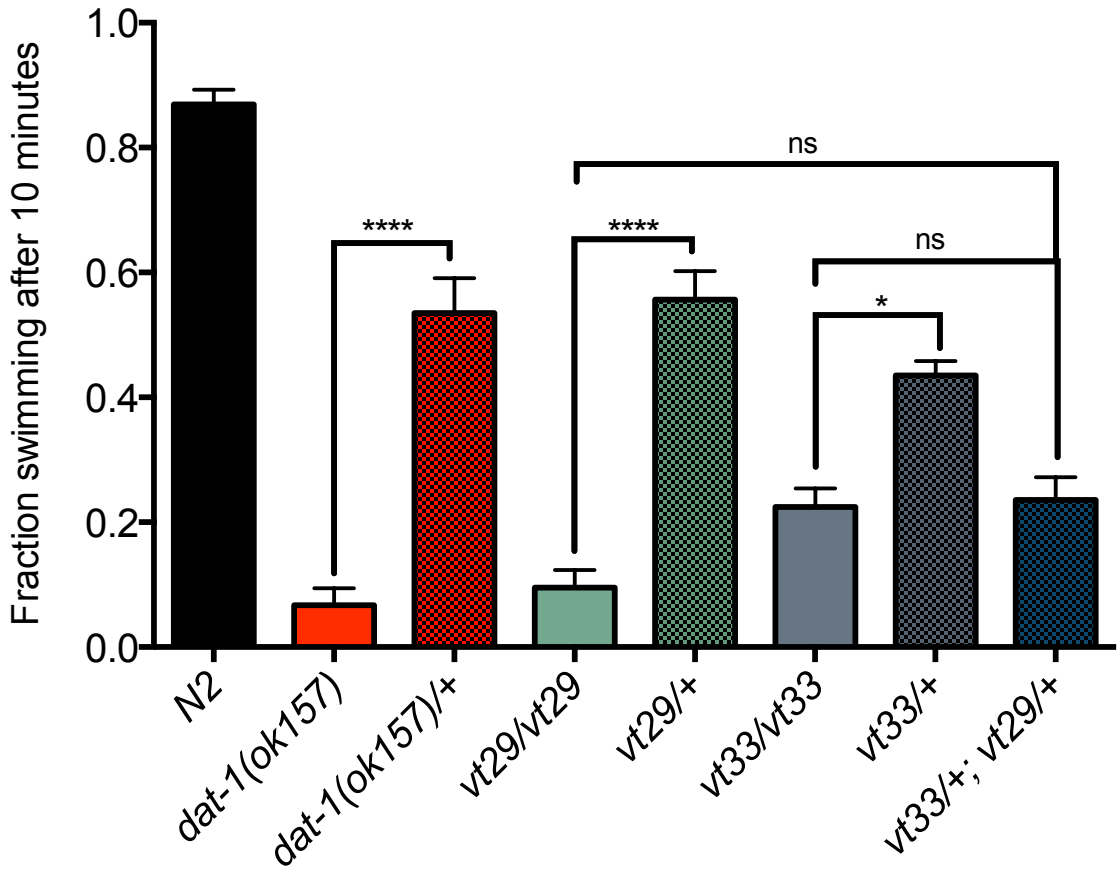

Figure 20 – Complementation Analysis of *vt29* and *vt33*. F_1 progeny were generated by cross of either N2 males, *vt29* males, or *vt33* males into the corresponding *dat-1*, *vt29*, or *vt33* hermaphrodite. Cross progeny were tested for Swip over 3 independent experiments. Data were analyzed by one-way ANOVA with selected Bonferonni multiple comparisons post tests between homozygote and heterozygote cross progeny. * and **** indicate a *p* value of <0.05 or <0.0001 respectively.

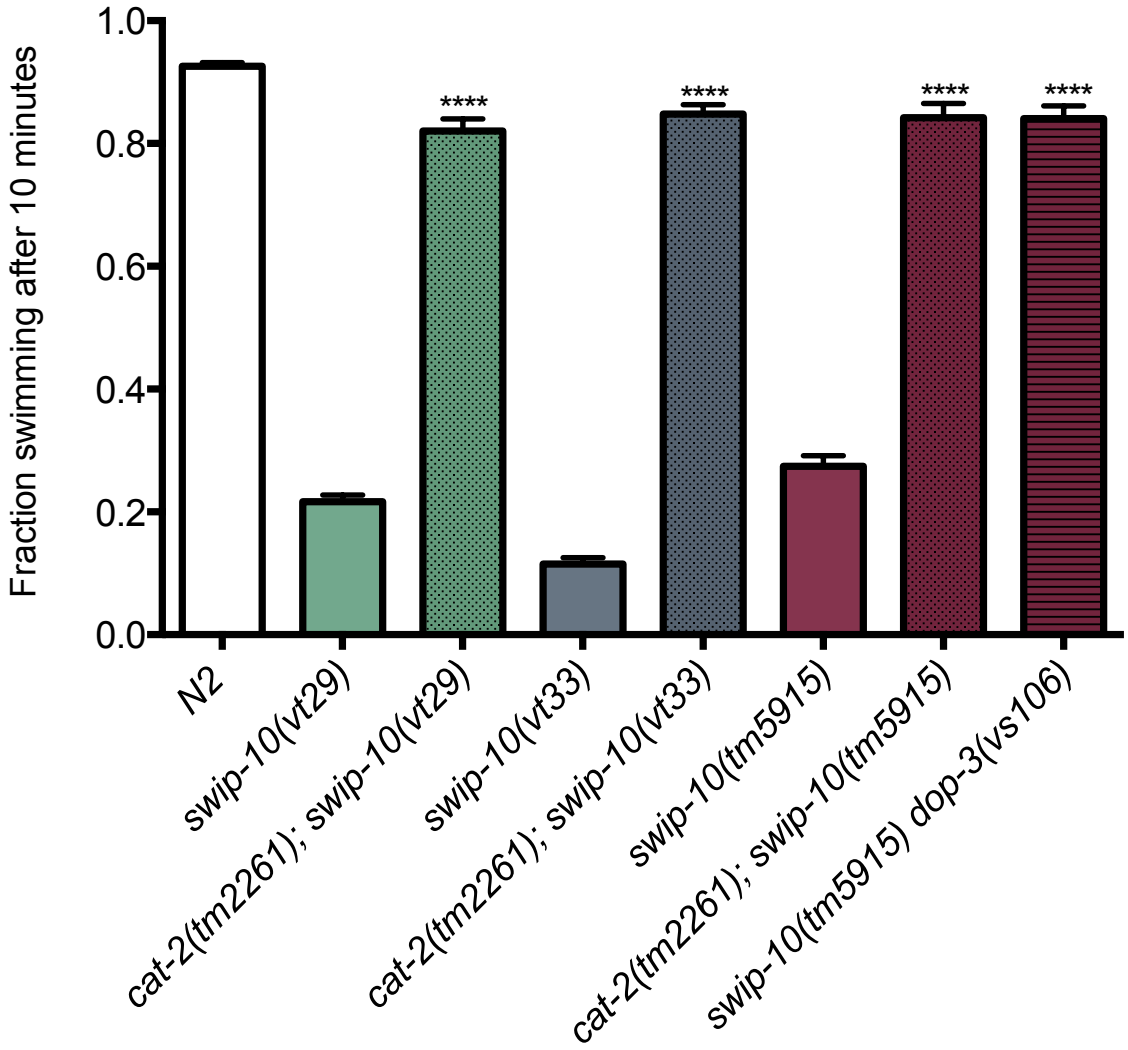

Figure 21 – *swip-10* Swip is *cat-2* and *dop-3* dependent. *swip-10(vt29)* and *swip-10(vt33)* were crossed to the *cat-2(tm2261*) strain and assayed for Swip. Sequencing of the *vt29* and *vt33* SNPs confirmed that the presence and homozygosity of these mutations. *cat-2(tm2261)* was crossed to *swip-10(tm5915)* and genotyped by PCR. *swip-10(tm5915)* was recombined with *dop-3(vs106)* and recombinant clones were identified by PCR. Swip assays were performed as described in the Methods section. Data were analyzed by one-way ANOVA with selected Bonferroni post tests between the double mutant strain and its corresponding single mutant allele. **** indicates a $p<0.0001$.

Furthermore, we determined that the Swip phenotype in *tm5915*, as in *vt29* and *vt33*, is DA dependent as double mutants lacking *cat-2*/TH, are suppressed to wildtype levels. Because of their proximity to *dop-3*, our previous study had only used reserpine and *cat-2* alleles to validate the DA dependence of *vt29* and *vt33* (Hardaway, et al., 2012). We recombined *tm5915* with *dop-3* and found that *dop-3* is required for the Swip phenotype, restoring the swimming behavior to near wildtype levels (Figure 21). To demonstrate that these mutations are required for the Swip we observe in *vt29* and *vt33*, we transgenically overexpressed a PCR fragment spanning the wildtype F53B1.6 genomic locus. Assay of Swip in both non-transgenic and transgenic progeny in multiple transgenic lines demonstrated that expression of the wildtype F53B1.6 locus rescues Swip in *vt29* and *vt33* (Figure 22). Thus, mutations in F53B1.6 are necessary and sufficient to trigger DA and *dop-3* dependent Swip. Hereafter we refer to F53B1.6 as *swip-10*.

Alignment of *swip-10* with vertebrate orthologs

As *swip-10* had not been described in any previous report, we used available bioinformatics tools to determine if any orthologs of *swip-10* existed in vertebrates, including humans. We discovered that *swip-10* has a highly conserved homolog throughout phylogeny. In mammals, the *swip-10* homolog is known as Mblac1 and has not been studied to date. To determine the extent of their homology, we performed a multiple sequence alignment of the *swip-10* protein sequence and its orthologs in *Caenhorhabditis briggsae, Drosophila*

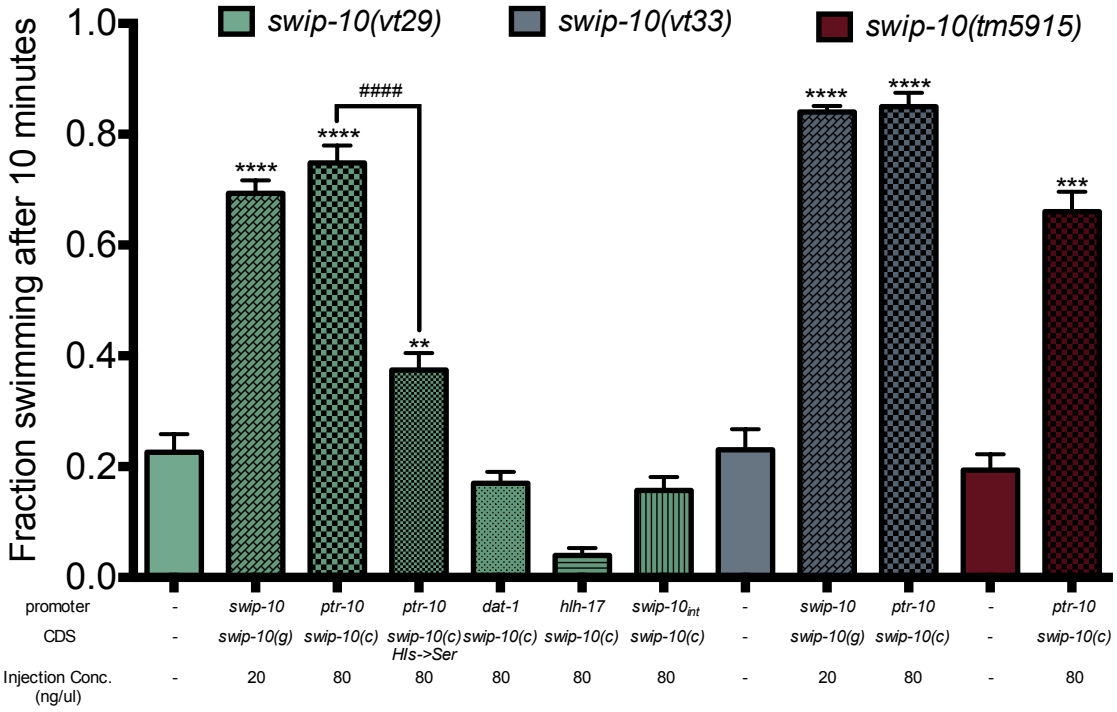

Figure 22 – Rescue of *vt29, vt33* and *tm5915* with exogenous F53B1.6 expression. A full length F53B1.6 genomic PCR fragment containing the endogenous F53B1.6 promoter(2nd and 9th bars) or an expression construct containing a cassette containing a full length F53B1.6 cDNA:GFP fusion under the control of a pan glial promoter(*ptr-10,* 3rd,10th and 12th bars), DA neuron specific promoter(*dat-1,*5th bar*)*, CEPsh promoter(*hlh-17*, 6th bar), or the *swip-10* 4th intron(7th bar) were injected into *swip-10(vt29)*. We found that expression of *swip-10* in glial cells, but not CEPsh glia, restores normal swimming behavior in *swip-10* mutants. 4th bar – mutation of histidine residues necessary for metal binding significantly reduces *swip-10* function. At least two independent transgenic arrays were recovered from each of the injections and tested for rescue of Swip. For testing, transgenic and non-transgenic progeny were picked onto separate plates by virtue of a fluorescent coinjection marker, allowed to acclimate for several hours, and then tested for Swip. For each transgenic line, at least 100 animals were tested. The bars indicate pooled values from each of the transgenic lines assayed. Data were analyzed by an unpaired student's *t* test between the transgenic and non-transgenic progeny that were assayed, where **, ***, and **** represent $p < 0.01$, 0.001, and 0.0001 respectively. Comparison of the His-> Ser mutant construct was performed by a *t* test between transgenic animals expressing the wildtype *ptr-10* rescue construct and transgenic progeny expressing the mutant construct. Non-transgenic progeny shown above are representative of each of the experiments performed.

melanogaster (fruit flies), *Danio rerio* (zebrafish), *Mus musculus*(mice), *Rattus norvegicus* (rats), and *Homo sapiens* (humans) using ClustaW. We determined that although the 5' end of the *swip-10* protein is not highly conserved, the vertebrate and invertebrate orthologs of *swip-10* bear extensive homology to the 3' end of the *swip-10* protein (Figure 23). Overall *swip-10* had a 39% sequence identity with human MBLAC1 and mouse Mblac1. We used available secondary structure prediction tools (PredictProtein and XtalPred) to identify whether the 3' end of the *swip-10* protein and its homologs contain known functional domains. *swip-10* and each of its vertebrate orthologs contain a metallo β-lactamase domain that is typified by several motifs that harbor histidine residues necessary for the binding of a catalytically active zinc ions (highlighted blue residues in Figure 23)(Callebaut, Moshous, Mornon, & de Villartay, 2002). These include the canonical HxHxDH motif that is present in the catalytic core of all metallo β-lactamase family members. Following the alignment of *swip-10* and its orthologs, we found that *swip-10(vt29)* is predicted to truncate this important domain and that *swip-10(vt33)* harbors a nonconservative mutation in a highly conserved glycine residue within the metallo β-lactamase domain (yellow highlighted residues in Figure 23). We also assayed secondary structural elements at the 5' end and determined that this end of the protein, while not conserved, contains a predicted signal peptide sequence in the first 18 amino acids of the N-terminus and a potential coiled-coil motif just 5' of the metallo β-lactamase domain. Thus prediction of *swip-10* structural elements suggests that it contains a highly conserved metallo β-lactamase domain at its 3' end, a

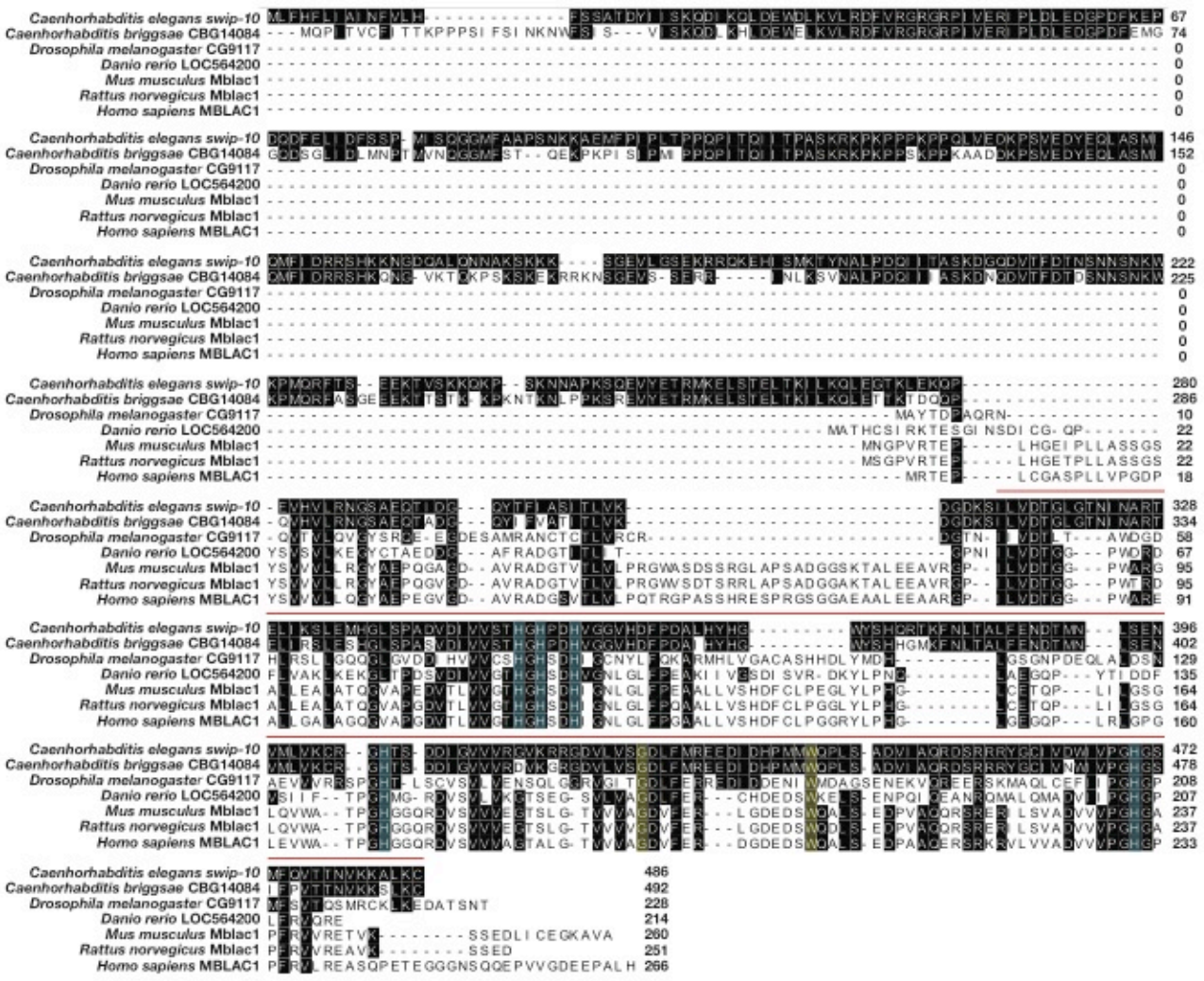

Figure 23 – Sequence Alignment of the isolated *swip-10* protein sequence. The *swip-10* protein is highly conserved with its nematode homolog CBG14084 at the 5' end. The vertebrate homologs have much shorter protein sequences and only begin to align at 260 amino acids into the *swip-10* protein sequence. Shaded residues indicate amino acids that match the *swip-10* sequence. Red bar indicates the span of the metallo β-lactamase domain that begins with a canonical "ILVDTG" motif. Blue boxes indicate histidine residues that are predicted to be critical for metal binding including a canonical HxHxDH motif that is typical of the entire metallo β-lactamase superfamily. Yellow boxes indicate amino acids that are altered in the strains isolated from the Swip-based mutagenesis screen. *swip-10(vt29)* harbors a SNP that results in the conversion of a conserved tryptophan at position 377 to a stop codon, resulting in a truncated metallo β-lactamase domain. The mutation in *swip-10(vt33)* converts a conserved glycine at position 362 to glutamic acid. Sequences were aligned using ClustalW(DNAStar).

nonconserved coiled- coil motif in the middle of the protein and a nonconserved secretory motif at its 5' end.

These analyses also revealed that three *swip-10* metallo β-lactamase domain containing paralogs exist in the worm: C23H3.9, C25D7.5, C03F11.2. None of these genes have been characterized via reporter fusions, there are no phenotypes reported via genomewide RNAi screens, and there are no alleles currently available to assess their impact on dopamine-regulated behaviors. To determine the extent of conservation between *swip-10* and its metallo β-lactamase paralogs, we performed multiple sequence alignment on the predicted protein sequences for each of these genes in parallel with *swip-10* (Figure 24). We found that *swip-10* was 36% identical to C03F11.2 largely due to extensive identity within stretches of the metallo β-lactamase domain, including the histidine residues predicted for metal binding and metallo β-lactamase activity. By comparison, *swip-10* was only 23 and 22% identical to C23H3.9 and C25D7.5 respectively.

Isolation of the *swip-10* cDNA

To determine how the *swip-10* gene is transcribed and is organized, we set out to isolate the *swip-10* cDNA. We located putative clones of the *swip-10* cDNA in a genomewide open reading frame (ORF) cloning project (WORFDB - http://worfdb.dfci.harvard.edu/) that included 3 ORF sequence tags (OSTs): one OST that spanned that the 5' group of exons (but included an exon that was not

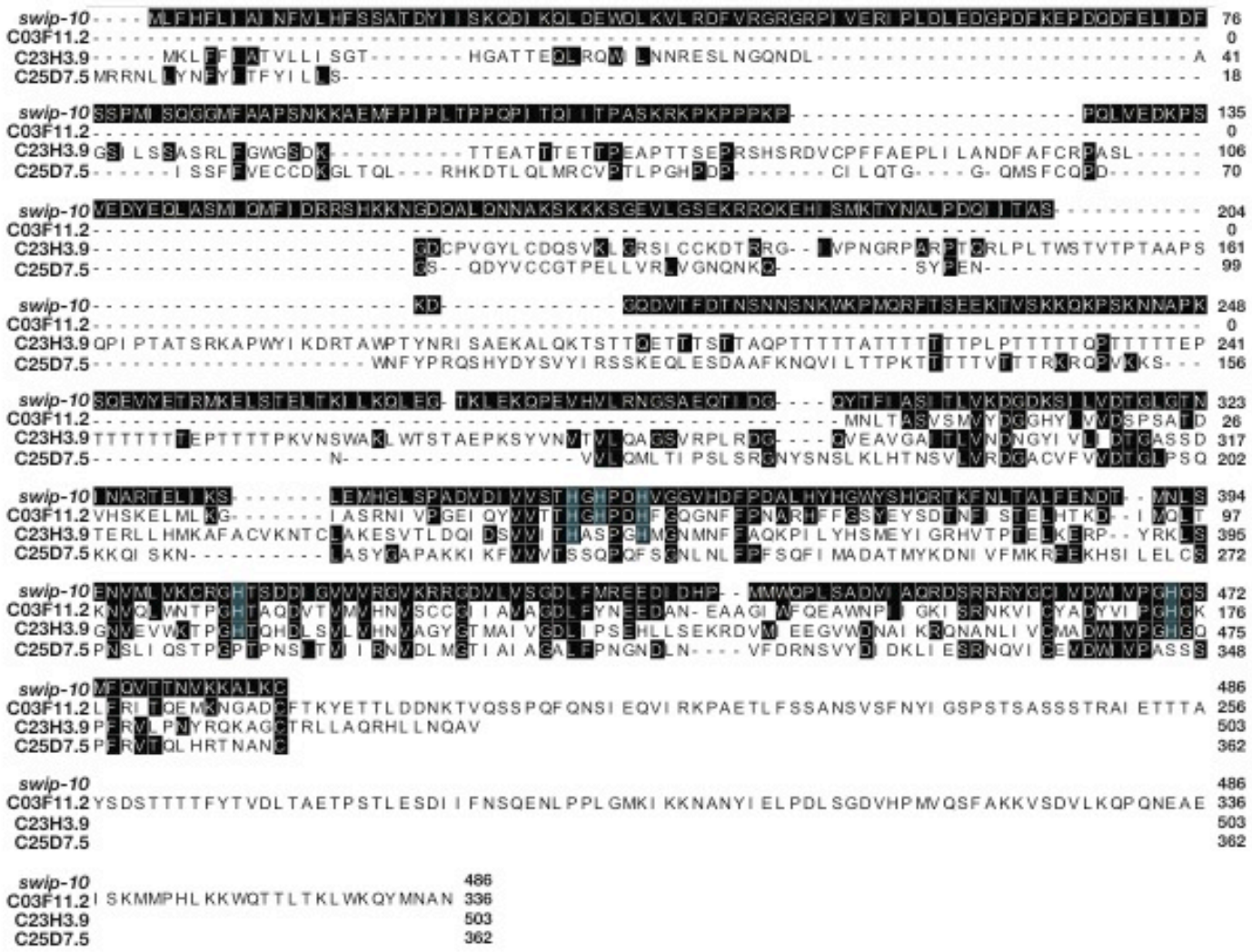

Figure 24 – Alignment of *swip-10* and its worm paralogs. *C. elegans* contains three other putative β-lactamase domain-containing genes known only as C03F11.2, C23H3.9, and C25D7.5. Blue shading indicate conserved histidine residues that are predicted to be required for β-lactamase activity. Sequences were aligned using ClustalW(DNAStar).

predicted), one OST that spanned the 3' group of exons, and one OST that spanned the full predicted full length ORF including the 5' and 3' group of exons. As there existed a predicted start site that was present in the latter OST containing the 3' metallo β-lactamase domain, we injected a PCR fragment containing only the large intron and the 3' group of exons into *swip-10(vt29)* to test if the 5' end of the gene was required for rescue. This fragment failed to rescue *swip-10(vt29)*. Combined with the presence of Swip in a deletion allele of the 5' group of exons (*tm5915)*, we therefore conclude that the F53B1.6 gene consists of two groups of 5 exons separated by a large 5th intron and that the 5' end of the sequence, while not conserved, is required for protein function. To pursue functional studies of *swip-10*, we amplified a full length *swip-10* cDNA from a wildtype cDNA library using gene specific primers at the predicted translational start site and the 3' end (see Methods). We did not observe the 1.2 Kb OST present in WORFDB, but rather a 1.4 Kb product that included an additional exon at the 5' end (Figure 25) that was also present in WORFDB OSTs.

DISCUSSION

In our previous report we described the implementation of a forward genetic screen to identify novel, conserved regulators of DA signaling using *C. elegans*. Using a combination of SNP mapping and whole genome sequencing we showed that two allelic mutant lines, *vt29* and *vt33*, harbor mutations in a previously undescribed gene F53B1.6 that we named *swip-10*. Genetic

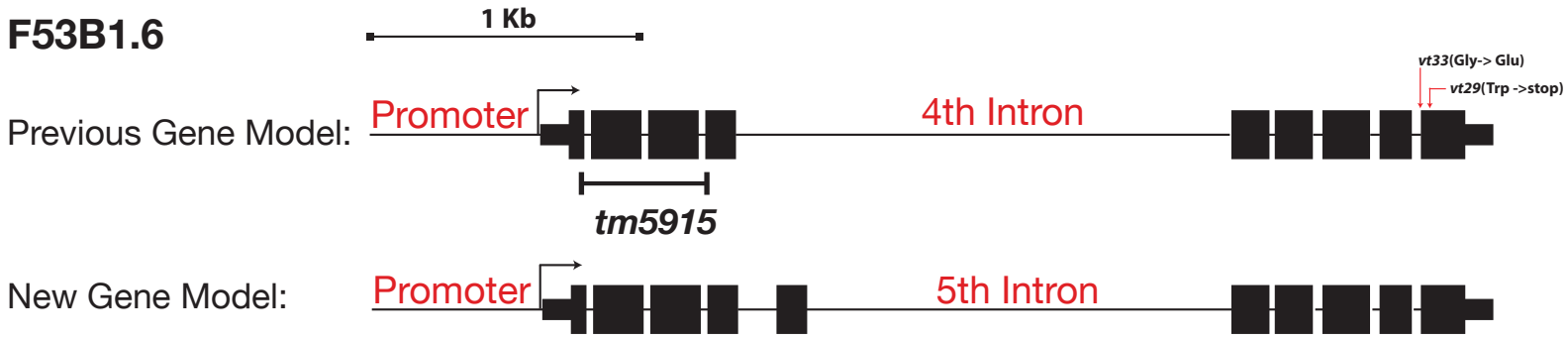

Figure 25 – **Gene model for *swip-10***. The top gene model represents the predicted model according to WormBase. The bottom model is the revised model prediction based on isolation of a 1.4 *swip-10* cDNA, functional studies using minimal PCR fragments spanning only the 3' end of the gene, and the presence of Swip in the *tm5915* deletion.

experiments using *vt29, vt33* and a novel allele *tm5915* demonstrated that mutations in *swip-10* all trigger the hyperdopaminergic phenotype Swip. Similar to *dat-1*, *swip-10* Swip requires the function of the tyrosine hydroxylase homolog *cat-2* and the D2-like receptor *dop-3* (Chase, et al., 2004; Sulston, et al., 1975). To establish that the mutations we observed in *vt29* and *vt33* were required for the Swip phenotype, we transgenically overexpressed the wildtype *swip-10* gene and observed that its overexpression significantly rescues Swip in *vt29* and *vt33*.

swip-10 is highly conserved throughout phylogeny. We identified its homologs in vertebrates by virtue of the presence of conserved functional domain known as a metallo β-lactamase domain. In addition, analysis of the *swip-10* protein sequence using secondary structure prediction algorithims revealed that the 5' end may harbor an 18 amino acid long signal peptide sequence and that the middle of the protein may contain a coiled coil motif. Neither of these domains, however, is conserved in the *swip-10* human homolog, MBLAC1. Anecodotally, imaging of the functional GFP-tagged *swip-10* cDNA was very difficult as the GFP is very diffuse (see Chapter IV), and some of the GFP may accumulate in the coelomocytes (data not available). This is consistent with the hypothesis that *swip-10* may be secreted by glia to act on its substrate. Importantly, bioinformatic analysis of glial-enriched transcripts have revealed an enrichment for secreted proteins that function in assembly of amphid neuron structures (Bacaj, Tevlin, Lu, & Shaham, 2008).

Through searching the *C. elegans* genomic and protein databases, we identified three *swip-10* paralogs that also contain metallo β-lactamase domains: C03F11.2, C23H3.9, and C25D7.5. To date, there has been no description of the expression pattern or the impact of mutations on worm phenotypes of these genes. As *swip-10* does not harbor overt morphological phenotypes, the disruption of other *swip-10* paralogs may have only subtle effects on *C. elegans* circuitry only revealed through behavioral screening or analysis of neuronal physiology.

To understand how the *swip-10* gene is transcribed, we searched available databases for ESTs and ORFs that might predict its exon organization. The available clones suggested that *swip-10* might be expressed as either: a full length cDNA containing both the 5' and 3' groups of exons, as just the 5' group, or just the 3' exons. Our original experiment expressing the full length genomic region of *swip-10* did not allow us to determine which of these regions were required for its rescue. Expression of truncated *swip-10* fragments not containing the 5' exons or the upstream promoter did not rescue *swip-10(vt29)*. We therefore concluded that the entire gene was required for a functional *swip-10* protein. We therefore isolated a full length cDNA of *swip-10* using gene specific primers to determine how the predicted gene model matches our empirically determined one. The cDNA we isolated was 1.4 Kb long and the organization of the exons matched the predicted except for an additional exon in the 5' group. The *swip-10* gene, therefore, consists of a 700 bp promoter, a

group of 5 exons at its 5' end, a large 5th intron, and a group of 5 exons at the 3' end. Importantly, expression of this cDNA can rescue *swip-10* (next chapter).

FUTURE DIRECTIONS

The isolation of *swip-10* prompts new questions about the role of metallo β-lactamase domain containing proteins in cellular physiology. Currently, we know little about how these genes are expressed and genomically organized. Analysis of their expression patterns using overlap PCR fusion and expression of GFP promoter fusions for C03F11.2, C23H3.9, and C25D7.5 may provide new insights into the diversity of gene expression for metallo β-lactamases.

To determine if *swip-10* has a unique role in affecting DA signaling, alleles of C03F11.2, C23H3.9, and C25D7.5 must be acquired. Assay of these lines using DA-dependent behavioral assays will be a critical first step toward determining if *swip-10*'s has a specialized role. Based on the expression patterns of these genes, we might assay the contribution of these genes to other neurotransmitter signaling pathways including 5HT, tyramine, octopamine, GABA, and ACH.

Chapter V

CHARACTERIZATION OF *SWIP-10* IN *C. ELEGANS*

INTRODUCTION

In the previous chapter we described the identification of the molecular lesion in the *vt29* and *vt33* strains as occurring in a novel, conserved gene that we named *swip-10*. In this chapter we describe the characterization of the *swip-10* gene expression pattern, the impact of its loss on DA neuron physiology, and our initial efforts to understand how *swip-10* impacts dopamine signaling through a novel pathway containing glutamate transporters and receptors.

MATERIALS AND METHODS

C. elegans strains, husbandry, and genotyping

C. elegans strains were cultured on bacterial lawns of OP50 and maintained at 12 to 20°C using standard methods (Brenner, 1974) unless otherwise noted. The wild-type strain is N2 Bristol.

BY810 *swip-10(vt29)* - G->A substitution 3289 bp downstream of start site. The following strains were used in this study:

BY828 *swip-10(vt33)* - G->A substitution 3243 bp downstream of start site

BY1010 *swip-10(tm5915)* - 339 bp deletion (bp 31-370 from start) generated by Shohei Mitani

The following lines were acquired from the Caenhorhabditis Genetics Center (U. Minnesota), the National Bioresource Project, or the noted lab by request:

cat-2(tm2261)
LX703 *dop-3(vs106)*
RM2702 *dat-1(ok157)*
MT6308 *eat-4(ky5)*
KP4 *glr-1(n2461)*
RB1808 *glr-2(ok2342)*
glr-2(tm669)
glr-4(tm3239)
glr-5(tm3506)
glr-6(tm2729)
glr-7(tm2877)
VM487 *nmr-1(ak4)*
nmr-2(tm3285)
mgl-1(tm1811)
mgl-2(tm355)
mgl-2(tm355); mgl-1(tm1811) – Avery Lab
mgl-3(tm1766)
ZB1106 *glt-3(bz34); glt-1(ok206)* – subsequently outcrossed
RB2185 *glt-4(ok2961)*
ZB1098 *glt-4(bz69)*
ZB1099 *glt-5(bz70)*
RB1615 *glt-5(ok1987)*
glt-6(tm1316)
glt-7(tm1641)
OS2649 *hlh-17(ns204)* – Shaham Lab
OS2659 *hlh-17(ns204) hlh-31(ns217) hlh-32(ns223)* – Shaham lab
OS1914 *nsIs105*(phlh-17:GFP) – Shaham Lab
OS1917 *nsIs108*(pptr-10:mRFP) – Shaham Lab
TQ800 *lite-1(Xu7)* - Xu Lab
TQ733 *XuIs14*(pdat-1:GCaMP, pdat-1:dsRed2) – Xu lab
VPR128 *vprIs128* (phlh-17:dsRed2)

Genetic Crosses

Crosses were performed using publically available integrated fluorescent reporter strains to mark chromosomes *in trans*. Single worm PCR were performed to confirm the presence of the indicated mutation. For all deletions, we used a three primer multiplex strategy that produces PCR amplicons with 100-200 bp difference between N2 and mutant. This was highly effective in

eliminating preferential amplification of a lower molecular weight species. In all cases, a synthetic heterozygous control was utilized to ensure that heterozygous clones could be identified within that experiment. All PCR reactions were performed with Platinum PCR Supermix (Life Technologies).

The following strains were generated by cross:

BY890 *eat-4(ky5); swip-10(vt29)*

PCR genotyping of *eat-4(ky5)* was performed using the following primers:

5' sense – gtgactgaaaagaaggggcgttt

3' antisense – TCTCCATGACACTAAGCTCATCTATTGTC

inner antisense – GCACCAGTTGCAGATGCAGC

BY891 *eat-4(ky5); swip-10(vt33)*

BY1103 *glr-1(n2461); swip-10(vt29)*

n2461 was determined by Sanger sequencing of PCR amplicons generated by:

sense - ggagttttcagGAGCAAATCTCAACAG

antisense- CCGAGTGCAGCCAACATTGAAAT

BY1102 *glr-2(ok2342); swip-10(vt29)*

PCR genotyping of *glr-2(ok2342)* was performed using the following primers:

5' sense – gcgaaATGAATAAGAACCTACTAGTATTCGGA

3' antisense – CTTCGTCTGATGGTGCctgagatt

inner antisense – tccacacaaaagtgaatcatatgcctatttg

BY919 *glr-4(tm3239); swip-10(vt29)*

PCR genotyping of *glr-4(tm3239)* was performed using the following primers:

5’ sense - TACCGATGTATGAACGGATgtaagtcac

3’ antisense – GCTTTTTCAGAAGGCGGAGGG

inner antisense – CTCGTCGATCTCTCCACCATTTATTTTTTAGT

BY926 *glr-5(tm3506); swip-10(vt29)*

PCR genotyping of *glr-5(tm3506)* was performed using the following primers:

5’ sense – GAACTTCTCATGCTGCACAGCAC

3’ antisense – GAATTGCATTGTCGATCCTCCGC

inner antisense – ACCAGGTAAAATACCCACCACGTAC

BY1032 *swip-10(tm5915) glr-6(tm2729)*

Recombinant clones were screened via PCR using the following primers:

5’ sense- GAAGAGCTTGGAAATCAAACTGAGTACAAC

3’ antisense – CCAAGAGCGAGGAGAAGAAACAAAC

inner antisense – CCATTGGATCCAAGAACAACGTTGC

BY1031 *swip-10(tm5915) mgl-1(tm1811)*

Recombinant clones were screened via PCR using the following primers:

5’ sense – GCAGCAGTAGTAGGTGGTAGTTATAGTTCTGTGTCTG

3’ antisense – gcggttgttccaaatccagatccagaaaattacatt

inner antisense – gctgaatgactggagtttctgaactgatgacgc

BY942 *mgl-2(tm355); swip-10(vt29)*

PCR genotyping of *mgl-2(tm355)* was performed using the following primers:

5’ sense – CTGATGGATGGGCTGATAGAAATGATGTT

3’ antisense - CTTCTTTTGAAACCGCGAACTGGC

inner antisense – cctaccgtttgattcatgaactttcagg

BY943 *mgl-3(tm1766); swip-10(vt29)*

PCR genotyping of *mgl-3(tm1766)* was performed using the following primers:

5’ sense – ggtcttgtagctctaacttcggaggg

3’ antisense – CCAATTCGGTATGTCCTTCAGCTACA

inner antisense – TGCAGGTTGTCTGGTGGAACAAC

BY914 *nmr-1(ak4); swip-10(vt29)*

PCR genotyping of *nmr-1(ak4)* was performed using the following primers:

5’ sense – GTGATCGAGATAGTGTAGATGCTGAATGG

3’ antisense – CCTATTCCATAGGCACTTCTTCCAAACA

inner antisense – ggggttgaagatgcagtaaaaatttttgg

BY923 *nmr-2(tm3285); swip-10(vt29)*

PCR genotyping of *nmr-2(tm3285)* was performed using the following primers:

5’ sense – GGTGATCCATATTGGGACAATGGGA

3’ antisense – CCCAATCACAGATGGATCCctgaa

inner antisense – CAGAGTGACCACTTTCACGTGAAAC

BY1052 *swip-10(tm5915) glr-6(tm2729) mgl-1(tm1811)* -

swip-10(tm5915) glr-6(tm2729) was recombined with *mgl-1(tm1811)*

BY1053 *glr-4(tm3239); swip-10(tm5915) mgl-1(tm1811)*

BY1054 *glr-4(tm3239); swip-10(tm5915) glr-6(tm2729)*

BY1097 *glr-4(tm3239); swip-10(tm5915) glr-6(tm2729) mgl-1(tm1811)*

BY1068 *glr-4(tm3239); glr-6(tm2729) mgl-1(tm1811)* –

swip-10(tm5915) was recombined with wild type *swip-10(+)* on LGX using BY1097

BY1101 *dat-1(ok157); glr-4(tm3239)*

PCR genotyping of *dat-1(ok157)* was performed using the following primers:

5’ sense - gcaatcacaacttggggaag

3’ antisense –aaagtggaagacacctatgttcatagc

inner antisense - ggttttccagatttgcagga

BY1088 *dat-1(ok157); glr-6(tm2729)*

BY1089 *dat-1(ok157); mgl-1(tm1811)*

BY920 *cat-2(tm2261); glt-1(ok206)*

PCR genotyping of *glt-1(ok206)* was performed using the following primers:

5’ sense - agttcatttttcagATGGTATCCTGGATAAGG

3’ antisense - gaaaacaaaacCGATTGAGTGAGATCTGG

inner antisense – GAGAGAACTCATGATAAGTGGGAGAATCAT

BY931 *cat-2(tm2261); glt-3(bz34)*

PCR genotyping of *glt-3(bz34)* was performed using the following primers:

5’ sense – AATCAAGCCGTCTCGTGTTCGC

3’ antisense – tgagagcattacCTGCATTGCATTC

inner antisense – gcgcctgatatttcgcagtttcc

BY927 *cat-2(tm2261); glt-4(bz69)*

PCR genotyping of *glt-4(bz69)* was performed using the following primers:

5’ sense – CCGATCGCAGAAAATCTGCCTGAAG

3’ antisense – ctgcaaaaaaagtttgtttcaaaggaaatagc

inner antisense – CCCATCAAACGATGCAACTCTTGTCC

BY1033 *swip-10(tm5915) glt-1(ok206)*

BY1057 *glt-3(bz34); swip-10(vt29)*

BY1058 *glt-3(bz34); swip-10(tm5915)*

BY1046 *swip-10(tm5915) glt-4(bz69)*

BY1098 *dat-1(ok157); glt-1(ok206)*

BY1099 *dat-1(ok157); glt-4(bz69)*

BY1100 *dat-1(ok157); swip-10(tm5915)*

BY1056 *swip-10(tm5915) lite-1(Xu7)*

Recombinant clones were genotyped for *lite-1(Xu7)* by response to brief UV illumination and the point mutation was confirmed by sequencing of PCR amplicons generated by the following primers:

sense – gcagTCTCAAATGACATTCTTCACCTTCC

antisense – TGGAGACTCTGGTTGTTCTTGATATCAA

BY1059 *XuIs14*(pdat-1:GCaMP, pdat-1:dsRed2)*; lite-1(Xu7)*

BY1060 *XuIs14; swip-10(tm5915) lite-1(Xu7)*

BY1061 *XuIs14; dat-1(ok157); lite-1(Xu7)*

swip-10 promoter: GFP manipulations

All PCR reactions performed for subcloning or germline transformations were performed using KAPA HIFI Hotstart Taq Polymerase. Additionally, PCR products and plasmids injected for germline transformation were purified via a Uprep column (Genesee Scientific) before generation of an injection mix.

Injection mixes were spun at max speed (13000 rpm) in a microcentrifuge prior to microinjection. All injection mixes were buffered to at least 100 ng/µl final concentration with pBSKII(-)(if necessary).

Promoter Fusions

Determination of *swip-10 cis* elements were performed using overlap PCR fusion. Three different fragments were assayed for their ability to drive the expression of a flourophore.

Minimal 5' promoter:

A fragment spanning -738 to the ATG start site was fused to CFP and injected at 50 ng/µl onto a *lin-15(n765ts)* background with a *lin-15(+)* rescue plasmid (pJM23) to generate *vtEx83, vtEx84*, and *vtEx85*.

5th Intron (Internal Promoter):

A fragment spanning 1013 to 2504 downstream of the ATG start site was fused to GFP and injected at 50 ng/µl onto a *lin-15(n765ts)* background with pJM23 to generate *vtEx191* and *vtEx192*. This fragment was also coinjected with p_{dat-1}:mCherry and pJM23 onto a *lin-15(n765ts)* background to generate *vtEx182-184*.

Full length Promoter (containing all putative cis elements):

A fragment spanning -738 upstream to 2504 downstream of the ATG start site was fused to CFP and injected at 50 ng/µl onto a *lin-15(n765ts)* background with p_{dat-1}:mCherry(20 ng/µl) to generate *vtEx94, vtEx95, vtEx96,* and *vtEx97*

swip-10 rescue experiments

A full length 4.3 Kb genomic fragment from -738 to 3569 downstream of the ATG start site was amplified and injected at 20 ng/µl onto *swip-10(vt29)* and *swip-10(vt33)* with $p_{unc-122}$:GFP to generate *vtEx74-75* and *vtEx76-78* respectively. To pursue functional studies related to the cell autonomous function of *swip-10*, we chose to use the *swip-10* cDNA exclusively owing to the presence of a large internal promoter. Total RNA was harvested from asynchronous N2 animals and first strand cDNA was generated using Superscript III First-Strand Synthesis System (Life Technologies). We amplified a 1.6 kB PCR product using the following primers: ATGCTTTTTCATTTTCTAATCGCTA(S) and TTAACATTTCAAAGCTTTCTT(A). This fragment was TA cloned into PCR8/GW/TOPO for further manipulations.

Rescue constructs that allow for cell autonomous expression of *swip-10* were generated in one of four backbones pRB1106-pRB1109, which contain unique restriction sites to allow for subcloning of either promoters, open reading frames, or 3' UTRs. In all cases an *unc-54* UTR was used at the end of tagged *swip-10* cDNA.

We fused GFP to the C-Terminus of the *swip-10* cDNA and subcloned this PCR fragment into pRB1106(*dat-1* promoter) using AscI and KpnI as 5' and 3' restriction sites to generate pRB1157. In all cases, insertion of the fragment and fidelity of the cassette was confirmed by sequencing. To express *swip-10* in glia, we amplified a 315 bp fragment of the *ptr-10* promoter from OS1917 worm lysate and subcloned it into pRB1157 using SphI and AscI as 5' and 3' sites to

generate pRB1158. To express *swip-10* in CEPsh glia, we amplified a 2.6 Kb product from p_{hlh-17}:GFP (kind gift of Shai Shaham) and subcloned it into pRB1106 using FseI and AscI as 5' and 3' sites to generate pRB1159. A 1.5 Kb fragment of the *swip-10* internal promoter was subcloned into pRB1106 using FseI and AscI as 5' and 3' sites to generate pRB1160. For expression of *swip-10* in the OL/ILso, we amplified a 2.1 Kb fragment of the *itx-1* promoter and subcloned it into pRB1106 using FseI and AscI as 5' and 3' sites. For expression of a lactamase dead version of *swip-10*, His residues at amino acid positions 351,353, 356, 405, and 470 were mutated to Serine via site-directed mutagenesis (Quickchange II XL – Agilent Technologies) in the pRB1158 backbone to generate pRB1162. These constructs were used to generate the following strains:

BY1004-1006(*vtEx159-161)* – pRB1157 was injected at 80 ng/µl onto *swip-10(vt29)* with p_{elt-2}:GFP(10 ng/µl), p_{dat-1}:mCherry(10 ng/µl), and $p_{unc-122}$:RFP(40 ng/µl).

BY1076-BY1078 – pRB1158 was injected at 80 ng/µl onto *swip-10(vt29)* with $p_{unc-122}$:RFP(50 ng/µl) to generate *vtEx200-vtEx202*.

BY1079-BY1081 – pRB1158 was injected at 80 ng/µl onto *swip-10(tm5915)* with $p_{unc-122}$:RFP(40 ng/µl) to generate *vtEx203-vtEx205*.

BY1090-BY1092 – pRB1158 was injected at 80 ng/µl onto *swip-10(vt33)* with $p_{unc-122}$:RFP(40 ng/µl) to generate *vtEx206-vtEx208.*

BY1093-BY1095 – pRB1162 was injected at 80 ng/µl onto *swip-10(vt29)* with $p_{unc-122}$:RFP(50 ng/µl) to generate *vtEx209-vtEx211*.

BY1104-BY1106 – pRB1159 was injected at 80 ng/µl onto *swip-10(vt29)* with $p_{unc-122}$:RFP(50 ng/µl) to generate *vtEx212-214*.

BY1107-BY1109 – pRB1160 was injected at 80 ng/µl onto *swip-10(vt29)* with $p_{unc-122}$:RFP(50 ng/µl) to generate *vtEx215-217*.

C. elegans Assay for Swip

In both batch and single worm analyses, we generated synchronous populations of these strains by hypochlorite treatment and harvesting arrested L1 animals. Early-mid stage L4 animals were identified by characteristic morphology and used for behavior as N2 animals show some stochastic Swip and quiescence bouts during the last larval molt. For automated analysis, single L4 hermaphrodites were placed in 20µL water or drug in a single well of a Pyrex Spot Plate (Fisher catalog number 13-748B), and 10 minute movies (uncompressed AVI format) of their swimming behavior were created and analyzed as described previously (Hardaway and Wang *et al.,* under review*)*. For testing behavioral responses to elevated osmolarity, 100 mM sucrose was dissolved in water immediately prior to testing.

C. elegans assay for Basal Slowing Response

Assays were performed as described in Chase *et al* with some modifications (Chase, et al., 2004). We prepared food free 35 mm NGM plates and used them

for 2-3 days of testing. For the food condition, we spread a thin layer of HB101 in a “donut” fashion around the edge of 35 mm plates with the bottom of a glass test tube. Bacteria were serially diluted, spread at several different dilutions, and incubated o/n at 37 degrees. The next day, food-containing plates were selected for BSR assay based on the density of bacterial growth, which was complete (not spotty), but also textured and not overgrown. Overgrown bacterial lawns were capable of producing non-DA dependent slowing by virtue of imposing a thicker matrix for worm locomotion. We picked mid-stage L4 animals and placed them at 15 degrees o/n to generate young adult hermaphrodites. On the day of testing, strains were blinded and experiments picked single young adults, rinsed them briefly in M9 (3-4 sec) to remove food, and placed them on either a food-free plate or directly adjacent to a bacterial source on a food-containing plate. After 30 seconds, we counted the number of body bends in a 20 second interval. On each day, 5 animals were scored in both conditions for each genotype. Data shown represents the cumulative average body bends over at least 3 days of experiments for two experimenters.

In vivo Ca^{2+} Imaging

Calcium imaging of freely-moving worms was performed on the CARIBN (Calcium Ratiometric Imaging of Behaving Nematodes) system as described previously (Piggott, Liu, Feng, Wescott, & Xu, 2011). The CARIBN system allows for the imaging of freely-behaving worms on the surface of an NGM plate in an open environment without any physical constraint. Briefly, 4 spots of freshly-

grown food (OP50 bacteria) were spotted on the surface of an NGM plate, with each one containing 2 µl of OP50 culture spaced 0.5~0.7 mm apart. Single young adult animals were picked into a food-free area of the plate. Images were acquired at 22Hz with 15 ms of exposure time per frame for 4 min. As it has been predicted that the mechanical stimulation of DA neuron dendrites produces an increase in DA neuron excitability, we recorded calcium transients from CEP soma during this behavior. G-CaMP/DsRed ratio was calculated as previously described (Piggott, et al., 2011).

Reversal Analysis and Speed Analysis

Assays were performed similar to (Zheng, Brockie, Mellem, Madsen, & Maricq, 1999). Briefly, L4 worms were picked to a fresh plate and incubated at 12-15 degrees o/n until worms reached the young adult stage. We avoided animals that were actively laying eggs in these analyses, preferring the 3-4 hours prior to active egg-laying bouts similar to the BSR assays. Food-free NGM plates were prepared fresh and used within a week. Plates containing precipitate were not used. We did not corral the animals using copper or fructose as these reagents can generate reversals that would be captured by the recording. Immediately prior to recording, plates containing young adults were placed at room temperature and allowed to acclimate to the ambient environment. For recordings, individual young adults were picked using an eyelash pick, rinsed briefly in a well containing 200 µl of M9 (not water) to remove food from the animal, and then placed on the food free NGM plate. Using this rinse method,

each worm only swims for <5 seconds. Assays using rinse of an entire plate or plate area yielded more inconsistent results. We picked as many animals in this way for 2 minutes (normally 10 worms) and then began a recording that lasted for seven minutes. For the recordings, the plate was illuminated with an LED illuminator passed through a housing unit containing a mirror and a polarizing filter beneath a base plate. The illuminator was placed on a camera stand beneath video recording components consisting of an AVT Stingray F-504B CCD Monochrome Camera and adjustable Nikon Zoom lens with C-mount adapter (MBF Biosciences-Williston, VT). Videos were recorded using the WormLab Image Capture module (MBF Biosciences-Williston, VT) using the native resolution 2456 X 2058 at 7.5 frames per second (fps). On average the field size for recording was 1.6 cm X 1.2 cm and the resolution <10 μM/pixel. We analyzed these videos using WormLab's tracking and analytical plugins – most notably speed and reversal. Proper head/tail and track assignment was validated by hand using available features in Wormlab.

Confocal Microscopy

Confocal microscopy of transgenic worm promoter fusions were performed using either a Zeiss LSM 510 or 710 confocal microscope and LSM or Zen capture software. Worms were immobilized using 20 mM Levamisole with 0.1% Tricaine in M9 on a fresh 2% agarose pad and sealed with 1 mM cover glass and wax.

Amino acid level measurements in *swip-10*

Worm pellets were homogenized, using a tissue dismembrator, in 100-750 ul of 0.1M TCA, which contains 10^{-2} M sodium acetate, 10^{-4} M EDTA, 5ng/ml isoproterenol (as internal standard) and 10.5 % methanol (pH 3.8). Samples were spun in a microcentrifuge at 10000 g for 20 minutes. The supernatant is removed and stored at –80 degrees. The pellet is saved for protein analysis. The supernatant is then thawed and spun for 20 minutes. Amino Acids are determined by the Waters AccQ-Tag system utilizing a Waters 474 Scanning Fluorescence Detector. Ten μl samples of the supernatant are diluted with 70 μl of borate buffer to which 20 μl aliquots of 6-Aminoquinol-N-Hydroxysuccinimidyl Carbamate and 10 ul 250 pmol/ul alpha-aminobutyric acid (as internal standard) are added to form the fluorescent derivatives. After heating the mixture for 10 minute at 37°, ten μl of derivatized samples are injected into the HPLC system, consisting of a Waters 2707 Autosampler, two 510 HPLC pumps, column heater (37 degrees C) and the Fluorescence detector. Separation of the amino acids is accomplished by means of a Waters amino acid column and supplied buffers (A – 19% sodium acetate, 7% phosphoric acid, 2% triethylamine, 72% water; B – 60% acetonitrile) using a specific gradient profile. HPLC control and data acquisition will be managed by Empower 2 software. Using this HPLC solvent system, the following amino acids elute in the following order: cysteic, homocystetic, aspartic, serine, glutamate, glycine, taurine arginine, threonine, alanine, proline, GABA, cystine, tyrosine, valine, methionine, lysine, isoleucine, leucine, and phenlyalanine.

RESULTS

Analysis of the *swip-10* expression pattern

To determine the relevant site of *swip-10* function, we first determined the *swip-10* endogenous expression pattern. Analysis of conserved nucleotides (UCSC genome browser) indicated that there existed putative *cis* elements in the region just 5' of the start site and within the large 5th intron (Figure 26A). We therefore generated a series of transgenic strains expressing PCR fusion fragments spanning three different regions (A, B + C) of the *swip-10* gene fused to a flourophore and imaged them during the L4 stage (Hobert, 2002) using confocal microscopy. *swip-10*$_{A}$, consisting of a 738 bp fragment immediately 5' of the predicted *swip-10* translational start site, was sufficient to drive the expression of GFP in the hypodermal cells in the head and tail, uterine muscle, and an unidentified single cell in the nerve ring (Figure 26B). *swip-10*$_{B}$, a 1.4 Kb region within the *swip-10* large intron, was sufficient to drive expression in multiple cell types, most notably glial cells in the head and tail (arrowheads in Figure 26C), the hypodermis, the RIA neuron pair (star) and other unidentified head cells. *swip- 10*$_{C}$, a 3.2 Kb fragment that spans from the A fragment to the end of the B fragment, was sufficient to drive expression of GFP in many of the aforementioned sites, including a robust expression in glial cells and motor neurons along the ventral nerve cord (not shown). However, we also observed weak, but detectable, expression of the *swip-10* transgene in DA neurons including the CEPs and PDEs (Figure 26D). While it's possible that some of the DA

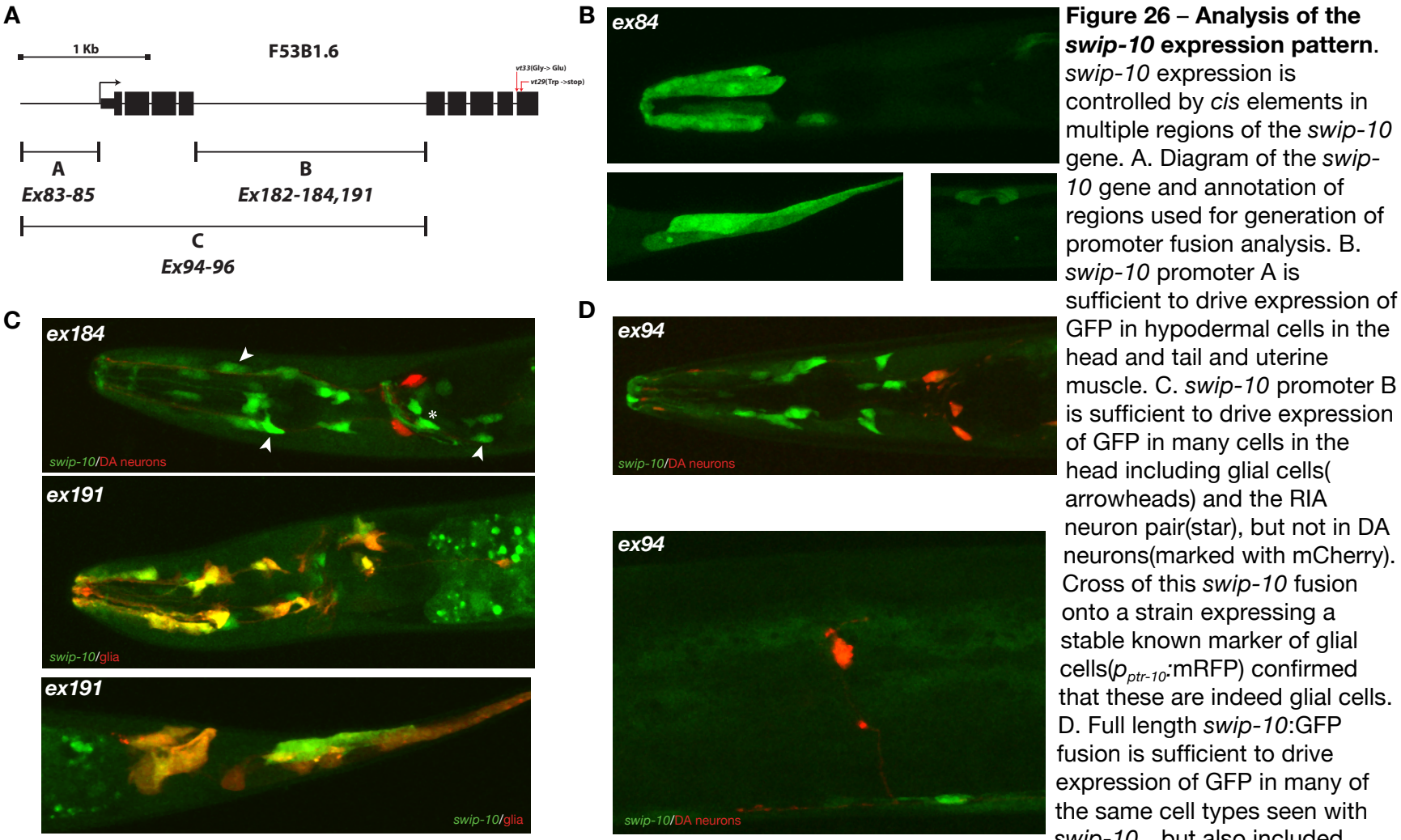

Figure 26 – Analysis of the *swip-10* expression pattern. *swip-10* expression is controlled by *cis* elements in multiple regions of the *swip-10* gene. A. Diagram of the *swip-10* gene and annotation of regions used for generation of promoter fusion analysis. B. *swip-10* promoter A is sufficient to drive expression of GFP in hypodermal cells in the head and tail and uterine muscle. C. *swip-10* promoter B is sufficient to drive expression of GFP in many cells in the head including glial cells(arrowheads) and the RIA neuron pair(star), but not in DA neurons(marked with mCherry). Cross of this *swip-10* fusion onto a strain expressing a stable known marker of glial cells(p_{ptr-10}:mRFP) confirmed that these are indeed glial cells. D. Full length *swip-10*:GFP fusion is sufficient to drive expression of GFP in many of the same cell types seen with *swip-10*$_B$, but also included weak expression in DA neurons(CEP and PDE) that we confirmed by coexpression of mCherry in DA neurons.

neuron expression may be an artifact of bleedthrough during confocal imaging, we believe that our choice of flourophores with very different excitation wavelengths precludes such a possibility. To confirm the expression we observed in glia, we crossed the *swip-10*$_B$ promoter fusion line to another transgenic line expressing an integrated copy of a pan glial fluorescent transgene (*ptr-10*:mRFP) (Yoshimura, Murray, Lu, Waterston, & Shaham, 2008). Imaging of both flourophores confirmed that *swip-10* expression colocalized with many *ptr-10*-expressing glial cells (middle panel in Figure 26C), though there are additional *swip-10 +/ptr-10 –* cells. Additionally, during the generation of these transgenic strains, we observed that the expression pattern of *swip-10* was regulated throughout development. We observed a strong *swip-10* expression in worm embryos and during early larval stages (Figure 27). Thus, we found that *swip-10* is highly expressed in a number of *C. elegans* tissues, including glia and DA neurons, and that this expression is coupled to the developmental stage of the animal.

Dissection of *swip-10* cell autonomy

With a *swip-10* cDNA in hand, we expressed a *swip-10* cDNA translationally fused to GFP (*swip-10*(c):GFP) under the control of cell specific promoters based on the endogenous expression pattern we observed using GFP promoter fusions. As predicted from the promoter fusion experiments, expression of a *swip-10* **genomic** fragment translationally fused to GFP led to expression in multiple cell types inconsistent with the cell specific promoter

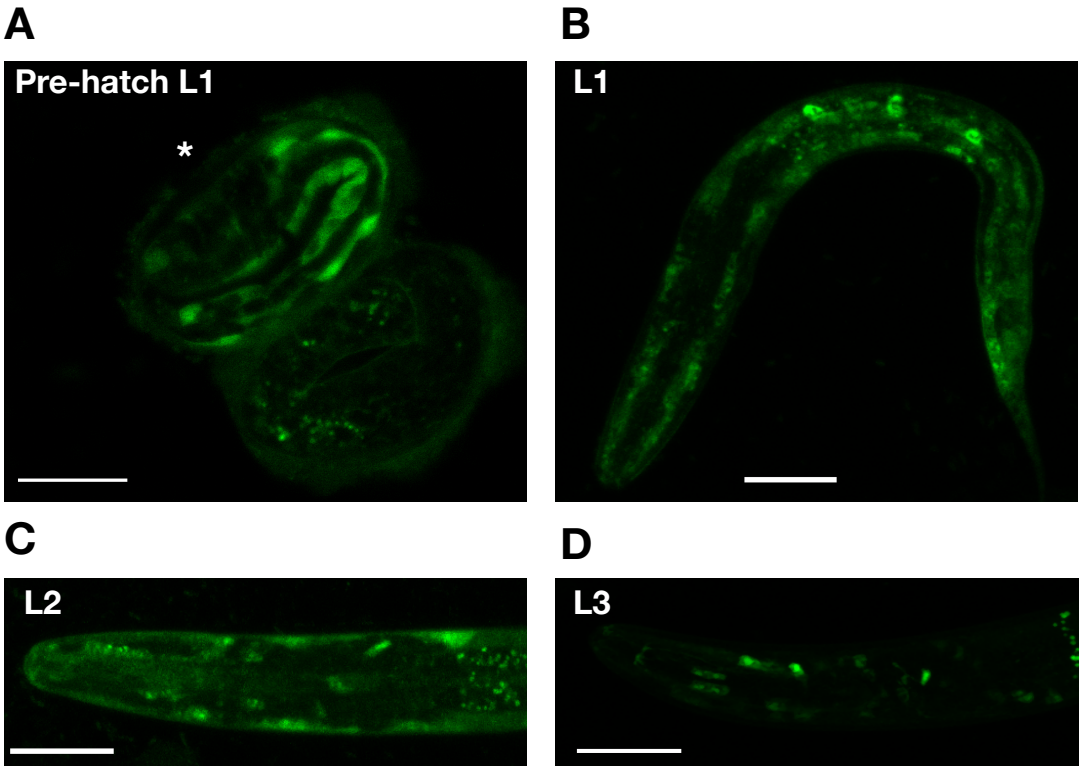

Figure 27 – Level of *swip-10* expression is regulated throughout development. *vtex191* progeny were picked at various larval stages and assayed for their *swip-10* expression pattern. **A**) *swip-10* is highly expressed in the developing embryo and the pre-hatch larval stage. Transgenic larva is indicated by the asterisk. **B**) L1 *swip-10* expression pattern. GFP is expressed faintly in the hypodermis and is not yet present in neuronal processes as previously shown **C)** Hypodermal *swip-10* expression persists in the L2 staged and cell bodies of head cells are more visible **D**) *swip-10* expression in L3 stage head. Hypodermal expression is lost and expression is restricted to cell bodies around the pharynx and nerve ring. Scale bar equal 20 μM in each of the images. Whereas the pre-hatch L1 represents a single confocal slice, panels B, C,+ D represent compressed z-stacks of the entire worm body or head.

used (i.e – expression in non-DAergic cells using the *dat-1* promoter). Having observed a dramatic expression in *C. elegans* glia, we used the *ptr-10* promoter to promote expression of *swip-10*(c):GFP and injected this transgene onto each of the *swip-10* mutant backgrounds. As seen in Figure 22, expression of *swip-10* in glia via *ptr-10* significantly rescued Swip in every allele of *swip-10*. Alternatively, we expressed *swip-10*(c):GFP specifically in DA neurons in *swip-10(vt29)* and did not observe rescue. One glial subclass, the CEPsh glia, is known to provide support for CEP DA neurons and they express a specific helix-loop-helix transcription factor known as *hlh-17* (Yoshimura, et al., 2008). Additionally, A recent report displayed that strains defective in *hlh-17* have altered dopaminergic phenotypes, including the basal slowing response (Felton & Johnson, 2011). We expressed *swip-10(c)*:GFP under an *hlh-17* promoter in the *swip-10(vt29)* strain, but did not observe rescue of Swip. Likewise, we tested *hlh-17* and *hlh-17, hlh-31, hlh-32* mutants for Swip to see if they demonstrated Swip (Yoshimura, et al., 2008), but observed that these mutants did not exhibit a significant Swip phenotype (Figure 28). Since we observed that the large 5th intron of *swip-10* was sufficient to drive GFP expression in glia, we used this promoter fragment to drive expression of the *swip-10(c)*:GFP cassette. Surprisingly, this construct failed to rescue *swip-10(vt29)*.

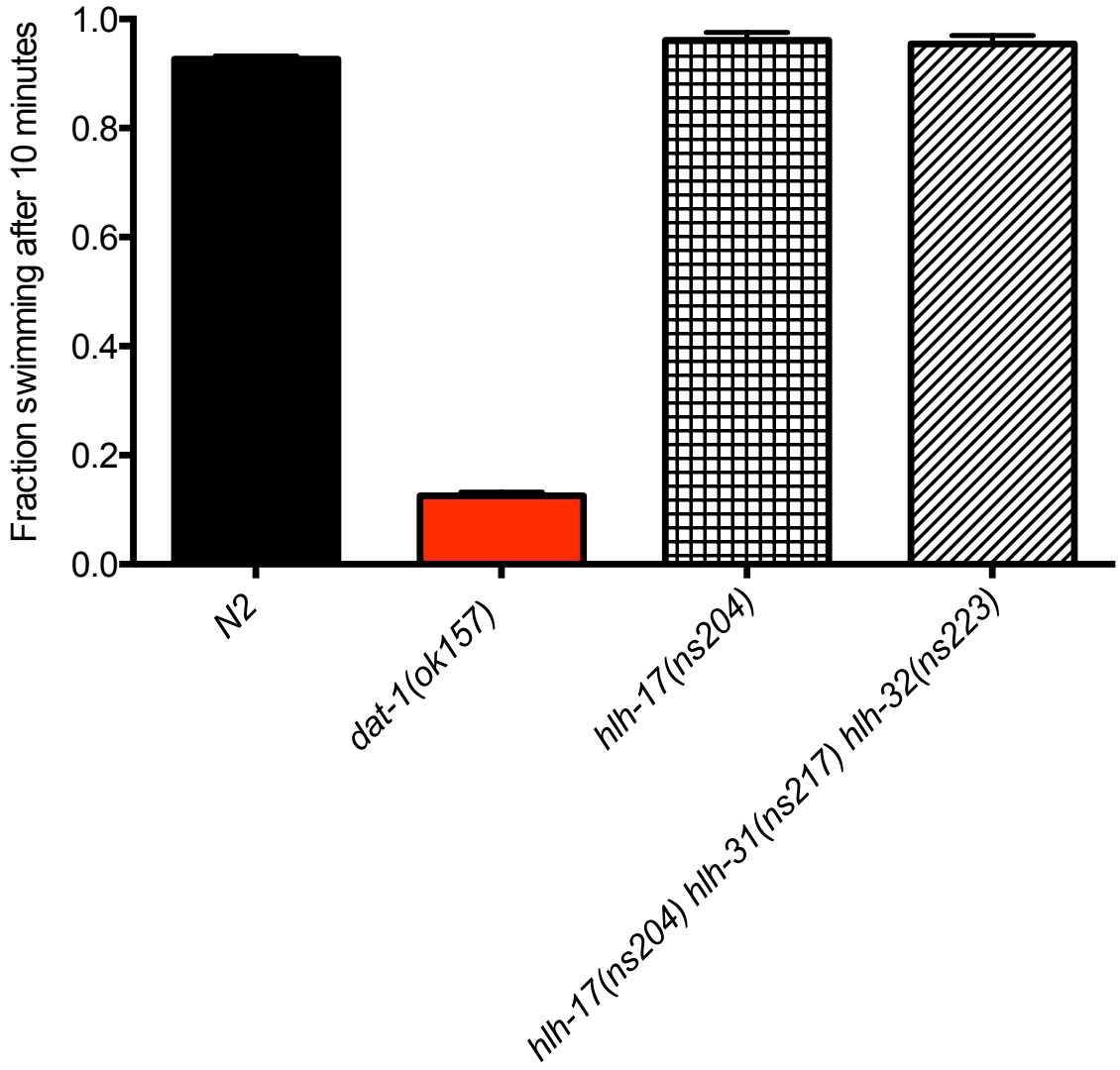

Figure 28 – Basal Swip of *hlh-17* and *hlh-17, hlh-31, hlh-32* mutants. Strains were tested by two experimenters over the course of three weeks. Each column represents the average of 48 trials tested over this period. Data were analyzed by one-way ANOVA with multiple Bonferroni post tests. No significant differences were observed between N2 and *hlh-17* or N2 and *hlh-17, hlh-31, hlh-32*.

swip-10 and its predicted metal binding residues

As we observed nearly complete rescue of the *swip-10* mutant strain with expression of the *swip-10* cDNA in glia, we sought to determine the requirement of amino acids within the metallo β-lactamase domain that are conserved throughout phylogeny. As the *vt29* and *vt33* mutations were both located proximal to these residues in the metallo β-lactamase domain, we hypothesized that these histidines are critical to *swip-10* function. We mutagenized five conserved histidines to serines in our glial expression construct and assayed its ability to rescue the *swip-10(vt29)*. We did observe a partial rescue of the *vt29* mutant, but the magnitude of this rescue was reduced relative to the histidine-containing wildtype gene (Figure 22). These data are consistent with the hypothesis that histidine-mediated metal binding is required for the activity of the *swip-10* gene.

swip-10 and DA neuron excitability

In our previous study we demonstrated that *swip-10* does not alter the function of *dat-1* as measured by uptake of the exogenous neurotoxic agent 6-OHDA and the subsequent death of the DA neurons (Hardaway, et al., 2012). With *dat-1* activity intact, we reasoned that *swip-10* likely functions in a pathway parallel of *dat-1*. We hypothesized that this pathway ultimately controls the amount of vesicular DA release. As we had also observed that *vt29* mutants display a decreased latency to paralyze and that *swip-10* functions in glia to regulate Swip, we hypothesized that loss of *swip-10* in glia results in an

increase in DA neuron excitability and an elevated rate of DA release that overwhelms endogenous *dat-1* activity present at DA neuron terminals (see Figure 53 in Discussion). To test our hypothesis, we performed *in vivo* Ca^{2+} imaging of CEP neurons expressing the calcium sensitive flourophore GCaMP and a calcium-independent flourophore dsRed2 during the BSR using the CARIBN (Calcium Ratiometric Imaging of Behaving Nematodes) system (Li, Feng, Sternberg, & Xu, 2006; Piggott, et al., 2011; Sawin, et al., 2000). As hypothesized by Sawin *et al.*, we observed that the excitability of DA neurons in wildtype animals is elevated upon entering a lawn of bacteria. Consistent with our hypothesis, we observed that *swip-10(tm5915)* animals displayed an elevated Ca^{2+} response to food, whereas the response of *dat-1* animals was similar to wildtype animals (Figure 29).

Characterization of Swip and basal slowing response in glutamate signaling gene mutants

Having demonstrated that loss of *swip-10* triggers an increase in DA neuron excitability and that *swip-10* functions in glia regulate Swip, we hypothesized that alterations in GLU signaling may underlie the increase in DA neuron excitability in *swip-10* mutants. To begin, we screened a number of strains harboring mutations in GLU signaling components including vesicular glutamate transporters (vGLUTs), plasma membrane transporters (GLTs), and glutamate

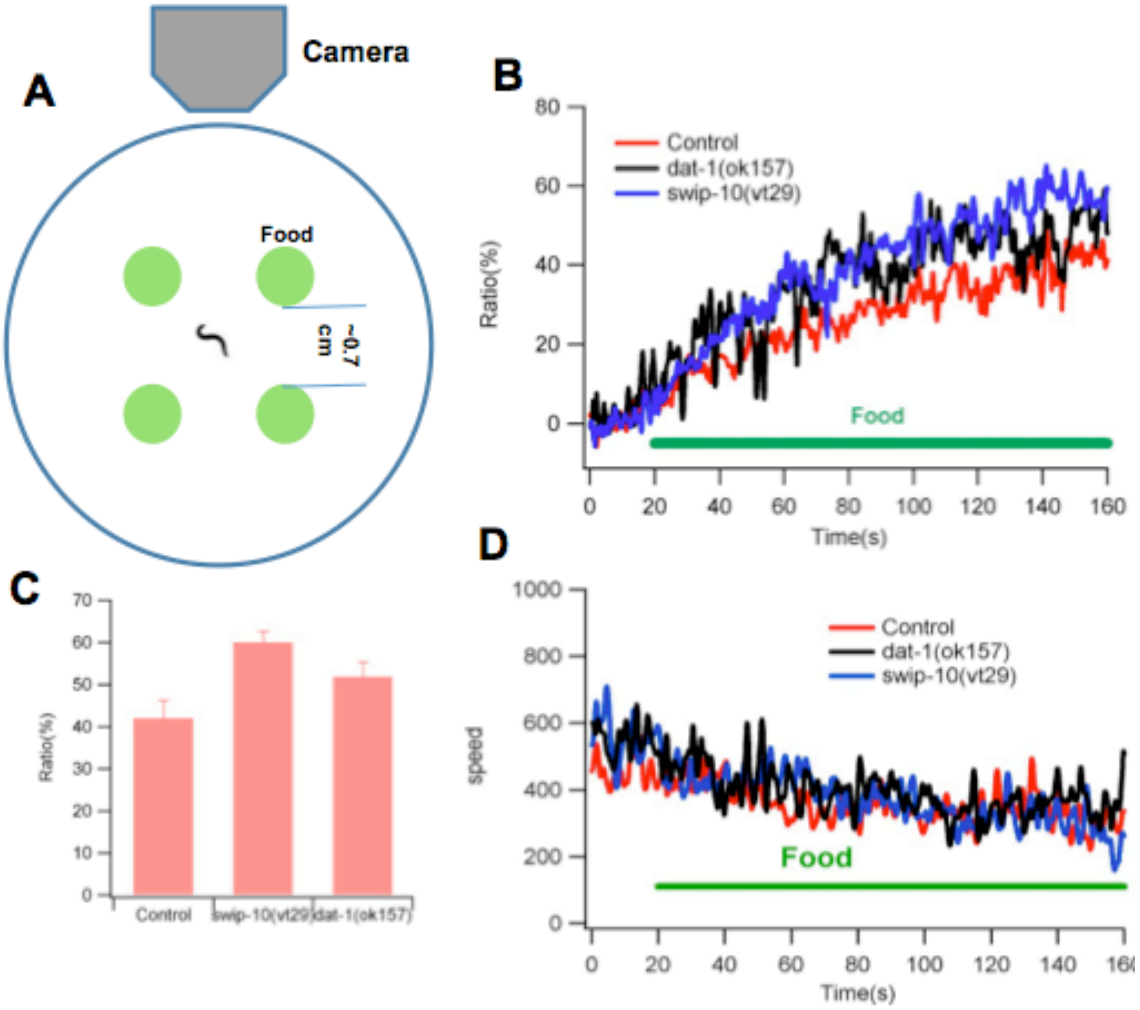

Figure 29 – *swip-10* mutation results in elevated DA neuron excitability during *in vivo* DA-dependent behavior. **A**. Schematic of BSR assay and CARIBN recording setup. See methods for details. Briefly, animals that were either wildtype , *dat-1*, or *swip-10(tm5915)* and containing an integrated GCaMP and dsRed2 transgene specifically in DA neurons and a mutation in the *lite-1* gene were placed on a plate and the fluorescence of CEP soma were recording during free movement on the plate. **B**. Average GCaMP/dsRed2 traces for wildtype, *dat-1(ok157)*, and *swip-10(tm5915)* animals(not *vt29)* during the response to a small lawn of food. **C**. Magnitude of fluorescence at 140 seconds after entering the lawn of food. Data were analyzed using a student's *t* test. *swip-10(tm5915)* animals have a significant elevation in the magnitude of their response, while *dat-1* animals do not. **D.** Average speed(μM/sec) of wildtype, *dat-1(ok157),* and *swip-10(tm5915)* animals during their response to the lawn of food. All three genotypes display a significant slowing in response to the lawn of food.

receptors (GLURs) using the Swip phenotype. Overall, we determined that the loss of glutamate signaling genes does not dramatically impact nematode swimming behavior relative to *dat-1* or mutations in other genes that we isolated in our mutagenesis screen (Hardaway, et al., 2012; P. W McDonald, et al., 2007).

Amongst the glutamate receptors (GluRs) that we assayed, we observed that although loss of *glr-2*(only *tm669* allele), *glr-4*, and *glr-5* signaling does result in a significant reduction in swimming behavior relative to N2, these mutations do not trigger dramatic Swip phenotypes (Figure 30). Similiarly, whereas *mgl-2* mutants do demonstrate some significant Swip, the penetrance of Swip is very low amongst the population of worms we assayed (Figure 31).

When we assayed strains harboring mutations in specific GLTs (Mano, Straud, & Driscoll, 2007), we found that mutations in *glt-1*, *glt-3*, and *glt-4* resulted in a highly significant Swip phenotype relative to N2 (Figure 32). Furthermore, when we assayed double mutant strains harboring mutations in both *glt-1* and *glt-3*, we observed a more penetrant Swip phenotype. These observations are consistent with the hypothesis that specific GLTs function in parallel pathways to regulate Swip penetrance. In an attempt to determine if loss of all three mutations could trigger Swip with penetrance comparable to *dat-1* and *swip-10*, we attempted to build the triple mutant strain. Unfortunately, recombinant progeny containing homozygous mutations for both *glt-1* and *glt-4* were sterile, precluding the possibility of assaying this strain. To determine if the Swip that we observed with loss of *glt-1,glt-3,* and *glt-4* was DA-dependent, we

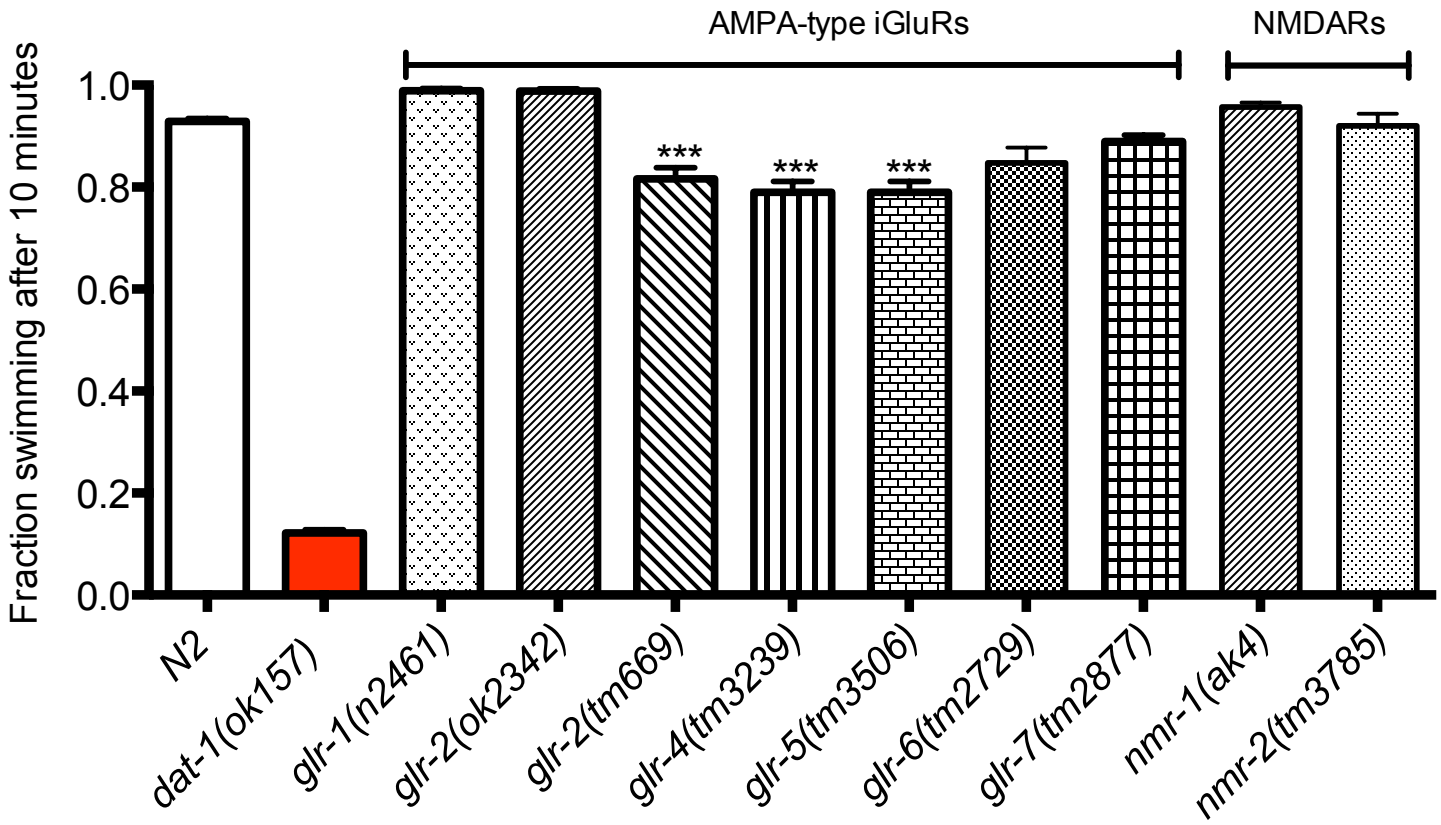

Figure 30 – Basal Swip behavior of ionotropic glutamate receptor mutants. *glr-2, glr-4*, and *glr-5* all show a significant reduction relative to N2, but not a robust Swip phenotype. Strains were tested by two experimenters over the course of three weeks. Each column represents the average of at least 48 trials tested over this period. Data were analyzed by one-way ANOVA with multiple Bonferroni post tests. *** indicate $p<0.001$.

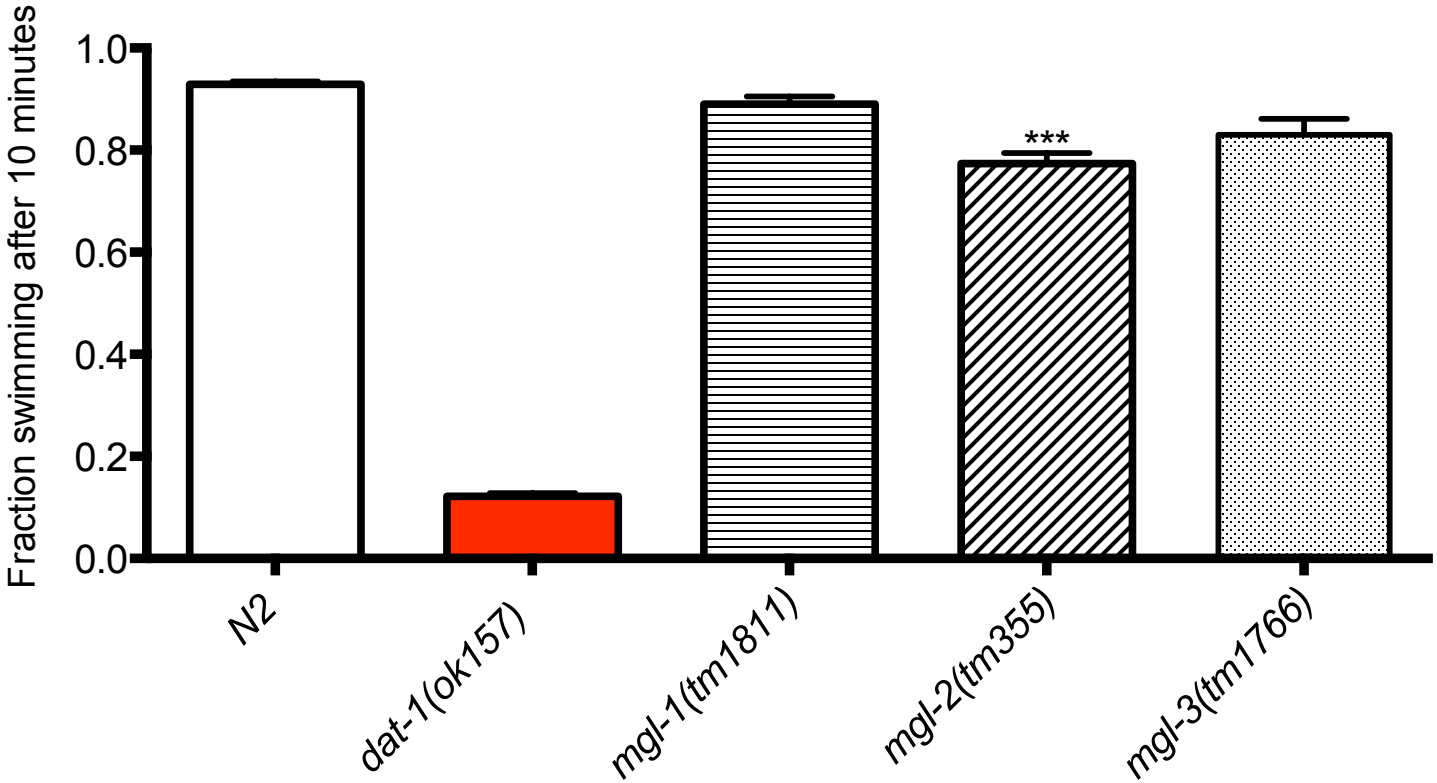

Figure 31 – Basal Swip of metabotropic glutamate receptor mutants. *mgl-2(tm355)* displayed a significant reduction relative to N2, but not a robust Swip phenotype overall. Strains were tested by two experimenters over the course of three weeks. Each column represents the average of at least 48 trials tested over this period. Data were analyzed by one-way ANOVA with multiple Bonferroni post tests. *** indicate $p<0.001$.

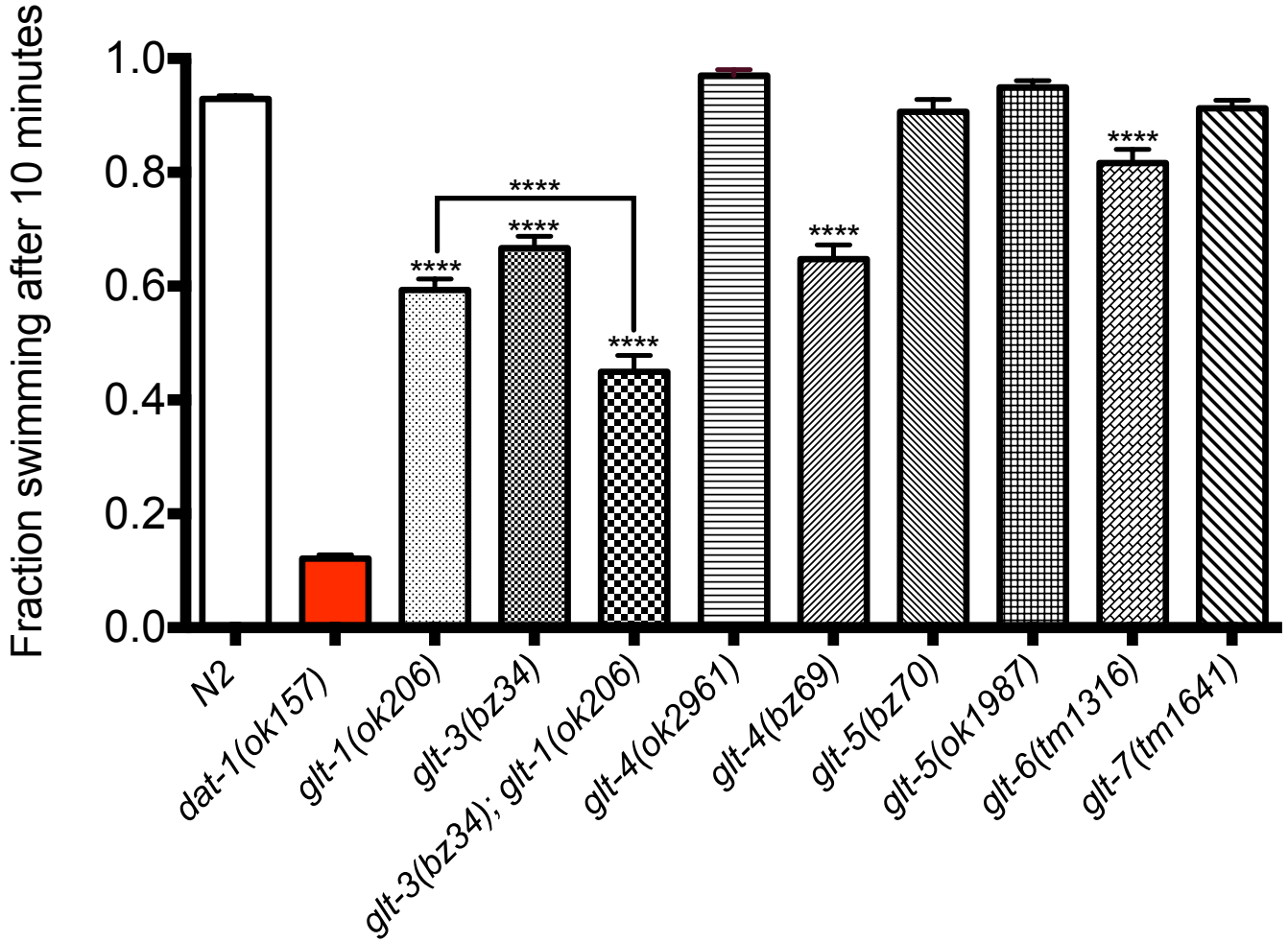

Figure 32 – Basal Swip behavior of glutamate transporter mutants. Loss of *glt-1*, *glt-3*, *glt-4,* and *glt-6* trigger a significant reduction in swimming behavior. Loss of *glt-3* and *glt-1* together can significantly enhance the amount of Swip. Strains were tested by two experimenters over the course of three weeks. Each column represents the average of at least 48 trials tested over this period. Data were analyzed by one-way ANOVA with multiple Bonferroni post tests. *** indicate $p<0.001$.

crossed these mutants to *cat-2* and assayed double mutant progeny for Swip. As seen in Figure 33, the loss of DA biosynthesis via the *cat-2* allele, similar to *dat-1* and *swip-10*, fully restored swimming behavior in these three lines. To further validate the Swip we observed in an unbiased way for *glt-1*, *glt-3*, and *glt-4*, we analyzed the kinetics of swimming behavior in these strains using SwimR. We observed a robust reduction in average swimming frequency for *glt-1*, but the reductions we observed for *glt-3* and *glt-4* were limited to specific times during the recording (Figure 34). These data suggest that Swip penetrant animals of these genotypes may have altered swimming kinetics such that in *glt-4* they paralyze and reverse and in *glt-3* they paralyze late during the 10 minute recording**.** Thus, loss of glutamate transport through *glt-1, glt-3*, and *glt-4* triggers a DA-dependent Swip phenotype.

To further enhance our understanding of how mutations in glutamate signaling pathways might impact DA signaling. We screened these mutants and alleles of *swip-10* for alterations in the BSR (Allen, et al., 2011; Chase, et al., 2004; Sawin, et al., 2000). Previously, alterations in BSR had been described as an all-or-none effect and as a readout of decreased extrasynaptic DA (Chase, et al., 2004; Kindt et al., 2007; Sawin, et al., 2000). Based on the partial penetrance and subtle Swip phenotype we observed previously, we hypothesized that alterations in DA signaling triggered by loss of glutamate signaling components and Swip-causing mutations may have more graded effects on BSR. Therefore, we analyzed the BSR phenotype of multiple strains as a percent change from

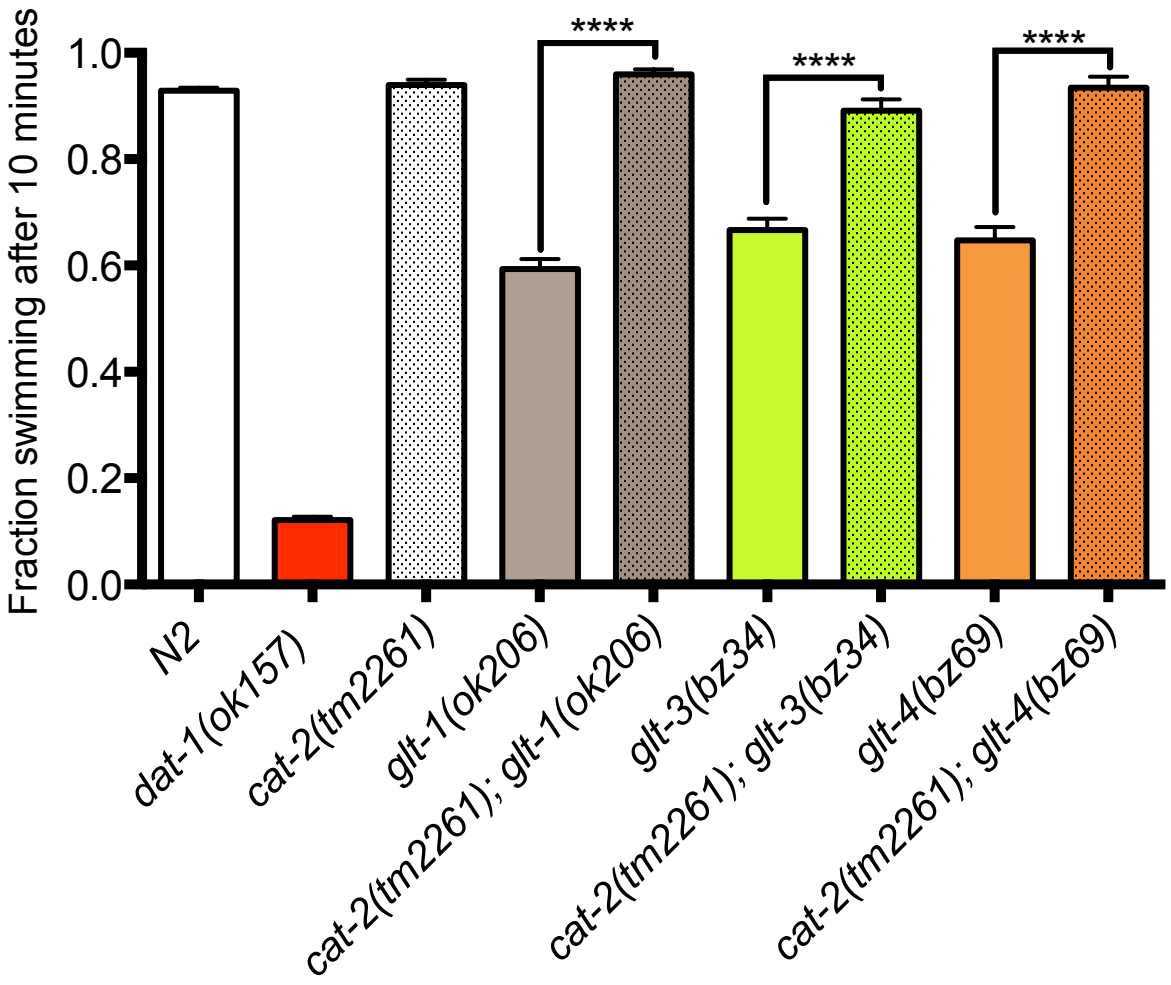

Figure 33 – *cat-2* suppression of Swip in glutamate transporter mutants. Double mutant strains were constructed as described in the Methods. Strains were tested by two experimenters over the course of three weeks. Each column represents the average of at least 48 trials tested over this period. Data were analyzed by one-way ANOVA with multiple Bonferroni post tests. *** indicate $p<0.001$.

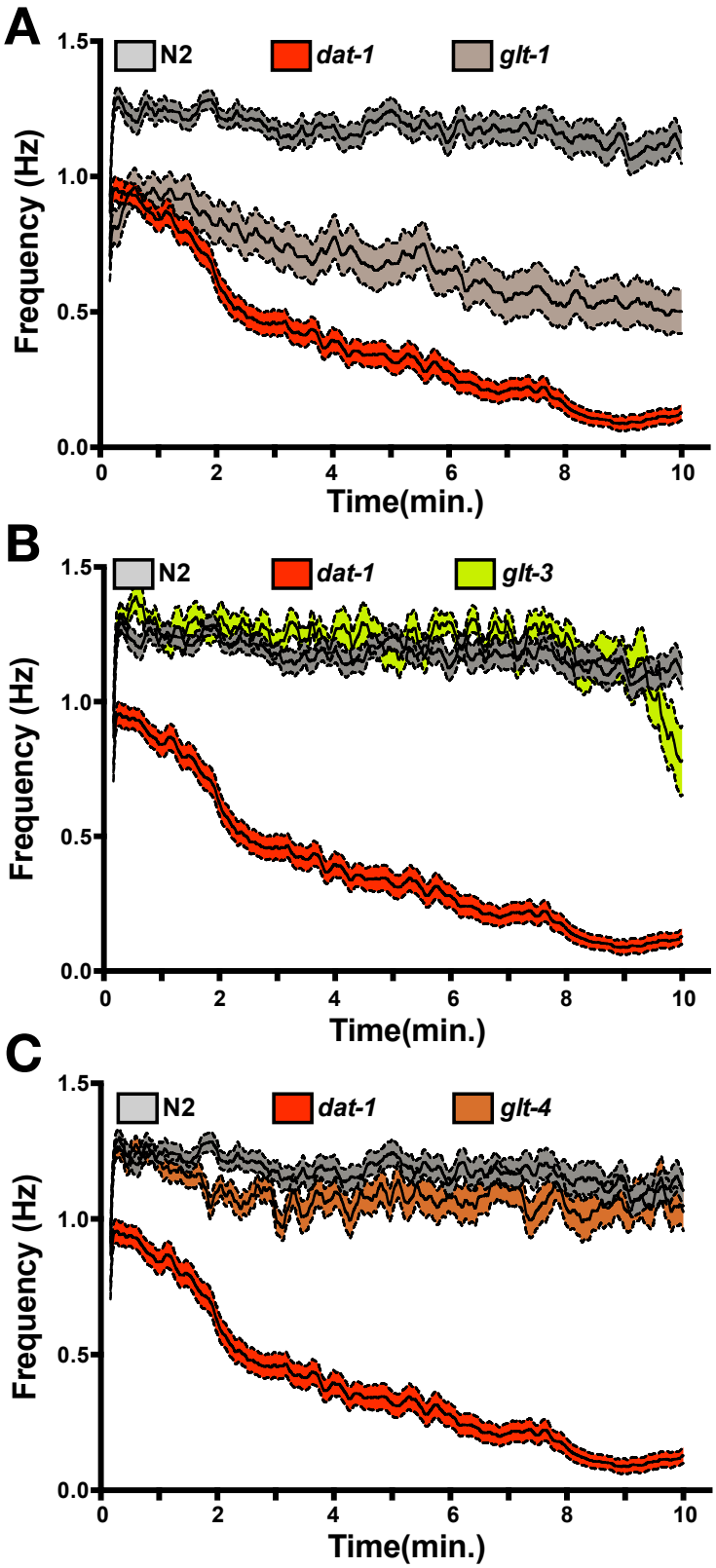

Figure 34 - Thrashing analysis of glutamate transporter mutants *glt-1, glt-3* and *glt-4*. A. Loss of *glt*-1 results in a significant reduction in average swimming frequency with points of significance in minutes 1-10. **B.** Loss of *glt*-3 triggers a decrease in swimming frequency in the final minute of the recording. **C.** Loss of *glt-4* results in a decrease in average swimming frequency with point of significance in the 2nd minute. For **A, B + C,** Single worm recordings were performed as described in the methods. Average traces represent at least 30 individual worm tracks. Data were analyzed by two-way ANOVA with multiple Bonferroni post tests at each time point.

their baseline locomotory on food- free plates. Consistent with previous reports, we observed a significant reduction in the magnitude of BSR with a loss of DA signaling (Figure 35). Surprisingly, there was a difference amongst two alleles of *cat-2* that we tested. While the previously tested *cat-2(e1112)* allele demonstrated virtually no BSR, we found that the unpublished *cat-2(tm2261)* allele exhibited some BSR, albeit at a reduced magnitude relative to N2. This BSR persists in spite of the fact that this strain has highly reduced levels of DA as measured by HPLC (Hardaway, et al., 2012). Consistent with Chase *et al*., we observed a blunted BSR in the *dop-3* mutant strain relative to N2. Interestingly, we observed a significantly blunted BSR in the *dat-1(ok157)* and *swip-10(vt33)*alleles, but not in the *swip-10(vt29)* alleles. We attribute this difference in *swip-10(vt29)* to a bimodal distribution of responders, where some *swip-10(vt29)* animals demonstrated no apparent BSR and other animals exhibited an exaggerated BSR which resulted in a wider standard deviation for this strain. Assays of this strain were also confounded by the fact that this strain moved at a slower rate on food-free plates relative to N2 (see later results).

Assays of BSR in ionotropic GLUR mutants revealed that, as in the Swip phenotype, signaling through ionotropic GLURs is largely dispensable for the BSR (Figure 36). The exceptions to this were *glr-1* and *glr-4*, that, when lost, result in a decrease and increase in the magnitude of the BSR relative to N2 respectively. Similar to Swip, we observed no alterations in the BSR of metabotropic GLU signaling mutants (Figure 37). Assay of BSR in GLT mutants

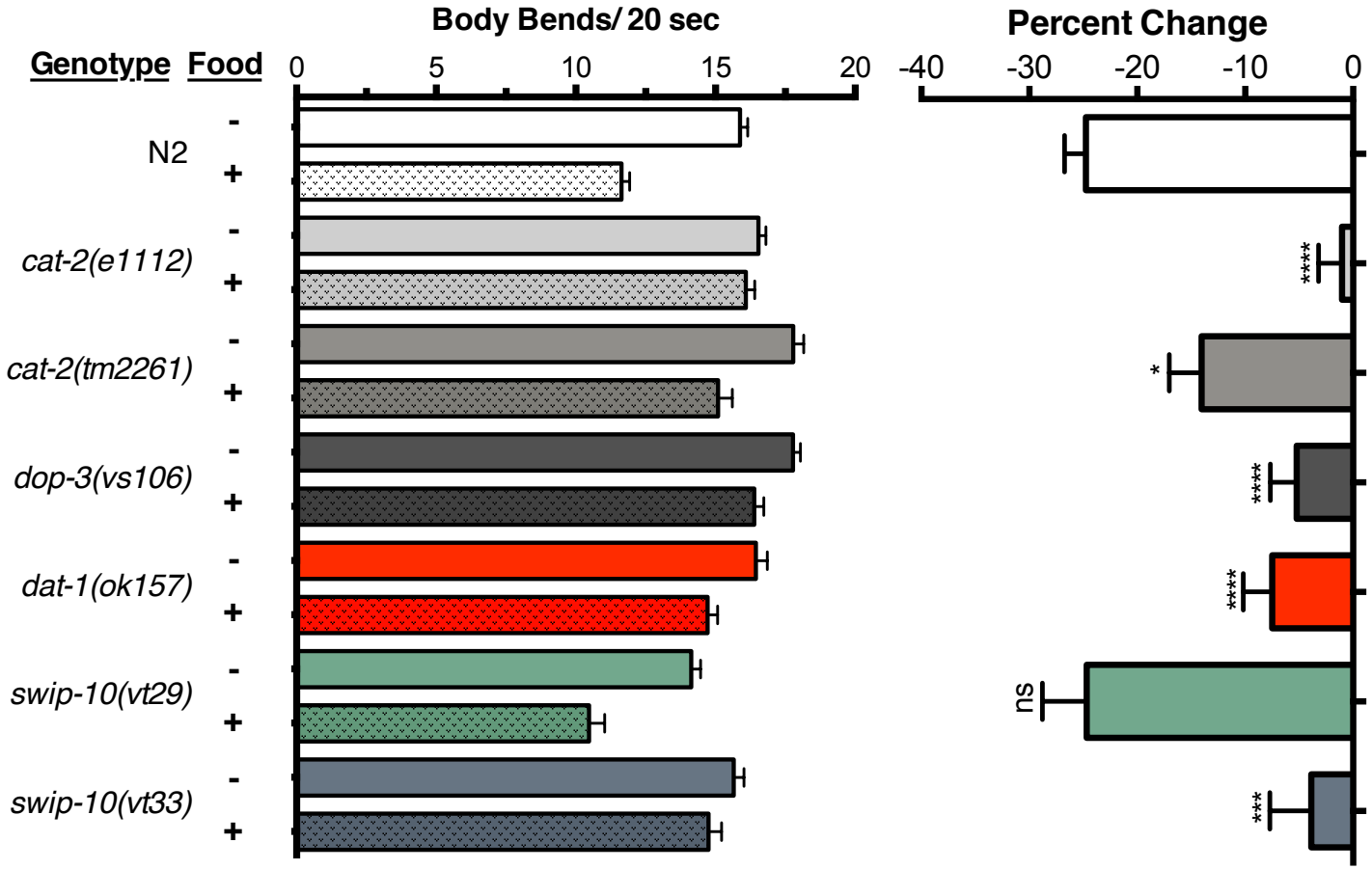

Figure 35 – Basal slowing response of *swip-10* alleles and *dat-1*. Assays were performed as described in the methods. Each column represents the average locomotory behavior of at least 30 animals tested over the course of three independent test days by two experimenters. Data is plotted as the raw counts over a 20 second interval on and off food and as the average percent change in body bends/20 sec for each animal tested over this period. Data were analyzed by one way ANOVA with Dunnet's post tests to the N2 strain. Both alleles of *cat*-2, dop-*3(vs106)*, *dat-1(ok157)*, and *swip-10(vt33)* demonstrated a significant reduction in the amount of slowing relative to N2.

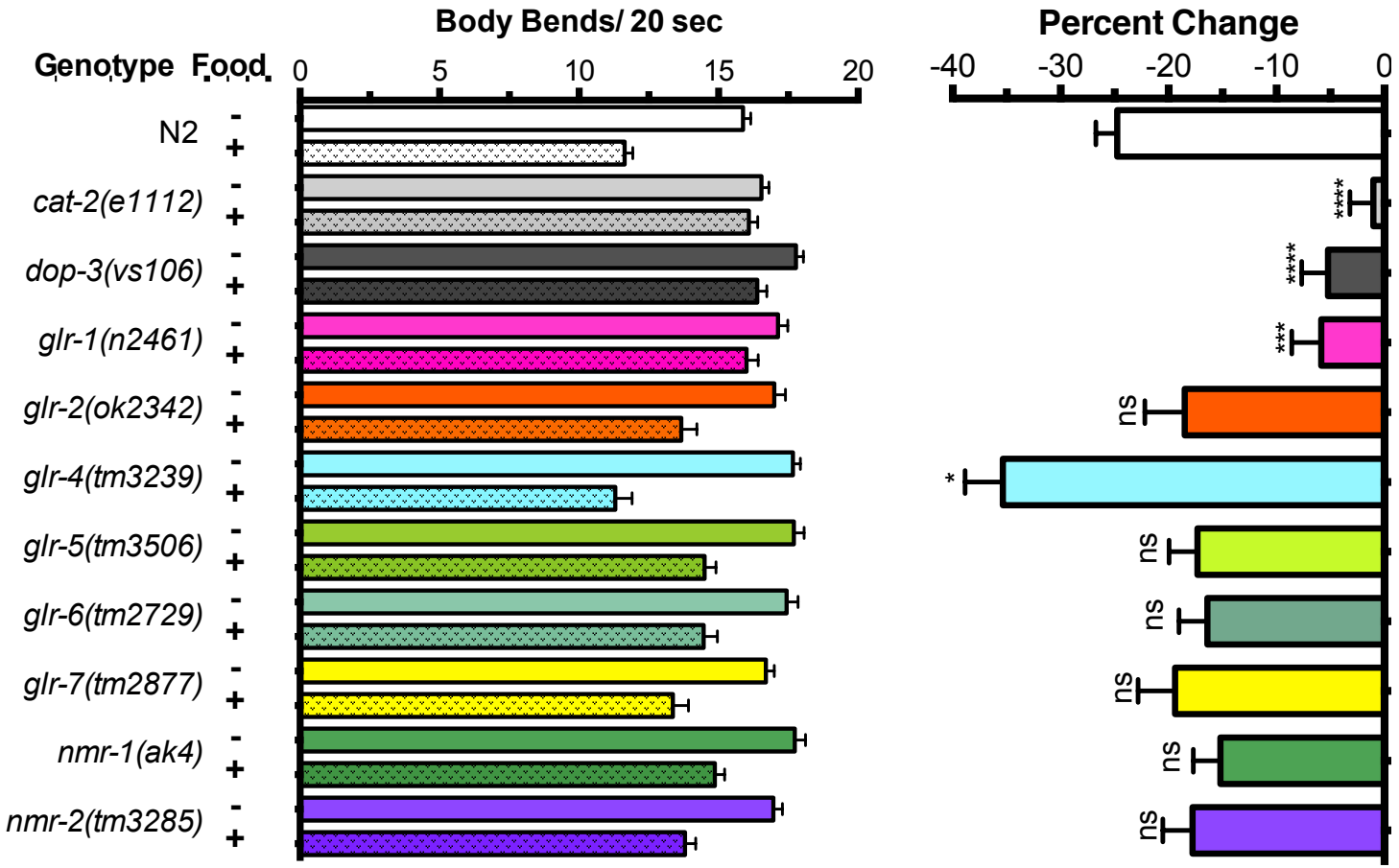

Figure 36 – Basal slowing response of ionotropic glutamate receptor mutants. Assays were performed as described in the methods. Each column represents the average locomotory behavior of at least 30 animals tested over the course of three independent test days by two experimenters. Data is plotted as the raw counts over a 20 second interval on and off food and as the average percent change in body bends/20 sec for each animal tested over this period. Data were analyzed by one way ANOVA with Dunnet's post tests to the N2 strain. *glr-1(n2461)* demonstrated a significantly blunted basal slowing response relative to N2 and *glr-4(tm3239*) demonstrated a significantly elevated basal slowing response relative to N2.

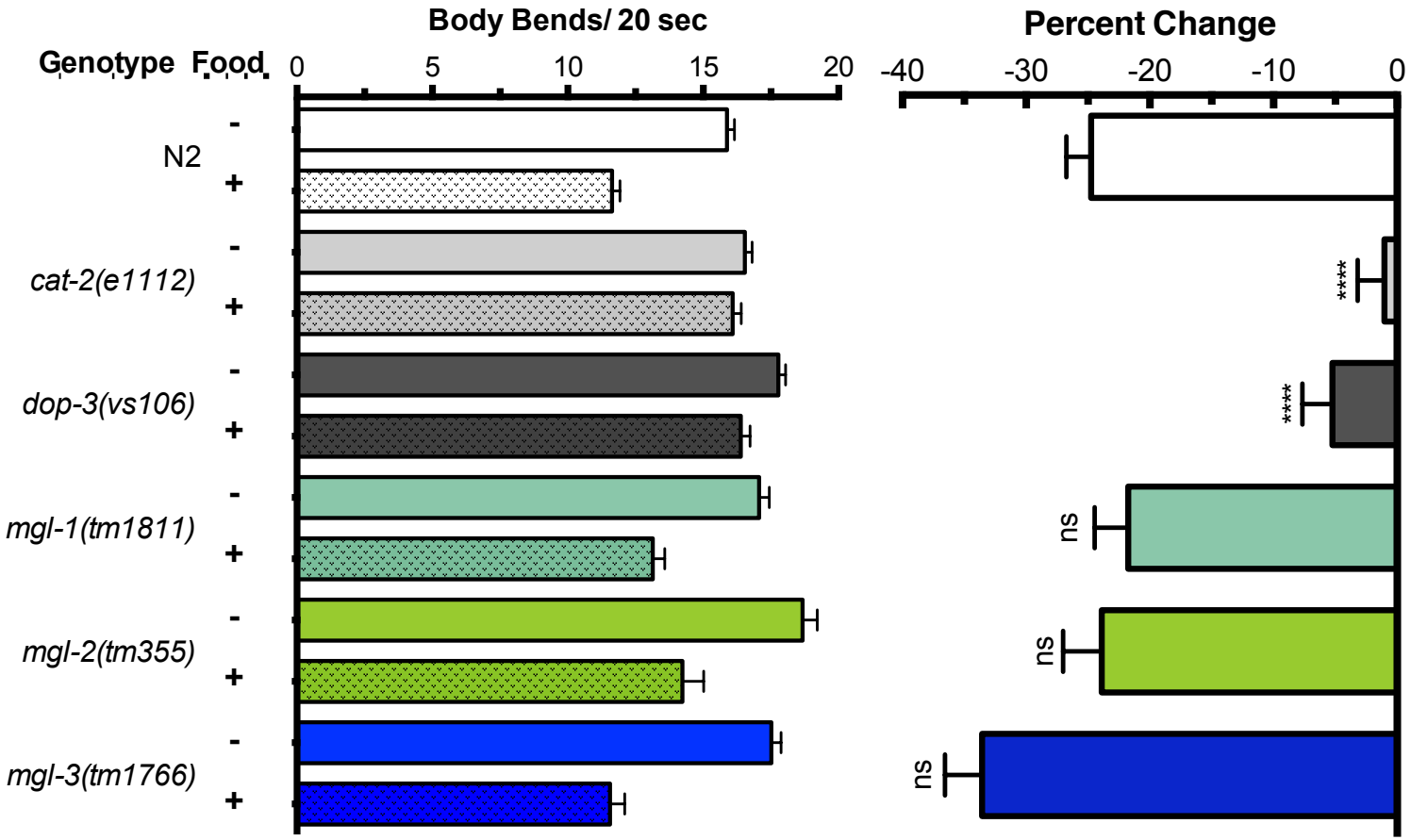

Figure 37 – Basal slowing response of metabotropic glutamate receptor mutants. Assays were performed as described in the methods. Each column represents the average locomotory behavior of at least 30 animals tested over the course of three independent test days by two experimenters. Data is plotted as the raw counts over a 20 second interval on and off food and as the average percent change in body bends/20 sec for each animal tested over this period. Data were analyzed by one way ANOVA with Dunnet's post tests to the N2 strain. We observed no significant differences for *mgl-1(tm1811)*, *mgl-2(tm355)* and *mgl-3(tm1766*) relative to N2.

revealed that loss of glt-1, but not in combination with glt-3, produced a significant reduction relative to N2 (Figure 38). Thus alterations in glutamate transport, in addition to their impacts on Swip, are capable of producing alterations in BSR. We also tested strains possessing a mutation in the primary) *eat-4*/vGlut for defects in BSR. *eat-4* mutants displayed a significant BSR relative to N2, though there may be alterations in its locomotory rate on food-free plates (Figure 39). Overall, these results suggested that alterations in GLU signaling pathways were capable of producing changes in DA-related behavioral phenotypes, but that these effects are graded and that multiple pathways function in parallel to mediate these effects.

Analysis of *swip-10* Speed using WormLab

During our analysis of the BSR in the *swip-10* lines we noted a decrease in the locomotory rate of these strains in plates containing no food. To validate this finding, we performed an analysis of their locomotory speed on plates using an automated tracking system. Similar to BSR, we calculated the average absolute speed value of wildtype, *dat-1* and *swip-10* mutants. *swip-10* demonstrated a striking reduction in their average speed, and, similar to Swip, this was suppressed by loss of *cat-2* (Figure 40). As previously reported, *dat-1* animals move at a rate similar to wildtype animals on plates. Thus there exist DA-dependent alterations in locomotion for *swip-10* in either water or during crawling on plates.

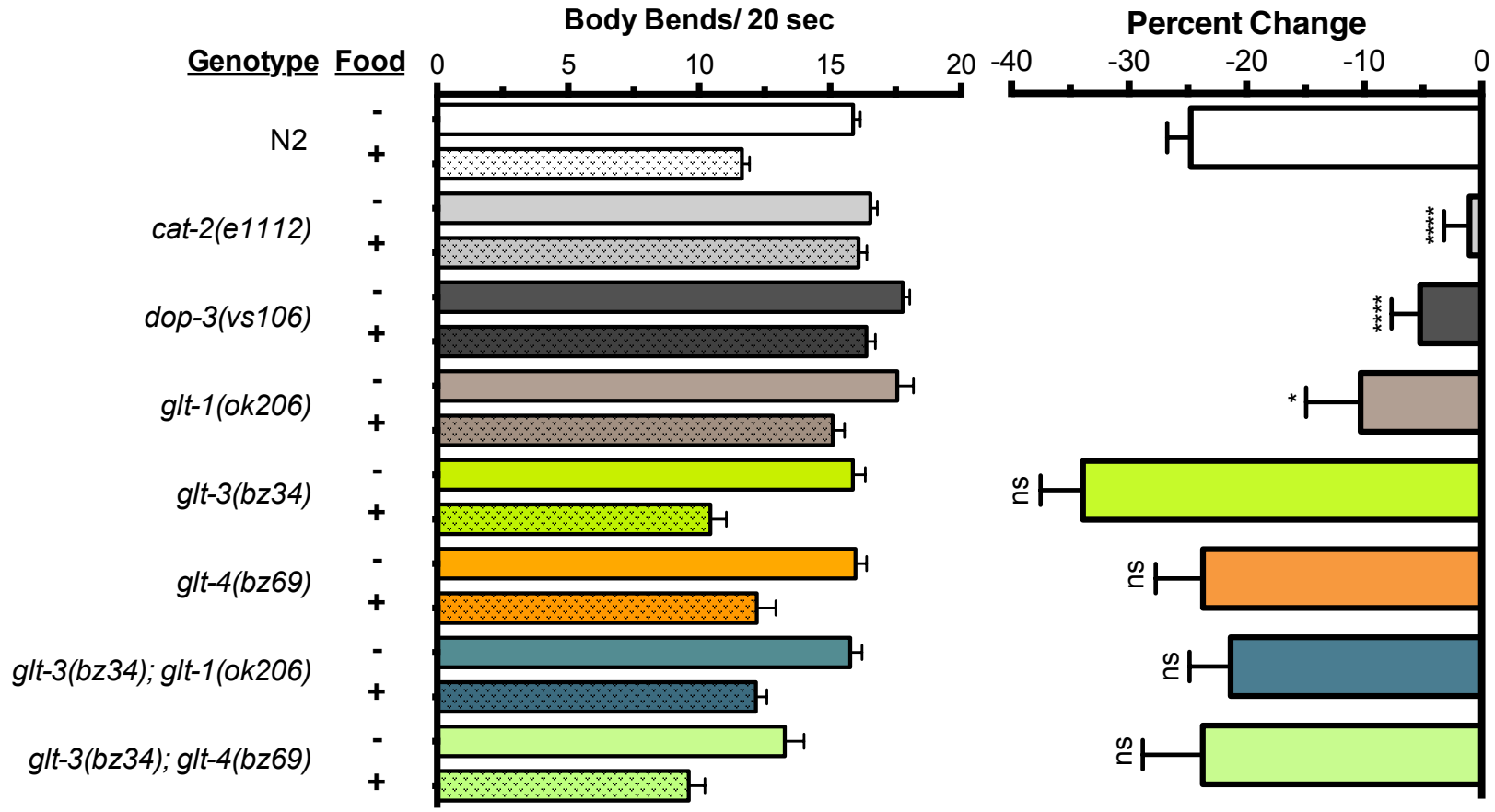

Figure 38 - Basal slowing response of glutamate transporter mutants. Assays were performed as described in the methods. Each column represents the average locomotory behavior of at least 30 animals tested over the course of three independent test days by two experimenters. Data is plotted as the raw counts over a 20 second interval on and off food and as the average percent change in body bends/20 sec for each animal tested over this period. Data were analyzed by one way ANOVA with Dunnet's post tests to the N2 strain. We observed a significant reduction in the magnitude of BSR for the *glt-1(ok206)* strain relative to N2.

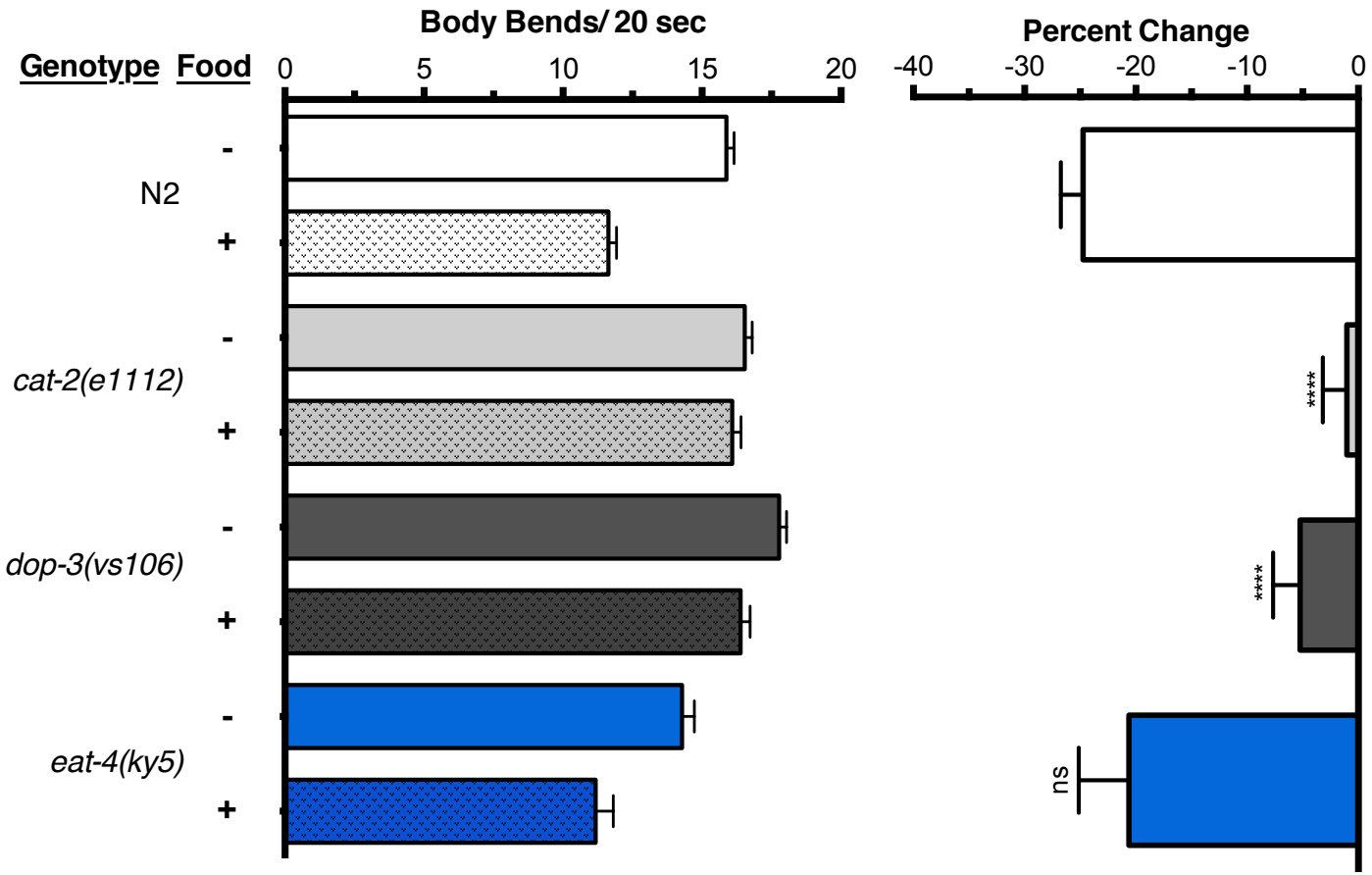

Figure 39 – **Basal slowing response of *eat-4(ky5)***. Assays were performed as described in the methods. Each column represents the average locomotory behavior of at least 30 animals tested over the course of three independent test days by two experimenters. Data is plotted as the raw counts over a 20 second interval on and off food and as the average percent change in body bends/20 sec for each animal tested over this period. Data were analyzed by one-way ANOVA with Dunnet's post tests to the N2 strain. *eat-4(ky5)* animals demonstrate a normal basal slowing response relative to N2.

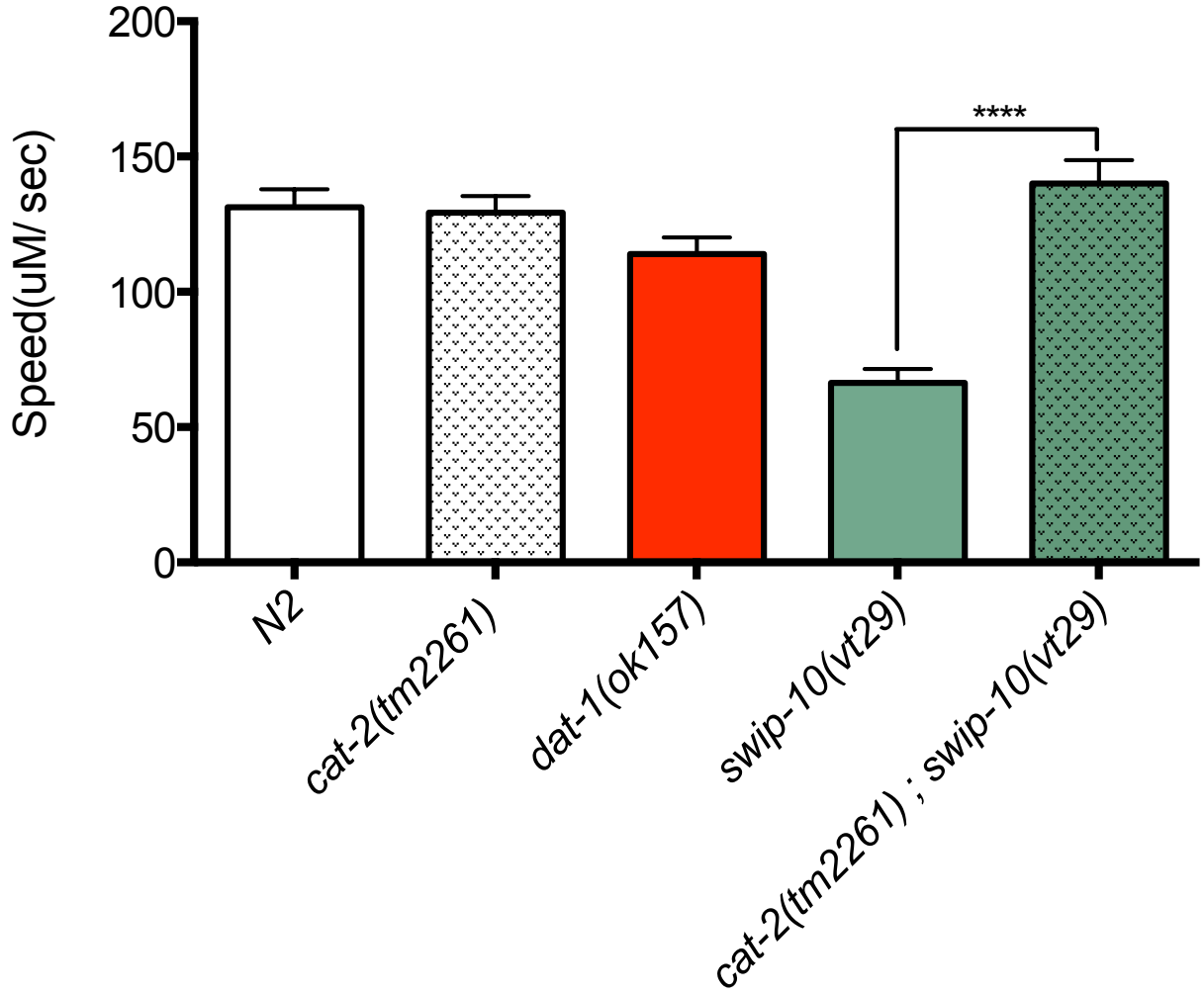

Figure 40 – Analysis of *swip-10* speed using WormLab. Experiments were performed as described in the methods and the absolute value of worm speed calculated during movement on a food-free NGM plate. Data were analyzed using one-way ANOVA with multiple Bonferonni post tests. **** indicates a *p* value <0.0001. swip-*10* is significantly suppressed from N2 and this is fully restored by loss of *cat-2*.

swip-10 interactions with *eat-4*(vGlut)

To determine if altered glutamate signaling is required for Swip in the *swip-10* mutants, we crossed the *vt29* and *vt33* strains to *eat-4*/vGlut and assayed double mutant progeny for their Swip phenotype. As seen in Figure 41, loss of *eat-4* alone is dispensible for normal swimming behavior and we observed a highly significant, yet incomplete, suppression in the *swip-10(vt33)* strain but not in the *swip-10(vt29)* strain as measured by manual Swip assays. As previous studies indicated that effects of GLU signaling mutations on DAergic phenotypes manifest in graded behavioral alterations, we measured the swimming behavior of *eat-4; swip-10* double mutants using SwimR (Hardaway and Wang, *under review*). Consistent with the manual assays, we did not observe a change in the average swimming frequency in the *eat-4* strain. Analysis of the average swimming frequency of these strains demonstrated that loss of *eat-4* results in an increased average swimming frequency in both *eat-4; swip-10(vt29)* and *eat-4; swip-10(vt33)* strains relative to the *swip-10(vt29)* and *swip-10(vt33)* mutants respectively (Figure 42). These studies establish that vesicular GLU signaling through *eat-4* contribute to the penetrance and kinetics of Swip in both *swip-10(vt29)* and *swip-10(vt33)*.

swip-10 interactions with *egl-3*

Studies using the expression of poly-A binding proteins in specific cell types had identified a DA neuron specific transcriptome (Spencer et al., 2011). They validated these data by the fact that classical genes necessary for DA

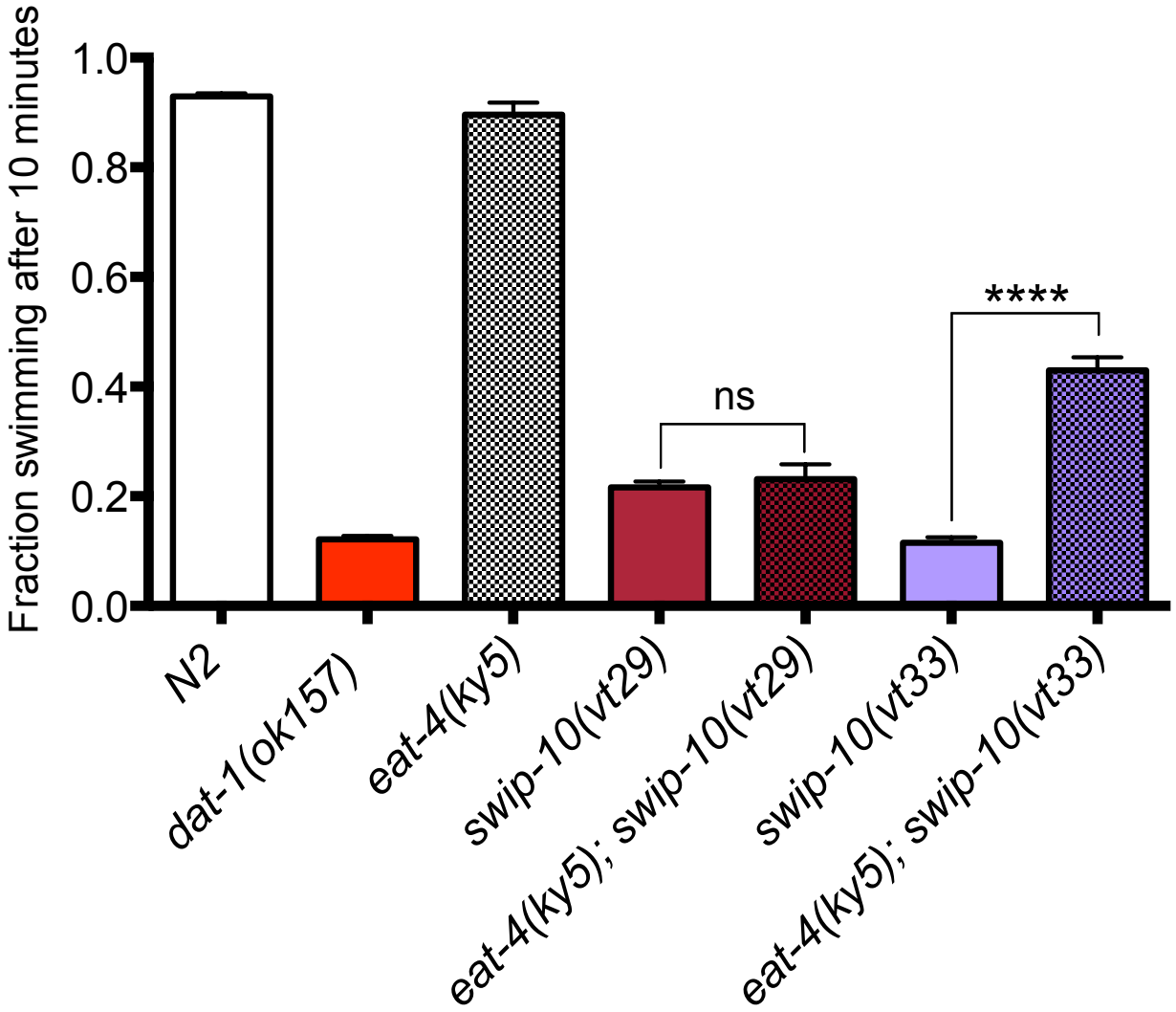

Figure 41 – *eat-4*(vGlut) significantly suppresses *swip-10(vt33)*, but not *swip-10(vt29)* as measured by manual Swip assays. Double mutant strains were constructed as described in the Methods. Strains were tested by two experimenters over the course of three weeks. Each column represents the average of at least 48 trials tested over this period. Data were analyzed by one-way ANOVA with multiple Bonferroni post tests. **** indicate $p<0.0001$.

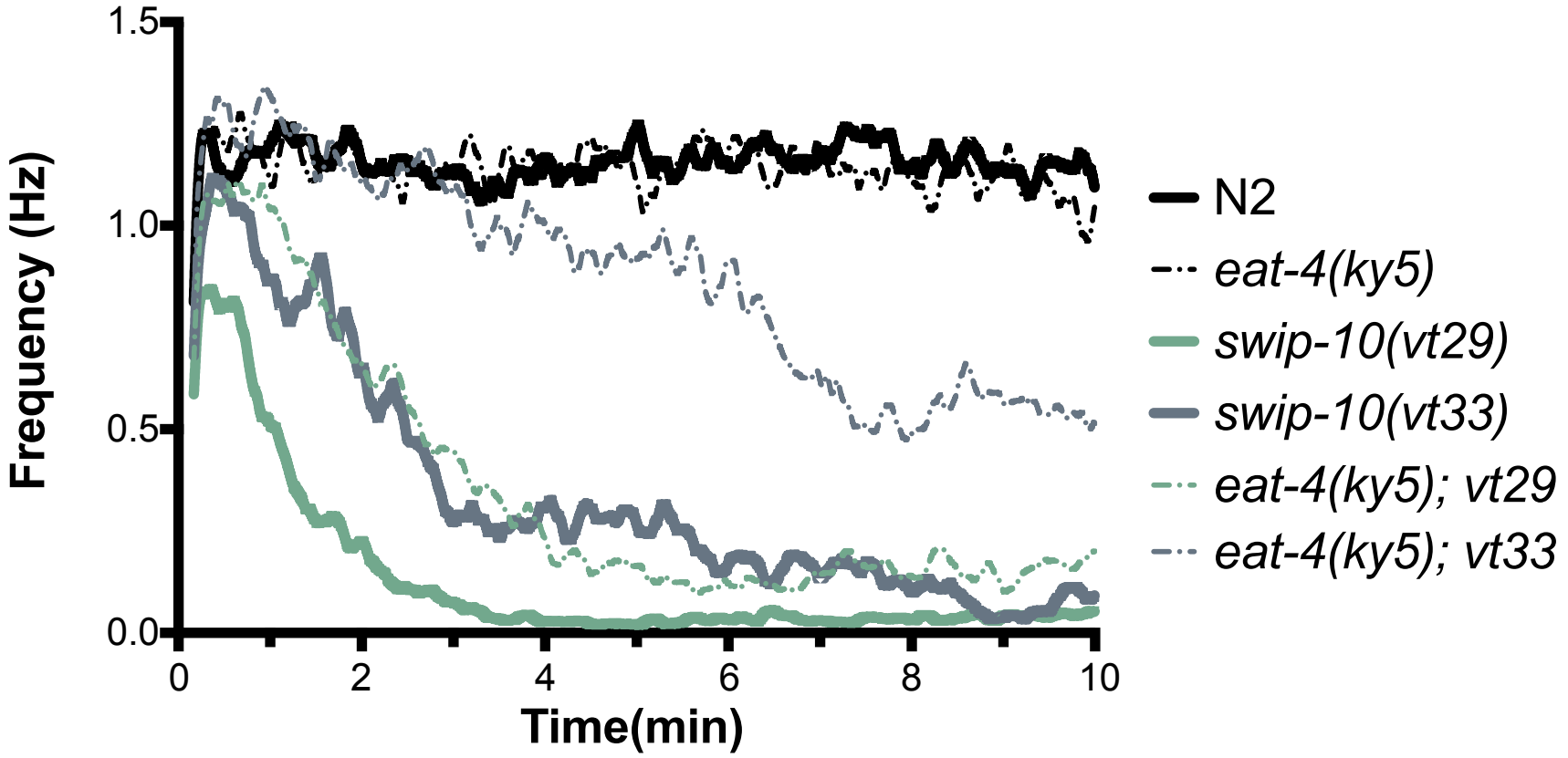

Figure 42 – *eat-4* suppresses *swip-10* as measured by kinetic thrashing analysis. Single worm recordings were made as described in the methods and videos were analyses as described in the Chapter VII Appendix. Curves represent the average thrashing frequency of at least 25 independent animals recorded over the course of several sessions. Data were analyzed by two-way ANOVA with multiple Bonferonni post tests at each time point. *eat-4; swip-10(vt29)* is significantly suppressed from *swip-10(vt29)* progeny during minutes 1-3 and *eat-4; swip-10(vt33)* is significantly suppressed from *swip-10(vt33)* from minutes 2-10.

signaling (*cat-1, cat-2*, *cat-4*, *bas-1*, and *dat-1*) and ion channels known to be enriched in DA neurons (*trp-4* and *asic-1*) were highly enriched relative to a pan-neuronal data set. In this data set, several neuropeptides were highly enriched. As neuropeptides have been shown to modulate the excitability of other neurons (Chalasani et al., 2010), we crossed the *swip-10(vt29)* and *swip-10 (tm5915)* alleles to a strain harboring a mutation in *egl-3* (Kass, Jacob, Kim, & Kaplan, 2001), the *C. elegans* preprotein convertase necessary for the production of most neuropeptides. Surprisingly, loss of *egl-3* fully suppressed the Swip phenotype present in *swip-10(vt29)* and *swip-10(tm5915)*(Figure 43). Thus, neuropeptide signaling through *egl-3* activity is required for Swip in *swip-10* mutants.

swip-10 interactions with glutamate receptors

Having observed that vesicular GLU signaling is required for Swip in *swip-10* mutants and that loss of GLURs does not drastically impair normal swimming behavior, we crossed *swip-10* into strains harboring mutations in distinct GLURs. In most cases we used the *swip-10(vt29)* allele, but for X-linked genes we recombined the glutamate receptor alleles with *swip-10(tm5915)*. Despite its requirement for normal BSR, we found that loss of *glr-1* did not affect the Swip phenotype of *swip-10* as measured by hand (Figure 44). Likewise, *glr-2, glr-5, nmr-1*, *nmr-2*, *mgl-2,* and *mgl-3* were all dispensable and had no effect on the amount of Swip we observed in *swip-10(vt29)*. Loss of the ionotropic GLURs *glr-4* and *glr-6* and the metabotropic GluR *mgl-1*

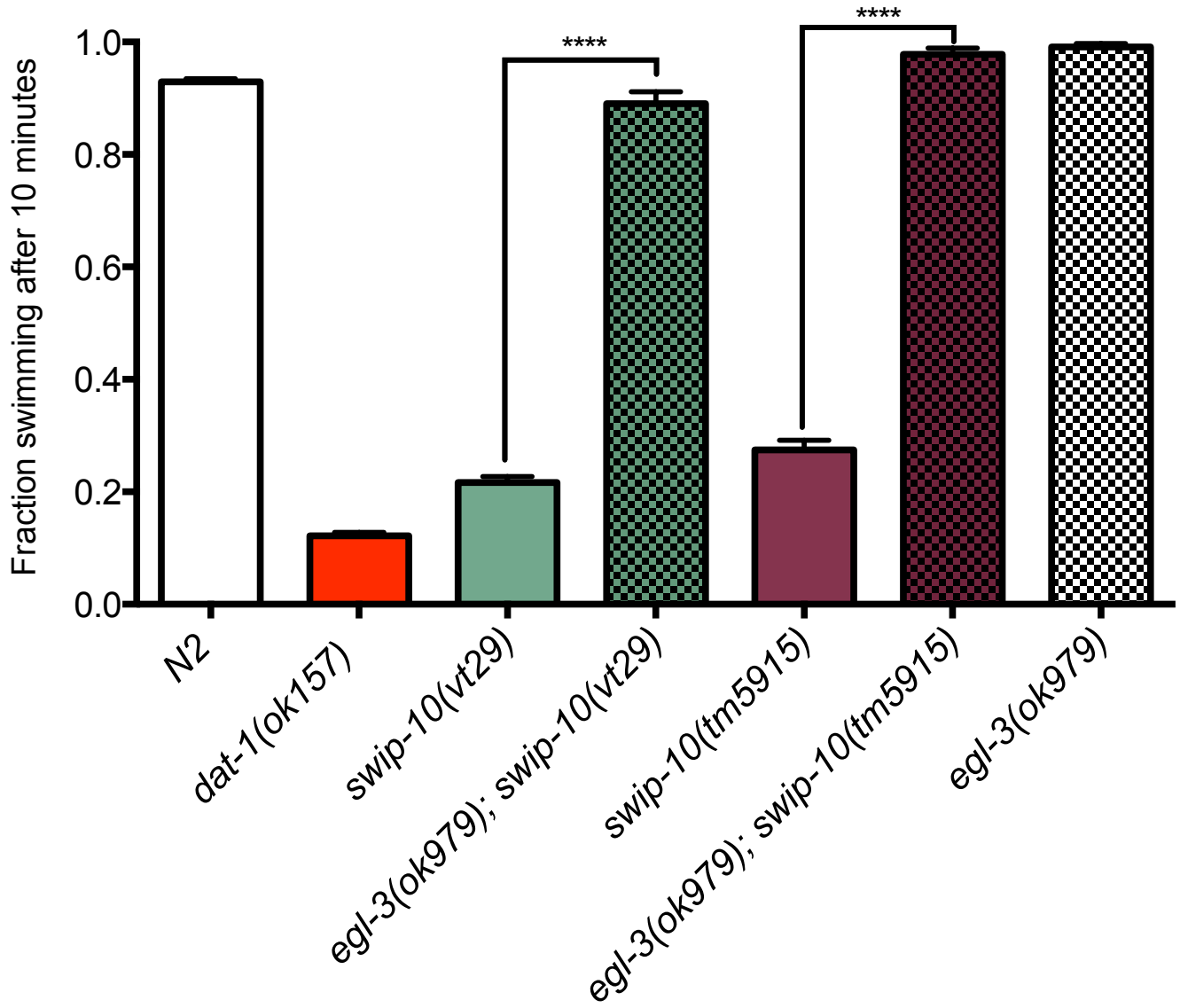

Figure 43 – Loss of *egl-3* fully restore the Swip phenotype *swip-10(vt29)* and *swip-10(vt33)*. Double mutant strains were constructed as described in the Methods. Strains were tested by two experimenters over the course of three weeks. Each column represents the average of at least 48 trials tested over this period. Data were analyzed by one-way ANOVA with multiple Bonferroni post tests. **** indicate $p<0.0001$.

significantly, yet incompletely suppressed the Swip phenotype in *swip-10* mutants (Figure 44). To confirm what we observed by hand, we used automated analysis of their swimming behavior in the single and double mutants and compared their average swimming frequency. As seen in Figure 45, we observed that the *glr-4; swip-10(vt29)*, *swip-10(tm5915) glr-6(tm2729),* and *swip-10(tm5915) mgl-1(tm1811)* strains all displayed a significantly elevated average swimming frequency relative to their single allele *swip-10* controls(Figure 45). To understand how these GLURs function in parallel to mediate Swip in the *swip-10* mutant, we constructed strains bearing mutations in each of these GLURs in combination. As in Figure 44, we observed that loss of two or more of these GLURs in combination could enhance the suppression of *swip-10*, though not completely restore it to wildtype levels. Importantly, loss of *glr-4*, *glr-6*, and *mgl-1* alone did not alter basal swimming behavior similar to the individual alleles (see Figure 30). In these analyses, we observed that loss of *glr-6* had the most significant effect on *swip-10* Swip either alone or paired with mutations in either *glr-4* or *mgl-1*. Thus, GLUR signaling through *glr-4, glr-6*, and *mgl-1* is required for the Swip in *swip-10* mutants and these receptors function in parallel to regulate the penetrance of the Swip phenotype.

We hypothesized that loss *swip-10* function in glia may impact the magnitude of excitatory signaling through *glr-4*, *glr-6*, and *mgl-1* and that the contribution of these receptors is specific. Additional studies in the lab studying the contribution of known ion channels such as *trp-4* and *asic-1* suggested that

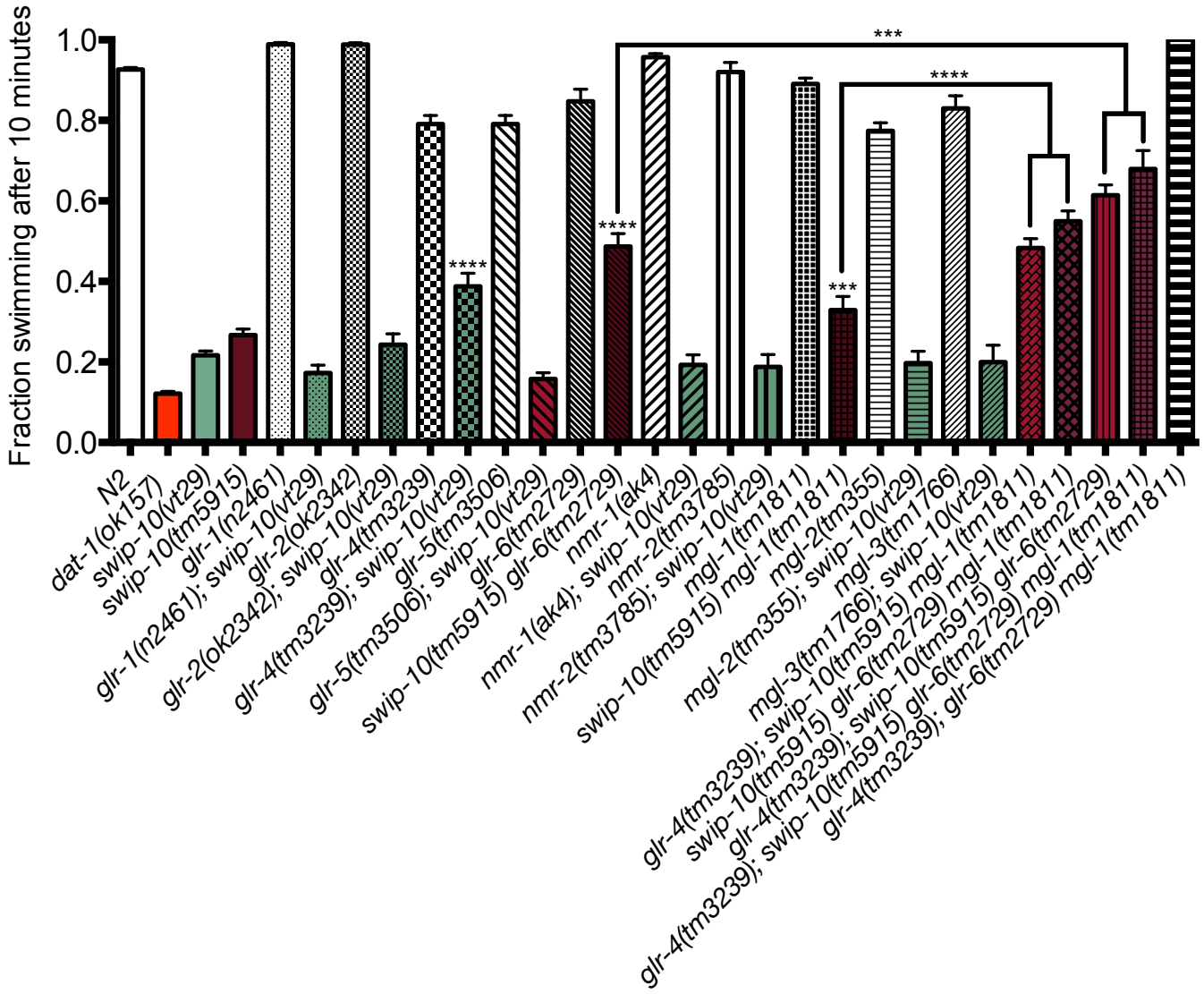

Figure 44 – Loss of specific GluRs significantly suppresses *swip-10* Swip. Double mutant strains were constructed as described in the Methods. Strains were tested by two experimenters over the course of at least three weeks. Each column represents the average of at least 48 trials tested over this period. Data from hese test days were alyzed by one-way ANOVA selected Bonferroni post *** indicate p<0.0001.

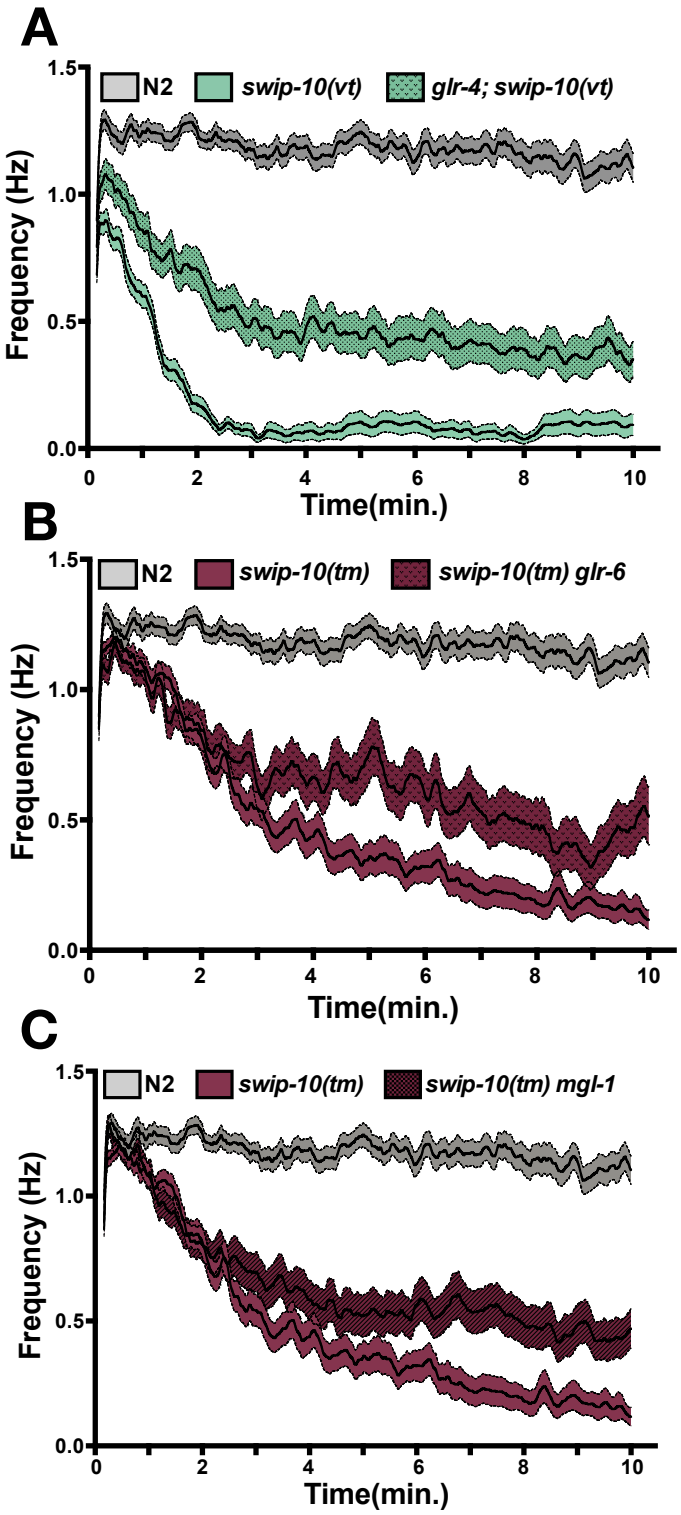

Figure 45 – *swip-10* is suppressed by loss of *glr-4, glr-6*, and *mgl-1*. A. Loss of *glr-4* significantly suppresses *swip-10(vt29)*. *swip-10* is significantly elevated from *swip-10(vt29)* starting in the 1st minute. **B.** Loss of *glr-6* significantly suppresses *swip-10(tm5915)* with points of significance in minutes 4-10. **C.** Loss of *mgl-1* significantly suppresses *swip-10(tm5915)* with points of significance in minutes 3-10. For **A, B,** + **C**, single worm recordings were performed as described in the methods and analyzed with SwimR. Data were analyzed by two-way ANOVA with multiple Bonferroni post tests at each time point.

these channels are dispensable for *swip-10* Swip, but required for *dat-1* Swip. Therefore, we tested the impact of *glr-4*, *glr-6*, and *mgl-1* on the Swip phenotype in *dat-1* mutants. As we hypothesized, loss of *glr-4* and *glr-6* had no impact on the *dat-1* Swip phenotype. Surprisingly, however, we observed a near complete restoration of swimming behavior in *dat-1; mgl-1* mutants (Figure 46). During the performance of these assays, we noticed that this strain did paralyze, but often transited between paralysis, swimming, and crawl-like motion. To gain a fuller picture of the impact of *mgl-1* on *dat-1* Swip, we analyzed the swimming behavior of this strain using SwimR. Loss of *mgl-1*, as in the hand assays, almost completely restored the average swimming frequency of the *dat-1* mutant (Figure 47). Inspection of individual worm tracks revealed a population of worms that exhibit only sporadic bouts of paralysis.

swip-10 **interactions with glutamate transporters**

As our behavioral analyses of *glt-1, glt-3*, and *glt-4* demonstrated a DA-dependent Swip phenotype, we hypothesized that *swip-10* may function in glia to regulate glutamate transporters. To test this hypothesis, we used a previously established epistatic paradigm to assay the *swip-10* Swip phenotype in combination with *glt-1, glt-3,* and *glt-4* (Hardaway, et al., 2012). As *glt-1* and *glt-4* are X-linked, we used the *swip-10(tm5915)* deletion allele for these studies. *dat-1* and *swip-10* both demonstrate a highly penetrant Swip phenotype that is suppressed by graded increases in the swimming media osmolarity such that a slight increase in osmolarity(100 mOsm) is sufficient to suppress these alleles

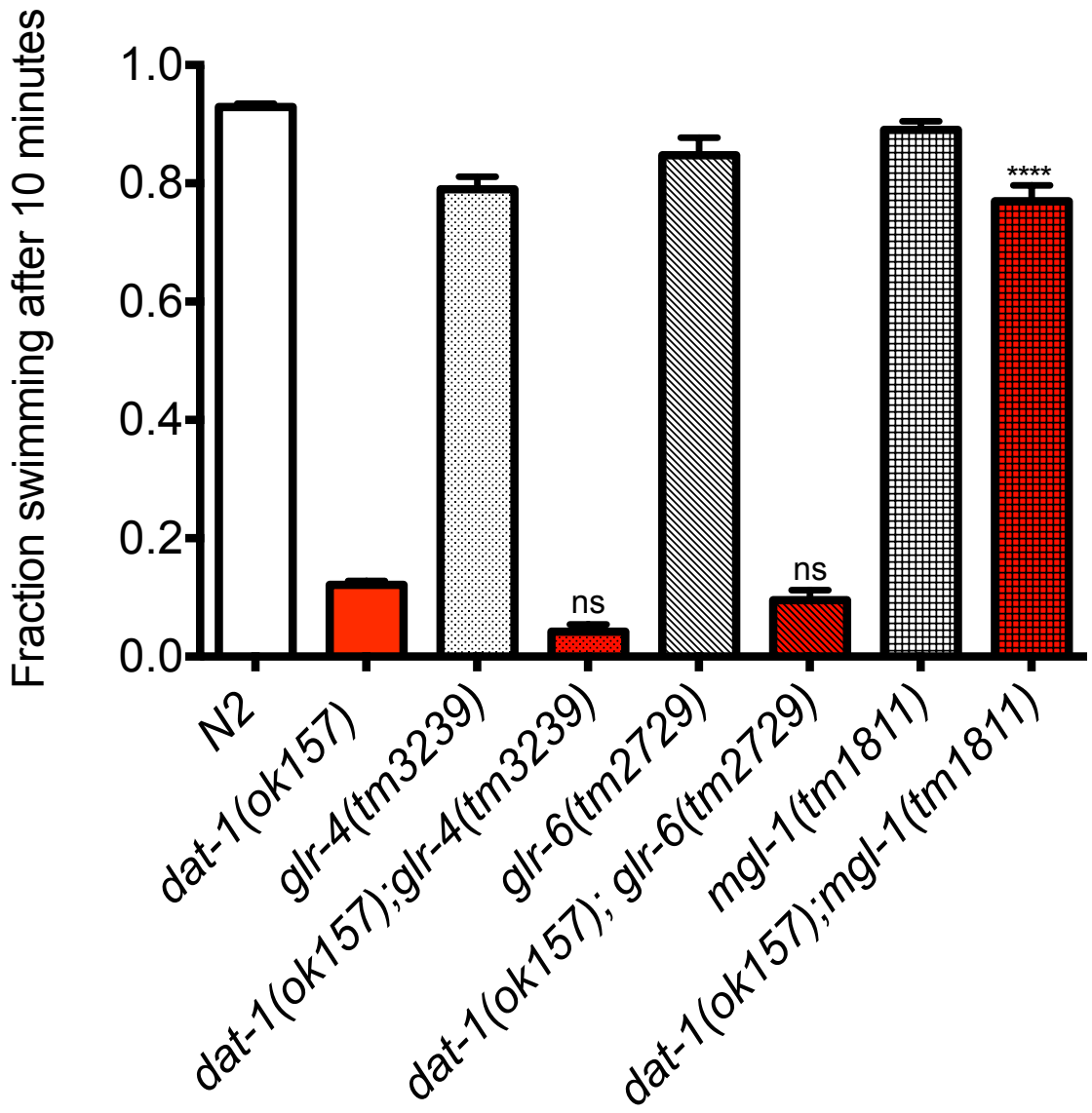

Figure 46 – *glr-6*, *glr-4*, and *mgl-1* interaction with *dat-1* Swip. Loss of *mgl-1* significantly restores the Swip of the *dat-1* strain. Double mutant strains were constructed as described in the Methods. Strains were tested by two experimenters over the course of three weeks. Each column represents the average of at least 48 trials tested over this period. Data were analyzed by one-way ANOVA with multiple Bonferroni post tests. **** indicate $p<0.0001$ for the post test to *dat-1*.

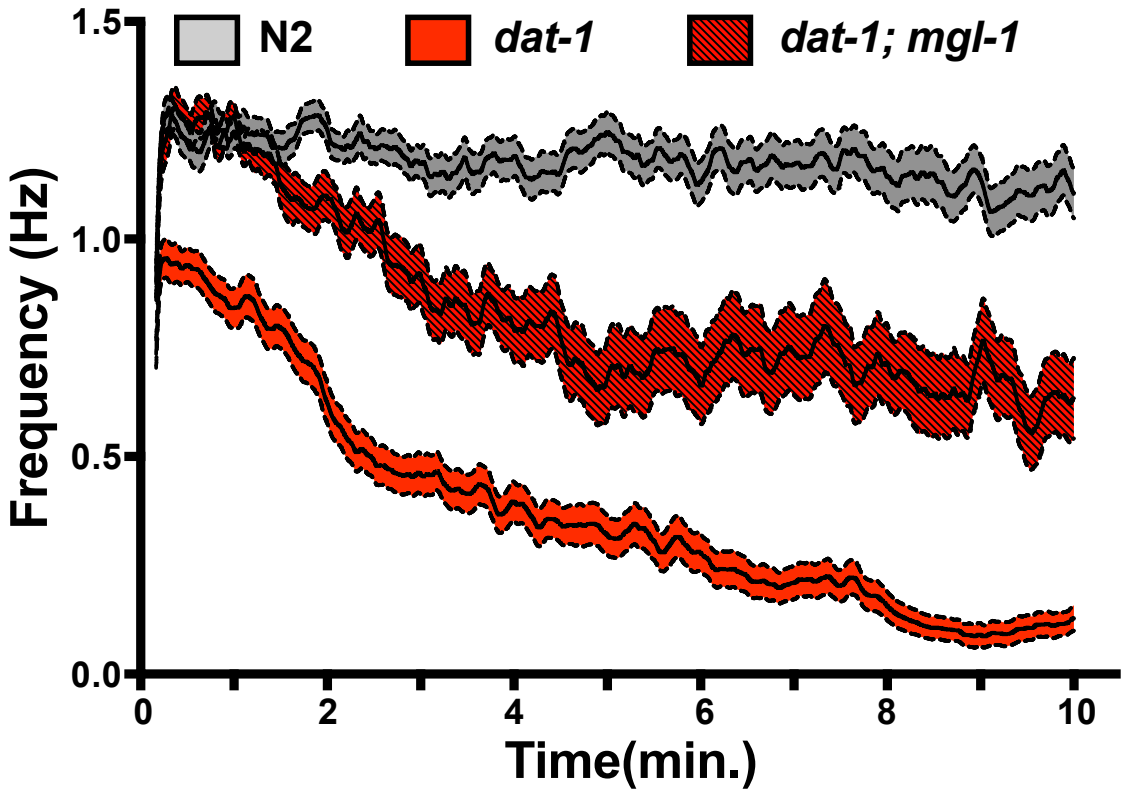

Figure 47 – Loss of *mgl-1* significantly suppresses *dat-1*. Single worm recordings were performed as described in the methods. Data were analyzed by two-way ANOVA with multiple Bonferonni post tests at each time point. *dat-1; mgl-1* thrashing frequency is significantly elevated from *dat-1* throughout the 10 minute period.

(Hardaway, et al., 2012). As we demonstrated in our previous report using the *swip-10(vt29)* allele, an increase in osmolarity reveals that loss of *swip-10* significantly enhances Swip in the *dat-1* strain (Hardaway, et al., 2012). This is consistent with our hypothesis that *dat-1* and *swip-10* function in parallel independent pathways to regulate DA signaling. As seen in Figures 48, 49, and 50, an increase in the osmolarity is sufficient to suppress the Swip phenotype of *glt-1, glt-3*, and *glt-4*. In keeping with our previous findings of *cat-2* suppression and osmolarity induced suppression of *dat-1* and *swip-10*, these findings add further evidence to our hypothesis that loss of *glt-1, glt-3,* and *glt-4* triggers DA-dependent Swip. Swip assays of double mutant strains containing either *dat-1* or *swip-10* and *glt-1* demonstrated that loss of *glt-1* significantly enhances *swip-10* Swip at intermediate osmolarity (Figure 49). Surprisingly, loss of *glt-1* did not enhance the *dat-1* allele. Therefore *glt-1* may function in a pathway shared with *dat-1*, but not with *swip-10. glt-4*, on the other hand, significantly enhanced Swip in the *dat-1* strain at 100 mOsm, but did not enhance *swip-10* (Figure 48). Assay of *glt-3*'s interaction with *swip-10* revealed that the loss of *glt-3* significantly, albeit partially, suppressed *swip-10* at basal or intermediate osmolarity (Figure 50). The impact of *glt-3* on *dat-1* Swip is still unknown at this time. Therefore, *swip-10* may function in a pathway containing *glt-4* and not *glt-1,* and that *glt-3* is required for the fully penetrant Swip phenotype of *swip-10*.

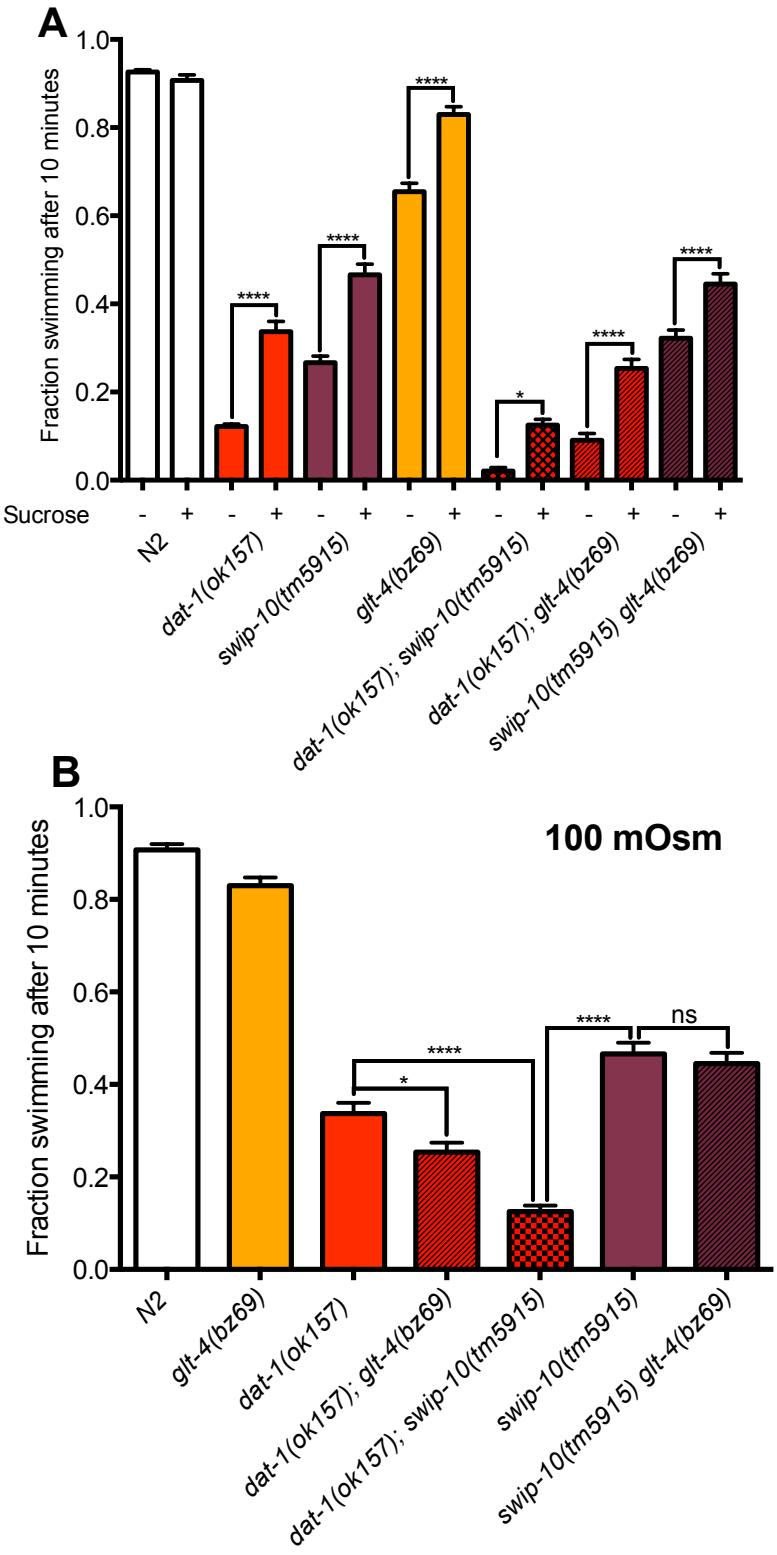

Figure 48 – *dat-1* and *swip-10* interactions with *glt-4*. A) Swip phenotype in water alone and in 100 mOsm-buffered water. Swip in each of these strains is significantly suppressed by elevated osmolarity. Data were analyzed by two-way ANOVA with Sidak's multiple comparison test comparing the osmolarity effect for each genotype. **B)** Swip behavior at 100 mOsm. *dat*-1 Swip is significantly enhanced by loss of *swip-10* and *glt-4,* whereas *swip-10* is not enhanced by loss of *glt-4*. Data were analyzed by one-way ANOVA with selected Holm-Sidak's post tests. For both **A** and **B,** assays were performed and double mutant strains constructed as described in the methods. Strains were tested by two experimenters over the course of three weeks. Each column represents the average of at least 48 trials tested over this period. Data were analyzed by one-way ANOVA with multiple Bonferroni post tests. * and **** indicate $p<0.05$ and 0.0001 for the post tests.

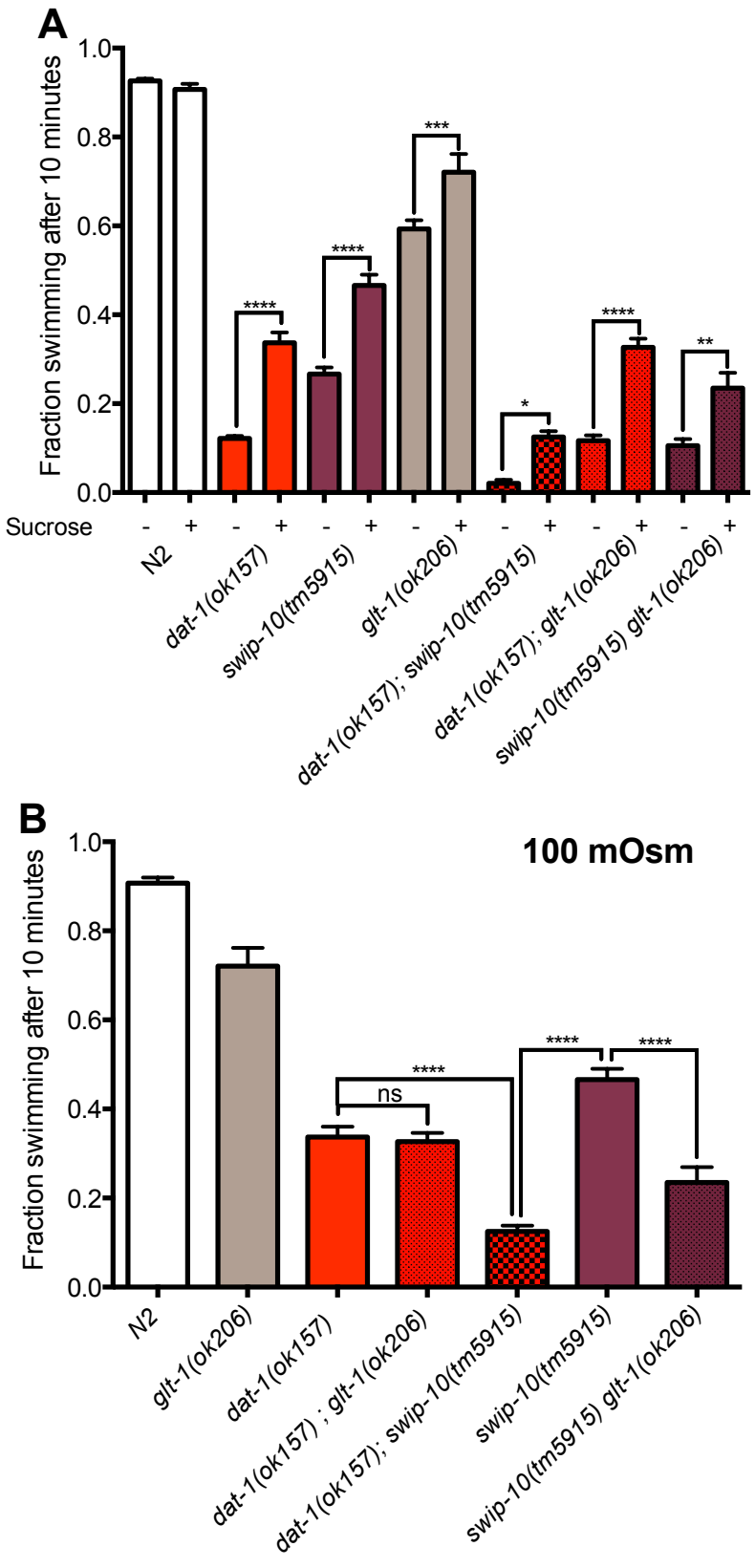

Figure 49 – *dat-1* and *swip-10* interactions with *glt-1*. A) Swip phenotype in water alone and in 100 mOsm-buffered water. Swip in each of these strains is significantly suppressed by elevated osmolarity. Data were analyzed by two-way ANOVA with Sidak's multiple comparison test comparing the osmolarity effect for each genotype. **B)** Swip behavior at 100 mOsm. *dat*-1 Swip is significantly enhanced by loss of *swip-10,* but not *glt-1,* whereas *swip-10* is enhanced by loss of *glt-1*. Data were analyzed by one-way ANOVA with selected Holm-Sidak's post tests. For both **A** and **B,** assays were performed and double mutant strains constructed as described in the methods. Strains were tested by two experimenters over the course of three weeks. Each column represents the average of at least 48 trials tested over this period. Data were analyzed by one-way ANOVA with multiple Bonferroni post tests. *, **, and **** indicate $p<0.05$, 0.01 and 0.0001 for the post tests.

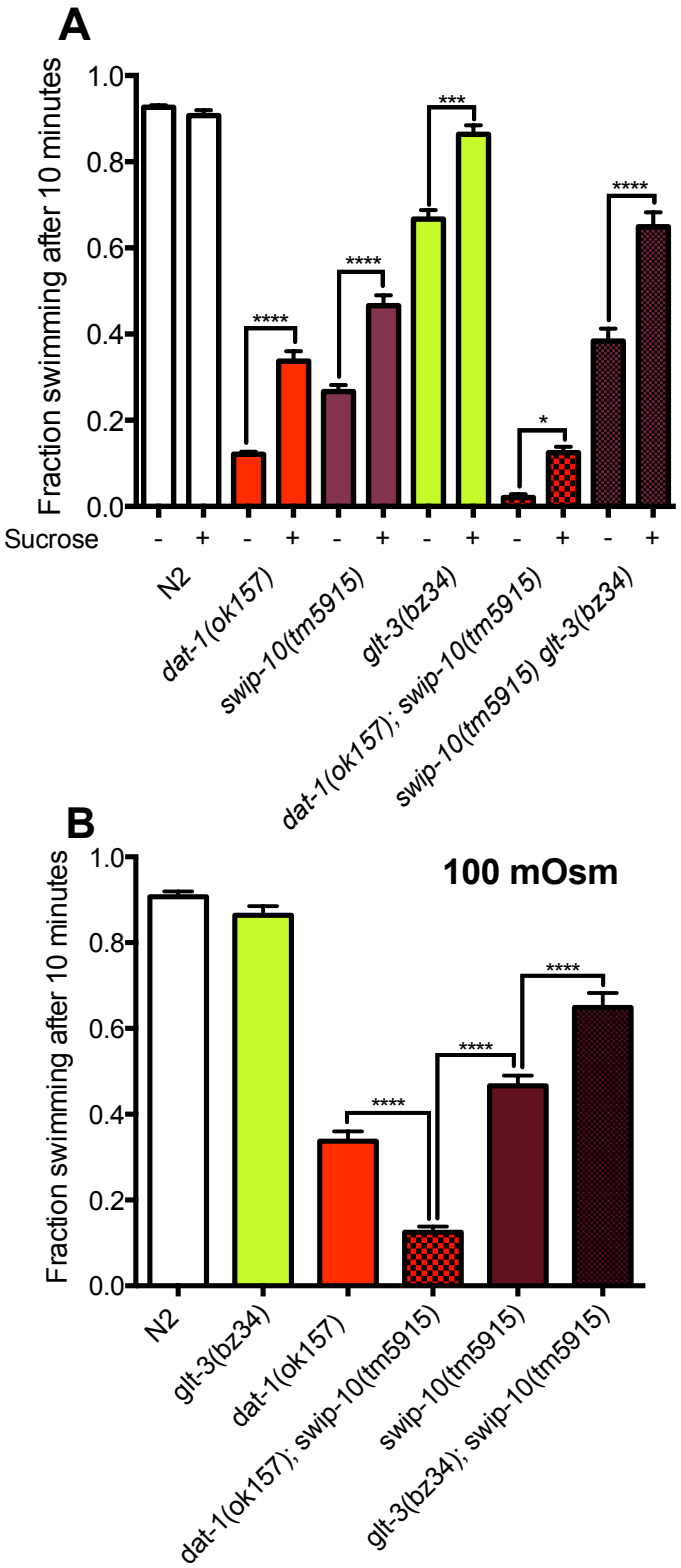

Figure 50 – *swip-10* interactions with *glt-3*. A) Swip phenotype in water alone and in 100 mOsm-buffered water. Swip in each of these strains is significantly suppressed by elevated osmolarity. Data were analyzed by two-way ANOVA with Sidak's multiple comparison test comparing the osmolarity effect for each genotype. **B)** Swip behavior at 100 mOsm. *dat*-1 Swip is significantly enhanced by loss of *swip-10. swip-10* is significantly suppressed by loss of *glt-3*. Data were analyzed by one-way ANOVA with selected Holm-Sidak's post tests. For both **A** and **B,** assays were performed and double mutant strains constructed as described in the methods. Strains were tested by two experimenters over the course of three weeks. Each column represents the average of at least 48 trials tested over this period. Data were analyzed by one-way ANOVA with multiple Bonferroni post tests. * and **** indicate $p<0.05$ and 0.0001 for the post tests.

swip-10 and GLT amino acid level measurements

Based on our previous data that *swip-10* requires GLUR signaling and that it may function in a pathway with *glt-4*, we hypothesized that the Swip phenotype may derive from gross alterations in the changes of excitatory or inhibitory signaling amino acids. Excitatory signaling at GluRs can occur through the ionic form of glutamic acid, GLU, and N-methyl-D-aspartic acid, whose precursor is aspartic acid. Additionally, extracellular GLU can also be passively affected through changes in extracellular 158ysteine and the export of GLU through the 158ysteine-glutamate exchanger (xC^-). Lastly, the increase in excitability of DA neurons in *swip-10* might also derive from a loss of inhibitory GABAergic signaling. To determine if loss of *swip-10* results in gross changes of these essential molecules, we performed HPLC on synchronized L4 tissue from wildtype, *dat-1*, *swip-10* and glutamate transporter mutants and determined the amount of these amino acids present. We did not observe any significant changes in the overall amino acid composition (Figure 51), including aspartic acid (Figure 52A), glutamic acid (Figure 52B), GABA (Figure 52C), and cysteine (Figure 52D). Thus loss of *swip-10* does not result in a gross change in the tissue composition of excitatory or inhibitory signaling molecules.

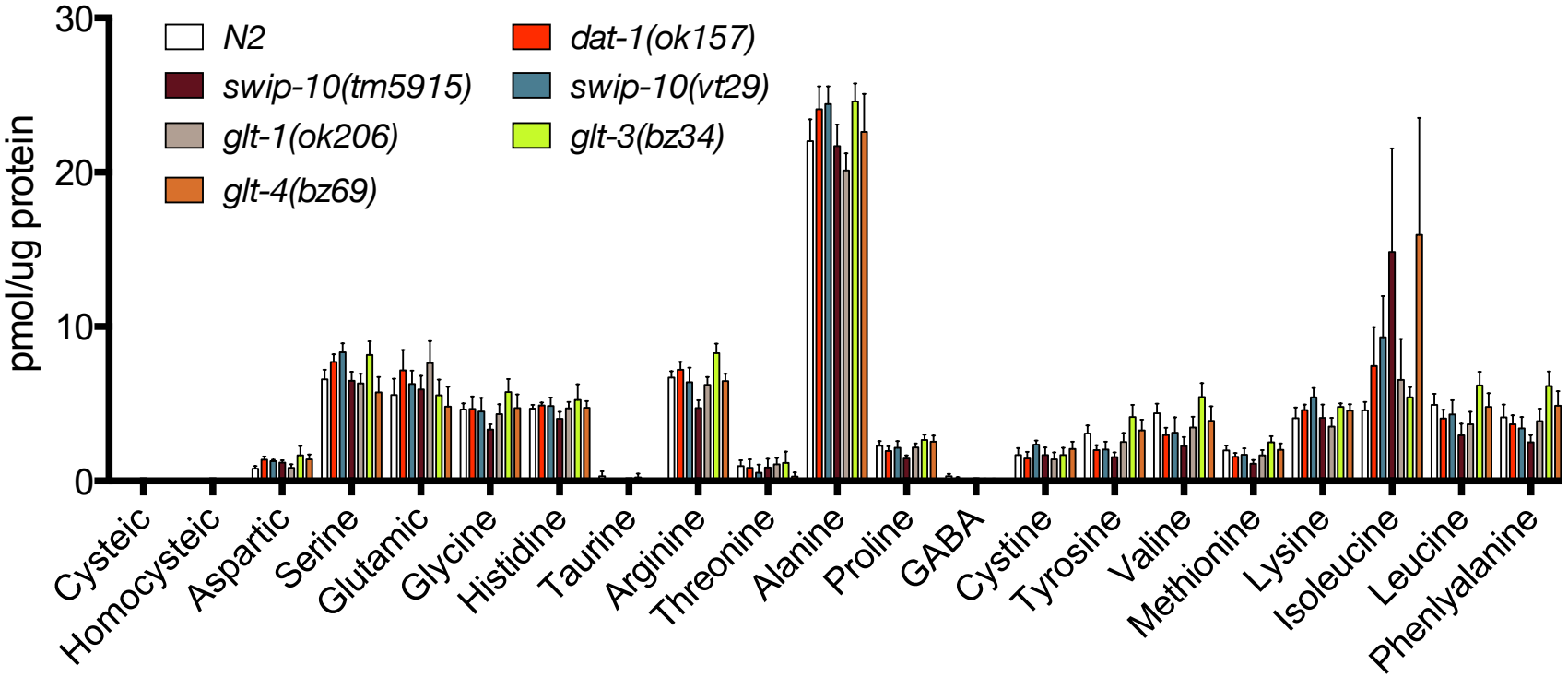

Figure 51 – Tissue amino acid composition of N2, *dat-1, swip-10*, *glt-1, glt-3*, and *glt-4*. Amino acid levels were determined by HPLC of synchronized L4 worm tissue as described in the methods. Data were analyzed by one-way ANOVA within each amino acid with Dunnet's post tests to N2. Overall, we observed no differences across the different amino acids measured.

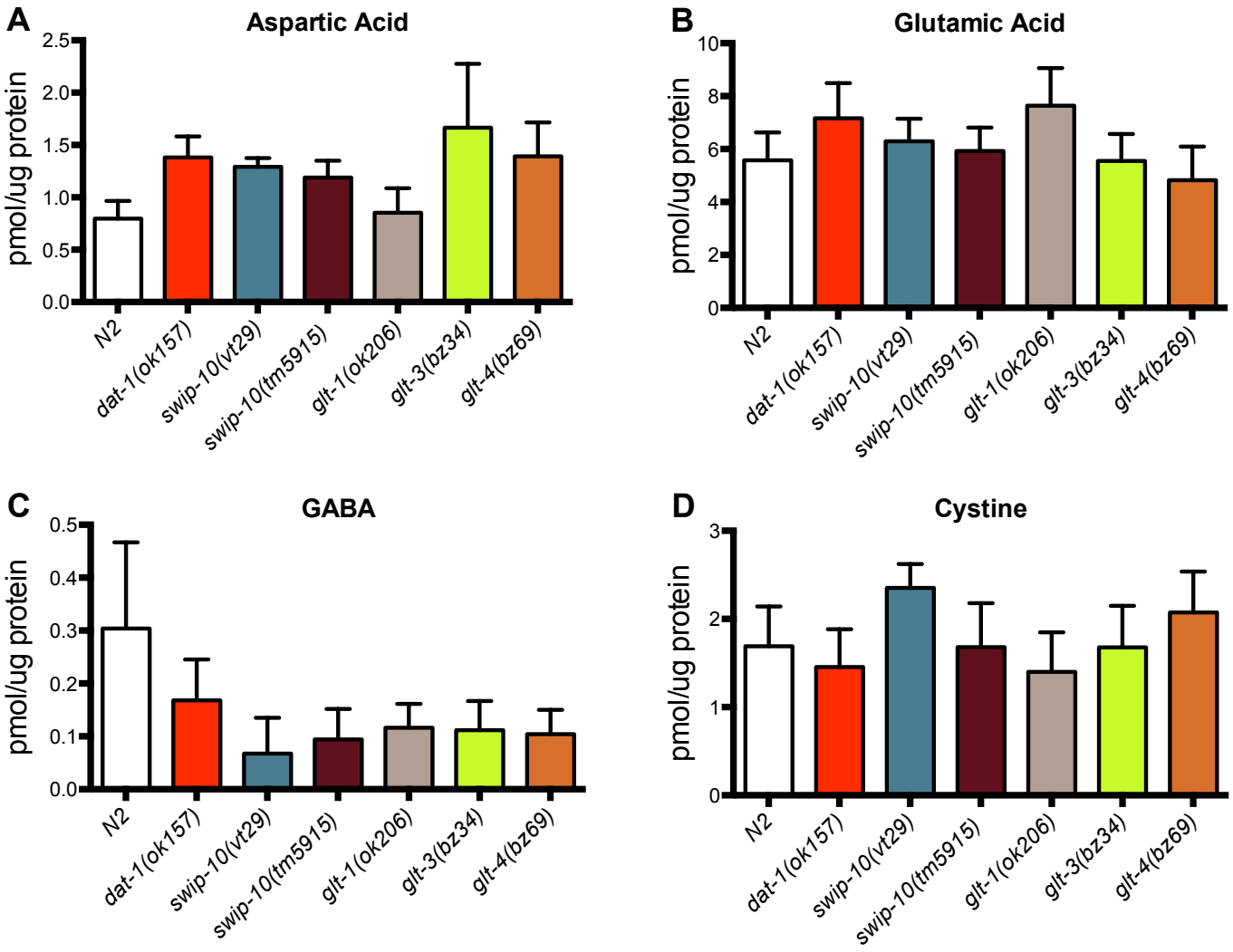

Figure 52 – Enlarged view of the HPLC measurement of Aspartic Acid, Glutamatic Acid, GABA, and Cystine for N2, *dat-1, swip-10, glt-1*, *glt-3* and *glt-4*. Amino acid level measurements were performed as described in the methods. Data were analyzed by one-way ANOVA with Dunnett's post tests to N2. We did not observed any significant changes.

DISCUSSION

Decades of research of CNS circuits have revealed that the brain is composed of neurons with genetic and developmentally defined patterns of gene expression and specific connectivity patterns (Arenkiel & Ehlers, 2009). It is embedded within a matrix of glia that perform a variety of complex functions including neuronal development, development and regulation of the brain's vasculature, and synaptic transmission (Clarke & Barres, 2013; Haydon, 2001; Lemke, 2001; Seifert, Schilling, & Steinhäuser, 2006). Despite their abundance in the brain, the role of glia in regulating behavior and ultimately neurological disease has long been overlooked. In the previous chapter we established that *swip-10* encodes a novel metallo β-lactamase regulator of DA signaling and that its loss results in a *dat-1* like Swip that is rescued by reserpine pretreatment, loss of *cat-2*/TH, and loss of *dop-3*/D2. In these studies, we describe the mechanism for how *swip-10* functions to regulate DA signaling.

To understand how the *swip-10* gene impacts the regulation of DA signaling, we began with determining its pattern of gene expression. The organization of *swip-10* required that we screen specific gene fragments for the presence of transcriptional *cis* elements. Using this transgenic approach, we observed that the regulation of *swip-10* gene expression is regulated by the presence of transcriptional elements immediately 5' of the predicted translational start site and within the large 5th intron situated between two groups of exons (Hobert, 2002). The 5' fragment was sufficient to drive GFP expression in mostly non-neuronal tissues like the hypodermis and vulval

muscle, whereas the intronic fragment was sufficient to express GFP in the hypodermis, but also in glia and some neurons. We compared the *swip-10* 5th intron GFP reporter to a known pan-glial marker and confirmed that *swip-10* is highly expressed in glia surrounding the anterior pharyngeal bulb. Interestingly, a fragment containing both 5' and intronic *cis* elements was sufficient for weak, but detectable GFP expression in DA neurons. We also observed that the expression of *swip-10* using any of these fragments, especially the intronic fragment, is detectable in the early embryo and persists with a more restricted expression pattern into adulthood. Considering the developmental profile of *swip-10*, its function in coordinating DA homeostasis may derive from its activity during the development of these tissues. Further experiments expressing *swip-10* under inducible promoters within certain cell types may help determine the temporal requirement for its function. Through additional experiments of the *dat-1* Swip temporal window, we have determined that the penetrance of Swip is highly dependent on the developmental stage of the animal. Though the biological mechanism of this regulation is unknown, the penetrance of Swip in *dat-1* and other mutants may derive from alterations in the connectivity and synaptic transmission of upstream neurons and glia. Alternatively, the penetrance of Swip in these strains may simply derive from the developmental trajectory of DAergic synapses that is not complete until L3-L4 (Sulston, et al., 1975).

To understand the precise site of *swip-10* function in regulating DA homeostasis, we transgenically overexpressed *swip-10* in specific cell types.

Our initial efforts using GFP-tagged genomic fragments under the expression different cell specific promoters demonstrated expression of GFP in off-target cells (data not shown). Consistent with our analysis of *swip-10 cis* elements, we hypothesize that the presence of the *swip-10* 5th intron precluded cell specific expression using a genomic fragment. Therefore we isolated a full length *swip-10* cDNA to use for investigation of *swip-10* cell autonomous function.

Having isolated the *swip-10* cDNA, we transgenically expressed it under the control of cell specific promoters on the *swip-10* backgrounds and tested transgenic progeny for rescue of Swip. Although we observed detectable expression of *swip-10* in DA neurons, expression of either tagged or untagged *swip-10* cDNA in these neurons did not rescue Swip. Consistent with the glial expression we observed using the *swip-10* promoter fusions, expression of the *swip-10* cDNA under the pan-glial promoter *ptr-10* significantly rescued the Swip in all alleles of *swip-10*. Thus, *swip-10* functions in glia to regulate DA signaling. CEPsh glia envelop and regulate the function and development of CEP DA neurons (Oikonomou & Shaham, 2010). Expression of *swip-10* in these cells (via the *hlh-17* promoter), however, did not rescue *swip-10* Swip. Likewise loss of the mammalian glial transcription factor Olig2 homolog *hlh-17*, whose expression is enriched in CEPsh, had been reported to generate dopaminergic phenotypes (Felton & Johnson, 2011). In our own assays of these lines, however, we did not observe any significant reductions in swimming behavior in *hlh-17* or *hlh-17 hlh-31 hlh-32* mutants. Importantly, whereas the *swip-10* 5th intron was sufficient to drive the expression of GFP, we could not rescue Swip

using this *swip-10* internal promoter to drive expression of the *swip-10* cDNA. Therefore, while the 5th intron of *swip-10* contains *cis* elements that are sufficient to drive expression of GFP in glia, they are not sufficient to permit function of the *swip-10* protein and rescue of Swip in a mutant allele. *ptr-10* is expressed in multiple glial cell classes: including sheath and socket cells of the inner/outer labial sensilla (OL/ILsh, OL/ILso, OLQsh, and OLQso cells), CEPsh glia, and sheath and socket cells of the deirid (ADE/PDEsh and ADE/PDEso cells). Unfortunately, cell specific promoters for many of these glial cell classes have not been described. Based on the robust expression that we observed in the promoter fusion experiments, we hypothesize that *swip-10* functions in sheath or socket cells of the inner and outer labial sensilla. The function of *swip-10* in the OL/ILso cells may be tested by use of the *itx-1* promoter (Haklai-Topper et al., 2011), but a cell specific promoter for the sheath cells has not been identified. The OL/ILsh and OL/ILso glia make supporting contacts with many neurons of the inner and outer labial sensilla, including the OLL neurons. Interestingly, the OLL mechanosensory neuron pair makes multiple synapses onto CEP neurons (wormatlas.org). Therefore *swip-10* may function in the OL sheath or socket cells to buffer the unknown chemical output of the OLL neurons onto CEP DA neurons. Mosaic analysis of using the *ptr-10* expression construct in combination with an SL2-mCherry cassette or by coinjection with a *ptr-10*:RFP plasmid will be necessary to precisely isolate the relevant glial cell type for *swip-10*'s role in regulating DA signaling.

Our previous study using the application of the DAT-dependent neurotoxin 6-OHDA had indicated that *dat-1* activity was intact in the *swip-10* mutant strain (Hardaway, et al., 2012). We hypothesized that loss of *swip-10* results in an increase in DA neuron excitability that results in elevated DA release that overwhelms the activity of endogenous *dat-1* that clears DA following release. Using *in vivo* Ca^{2+} imaging during BSR, we demonstrated that an encounter with a lawn of food is sufficient to drive CEP DA neuron excitability and that loss of *swip-10* results in an increase in excitability during this DA-dependent behavior. The rescue of this behavior using glial specific *swip-10* will be important to link the function of *swip-10* in glia in regulating Swip with *swip-10*'s role in regulating DA neuron excitability.

Having described the cell autonomous function of *swip-10* in glia and its impact on DA neuron excitability, we hypothesized that the increase in DA neuron excitability in *swip-10* may derive from an increase in GLU signaling. Although a previous study had illustrated that DA and GLU function in parallel to promote area-restricted search behavior in the worm (Hills, Brockie, & Maricq, 2004), no study to date has systematically assayed the impact of GLU signaling mutations on dopaminergic behaviors. Using Swip and the BSR assays, we screened through available mutant alleles in genes necessary for GLU signaling including both ionotropic and metabotropic GLURs and vesicular and plasma membrane transporters (P J Brockie, Madsen, Zheng, Mellem, & Maricq, 2001; P. J. Brockie & Maricq, 2006; Penelope J Brockie & Maricq, 2003; Dillon, Hopper, Holden-Dye, & O'Connor, 2006; C. Kang & Avery, 2009; R. Y. Lee,

Sawin, Chalfie, Horvitz, & Avery, 1999; Mano, et al., 2007). We did not observe major changes in the Swip phenotype of strains containing mutations in GLURs, but we did observe a loss of normal BSR with a loss of *glr-1* and an elevated BSR with a loss of *glr-4*. Allen *et al*. observed that the function of *glr-1* at command interneurons is necessary for modulating cholinergic output of motor neurons, thus we hypothesize that this loss of BSR is likely due to its function in the interneurons rather than its role in DA neurons (Allen, et al., 2011). *glr-4* expression is enriched in wide variety of neurons in the nerve ring, DB motor neurons, and analysis of DA neuron transcriptomes revealed the presence of *glr-4* transcript in these cells. Further work will be necessary to determine how *glr-4* contributes to normal BSR. Our assays of Swip in lines containing mutations in the glutamate transporters *glt-1*, *glt-3*, and *glt-4* revealed that loss of these transporters triggers an incomplete, yet highly significant, Swip phenotype. Furthermore, assays of strains containing mutations in multiple GLTs revealed that these GLTs likely function in parallel pathways to mediate the Swip phenotype. Unfortunately, it was impossible to assay a line containing a loss of all three GLTs, as *glt-1 glt-4* double mutants were not viable. To validate that the Swip in these strains was DA-dependent, we crossed these alleles to *cat-2* and observed that loss of *cat-2* fully restored the Swip phenotype of all three GLT alleles. Similarly, we observed that the Swip of these three alleles was suppressed by an increase in the swimming media osmolarity. Similar to Swip, we observed that loss of *glt-1* significantly impaired the magnitude of BSR relative to N2. Thus altered GLU signaling through loss of specific GLURs and

GLTs can evoke changes in DAergic behaviors and that loss of *glt-1*, *glt-3*, and *glt-4* can trigger DA-dependent Swip.

During our analyses of BSR in glutamate signaling mutants, we also tested the BSR of Swip-harboring strains including *dat-1* and *swip-10* as the effect of presynaptic or upstream mutations had not been described elsewhere. Surprisingly, loss of *dat-1* impaired normal BSR. We observed a loss of BSR in the *swip-10(vt33)* allele, but not in the *swip-10(vt29*) allele. Analysis of the latter allele was confounded two factors: 1) the presence of a bimodal distribution of animals that do not exhibit BSR and those that exhibit exaggerated BSR and 2) a decrease in their basal locomotory rate on food-free plates. We confirmed the latter finding and its DA dependence by use of an automated platform, WormLab, which provides for a more systematic analysis of locomotory kinetics on plates. In combination with the changes in DA neuron excitability, we hypothesize that that loss of *swip-10* results in an increase in extrasynaptic DA that is context-independent. While DA-dependent locomotory alterations for *dat-1* are only revealed when these animals are placed in water, an environment that we believe is capable of evoking dramatic increases in DA neuron excitability, *swip-10* mutants are hyperdopaminergic due to a persistent change in DA neuron activity. Simply put, DA neurons in the *swip-10* mutant are firing all the time, resulting in constitutive DA release. Initially, we hypothesized that strains that we suppose to be hyperdopaminergic (i.e. – *dat-1* and *swip-10*) would all demonstrate an exaggerated BSR through elevated DAergic tone on postsynaptic *dop-3* receptors. Due to the complexity of *dop-1*/*dop-3*

antagonism (Allen, et al., 2011; Chase, et al., 2004) or due to compensatory changes in tissue DA levels in Swip-harboring mutants (Hardaway, et al., 2012), we have revised our hypothesis. We hypothesize that BSR requires that the worm possess a wide dynamic range in the amount of extrasynaptic DA to control the amount of ligand available to act on postsynaptic *dop-1* and *dop-3*. In this model, a loss of the ligand or a gain in the amount of DA would be predicted to alter the amount of postsynaptic signaling and eventually behavior. Thus, strains that are hyperdopaminergic **or** hypodopaminergic have a narrower dynamic range of DA available for postsynaptic signaling than wildtype animals. Furthermore, it is unknown how chronic elevations in DA signaling in the *dat-1* and *swip-10* mutants impact the desensitization of pre and postsynaptic DA receptors and whether this contributes to the alterations in BSR that we observe. Based on changes in DA receptor expression levels in the DAT-/- mouse, we hypothesize that there are changes in DA receptor levels in the *dat-1* and *swip-10* strains (Giros, et al., 1996).

As a primary test of GLU signaling requirements on *swip-10,* we crossed *swip-10* to lines containing mutations in the only characterized vGLUT in *C. elegans*: *eat-4*. Loss of *eat-4* significantly suppressed Swip in the *swip-10* alleles *vt29* and *vt33*. Importantly, the suppression that we observed was incomplete. We hypothesize that loss of *eat-4* may decrease the overall extrasynaptic GLU content of the worm, but that Swip in the *swip-10* strain may derive from either 1) global changes that effect the overall extrasynaptic GLU content or 2) local changes in synaptic GLU that do not all use *eat-4*. A search of the worm gene

databases revealed that two other vGLUT orthologs exist (named *vglu-2* and *vglu-3*). Alleles of these vGLUTs are available, but their expression patterns have not been thoroughly characterized. Enrichment of their expression in neurons presynaptic to DA neurons may indicate that multiple vGLUTs contribute to elevated GLU release onto DA neurons in the *swip-10* mutant.

In combination with our analysis of DA neuron excitability, we hypothesized that *swip-10* hyperdopaminergia may require contribution of GLURs either in DA neurons or other neurons known to project to DA neurons. As loss of these GLURs by themselves did not evoke highly penetrant Swip phenotypes, we could assess the impact of these GLURs on *swip-10* through genetic analysis of GLUR loss on the *swip-10* background. We constructed double mutant strains of *swip-10* in combination with different GLUR alleles and assayed them for suppression of Swip. We observed that the majority of the GLURs that we tested including *glr-1, glr-2, glr-5, nmr-1, nmr-2, mgl-2,* and *mgl-3* did not affect the penetrance of Swip in the *swip-10* strain. We did find that loss of *glr-4, glr-6*, and *mgl-1* all produced a significant, yet incomplete, suppression of *swip-10*. Assays of triple mutant strains containing loss of two of these three GLURs on the *swip-10* background demonstrated that these receptors function in parallel to promote Swip in the *swip-10* mutant and a loss of all three receptors generated the most robust suppression of *swip-10*, though not to N2 levels. Importantly, we have not yet assayed the contribution of *glr-7* to *swip-10*, and there are no alleles available to test the contribution of *glr-3* and *glr-8*. However incomplete the suppression of *swip-10* Swip, these experiments

clearly demonstrate that *swip-10* hyperdopaminergia requires the function of two ionotropic and one metabotropic GLURs. To determine the specificity of these GLURs for *swip-10* Swip, we crossed them to the *dat-1* mutant and assayed their suppression of Swip in the *dat-1* mutant. Loss of *glr-4* and *glr-6* on the *dat-1* strain had no effect *dat-1* Swip penetrance. Loss of *mgl-1*, however, led to a nearly complete suppression of *dat-1* Swip. Moreover, we determined that the loss of *mgl-1* on the *dat-1* background promoted more frequent Swip reversal and crawling behavior. Future studies of rescue of the *mgl-1* gene and its expression within specific cell types will be necessary to determine the site of *mgl-1* function and the mechanism of *dat-1* Swip suppression. These studies establish that *swip-10* Swip, relative to *dat-1* Swip, is mediated by a host of GLURs as opposed to just *mgl-1*. We hypothesize that this shift in the GLUR contribution can be accounted for by a change in the amount of extrasynaptic GLU around these GLURs either in DA neurons or upstream neurons (Figure 53 and 54).

As we had demonstrated that *swip-10* requires the function of GLURs and that loss of GLTs can also generate Swip, we sought to determine whether *swip-10* functions in a pathway with either *glt-1, glt-3*, and *glt-4* using genetic epistasis experiments. We used a previously established paradigm, whereby an

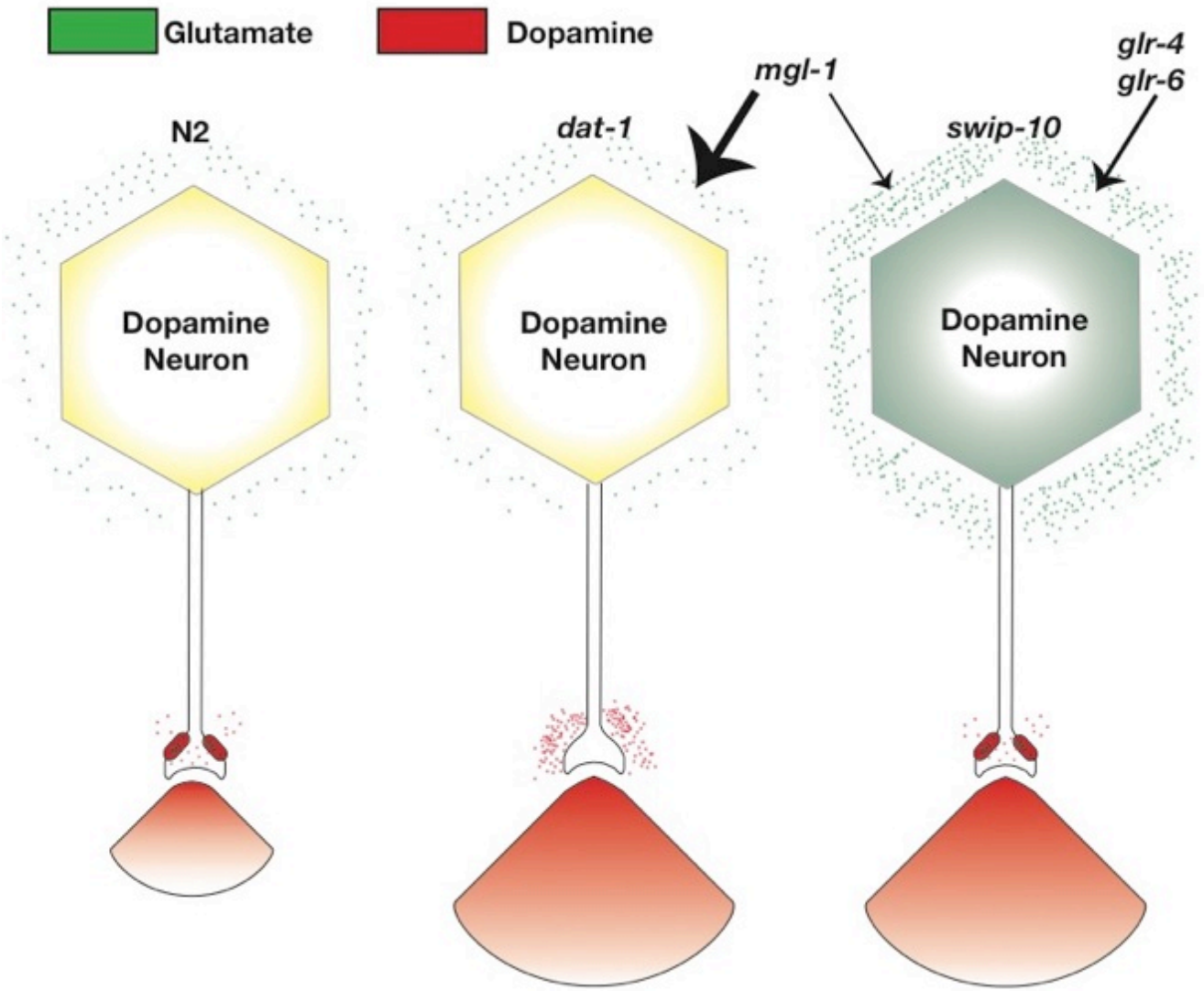

Figure 53 – Schematic of *glr-4, glr-6*, and *mgl-1* contributions to *dat-1* and *swip-10*. N2 animals maintain normal extrasynaptic DA levels through the uptake of DA through *dat-1* and the buffering of DA neuron excitability that is regulated by the amount of glutamate levels and excitatory signaling. Swip in the *dat-1* mutant is triggered by the loss of DA clearance but requires signaling of *mgl-1*, but not *glr-4* and *glr-6.* Swip in the *swip-10* mutant persists despite the normal function of *dat-1* and requires the contribution of *mgl-1*, *glr-4*, and *glr-6* mediated by an increase in tonic glutamate levels.

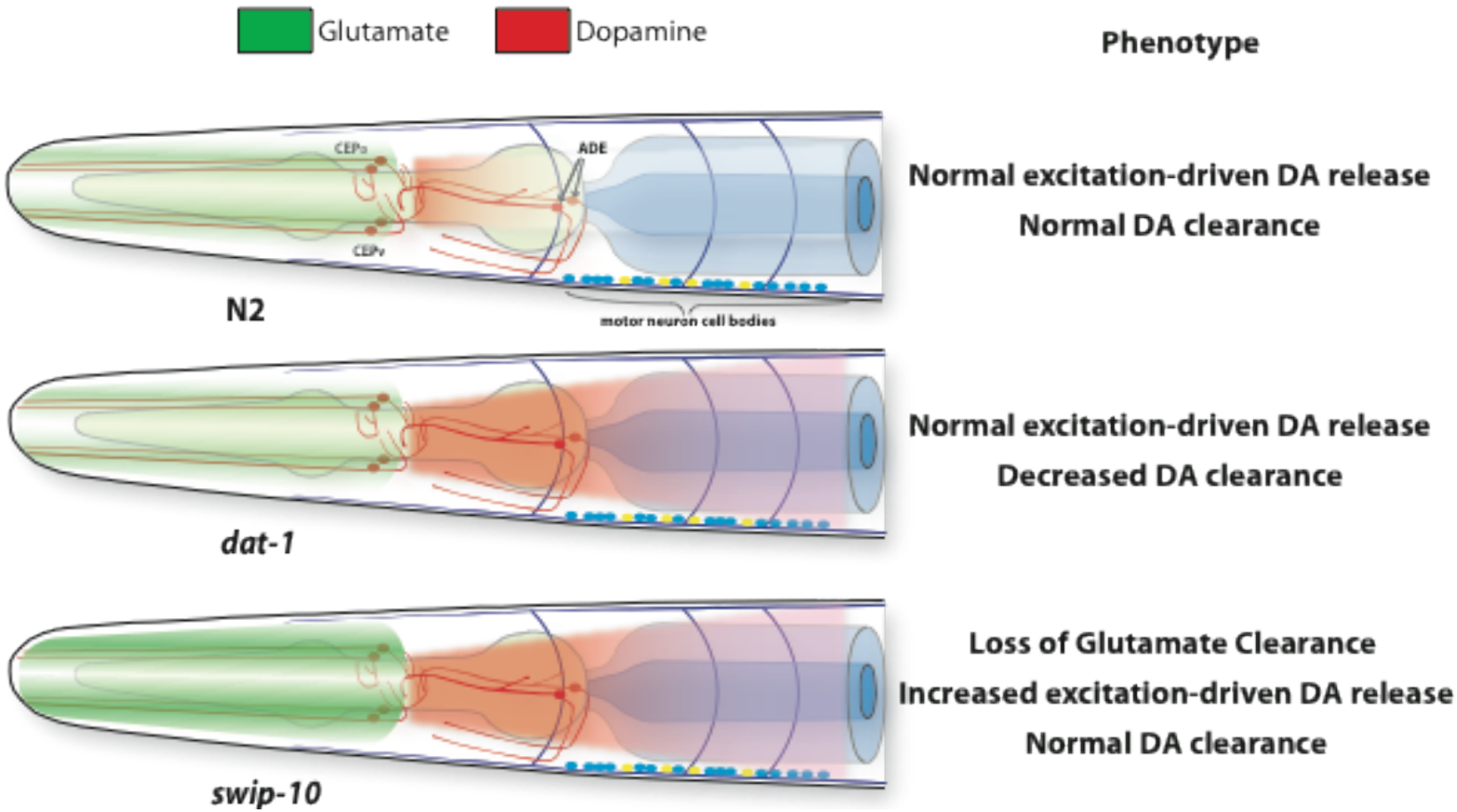

Figure 54 – Circuit level diagram of glutamate and dopamine contributions to Swip in the *dat-1* and *swip-10* strains. An increase in extrasynaptic DA in both strains is sufficient to trigger Swip, but the increase in extrasynaptic DA in the *swip-10* mutant is due to an increase in glutamate-mediated excitation-driven DA release as opposed to a loss of DA clearance through *dat-1*.

increase in osmolarity is sufficient to suppress the Swip in *dat-1* or *swip-10*, and that this suppression can reveal when two genes function in parallel, independent pathways to regulate the penetrance of Swip. Using this approach and a combination of *dat-1* and *swip-10* GLT double mutant strains, we found that, although loss of *glt-1* is capable of generating DA-dependent Swip, it significantly enhances Swip in the *swip-10* mutant and likely functions in pathways parallel and independent of *swip-10*. Surprisingly, loss of *glt-1* did not enhance the Swip of the *dat-1* mutant. Thus, *glt-1* and *dat-1* may cooperate through a shared pathway to regulate Swip. Analysis of *glt-4* revealed that it significantly enhances *dat-1*, but does not significantly enhance *swip-10*. Thus we conclude that *swip-10* functions in a genetic pathway containing *glt-4*. We have yet to construct the *dat-1; glt-3* strain, but we observed that loss of *glt-3* significantly rescued the *swip-10* strain at either osmolarity. Contrary to the presence of Swip in the *glt*-3 mutant strain, we hypothesize that *glt-3* activity may also be required for the recycling of GLU and its rerelease in addition to its predicted role in sodium dependent GLU clearance. Loss of *glt-3* function, in this case however, does not result in a global change in tissue GLU or aspartate levels as we did not observe any change in these amino acids, or cystine and GABA, in the *glt-1, glt-3*, or *glt-4* mutant lines using HPLC. Therefore, we hypothesize that changes in GLU signaling may be localized to synapses that are regulated by *glt-4.* Mano *et al*. observed that *glt-1*, by adulthood, is expressed mainly in the head muscle cells, but is enriched in hypodermal cells early in development (Mano, et al., 2007). Though our Swip analysis at the L4

stage of *swip-10 glt-1* double mutants suggest that these genes function in parallel, it is possible that *swip-10* may regulate *glt-1* function at an earlier larval stage. *glt-3*'s expression is pronounced in the excretory cell, a structure dedicated to excretion and electrolyte balance, and weakly in the pharynx. We predict that *glt-3* may function to regulate overall extrasynaptic GLU levels in the nerve ring thereby elevated extrasynaptic GLU may be capable of driving DA neuron excitation and DA release. The mechanism by which *glt-3* suppresses *swip-10* is more elusive. As these deletions are constitutive, compensatory changes in GLU neurotransmission such as reduced release or receptor desensitization are a possible mechanism for this effect. *glt-4* expression is enriched within neurons in the surrounding the nerve ring. In the description of its expression pattern the authors noted that *glt-4* expression colocalized with neurons also expressing *eat-4*. Therefore, they consider *glt-4* a presynaptic GLT, though a number of cells expressing *glt-4* were unidentified. In the description of the expression pattern of all *C. elegans* GLTs, they did not note any expression in worm glia. Therefore the actions of *swip-10* in a GLT pathway would have to function non cell- autonomously. We noted that the *swip-10* protein contains a nonconserved signal peptide sequence that may mediate secretion of the protein and hypothesize that *swip-10* may be secreted by glia to act on its substrate at distant sites in a *glt-4* pathway. In our review of the *C. elegans* glia literature there is no mention of glia's importance in regulating GLU neurotransmission in the worm. Considering the importance of glia like astrocytes in regulating synaptic and extrasynaptic GLU levels in mammals and

other invertebrates like *Drosophila* through the actions of GLTs, (Danjo, Kawasaki, & Ordway, 2011; Freeman & Doherty, 2006; Grosjean, Grillet, Augustin, Ferveur, & Featherstone, 2007; Stacey et al., 2010) (Nave & Trapp, 2008), we consider it highly unlikely that *C. elegans* glia do not harbor regulatory proteins necessary for GLU clearance. Rather, we suggest that the importance of glia in regulating GLU signaling derives from an evolutionarily ancient species and that its role has been previously unappreciated in *C. elegans*. Further studies of cell ablations of specific glia and measurements and their impact on synaptic GLU levels and GLU-regulated behaviors will be necessary to answer this question.

In summary, we identified a highly conserved gene in *C. elegans* that, when lost, triggers a hyperdopaminergic phenotype through an increase in DA neuron excitability. This gene is highly expressed and functions in worm glia to regulate the amount of excitatory signaling through 3 independent GLURs likely through the activity of *glt-4*, a neuronal GLT that, by itself, is necessary for maintenance of DA signaling.

FUTURE DIRECTIONS

The precise cell autonomous role of *swip-10* is still unknown. Our studies establish that *swip-10* functions in glia, but we do not yet know which glia are important for the regulation of Swip. The use of mosaic analysis using an expression plasmid containing an SL2-mCherry cassette or by coinjection of the *ptr-10*:RFP marker plasmid in tandem with the previously established functional

ptr-10: swip-10 cDNA:GFP construct and the generation of transgenic lines with mosaic transmission would allow for this type of analysis. Animals harboring expression of RFP or mCherry in specific glia could be tested separately by manual or automated Swip to determine which glia must express *swip-10* to rescue Swip.

Although we have established that DA neuron specific ion channels function cell autonomously to regulate Swip in a *dat-1* animal (see Chapter X), these ion channels exert only modest effects on *swip-10*. Therefore Swip in the *swip-10*, consistent with our previous data, derives from a polyneuronal and glial-interacting circuit. In keeping with our hypothesis of the importance of the OL/IL glia and the OLL mechanosensory neuron pair, *in vivo* Ca^{2+} imaging of the OLL neuron using a *ser-2*$_{prom3}$*:*GCaMP transgene during BSR and/or photostimulation of these neurons using *ser-2*$_{prom3}$*:*ChR2 during swimming and BSR, and ablation of these neurons on the *swip-10* and *dat-1* backgrounds will be important experiments to consider in illustrating how *swip-10* functions within the Swip-interacting native circuit to regulate DA homeostasis.

In our previous study, we noted that 6-OHDA exerts normal neurotoxic effect on *swip-10* animals. Although we measured this effect over an acute time scale, we did not, however, assay the integrity of DA neurons throughout the worm lifespan. The effects of many Parkinson's Disease associated genes on DA neuron viability has been thoroughly studied (Caldwell & Caldwell, 2008; Cao, et al., 2005; Hamamichi, et al., 2008; Iwatsubo, 2007; Kuwahara et al., 2006; Lakso et al., 2003), therefore a longitudinal measurement of DA neuron

morphology on the *swip-10* or GLT mutant background should be possible. We hypothesize that because *swip-10* animals contain a persistent elevation in DA neuron excitability that requires GLURs, these animals will demonstrate age-dependent neurodegeneration relative to the N2 strain.

We observed that loss of *egl-3* completely suppressed the *swip-10* strain. At this time, we have no further data to support an explanation for this result. We hypothesize, however, that neuropeptide signaling through *egl-3* may be required postsynaptically at the motor circuit to mediate DA's effects. A cross of *egl-3* into the *dat-1* mutant would be sufficient to demonstrate if *egl-3*'s function generalizes to other hyperdopaminergic strains. We hypothesize that *egl-3* would suppress this strain and other Swip-harboring strains. Finally, assay of *egl-3*'s response to exogenous DA would be sufficient to determine its requirement for DA modulation of the postsynaptic motor circuit. We hypothesize that *egl-3* and neuropeptides are necessary for DA signaling onto DA receptors expressed by motor neurons.

In these studies, we screened through a number of strains harboring mutations in GLU signaling genes. There are a number of strains that we might still screen or repeat to complete our analysis of the entire GLU signaling network. *vglu-2* and *vglu-3* are other vGLUT homologs in the worm and mutant alleles are available to screen for Swip and BSR. Though we did observe suppression of *swip-10* with loss of *eat-4*, we may observe a more dramatic suppression of Swip with a loss of *vglu-2* or *vglu-3*. We screened *swip-10*'s interaction with all GLURs with an available allele except for *glr-7*. We

hypothesize that, based on the expression pattern and level of *glr-7* transcript in DA and other neurons, that *glr-7* is not required. Similarly, there are no current alleles available for the AMPA receptors *glr-3* and *glr-8* which precludes an analysis of their contribution to *swip-10*. Through these genetic analyses we observed that loss of *glr-4, glr-6,* and *mgl-1* in parallel generates a robust suppression of *swip-10*. Analysis of BSR in the triple *glr-4; glr-6 mgl-1* strain may reveal a reduction in this behavior, consistent with the hypothesis that these GLURs function in parallel to mediate changes in DA neuron excitability. Similarly, at the time of performing the BSR assays on GLU signaling components, the *swip-10(tm5915)* allele was not yet available. Assay of this strain would provide parallel evidence to the phenotypes we observed using *vt29* and *vt33* that include the reduction in overall locomotory rate on food-free plate. Using Wormlab and the *swip-10(tm5915)* allele in combination with *cat-2*, *dop-3* and GLUR alleles, there is a need to establish that the reduction in speed in the *swip-10* mutant is not allele specific and that this reduction is mediated by DA, *dop-3*, and the same GLURs that are mediating Swip.

The contribution of GLUR signaling to *dat-1* and *swip-10* is a compelling line of research. Future analyses using transgenic restoration of these GLURs on the *glr-4; swip-10 glr-6 mgl-1* and *dat-1; mgl-1* backgrounds will help augment our understanding of the cell autonomous function of these GLURs and how *swip-10* mutations alter a network of GLU signaling genes.

Our analysis of *swip-10* genetic interactions with GLTs establish that *swip-10*, unlike *dat-1*, likely functions in a pathway with *glt-4* to mediate Swip.

glt-1, on the other hand, functions in a parallel pathway to *swip-10* and may interact genetically with *dat-1*. Our analysis of *glt-3* and its interaction with *dat-1* is still incomplete however.

Lastly, our epistasis experiments clearly establish genetic interactions between *swip-10* and GLU signaling components, but we do not yet understand the molecular mechanism by which *swip-10* alters GLU signaling. Future studies investigating *swip-10*'s contribution to glutamatergic behaviors such as spontaneous reversal would provide parallel evidence for our hypothesis that *swip-10* are hyperglutamatergic (P J Brockie, Mellem, Hills, Madsen, & Maricq, 2001; Mellem, Brockie, Zheng, Madsen, & Maricq, 2002; Zheng, et al., 1999). Additionally, the molecular mechanism by which *glt-4* is regulated by *swip-10* is still unknown. Analysis of *glt-4* transcription by use of the available *glt-4*:GFP reporter may reveal *swip-10*'s contribution to *glt-4* transcription.

Recently, a group reported the development and *in* vivo analysis in *C. elegans* of a GFP-based glutamate sensor called iGluSnFr (Marvin et al., 2013). The expression of this sensor has already been tested in DA neurons (Snarrenberg and Hardaway, unpublished) and the relative baseline fluorescence of this sensor or the imaging of this sensor on the *dat-1* and *swip-10* background using fluorescence recovery after photobleaching (FRAP) may serve as an effective proxy for synaptic GLU levels. Similarly, measurement of synaptic release using FRAP of a $p_{asic\text{-}1}$:: *snb-1*:pHlourin transgene in DA neurons have already been established and implemented in the lab (Bermingham and Baas, unpublished)(Voglis & Tavernarakis, 2008). A line containing the *swip-10*

mutation in combination with the $p_{asic\text{-}1}$:: *snb-1*:pHlourin transgene has been generated and archived for these experiments.

Chapter VI

IDENTIFICATION AND CHARACTERIZATION OF Mblac1

INTRODUCTION

In the previous chapter, we described the identification and characterization of *swip-10* in the nematode *C. elegans*. In this chapter, we analyze the expression pattern of Mblac1 RNA and protein in the mouse brain and in cultured cells, begin our efforts to identify the endogenous Mblac1 substrate, and describe how this protein fails to interact with β-lactam containing substrates.

MATERIALS AND METHODS

Isolation of RNA

Total RNA was isolated from either whole brain, distinct brain regions or peripheral tissues in 14-16 week old C57/BL6 male mice. An appropriate amount of Trizol (Sigma) was added to the tissue and Total RNA was isolated according to the manufacturer's instructions. We repeated the Trizol extraction to ensure that gDNA was not present in our samples.

RT-PCR

To generate first-strand cDNA, we used 500 ng of total RNA as input in a reverse transcriptase reaction using Superscript III RNA Polymerase (Life Technologies). cDNAs were diluted to 100 ng/μl and used as template for

polymerase chain reaction. PCR reactions were performed using Platinum PCR Supermix (Life Technologies) according to the manufacturer's instructions. PCR products were sequenced with the sense primer to validate their identity. The primers used were:

Mblac1:

RB4442(For) – CCTGGGGCTGTTTCCCGAGGCAG

RB4393(Rev) - TGCCTTCACATATCAAATCCTC

Mblac2:

RB4394(For) - ACCTCTACTCCTCTGGCCTCTT

RB4443(Rev) – GCCCAGGAAGCACCTTCTCCACAAG

Lactb2:

RB4396(For) – GGAATCCCCAGAGAGAAGAAAT

RB4444(Rev) – GGATGACTGGGCCATGTCCTGG

Gapdh:

RB4495(For) – GCACAGTCAAGGCCGAGAAT

RB4496(For) – GGCCTTCTCCATGGTGGTGAA

In situ hybridization of Mblac1 and Mblac2

Experiments were performed as described in Wu *et al.* with some modifications (Wu et al., 2009; Wu & Levitt, 2013). Prior to probe generation 564 bp Mblac1 and 524 bp Mblac2 cDNA fragments at the 3' end of each gene were subcloned into pBSKII(-) using 5' BamHI and 3' XbaI sites to generate pRB1165 and pRB1166 respectively. Digoxigenin cRNA probes for Mblac1 and Mblac2 were

generated by *in vitro* transcription from these vectors using a DIG RNA labeling kit (Roche) and T3 RNA polymerase (Roche). Brains were dissected and frozen fresh with liquid N_2 cooled isopentane and stored at -80°**.** Brains were embedded in TFM tissue freezing media (Triangle Biomedical Sciences) and sectioned at a thickness of 20 μM using a cryostat. Slides were fixed in 4% paraformaldehyde (PFA)/PBS for 20 min. at RT, washed with PBS, and incubated in Proteinase K(1 μg/ml) solution for 15 min. at RT. Slides were acetylated by incubating with triethanolamine (TEA-HCl, pH 8.0) for 10 min. after drop additions of acetic anhydrate(0.25% TEA volume). We prehybridized the slides for 2 hr at 60° in hybridization solution (50% deionized formamide, 5X SSC, pH 7.0, 1X Denhardt's solution, 0.1% Tween-20, 0.1% CHAPS, 5 mM EDTA, pH 8.0, 100 μg/ml heparin, 300 μg/ml yeast tRNA in DEPC-H_2O). Hybridization of slides with cRNA probes was carried out in hybridization solution at 60° for 16-18 hrs. Slides were first washed three times for 45 min at 65° in washing solution (2X SSC, pH 4.0, 50% formamide, 1% SDS in distilled H_2O) and then three times for 15 min in TBST (25 mM Tris-HCl, pH7.5, 136 mM NaCl, 2.68 mM KCl, 1% Tween-20 in distilled H_2O) with light agitation at RT. We blocked the slides for 1 hr at RT with blocking solution (100 mM Tris-HCl, pH7.5, 150 mM NaCl, containing 1.5% blocking agent – Roche) and then incubated them o/n with alkaline-phosphotase conjugated anti-DIG Fab fragments (1:2,000, Roche). To color the sections, we incubated them in NTMT solution (100 mM NaCl, 100 mM Tris- HCl, pH 9.5, 25 mM MgCl2, 1% Tween-20, 2 mM

levamisole) with 0.2 mM 5-bromo-4-choloro-3-indolyl phosphate (BCIP) and 0.2 mM nitroblue tetrazolium (NBT; Roche) until color was evident.

Development of an Mblac1 Polyclonal Antibody

Mblac1 cDNA (ThermoFisher) was amplified and subcloned in frame to glutathione S-transferase (GST) within pGEX2T using BamHI and EcoRI sites at the 5' and 3' ends respectively to generate pRB1163. pRB1163 was transformed into BL21 competent cells. Expression of a full length GST-Mblac1 protein was induced via IPTG addition and purified from crude bacterial cell lysates via GST affinity chromatography. GST-Mblac1 with adjuvant was injected into two rabbits (#4979 + 4980) over the course of several months to produce GST-Mblac1 antiserum. Antiserum from both rabbits was tested at several dilutions via western blotting against GST-Mblac1 protein and Mblac1 transfected cells. Specificity of Mblac1 immunoreactivity was confirmed by preadsorption of the antiserum with GST-Mblac1 protein. For purification of the Mblac1 antiserum, we cloned Mblac1 cDNA in frame to maltose binding protein (MBP) within pMal-cR1 using EcoRI and BamHI sites at the 5' and 3' ends respectively to generate pRB1164. Full length MBP-Mblac1 protein was generated as previously described with addition of 100 uM $ZnSO_4$ (Sigma-Aldrich) to the culture media during induction. The protein was purified via amylose affinity chromatography (New England Biolabs) and concentrated for further use. MBP-Mblac1 protein was conjugated to amylose resin, and 4980 serum was passed over the column multiple times, washed with column buffer,

and eluted with 150 mM Glycine pH 2.0. 400 μl fractions were collected and immediately neutralized in 2 M Tris-HCl pH 8.0. Fractions were pooled and dialyzed in excess 1X PBS containing additional 150 mM NaCl at 4 degrees overnight. Dialysate was then concentrated for further experiments and testing. For these experiments, we used several affinity-purified lots from Rabbit #4980 serum.

Immunohistochemistry

WT C57/BL6 males aged 10-15 weeks were anesthetized with Nembutal and cardiac perfused with 4% paraformaldehyde. Brains were removed and post-fixed for up to one week in 4% paraformaldehyde. The tissue was cryoprotected overnight in 20% sucrose at 4 degrees and sliced at 40 μM using a freezing microtome. Sections were collected in cryoprotectant and stored at -20 degrees until experiments were performed. For peroxidase staining, sections were washed 3X in TBS to remove cryoprotectant and endogenous peroxidase activity was quenched with 0.5% hydrogen peroxide and 10% methanol in TBS. Sections were blocked for 1 hour at RT using 3% normal goat serum (Jackson Research Labs) in TBS containing 0.1% Triton X-100 (TBST) and incubated with Mblac1 primary antibody (100-1000 ng/ml) at 4 degrees overnight. The following day, the sections they were washed 3X with TBS and incubated with biotinylated Goat anti-Rabbit (1:1,000) secondary antibody for 1 hour at RT. Following 3X washes with TBS, Mblac1 immunoreactivity was detected by applying avidin/horseradish peroxidase conjugate and 3,3'-diaminobenzodine

(3-7 min.). High resolution images of peroxidase based IHC were capture at 5-20X on an upright AxioImager 2 microscope and then stitched using AxioVision software. For immunofluorescence, sections were washed 3X in TBS and blocked in 10% normal goat or donkey serum in TBST for 1 hour at RT. Sections were then incubated in primary antibody cocktails for two days at 4 degrees. Antibodies used in these studies were Rabbit α Mblac1(5 ug/ml), GFAP(mAb360 - Millipore) at 1:1,000, S100β(SAB1402349 - Sigma) at 1:200, MAP2(M4403 – Sigma) at 1:100, vGlut2(ab2251 – Millipore) at 1:1,000, GLT-1(courtesy Robinson lab) at 1:100, Doublecortin(ab2253 – Millipore) at 1:1,000 and GAD67(mAb5406) at 1:500. Sections were then washed 3X with TBS and incubated with host appropriate AlexaFlour488 or 546 conjugated secondary antibodies at 1:1,000 for 1 hour at RT in the dark. Sections were washed 3X with TBS and incubated with 4',6-diamidino-2-phenylindole (DAPI) at 1:1,000. Sections were mounted on glass slides and sealed for imaging. All images were captured on an Zeiss LSM 710 confocal microscope and processed offline in ImageJ.

Mammalian Cell Culture

Human embryonic kidney cells containing a stable integrated SV40 large antigen (HEK293T) cells were cultured in DMEM containing 10% fetal bovine serum (FBS) containing L-glutamine and 1 mM L-glutamine. Note that antibiotic was not included for β-lactamase activity assays. Immortalized mouse fibroblast 3T3 cells were cultured in DMEM containing 4.5 g/L glucose and 1.5 g/L sodium

bicarbonate supplemented with 10% bovine calf serum. All cell lines were maintained in incubators at 37° with 5% CO_2.

Western Blot and Immunoprecipitation Analyses

For western blot analyses in 3T3 cells, cells were trypsinized for 5 min. at 37°, harvested with phosphate-buffered saline (PBS) and transferred to a 1.5 ml microfuge tube. Protein was solubilized from the cell pellet by incubation with RIPA buffer (50 mM Tris-HCl, pH 7.4, 150 mM NaCl, 1% Triton X-100, 1% sodium deoxycholate, 0.1% SDS, 1 mM EDTA) at 4 degrees for 1 hour with gentle agitation. Following solubilization, insoluble material was removed from the extracts by centrifugation at 13,000 rpm for 15 minutes. The protein concentration of the supernatant was determined by use of the colorometric bicinchoninic acid (BCA) method and absorption at 562 nM using an Omega Series plate reader (BMG Labtech). Total protein was denatured by incubation with 2X Laemli buffer at 95° for 5 min. Insoluble material was removed from the samples by centrifugation at 13,000 rpm for 15 min at RT. 15-25 μg of total cell protein were separated using SDS-PAGE and then transferred to an immobilon PVDF membrane (Millipore). Membranes were then baked at 37° and reactivated by methanol application. We blocked the membranes using PBS containing 0.1% Triton X-100 (PBST) and 5% bovine serum albumin (BSA). To detect Mblac1 we incubated the membranes overnight with the previously described Mblac1 affinity purified antibody at a concentration of 1 μg/ml diluted in 5%

BSA/PBST. For expression of human and mouse cDNAs, we cloned full length cDNAs using BamHI and EcoRI sites at the 5' and 3' ends to generate pRB1167(Mouse Mblac1), pRB1168(Human MBLAC1), pRB1169(Mouse Mblac2), and pRB1170(Human MBLAC2). Original cDNAs were obtained from Thermo-Fisher.

Measurement of β-lactamase Activity

We used the mammalian heterologous expression vectors described above in parallalel with a construct expressing a truncated non-secreted version of the TEM-1 β-lactamase (Bla)(Hasegawa, Jackson, Tsien, & Rao, 2003). We transfected HEK293T cells in six-well plate using TransIT-LT1 (Mirus Bio, Madison, WI), grew them for 48-72 hours, cells were harvested by rinse with PBS containing 100 μM $ZnSO_4$. We washed the cell pellets twice using the same buffer. Cell lysates were generated by four repeated freeze thaw cycles for 10 min. in liquid nitrogen and in a 37 degree water bath. Following cell lysis, we spun the lysates at 13,000 rpm to remove insoluble material and transferred the supernatant to a fresh tube. 90 μl of cell lysate was transferred on ice to a microtiter plate in quadruplicate and the substrate was added just prior to recording the absorbance on a Omega microplate reader (BMG Labtech) at 486 nM for Nitrocefin (de Seny et al., 2002) and both 346 and 405 nM for CENTA (C Bebrone et al., 2001). For nitrocefin (Millipore), we dissolved the compound in dimethyl sulfoxide (DMSO) according to the manufacturers instructions and then diluted this to a working stock of 1 mM with phosphate buffer (100 mM, pH 7.0).

For CENTA, we dissolved the substrate in 50 mM phosphate buffer (pH 7.0) to a final concentration of 1 mM. For both substrates, we added them to the cell lysates at a final concentration of 100 μM.

Confocal Microscopy

Confocal microscopy of immunofluorescent staining of mouse brain sections was performed using Zeiss LSM710 and the Zen software.

RESULTS

Expression of Mammalian Mblac1 and Mblac2

As we had observed robust expression of *swip-10* in glia and some neurons in *C. elegans*, we hypothesized that Mblac1 is expressed in the mammalian brain. During our identification of Mblac1 and analyses of functional domains using secondary structure prediction, we noted the existence of other genes containing metallo-β-lactamase domains. Preliminary experiments of Mblac1 and another metallo-β-lactamase, Mblac2, using *in situ* hybridization by the Allen Brain Institute supported our hypothesis that these metallo-β-lactamase domain-containing genes were expressed in the brain (Mblac1 - http://mouse.brain-map.org/experiment/show/68920662, Mblac2 - http://mouse.brain-map.org/experiment/show/72283390). To validate these experimental results we performed reverse transcriptase polymerase chain reaction (RT-PCR) on these three genes in parallel with a loading control RNA isolated from peripheral tissues such as the liver, lung, and the heart, whole

brain, and several distinct brain regions like the olfactory bulb, striatum, hippocampus, cerebellum, and the cortex. Similar to the available experiments at Allen, we observed that Mblac1 and Mblac2 were expressed throughout the brain including each of the regions we assayed (Figure 55). We also found that these two genes were expressed in each of the peripheral tissues we assayed.

Distribution of Mblac1 and Mblac2 RNA in mouse brain

To determine the distribution of Mblac1 transcript, we performed *in situ* hybridization on coronal sections. We observed high levels of Mblac1 RNA in the same brain regions that we tested with RT-PCR including the cerebellum (Figure 56A), the cingulate cortex (Figure 56B), the medial habenula (Figure 56C), the hippocampus (Figure 56D), and in cells lining the lateral ventricle (Figure 56E). Together with our RT-PCR experiments, these experiments establish that Mblac1 RNA is expressed in several areas of the mammalian brain.

Development and Affinity Purification of Mblac1 Antiserum

To probe for the expression of Mblac1 protein, we developed antiserum against a full-length GST-Mblac1 protein and tested its ability to detect Mblac1 expression in transfected cells. We found that antiserum (Rabbit #4980) could detect a protein of the predicted molecular weight in HEK293T cells overexpressing mouse Mblac1, but not human MBLAC1 (Figure 57A). To remove any potential contaminants, we affinity purified the antiserum and tested it as before in mouse Mblac1 transfected cells. Again, we found that our Mblac1

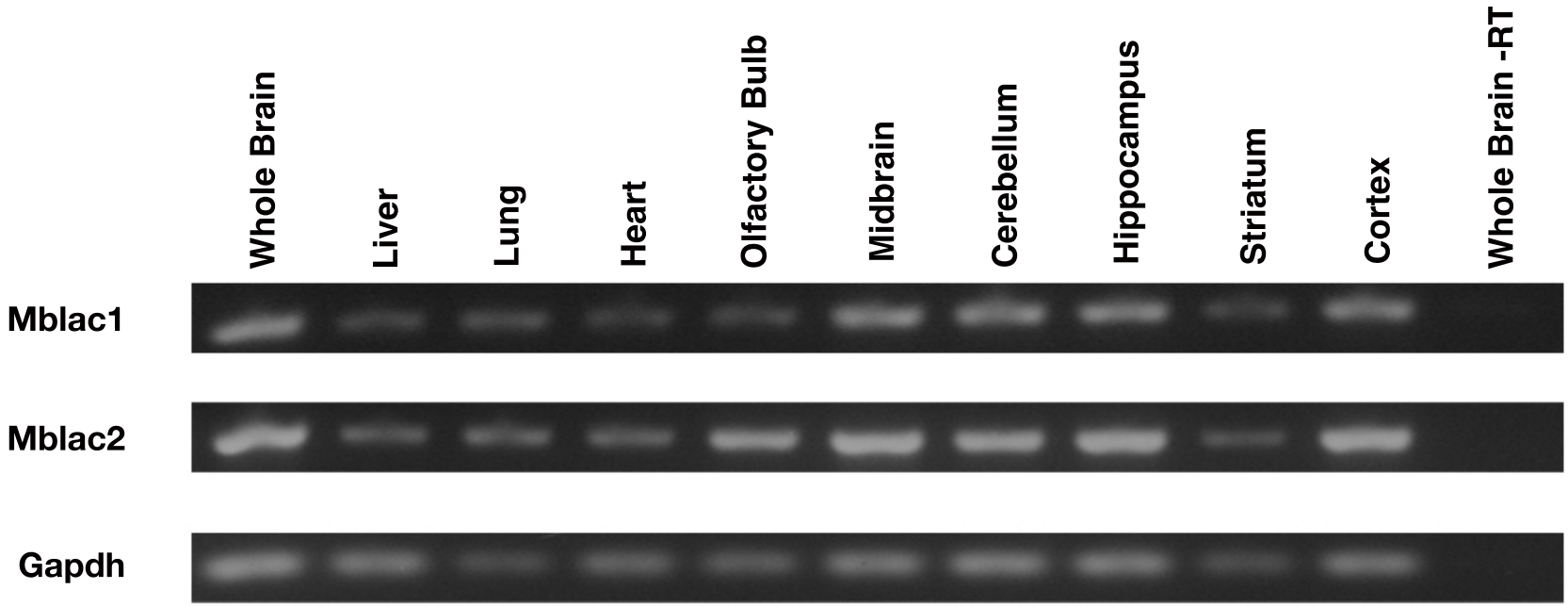

Figure 55 – RT-PCR of Mblac1 and Mblac2 from Mouse brain and peripheral tissues. Experiment, including RNA isolation, reverse transcription, and PCR was performed as described in the Methods. Significant Mblac1 and Mblac2 transcript was detected in each of the tissues we isolated, but not in whole brain libraries treated minus the reverse transcriptase enzyme.

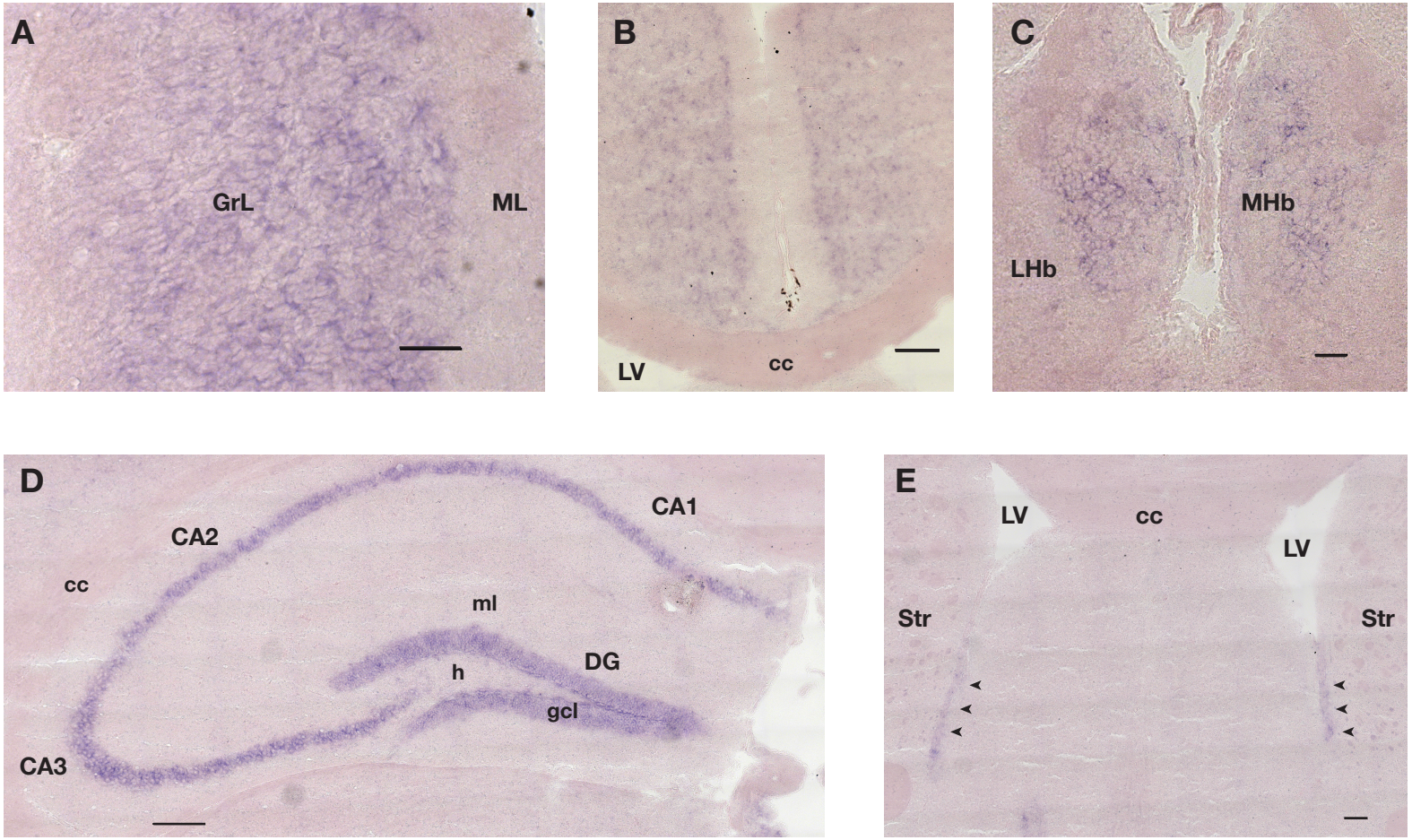

Figure 56 – *In situ* hybridization of Mblac1 in various mouse brain regions. Mblac1 RNA is present in the granular layer of the Cerebellum(**A),** cingulate cortex(**B**), medial habenula(**C),** the cellular layer of the hippocampus(**D**), and cells lining the lateral ventricle(**E**). Scale bar equals 50 μM in each image. Abbreviations are GrL – granular layer, ML – molecular layer, LV – lateral ventricle, cc – corpus callosum, MHb – medial habenula, LHb – lateral habenula, h – hilus, gcl – granule cell layer, DG – dentate gyrus, Str – striatum

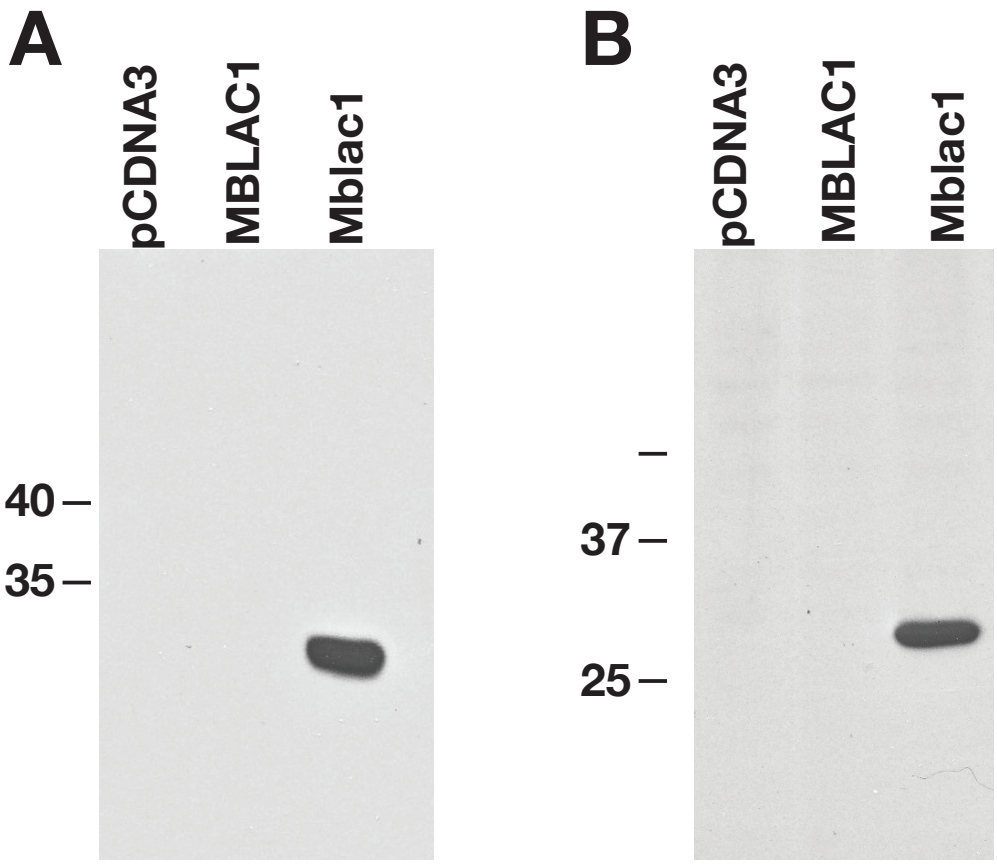

Figure 57 – Development and Purification of Mblac1 antiserum. A. Western blot of transfected cell lysates using 4980 antiserum(1:30,000). We detect a band of the predicted molecular weight in cells expressing mouse Mblac1. We do not detect human MBLAC1 protein with this antiserum. **B.** Western blot of transfected cell lysates using affinity purified Mblac1 antibody(1 μg/ml). We detect a band of the predicted molecular weight in cells expressing mouse Mblac1 but not human MBLAC1. For both **A** and **B**, we transfected HEK293T cells with pCDNA3 alone or pCDNA3 containing mouse(Mblac1) or human(MBLAC1). Cell lines and western blots were performed as described in the methods.

polyclonal antibody could reliably detect transfected Mblac1 at the predicted molecular weight.

Identification of Immortalized Cell Line expressing Mblac1

To gain a better understanding of Mblac1's subcellular expression pattern, we screened a number of immortalized cell lines for the expression of endogenous Mblac1. Our previous experiments using HEK293T cells transiently transfected with Mblac1 had already demonstrated that these cells do not express Mblac1 endogenously. Based on the expression of Mblac1 in peripheral tissues we observed with RT-PCR and the expression of *swip-10* in hypodermal cells, we screened NIH 3T3 cells and observed a band of the predicted molecular weight (28 kD) that was blocked by preadsorption of the Mblac1 antibody with a full length Mblac1 protein (data not shown).

Mblac1 Subcellular Expression Pattern in 3T3 cells

Having identified a cell line that expresses Mblac1 endogenously, we used 3T3 cells and crude subcellular fractionation to determine the subcellular expression pattern of Mblac1 (Holden & Horton, 2009). Using additional proteins to validate our fractionation protocol, we observed that Mblac1, like Gapdh, was expressed in the cytosol. Calnexin and Lamin B1 were enriched in the organellar and nuclear fractions respectively (Figure 58). Importantly, although we detected significant Lamin B1 protein in our cytosolic fraction, but we never observed any Mblac1 expression in the nuclear fraction. Along with our studies of Mblac1

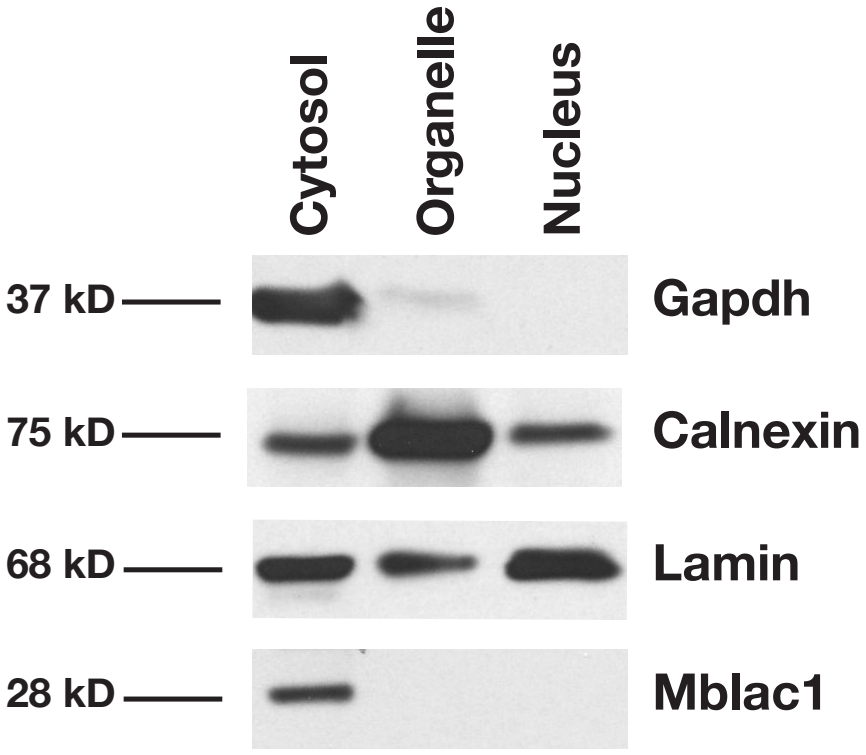

Figure 58 – Western blot analysis of Mblac1 in fractionated 3T3 cells. Crude subcellular fractionation were performed as described in the methods with 200 ug/ml digitonin for the cytosolic fraction and we probed three cellular fractions for the expression of known subcellular markers and Mblac1. We detected Mblac1 expression solely in the cytosolic fractions similar to Gapdh.

expression in native brain tissue sections (see next section), these data suggest that Mblac1 is a cytoplasmic protein.

Expression of Mblac1 Protein in mouse brain

To determine if Mblac1 protein is expressed in native tissue, we harvested protein from striatum, midbrain, cerebellum, hippocampus, and cortex and probed for its expression using western blots. As shown in Figure 59, we detected a band of the predicted molecular weight (28 kD) in all of these brain regions. Importantly, using this antibody we also detected a doublet just below 50 kD and a single band ~70 kD, but only the 28 kD band was blocked by preadsorption of the primary antibody with Mblac1 protein. We hypothesize that these bands are proteins with similar antigenicity to Mblac1, but that endogenous Mblac1 is expressed at the predicted molecular weight of 28 kD.

Distribution of Mblac1 expression in the mouse brain

To determine how Mblac1 expression is distributed in the mammalian brain, we used peroxidase-based immunohistochemistry using our Mblac1 antibody. We detected a high level of Mblac1 expression throughout all regions of the brain, but with a very consistent pattern of staining in certain areas (Figure 60). Mblac1 protein was enriched in areas that we had observed in analyses of Mblac1 transcript including the anterior cingulate cortex (Figure 61A), medial habenula (Figure 61D), hippocampus (Figure 61E), and the subventricular zone (Figure

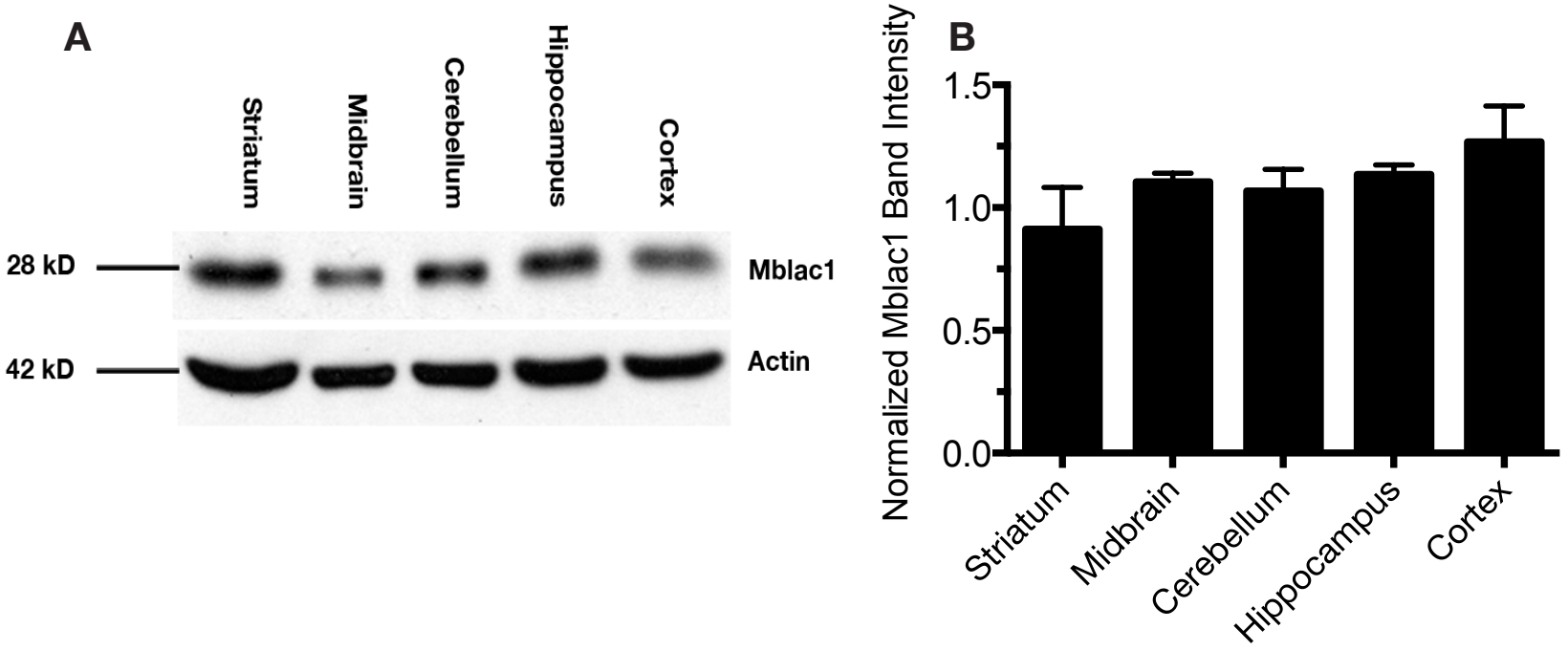

Figure 59 – Mblac1 protein is expressed throughout the mammalian brain. **A**) Representative blot of Mblac1 and loading control(β-actin) from native brain tissue **B**) Quantification of Mblac1/β-actin band density from 6 mice. Experiments were performed as described in the Methods and band density was determined using NIH ImageJ. Normalized values were analyzed by one-way ANOVA with multiple Bonferonni post tests.

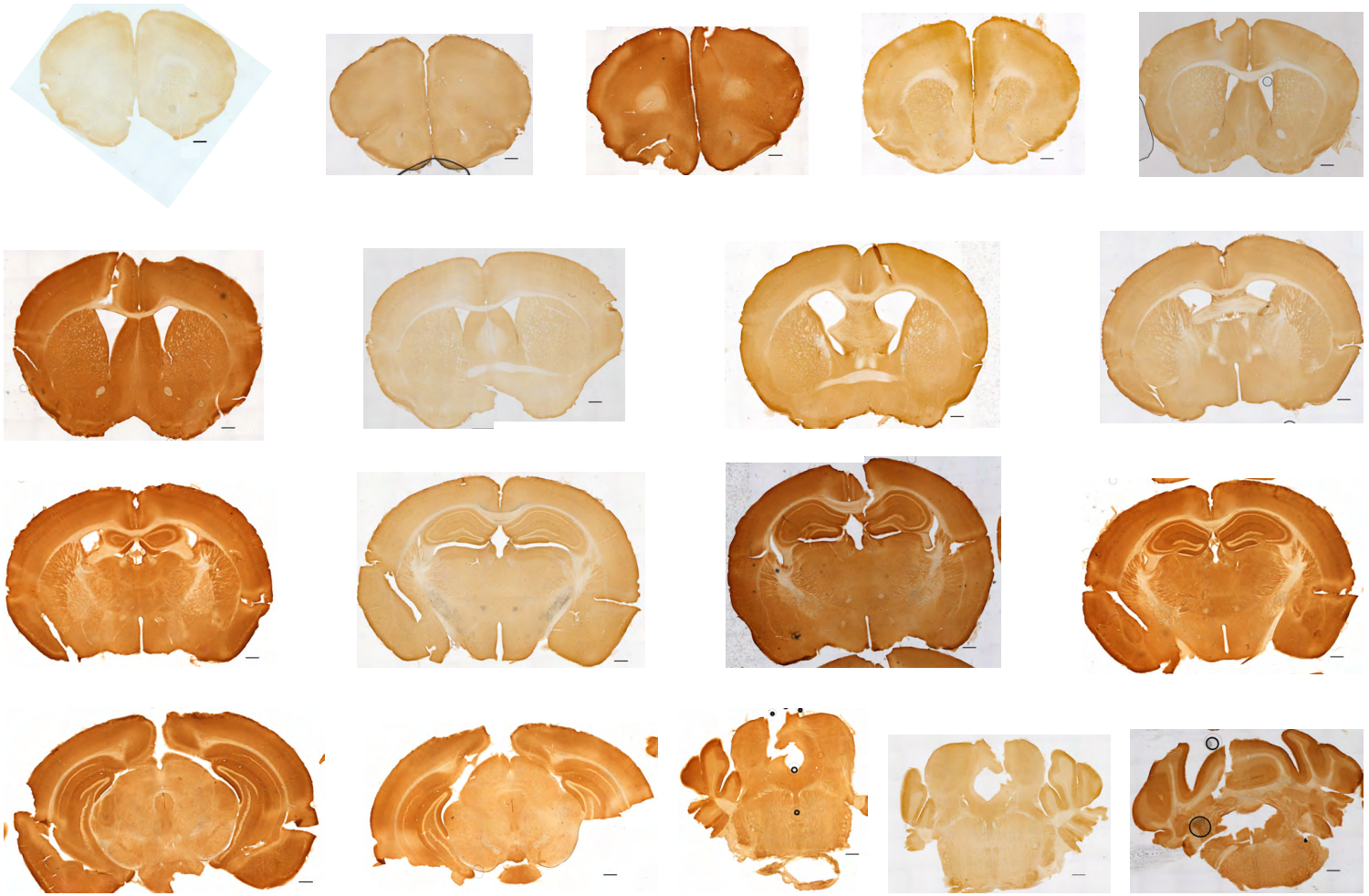

Figure 60 – Immohistochemical staining of Mblac1 in the wildtype mouse brain. Representative rostral and caudal coronal sections display that Mblac1 is expressed in multiple regions of the brain. Experiments were performed and sections were imaged as described in the methods section. Scale bar equals 500 μM in bottom right hand corner of each section.

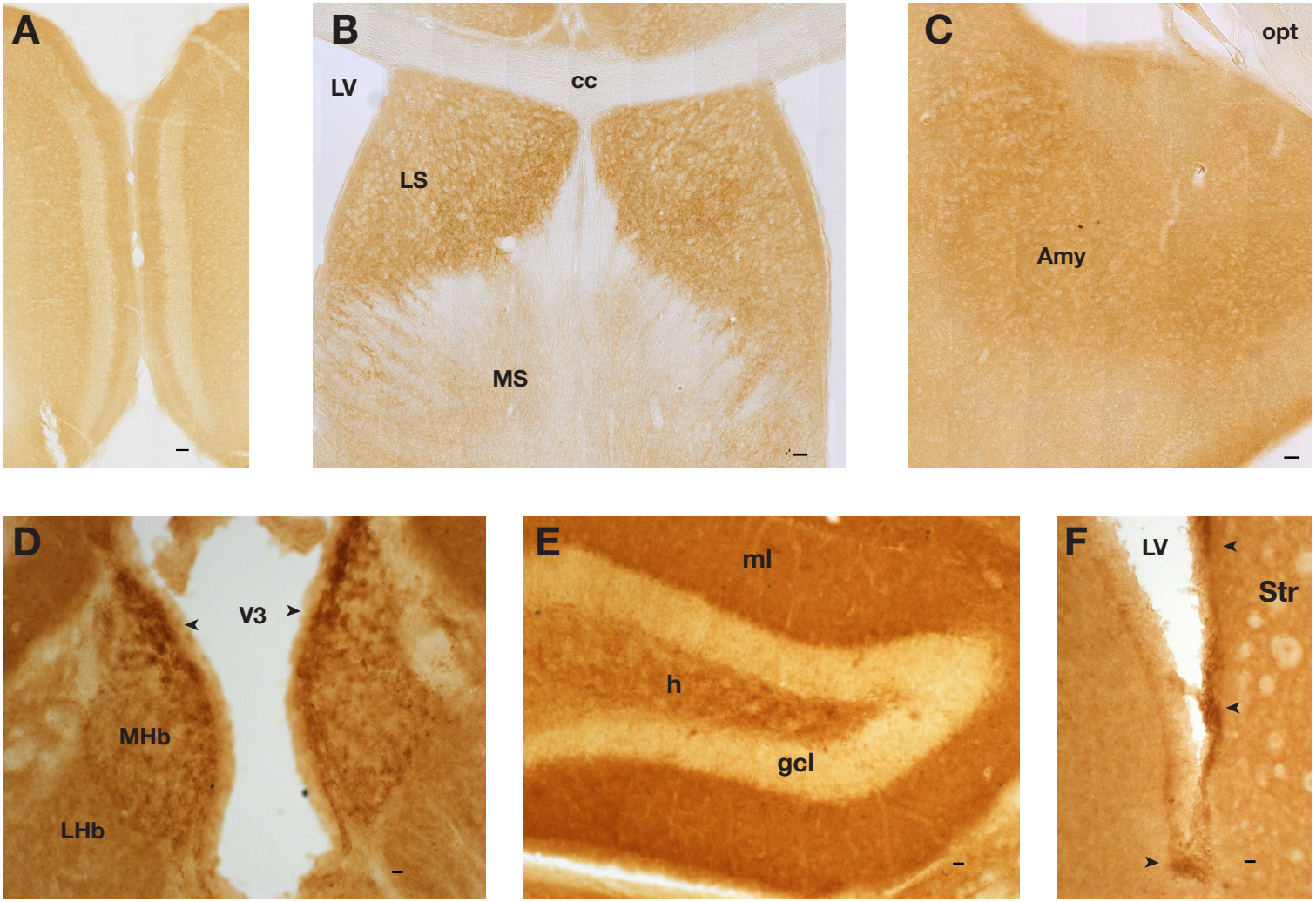

Figure 61 – High resolution images of Mblac1 immunohistochemistry. in **A**) Anterior Cingulate Cortex, **B**) Lateral Septal nucleus, **C**) Amygdala, **D**) Medial Habenula, **E**) Dentate Gyrus, and **F**) Subventricular Zone. Experiments were performed and sections were imaged as described in the methods section. Scale bar equals 50 μM in **A** and **B** and 20 μM in **C-F**.

61F). We also observed significant staining in throughout portions of the lateral septal nucleus (Figure 61B) and in other portions of the limbic system including the nucleus accumbens (see top right sections in Figure 60) and the amygdala (Figure 61C).

Immunofluorescent Characterization of Mblac1 Expression

To gain an understanding of how the Mblac1 expression pattern is defined at a molecular and genetic level, we performed immunofluorescence of Mblac1 in parallel with markers of specific neuronal and glial markers. We used association of the *swip-10* phenotypes and the distribution of known CNS molecules as our guide focusing on specific regions of robust Mblac1 staining including the medial habenula (MHb), dentate gyrus (DG), lateral septal nucleus (LS), dorsal peduncular cortex (DPC), subventricular zone (SVZ), lateral cerebellar nucleus (LCN), and the trapezoidal body nucleus (TB).

As we had observed robust expression of *swip-10* in *C. elegans* glia, we performed immunofluorescent staining for Mblac1 and known glial markers glial fibrillary acidic protein (GFAP), S100β, and glutamine synthetase (GS). Suprisingly, we did not observe colocalization of Mblac1 with any of these markers in the MHb, DG, DPC, or LS (Figures 62, 63, and 64). We did observe an enrichment of GS immunoreactivity in the DPC (Figure 64A), but analysis of both proteins at high resolution demonstrated that they display non-overlapping patterns of expression. As our characterization of *swip-10* suggested a connection to glutamate transporters (GLTs), we performed immunofluorescent

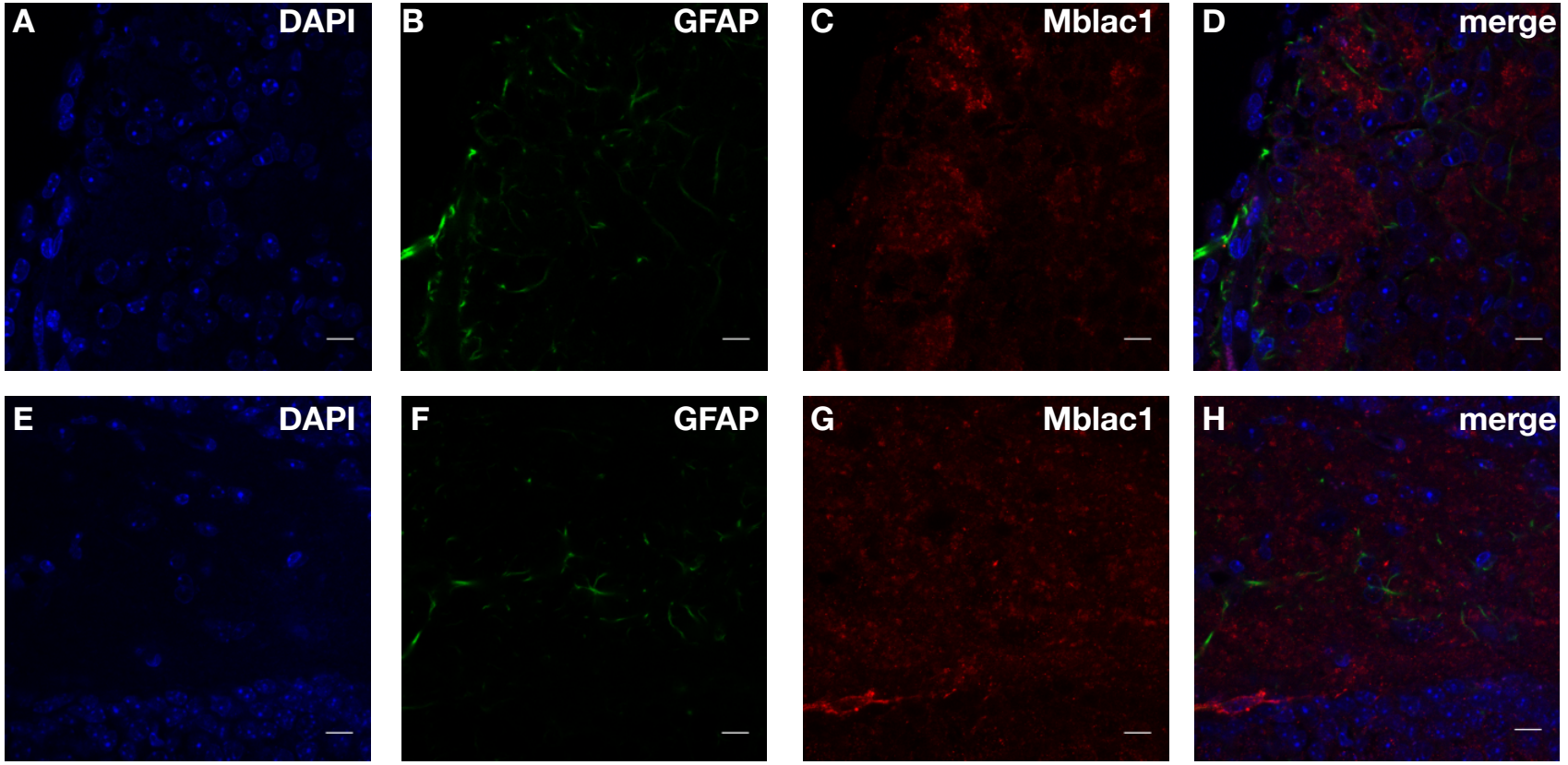

Figure 62 – Mblac1 and GFAP expression are not colocalized. **A-D**) 63X image of Mblac1 and GFAP in the MHb. GFAP+ fibers do not colocalize with Mblac1. **E-F**) 63X image of Mblac1 and GFAP staining in the DG. GFAP+ fibers do not colocalize with Mblac1. Scale bar indicates 10 μM for all panels. Dorsal is up for all confocal images.

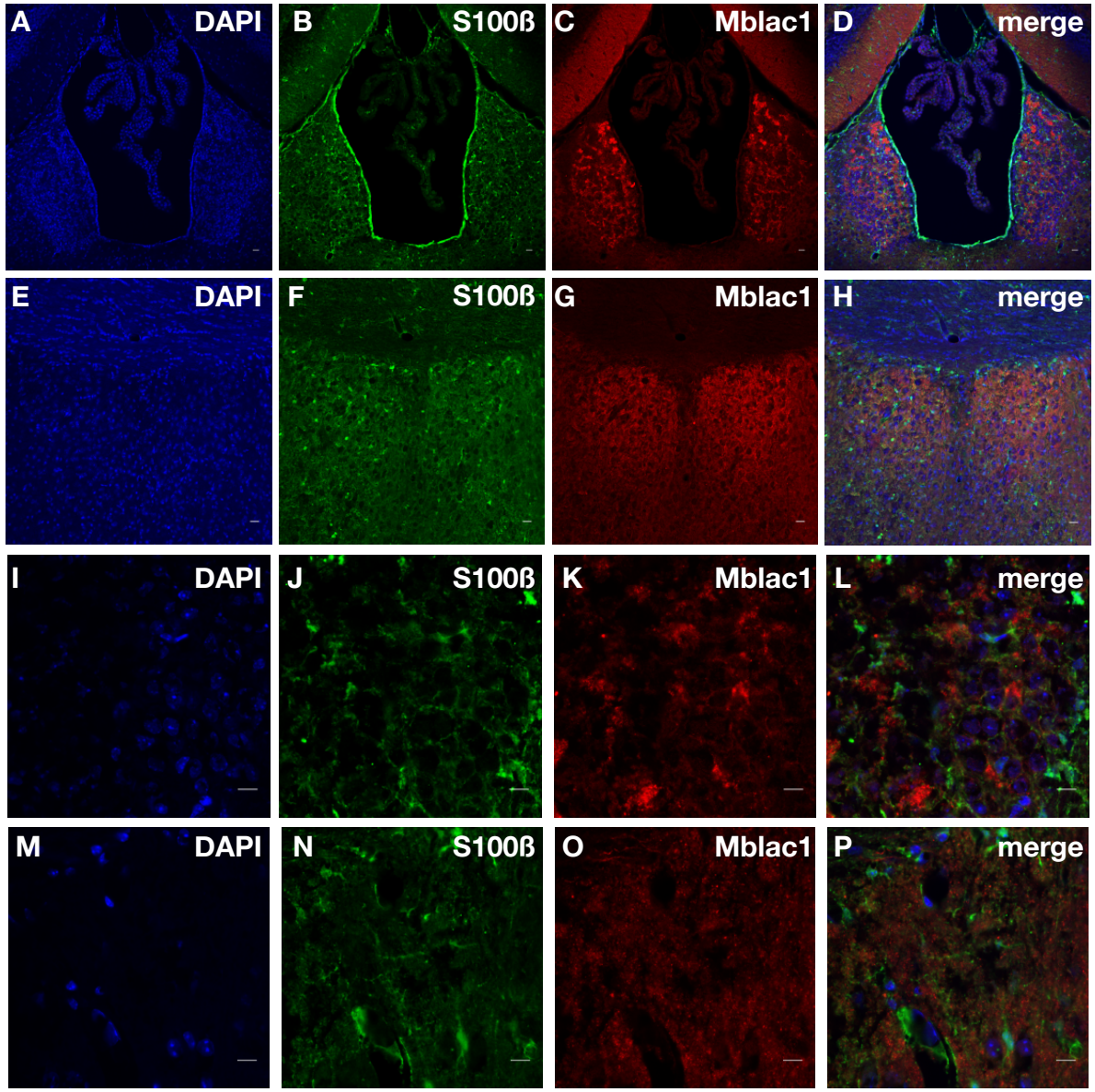

Figure 63 - **Mblac1 and S100β expression are not colocalized**. **A-D)**10X image of Mblac1 and S100β in the MHb. **E-H**) 10X image of Mblac1 and S100β in the DPC. **I-L**)63X image of Mblac1 and S100β in the MHb. Mblac1 and S100β do not colocalize. **M-P**)63X image of Mblac1 and S100β in the DPC. Mblac1 and S100β do not colocalize. Scale bar indicates 20 μM for **A-H** and 10 μM for **I-P**.

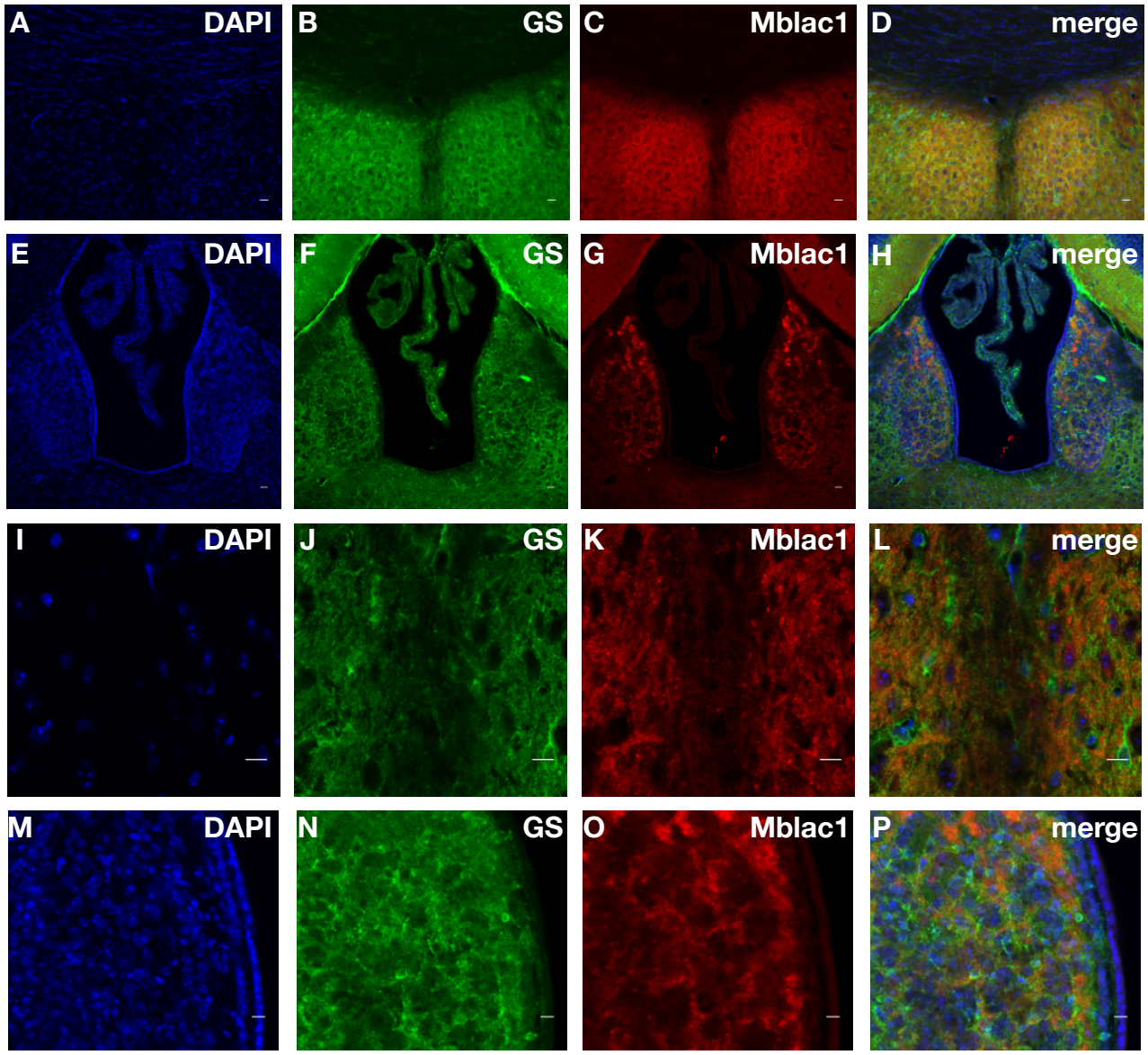

Figure 64 - **Mblac1 and GS expression are not colocalized**. **A-D)**10X image of Mblac1 and GS in the DPC. **E-H**)10X image of Mblac1 and GS in the Medial Habenula. **I-L**)63X image of Mblac1 and GS in the DPC. Mblac1 and S100β do not colocalize. **M-P**) 63X image of Mblac1 and GS in the MHb. Mblac1 and S100β do not colocalize. Scale bar indicates 20 μM for **A-H** and 10 μM for **I-P**.

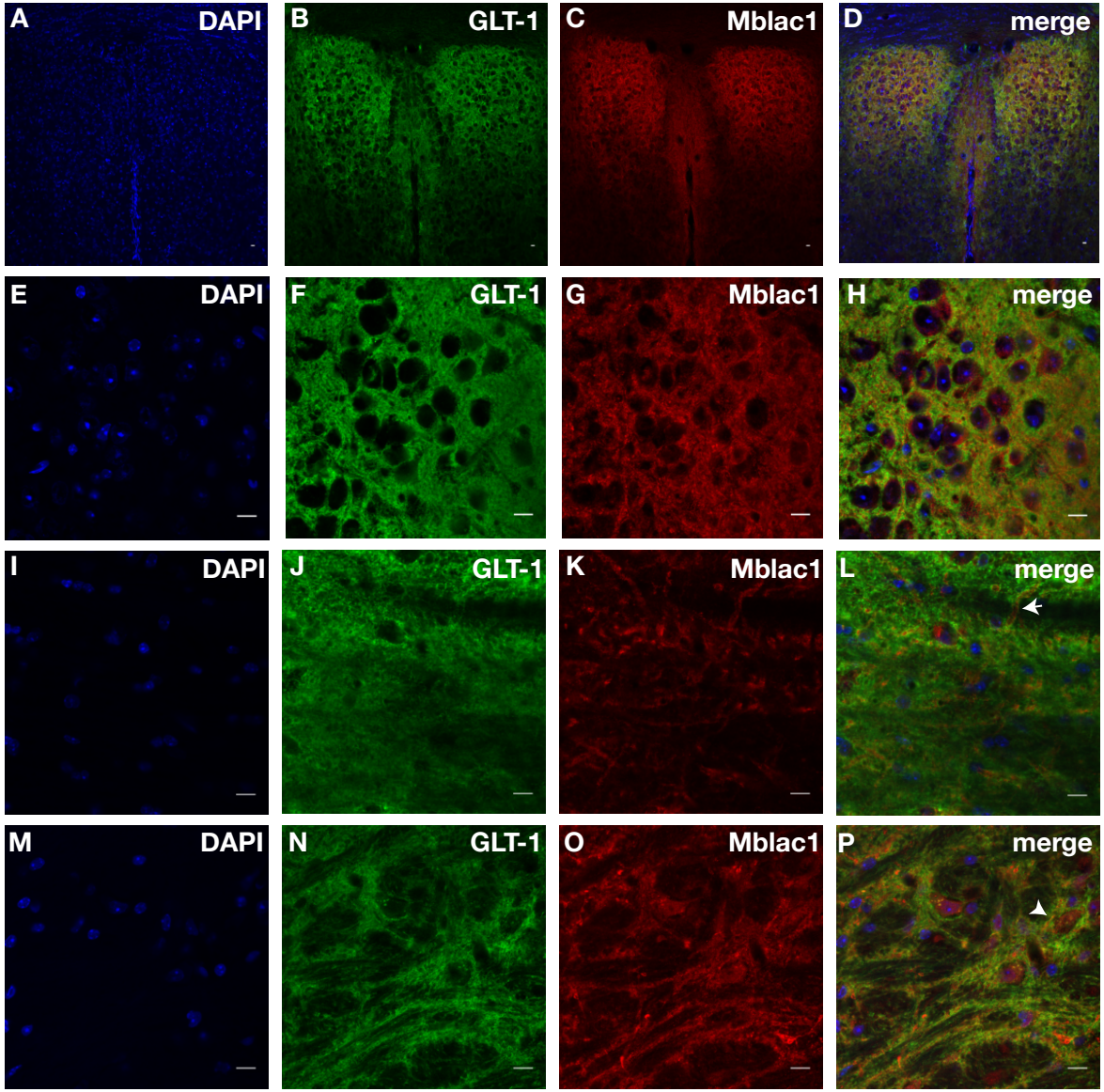

Figure 65 – Mblac1 is expressed in EAAT2/GLT-1 containing fibers. **A-D**) 10X image of Mblac1 and GLT-1 in the DPC. **E-H**)63X image of Mblac1 and GLT-1 staining in the DPC. **I-L**)63X image of Mblac1 and GLT-1 at the midline between rostralmost dorsal hippocampi. Arrowhead denotes an Mblac1 positive fiber expressing GLT-1. **M-P**) 63X image of Mblac1 and GLT-1 staining in the TB. Arrowhead indicates an Mblac1+ fiber surrounded by GLT-1 immunoreactivity. Scale bar indicates 20 μM for **A-D** and 10 μM for **E-P**.

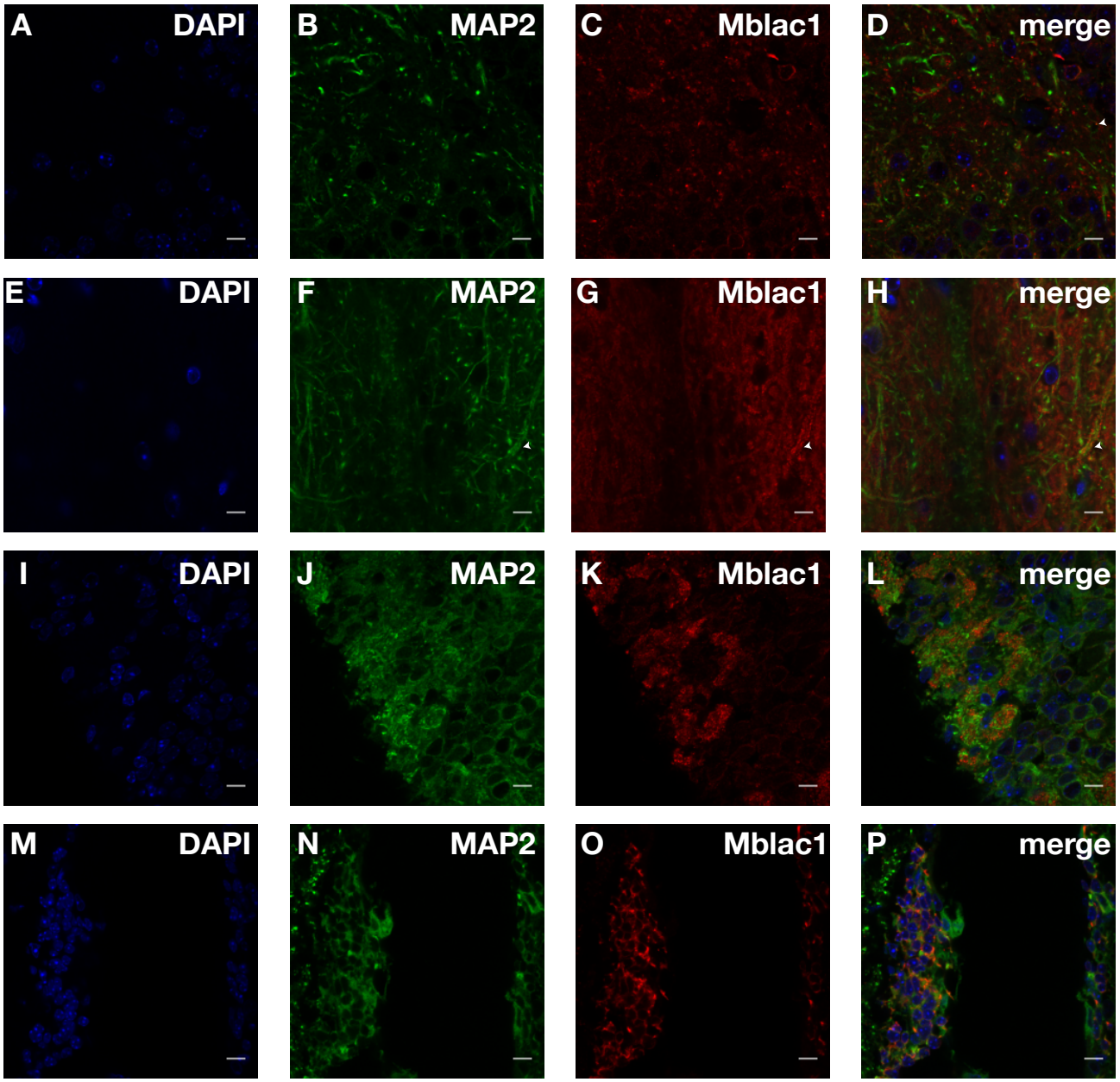

Figure 66 – **Mblac1 apposes the dendritic marker MAP2 except for in the SVZ**. **A-D**)63X image of Mblac1 and MAP2 expression in the DG. Arrowhead denotes a site of MAP2 and Mblac1 apposition. **E-H**)63X image of Mblac1 in the DPC. Arrowhead denotes a MAP2+ dendrite surrounded by Mblac1+ puncta. **I-L**)63X image of Mblac1 and MAP2 in the MHb. Mblac1 and MAP2 show non-overlapping, yet adjacent patterns of expression in the MHb. **M-P**) Mblac1 and MAP2 colocalize in the SVZ.

staining for Mblac1 and the dominant astrocytic glutamate transporter EAAT2/GLT-1. We observed a striking enrichment of GLT-1 in areas of intense Mblac1 staining like the DPC (Figure 65A-D) and the TB (Figure 65M-P) but not in the MHb. At high resolution in the DPC and hippocampal midline, we detected a high # of Mblac1+ cross sections (Figure 65E-L) surrounded by GLT-1 immunoreactivity. Thus Mblac1 is expressed in GLT-1 expressing fibers, but does not colocalize with known astrocytic filament proteins.

To determine if Mblac1 was expressed in neurons we stained for Mblac1 in parallel with the neuronal dendritic marker MAP2. We found Mblac1 was often expressed apposed to MAP2 fibers in the DG (Figure 66A-D), DPC (Figure 66E-H), and the MHb (Figure 66I-L). Surprisingly, we noticed that MAP2 colocalizes with Mblac1+ cells in the SVZ. As Mblac1 was expressed opposite dendrites, we reviewed the literature for patterns of expression that resembled Mblac1. The neuronal vesicular glutamate transporter 2(vGlut2) has a very robust expression pattern in the MHb (Qin & Luo, 2009) which we were able to replicate. We observed a striking gross overlapping pattern of expression with vGlut2 and Mblac1 in the MHb and LCN (Figure 67A-D and not shown). At high resolution, we found that Mblac1 is expressed immediately adjacent to vGlut2 in the MHb and colocalizes with vGlut2 in the LCN (Figure 67E-L). Conversely, we did not observe any consistent colocalization with the GABAergic neuronal marker GAD67 (Figure 68). Therefore Mblac1 is expressed in or near glutamatergic axon terminals in addition to being expressed in GLT-1 containing fibers.

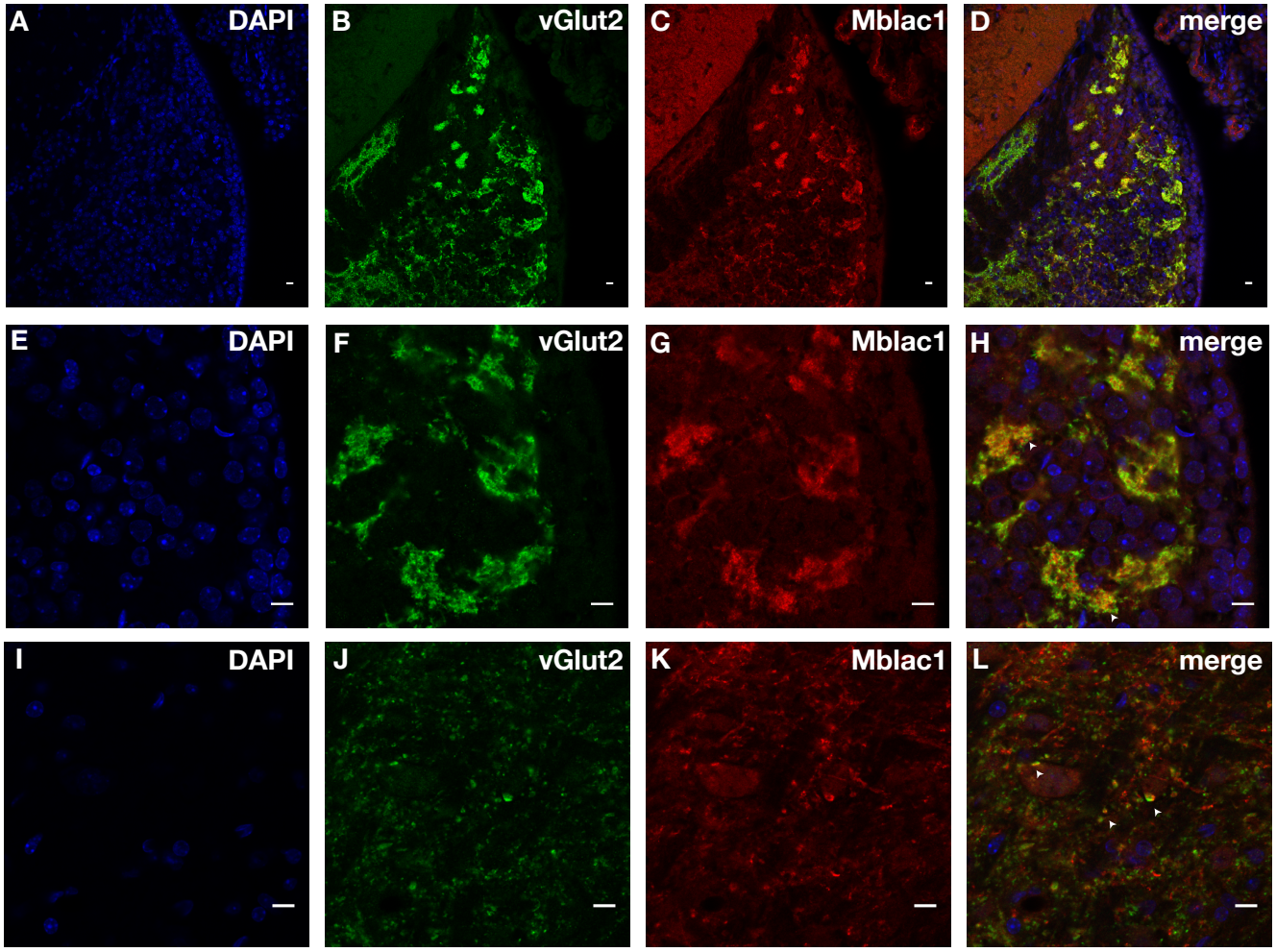

Figure 67 – Mblac1 is expressed adjacent to the glutamatergic axon terminal marker vGlut2. Immunoflourescence and confocal microscopy was performed as described in the methods **A-D)** 20X image of MHb. **E-H**) 63X image of MHb. Arrowheads indicate example areas where Mblac1 and vGlut2 are expressed in at a high density adjacent to one another. **I-L**) 63X image of LCN. Arrowheads indicate colocalized Mblac1 and vGlut2. Scale bar indicates 10 μM for all images. Dorsal is up for all confocal images.

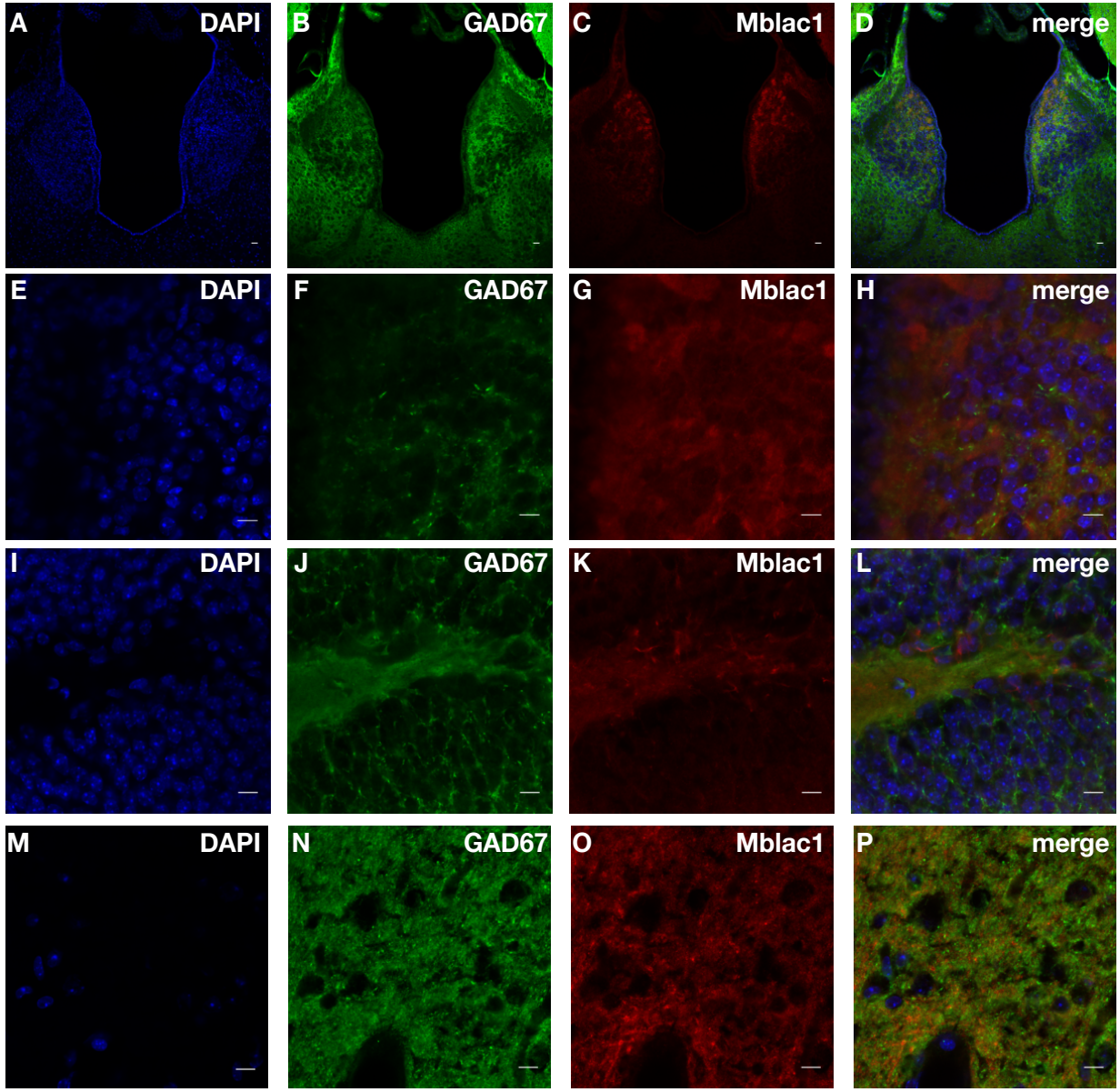

Figure 68 – Mblac1 and GAD67 expression are not colocalized. **A-D**) 10X image of Mblac1 and GAD67 expression in the MHb. **E-H**) 63X image of Mblac1 and GAD67 expression in the MHb. Mblac1 and and GAD67 expression do not overlap. **I-L**) 63X image of Mblac1 and GAD67 in the DG. Mblac1 and GAD67 expression do not overlap. **M-P**) 63X image of Mblac1 and GAD67 in the LS. Mblac1 and GAD67 are expressed near one another but do not colocalize or share fibers. Scale bar indicates 20 μM for **A-D** and 10 μM for **E-P**.

To characterize the expression that we observed in the SVZ, we performed immunofluorescence for both Mblac1 and the neural stem cell marker doublecortin (DCX) (Seri, Garc a-Verdugo, Collado-Morente, McEwen, & Álvarez-Buylla, 2004). We observed complete colocalization of Mblac1 with DCX in the SVZ that did not differ dorsoventrally (Fig. 69A-H) (Ihrie et al., 2011). To our surprise, we observed that Mblac1 is also colocalized with DCX+ cells in the subgranular zone of the DG (Fig. 69I-L). Although we observed that there are additional areas of Mblac1 staining in the DG, these are consistent with the hypothesis that one of the population of cells expressing Mblac1 in the DG are neural stem cells.

Evaluation of β-lactamase activity using chromogenic β-lactamase substrates

β-lactamases make up a very broad family of enzymatic molecules amongst prokaryotes and can be segregated into Classes A-D. Classes A, C, + D all utilize a serine residue in the active site to hydrolyze β-lactam rings, a cyclic amide that is present in many types of β-lactam antibiotics like penicillin and ampicillin. Class B β-lactamases include the metallo β-lactamases that require the presence of metal ions in the active site to mediate hydrolytic activity (Carine Bebrone, 2007). The emergence of antibiotic resistant bacteria by the expression of novel metallo β-lactamases is a growing problem (Yong et al., 2009). To aid in the clinical diagnosis of antibiotic resistant infections, multiple β-lactam containing chromogenic substrates have been developed that can be

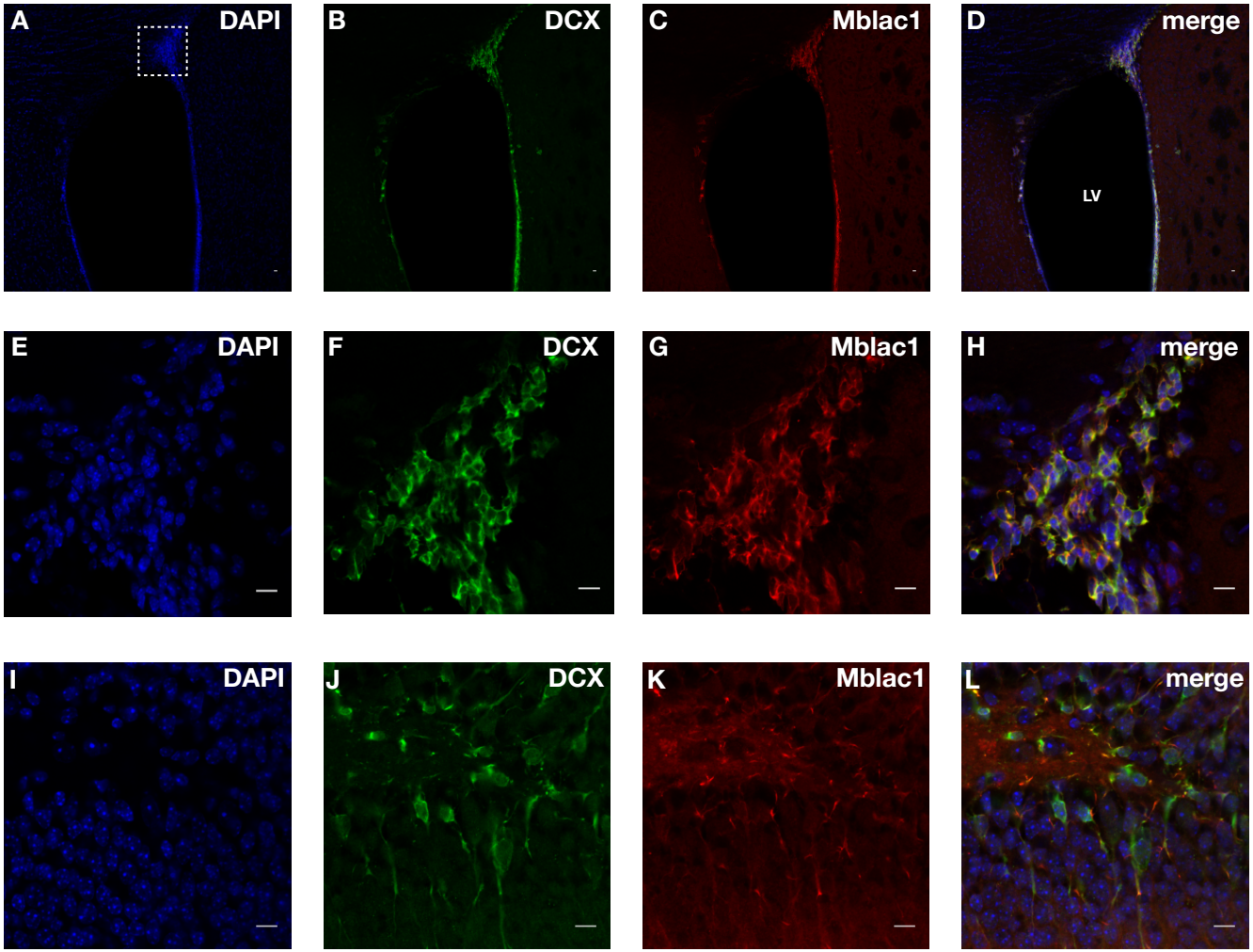

Figure 69 – Mblac1 colocalizes with the neural stem cell marker Doublecortin (DCX). Immunoflourescence and confocal microscopy was performed as described in the methods A-D) 10X images of the subventricular zone(SVZ). Dotted line box indicates magnified image in E-H. E-H) 63X images of dorsal SVZ. Mblac1 and DCX expression completely overlaps in the SVZ I-L) 63X image of subgranular zone(SGZ). Mblac1 is expressed in DCX+ cells. Scale bar indicates 20 μM for A-D and 10 μM for E-L.

used as a readout of β-lactamase activity (C Bebrone, et al., 2001; O'Callaghan, Morris, Kirby, & Shingler, 1972). To determine if Mblac1 can cleave β-lactams, we expressed Mblac1 in HEK293T cells as before and assayed β-lactamase activity by two chromogenic substrates: Nitrocefin and CENTA. While we were able to detect a significant β-lactamase activity of the *E. coli* β-lactamase TEM-1 using this method, we did not detect any significant β-lactamase activity of Mblac1 using this method (Figure 70). These data suggest that Mblac1 does not cleave β-lactam rings and that its endogenous substrate is not likely to contain this chemical group.

DISCUSSION

In this chapter we describe our initial efforts to characterize the expression pattern of the *swip-10* homolog, Mblac1. To date, there are no reports describing the Mblac1 gene.

Using a combination of RT-PCR and *in situ* hybridization, we show that Mblac1 RNA is present throughout the brain yet is enriched in particular brain regions. Of these regions we note a high density of Mblac1 RNA in the cingulate and entorhinal cortices, the hippocampus, the MHb, and the SVZ.

We then developed and purified an Mblac1 antibody and used it to probe the expression of Mblac1 in transfected cells and in native brain tissue via Western blots. Though our primary antibody exhibits a high level of specificity in western blots of Mblac1 transfected cells, this antibody does not recognize human MBLAC1. Using antiserum from another host (#4979), we were able to

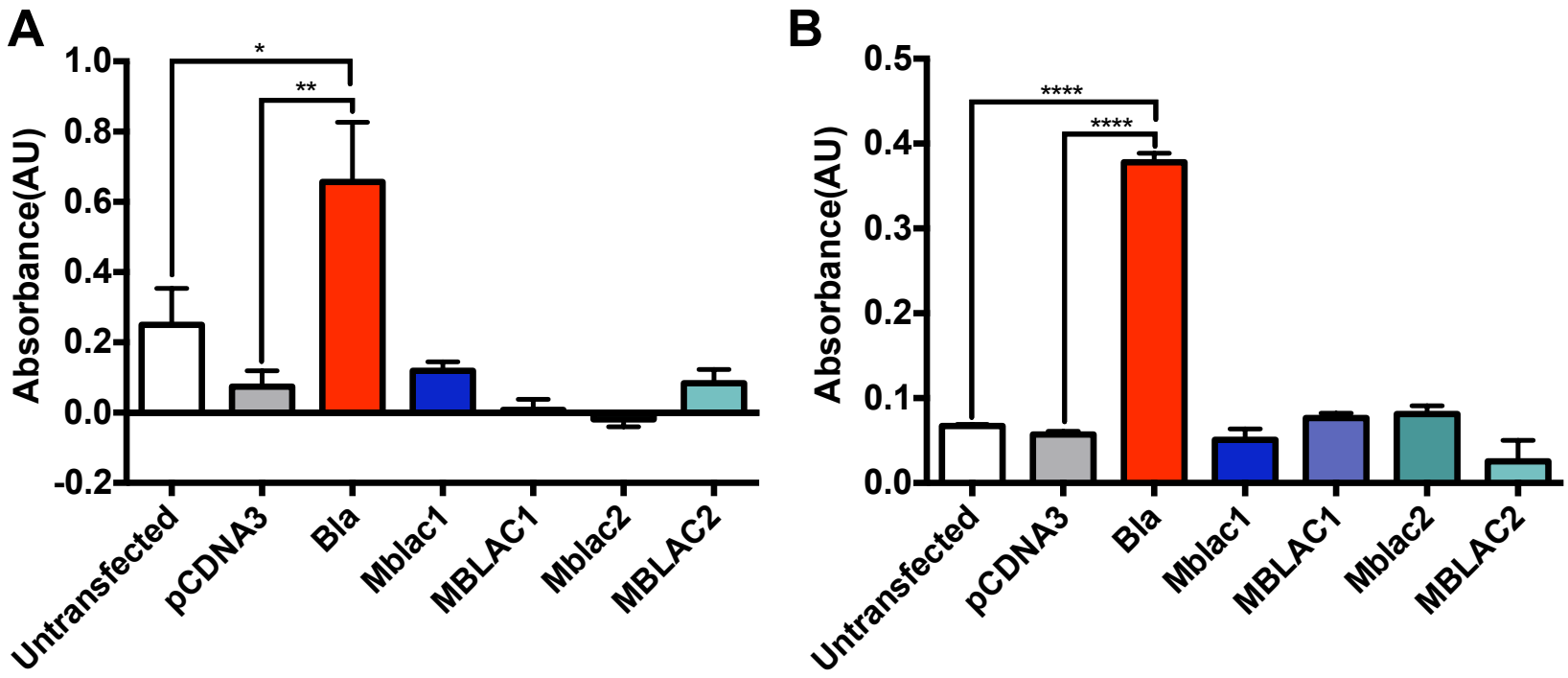

Figure 70 – Measurement of Mblac1 β-lactamase activity using chromogenic substrates. Cell lysates from HEK293T cells transfected with the indicated gene were treated with one of two β-lactamase substrates to measure β-lactamase activity as described in the methods. Data were analyzed by one-way ANOVA with multiple Bonferroni post tests. Whereas the *E. coli* protein TEM-1(Bla) can cleave these substrates, Mblac1 and Mblac2 do not exhibit any specific cleavage of either **A)** Nitrocefin or **B)** CENTA.

detect the expression of transfected human MBLAC1 in this way. Thus antiserum from another rabbit may prove a vital tool in elucidating the expression of human MBLAC1 in post mortem brain tissue.

To understand how Mblac1 expression is distributed in the cell, we screened immortalized cell lines for the expression of endogenous Mblac1. We identified the 3T3 embryonic fibroblast cell line as expressing endogenous Mblac1 that could be blocked by peptide preincubation. Based on the expression of *swip-10* in glia, we screened C6 glioma cells for Mblac1 expression. Surprisingly, we did not observed a specific Mblac1 band of the predicted molecular weight. Using 3T3 cells, we carried out crude subcellular fractionation to determine which cellular compartment is enriched for Mblac1 expression. With this approach, we determined that Mblac1 is expressed in the cytosol and not in organelles or the nucleus.

Next, we used our custom antibody to probe the expression of Mblac1 in mouse brain tissue via western blots and immunohistochemistry. We detected bands of the predicted molecular weight (28 kD) that could be blocked by peptide preadsorption of the primary antibody in cortex, striatum, midbrain, hippocampus, and cerebellum. These studies did not reveal any significant differences in the relative amount of Mblac1 in these brain regions so we moved to immunohistochemistry to get a more precise view of how Mblac1 expression is distributed throughout the brain. In multiple experiments using either antiserum or affinity purified antibody, we observed a very consistent pattern in areas proximal to the areas we observed in the *in situ* hybridization experiments.

Importantly, whereas Mblac1 RNA was enriched in neuronal layers of nuclei like the hippocampus and the cingulate cortex, we observed the majority of Mblac1 protein in the molecular layer of the HIPP or surrounding the neuronal layer of the cingulate. As in the *in situ* we observed a striking expression in the MHb and in cells that make up the SVZ. In terms of the intensity of staining that we observe in these areas, the cells in the SVZ have the most pronounced level of staining. In immunohistochemistry experiments titrating the amount of Mblac1 primary antibody, we observed staining of these cells at relatively low amounts of primary where staining in other known nuclei was limited.

We have established that *swip-10* hyperdopaminergia may derive from alterations in GLU signaling that drive the excitability of DA neurons and that its function is required in glia. In mammals, astrocytes are critical for the termination of synaptic and extrasynaptic GLU. We were therefore surprised to find that Mblac1 did not colocalize with known astrocyte markers like GFAP, S100β, or GS. Not deterred, we used immunofluorescence to determine if GLT-1 and Mblac1 were coexpressed. In certain areas of the brain like the HIPP and the TB, we observed that Mblac1 and GLT-1 are expressed in shared fibers. Other areas of the brain such as the MHb are not rich in GLT-1 expression, so their coexpression in this area is unlikely. The MHb is rich in the expression of another GLT called GLAST, so immunofluorescence for both Mblac1 and GLAST may be an important step in determining if Mblac1 might have a broader role in its coexpression near GLTs (Gampe, Hammer, Kittel, & Zimmermann, 2012).

Based on the pattern of expression we observed in the MHb, another candidate that shared a similar glomerular pattern of expression was vGlut2 (E Herzog et al., 2004; Etienne Herzog, Takamori, Jahn, Brose, & Wojcik, 2006). We observed that Mblac1 and vGlut2 were grossly expressed in shared terminal fields of the MHb and appear to colocalize in deep cerebellar nuclei. 3D reconstruction of MHb Z-stacks in these experiments did not suggest that Mblac1 expression is along vGlut2 containing axons, but a costain for acetylated tubulin and Mblac1 would be more informative. These studies suggest that robust Mblac1 expression exists in areas of dense glutamatergic innervation. Importantly, we demonstrated that Mblac1 does not colocalize with the known dendrite marker MAP2.

Lastly, based on our literature review, we hypothesized that the striking staining pattern that we observed in the SVZ cells were neural stem cells. We observed that Mblac1 colocalizes with the neural stem cell marker DCX in the SVZ and in the SGZ of the dentate gyrus. Therefore, in addition to its expression near vGlut2 and in GLT-1 containing fibers, Mblac1 expression is highly enriched in neural stem cells.

Using chromogenic β-lactamase substrates, we sought to probe the activity of Mblac1. Unlike TEM-1, however, Mblac1 nor Mblac2, was able to specifically cleave these β-lactam containing compounds. Similary, other β-lactamase containing genes in humans like CPSF-73 and Artemis have been cloned and characterized that do not cleave β-lactams (Dominski, Yang, & Marzluff, 2005; Ma, Pannicke, Schwarz, & Lieber, 2002; Mandel et al., 2006;

Moshous et al., 2001; RYAN, 2004). We hypothesize that Mblac1 has an alternative substrate that does not contain this core chemical group.

FUTURE DIRECTIONS

Mblac1 Expression Pattern

To enhance our understanding of the pattern of Mblac1 expression in the brain, there are a few immunofluorescent stains that might inform about its localization including GLAST, NeuN, and acetylated tubulin to determine if it localizes in fibers with another known GLT and whether Mblac1 is expressed in neurons. To determine the exact site of expression in areas of dense Mblac1 expression like the MHb, immunoelectron microscopy of Mblac1 will reveal how Mblac1 is expressed around synapses. A collaboration to facilitate these efforts is currently underway.

Impact of Mblac1 on Neuronal Physiology

Our studies of *swip-10* revealed that its loss results in an increase in DA neuron excitability. To test if Mblac1 has a conserved role as a regulator of neuronal physiology, we have begun efforts to understand the impact of viral Mblac1 overexpression or knockdown in astrocytes on neuronal cocultures. Our preliminary studies have established that 1) Mblac1 is expressed in astrocytic cultures 2) The expression of Mblac1 is upregulated when neurons are cocultured with these glia 3) Neuron-induced upregulation of Mblac1 is more exaggerated when Mblac1 is virally overexpressed in astrocytes and 4) Whole

cell patch clamp recordings of spontaneous excitatory postsynaptic currents (sEPSCs) in neurons cocultured with and without astrocytic Mblac1 overexpression suggest that Mblac1 overexpresssion in astrocytes increases the frequency, yet reduces the amplitude of sEPSCs. These data are consistent with the hypothesis that alterations in Mblac1 gene dosage in astrocytes impacts postsynaptic excitatory signaling. The detailed mechanism of Mblac1's role in regulating GLU clearance or release is still unknown at this time.

Identification of the Mblac1 substrate

Our studies demonstrate that Mblac1 contains a metallo β-lactamase domain and that, in the case of *swip-10*, this domain is required for its function. It does not, however, appear to function as known prokaryotic metallo β-lactamases by cleavage of β-lactam bonds that can inactivate cephalosporin antibiotics. To discover the endogenous substrate, we are currently utilizing mass spectroscopy of Mblac1 protein incubated with and without mouse whole brain extract. We hope that these analyses may reveal a mass peak that is sensitive to Mblac1 expression.

Mblac2/MBLAC2

We identified a second metallo β-lactamase that is of similar length to Mblac1 and contains some sequence similarity to *swip-10* and Mblac1 (Figure 71). Analysis of the sequence similarity between *swip-10* and mouse and human Mblac1/2 demonstrated that *swip-10* is most similar to Mblac1 (39%) and that

Mblac1 is more closely related to *swip-10* than Mblac2 (29%). During our previous RT-PCR experiments we also confirmed that demonstrated that Mblac2 and another metallo β-lactamase, Lactb2, were expressed throughout the brain. Importantly, analysis of the Mblac2 RNA expression pattern using *in situ* hybridization revealed some overlapping and nonoverlapping areas of expression with Mblac1 (data not shown). Mblac2 transcript is present in areas of the hypothalamus where there is no Mblac1 transcript. Analysis of Mblac2 protein expression in brain sections via a recently generated commercial antibody revealed that this protein, though it is expressed in some overlapping areas of Mblac1 like the medial habenula, SVZ, hippocampus, and cerebellum, has a different cellular pattern within these nuclei. In the SVZ, for example, Mblac2 is likely expressed in a less dense and particular cell type known as tanacytes, whereas Mblac1 is expressed in a large swath of neural stem cells.

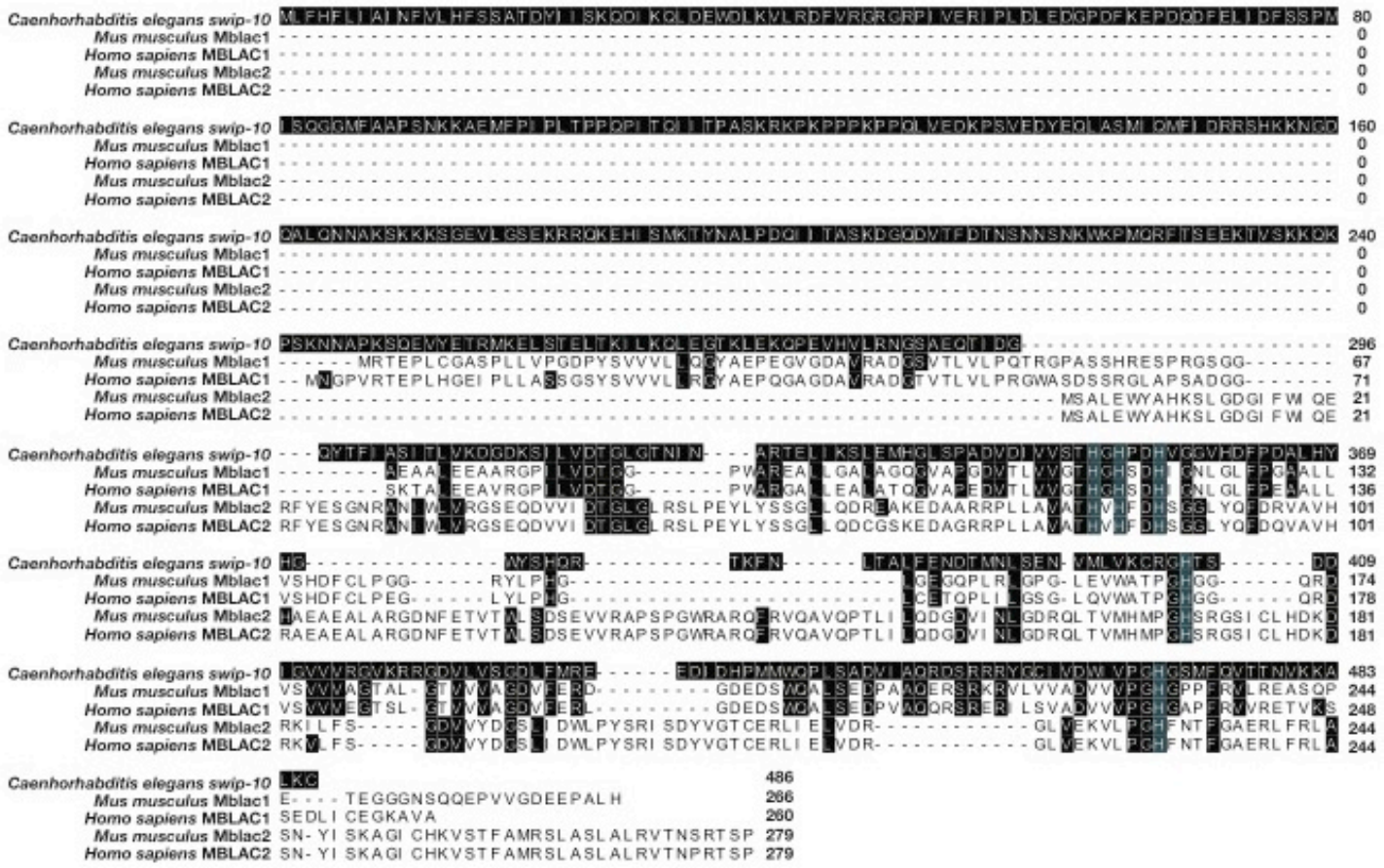

Figure 71 – Alignment of *swip-10* with Mblac1 and Mblac2. Black shading indicate residues that match *swip-10*. Blue shading indicates conserved histidine residues necessary for metal binding. Multiple Sequence alignment was performed using ClustalW in DNAStar.

Chapter VII

CONCLUSIONS AND FUTURE DIRECTIONS

INTRODUCTION

These studies have demonstrated that the nematode *C. elegans* remains a powerful force in the identification of novel, conserved genes. With its rapid lifespan, the ability to carry out forward and reverse genetic screens, a transparent cuticle, and the availability of molecular biological tools to carry out rapid transgenesis, *C. elegans*' holds promise to open new avenues of research that might be impractical or impossible using other model systems. Futhermore, more advanced neurophysiological approaches such as calcium imaging and optogenetics provide direct real time control or measurement of neural activity during behavior. Our forward genetic screen, though small in scale, has resulted in the isolation of a novel gene that regulates DA signaling through a novel pathway and whose mammalian homolog is expressed in the brain. In addition to the characterization we have already performed, these studies have stimulated a new line of research as to the function of mammalian metallo β-lactamases in the CNS including Mblac1 and Mblac2. Though future studies will be necessary to fully describe their mechanism of action, the impact of *swip-10* on DA neuronal excitability and DA-regulated behaviors suggests that one or both of these genes may be important in regulating the physiology of neurons in the brain.

SWIP-10/MBLAC1 AND ITS CONNECTION TO β-LACTAM ANTIBIOTIC EFFECTS ON THE CNS

In addition to their role in regulating neuronal excitability, we propose a hypothesis that Mblac1, possibly Mblac2, represent important potentially druggable targets for neuropsychiatric and neurological disorders. We hypothesize that manipulation of these proteins with pharmacological agents may have a dramatic impact on CNS neurocircuitry through alterations in the amount of extrasynaptic GLU. In the following section I describe the current state of knowledge about the impact of β-lactam antibioitics on brain disorders, why we hypothesize that Mblac1 may represent its target, the data that is consistent or inconsistent with this hypothesis, and what we propose to test our hypothesis.

In 2005, researchers at Johns Hopkins and Columbia University made an important discovery that we believe represents the key link to understanding Mblac1's function in the CNS. Previous work had shown that either inhibition of GLTs in organotypic slices or genetic loss of the astroglial GLTs GLAST and GLT-1 in a mouse was sufficient to produce excitotoxicity (Rothstein et al., 1996; Rothstein, Jin, Dykes Hoberg, & Kuncl, 1993). They postulated that loss of GLT-1 protein and GLU transport activity was a valid model of amyotrophic lateral sclerosis (ALS) as studies of post mortem tissue in ALS patients demonstrated a highly significant reduction in GLT-1 protein (Rothstein, Martin, & Kuncl, 1992). Thus they hypothesized that compounds that increased the amount of GLT-1 protein might be neuroprotective. In this study, the authors

screened a library of 1,040 FDA-approved compounds for their protective effects on organotypic rat spinal cord slices bathed in glutamate (Rothstein et al., 2005). The overwhelming majority of compounds that they screened had no effect on the amount of toxicity, but they observed that compounds of the β-lactam antibiotic class consistently protected the slices **and** elevated the amount of GLT-1 protein. These compounds were sufficient to activate the human GLT-1 promoter *in vitro* and increase transcription and protein expression of GLT-1 *in vivo* in a mouse brain. To validate the relevance of these compounds in a disease model of ALS, they treated G93A superoxide dismutase 1 (SOD1) mice with one particular β-lactam compound: ceftriaxone (CEF). They found that CEF treatment significantly increased the lifespan, body weight, grip strength relative to saline treated animals. Moreover, treatment with CEF increased the amount of GLT-1 protein in these animals and prevented the death of motor neurons in the SOD1 G93A. These studies established a clear link between the effects of β-lactam antibiotics on the CNS, the regulation of GLT-1 activity, and identified a novel compound class to pursue in the treatment of ALS. Future studies have shown that β-lactams like CEF may have broader effects in the treatment of brain disorders.

One of the hallmarks of addictive psychoactive drugs like cocaine is that their acute use results in an increase in the amount of DA release in the NAc, but the neuroadaptive changes that result in chronic use of these drugs and behavioral hallmarks of addiction like tolerance, withdrawal, and relapse are still unclear. Work over the past decade has established that these aspects of

addiction are the result of alterations in the connectivity, morphology, and neurotransmission in pathways that ultimately converge on the NAc (S E Hyman & Malenka, 2001). One of the hypotheses postulated to account for these effects is that chronic exposure to cocaine or other drugs of abuse is that they alter the amount of extrasynaptic GLU that produces enduring changes in the physiology of NAc medium spiny neurons and ultimately behavioral elements of the phases of addiction (Kalivas, 2009). Baker and colleagues showed that animals that have undergone cocaine self-administration and 3-week withdrawal have a specific decrease in the amount of extrasynaptic GLU in the NAc as measured by no-net flux microdialysis (Baker et al., 2003). They found that restoration of the GLU levels could be accomplished by application of a drug called N-acetylcysteine (NAC) that acts on xC^- to promote passive exchange of cysteine into the cell for GLU out of the cell. Later work by Knackstedt *et al*. showed that that this same self-administration and extinction paradigm was capable of reducing the amount of GLT-1 and xC^- protein expression and a reduction in the amount of glutamate uptake (Knackstedt et al., 2009). As ceftriaxone upregulates the amount of GLT-1 expression, they treated the drug self-administered animals and drug naive animals with NAC and CEF and found that both of these compounds restored the amount of xC^- and GLT-1 in the drug-treated animals with no effect on drug-naïve animals. To determine if CEF had effects in a behaviorally relevant addiction model, they challenged the drug withdrawn saline and CEF-treated animals with a cue previously paired with drug administration. Whereas the saline treated animals reinstated drug-seeking

behavior (lever presses), the CEF treated animals exhibited a significant reduction in cue-induced reinstatement. Another lab has also validated these results using a similar self-administration and withdrawal paradigm (Sari, Smith, Ali, & Rebec, 2009). Recently, Knackstedt and colleagues validated their previous results and demonstrated that cocaine self-administration results in an increase in sEPSC or ePCSC frequency and amplitude on MSNs in the NAc that were normalized by CEF (Trantham-Davidson, LaLumiere, Reissner, Kalivas, & Knackstedt, 2012). What is unclear in these studies is why loss of these of these GLTs (GLT-1 and xC^-) results in a **decrease** in extracellular GLU and an increase in excitatory neurotransmission. A model that has been proposed is that the amount of extracellular glutamate exerts drive on presynaptic GLURs mGluR2/3 and mGluR5 and that this drive is necessary for the development of plasticity that alters GLU release (Bellesi & Conti, 2010; Moussawi et al., 2009; Moussawi et al., 2011). Thus elevation of extracellular GLU via NAC or CEF treatment restores cocaine-induced metaplasticity, that is the loss of drug or behaviorally induced plasticity after chronic cocaine treatment. The effects of CEF on drug-induced behavior may be more complicated as Ward *et al.* demonstrated that CEF reduces cocaine self-administration on a fixed ratio schedule without affecting the acquisition of sweet food reinforcement (Ward et al., 2011). Additionally, Rasmussen and colleagues showed that chronic CEF treatment inhibited acute AMPH-induced hyperactivity and acute and sensitized AMPH-induced stereotypies (Rasmussen, Unterwald, & Rawls, 2011; Sondheimer & Knackstedt, 2011). Nonetheless, although an exact understanding of how NAC

and CEF alter drug-induced plasticity, neurotransmission, and behavior is not yet available, these studies establish that drugs like CEF may have broader activity in multiple brain disorders like addiction in addition to ALS.

The breadth of behavioral or disease paradigms that are ameliorated by CEF are on the rise, which suggests that alterations in GLU signaling may underlie the etiology of multiple CNS disorders. Considering the ubiquity of the GLU in the CNS, this is perhaps not surprising. Following the identification of CEF, another lab determined that CEF administration exerts antidepressant effects in mice (Mineur, Picciotto, & Sanacora, 2007). Similar to traditional antidepressants and serotonin selective reuptake inhibitors (SSRIs), ceftriaxone decreased the immobility time in the tail suspension and forced swim tests and decreased the latency to feed in the novelty-suppressed feeding paradigm. The authors therefore determined that ceftriaxone has antidepressant effects in mice. Further work by Lipski *et al.* determined that, similar to Rothstein *et al*., ceftriaxone was neuroprotective in oxygen glucose deprivation model of stroke (Lipski et al., 2007). Perhaps the best illustration of the broad neuroprotective role of CEF is a recent study that demonstrates that CEF protects against the neurochemical and behavioral effects of 6-OHDA (Leung et al., 2011). Together these studies demonstrate that CEF and the upregulation of GLT-1 (and perhaps xC^-) has broad role in CNS disorders and prompts two important questions 1) where does CEF bind and accumulate in the brain and 2) What is the molecular target of this drug?

We hypothesize that Mblac1 is the target of β-lactam compounds like CEF, and that CEF accumulates in Mblac1 expressing cells in the brain. Based on our studies in worms, we found that *swip-10* acts in glia cells and may function in a pathway containing a GLT. Additionally, in collaboration with Jens Meiler's group, we determined a predicted structural model for the *swip-10* metallo β-lactamase that had 27% sequence similarity to di-Zn metallo β-lactamase VIM-4 from *P. aeruginosa* (Loktis, Sheehan, and Combs). We used this model to determine if the catalytic binding site could accomodate macromolecules like DNA or RNA or small molecules like CEF. Unlike other mammalian β-lactamases like Artemis or CPSF-73, these molecules are likely too large to dock in the predicted model of *swip-10*. The docking of CEF or penicillin within the binding site, on the other hand, was more likely. Thus it is structurally plausible that β-lactams can bind within the catalytic site of *swip-10*. Whether *swip-10*/Mblac1 acts on an endogenous β-lactam-containing compound is still unknown, but these analyses imply that *swip-10* is not likely to act on a nucleic acid and that its molecular target is most likely a peptide or a small molecule. Currently, we are carrying out similar computational analyses with Mblac1 to validate that these same principles can be applied to the mammalian homolog.

Our studies of Mblac1 expression *in vivo* are consistent with our hypothesis that it functions in a pathway that is regulated by β-lactams and contains GLT-1. We demonstrated that it is expressed directly adjacent to vGlut2 and in GLT-1 containing fibers. Our GLT-1 colocalization and

fractionation experiments both demonstrate that Mblac1 is expressed in the cytosol. We hypothesize that β-lactams are likely to accumulate in overlapping GLT-1/Mblac1-containing fibers. Currently, we are using CEF-crosslinked resin to pull down potential binding partners from whole brain protein lysates and using matrix associated laser desorption ionization (MALDI) imaging of CEF-treated brain sections to determine the areas where this compound accumulates in the brain. Unfortunately, we were not able to detect significant β-lactamase activity using prokaryotic chromogenic substrates. This does not preclude the possibility that CEF acts on Mblac1, rather it suggests that we must use the endogenous substrate and its modified product as a way to assay CEF's effect on this enzyme. We are currently using mass spectroscopy of Mblac1-treated brain lysate with and without CEF as a way to identify the Mblac1 substrate and whether this interaction is sensitive to CEF. We hypothesize that the Mblac1 target will be sensitive to CEF and will provide us with a novel mechanism to understand the regulation of GLU signaling and GLT-1.

Lastly, Mblac1's expression in neural stem cells may hold the key to understanding CEF's actions. It has been established that stem cells have an inherently glial nature, and Mblac1 may have a critical role in the differentiation or function of glial precursors in these stem cells (Kriegstein & Álvarez-Buylla, 2009). One potential way to explain the breadth of literature on the effect of β-lactams on CNS disorders is that CEF effects on Mblac1 and the production of its product ultimate control the production of new glia or neurons. In all of the previously mentioned studies, there have been no controls to rule out this

possibility such as western blotting for GFAP (in addition to GLT-1) or BrdU labeling to label newly generated cells. Another reason this hypothesis deserves a more critical examination is that CEF has been shown to produce antidepressant like effects (Mineur, et al., 2007). In the past 10 years, there is a growing body of evidence that the effects of antidepressants on CNS circuitry ultimately require that they increase hippocampal neurogenesis in the SGZ of the DG. As we observe Mblac1 expression in these cells, we hypothesize that Mblac1 may function in a pathway with antidepressants to regulate the production or maintenance of new neurons and/or glia.

GENETIC MANIPULATION OF MBLAC1

We have begun to gauge the impact of Mblac1 gene dosage alteration via lentiviral overexpression of this gene in mouse astrocytes and neuron cocultures. Our preliminary evidence suggests that Mblac1 overexpression increases the frequency and decreases the amplitude of spontaneous excitatory postsynaptic currents in postsynaptic neurons. These data suggest that Mblac1 overexpression in astrocytes may increase glutamate release probability, but decrease the number of postsynaptic AMPA receptors available for glutamate. Future studies repeating these experiments with Mblac1 overexpression and using viral knockdown of Mblac1 will be informative in connecting Mblac1 to the regulation of neuronal physiology similar to *swip-10*.

In *in vitro* preparations of astrocytes cultured in isolation the expression of the astrocytic glutamate transporter EAAT2/GLT-1 is limited. Similar to Yang

et al., GLT-1 expression is upregulation by the overlay of neurons on astrocytes (Yang et al., 2009). Over several experiments, we have observed that Mblac1 expression is linked to neuronal coculture such that the amount of Mblac1 expression relative to a loading control is increased when neurons are applied. These studies suggest that Mblac1 expression is dynamic in astrocytes or that Mblac1 may be partially expressed by neurons. Importantly, the neuron induced increase of Mblac1 expression is magnified in astrocytes that are virally overexpressing Mblac1. Thus these data are consistent with the expression of Mblac1 being linked to neuronal induction similar to GLT-1. Current efforts to develop a lentivirus to knockdown Mblac1 expression via Mblac1-specific shRNAs in these preparations are underway. The previously described connection to β-lactam antibiotics have led us to hypothesize that antagonism or binding of these compounds to endogenous Mblac1 may be required for the upregulation of GLT-1 that occurs during chronic CEF administration.

In addition to developing a knockdown virus for manipulation, we are interested in developing genetic tools to determine the physiological role of Mblac1 *in vivo*. The International Knockout Mouse Consortium is currently using traditional homologous recombination to generate a Mblac1 knockout mouse (http://www.knockoutmouse.org/genedetails/MGI:2679717) and the Texas Institute for Genomic Medicine has screened positive ES cells containing a GeneTrap that is inserted in the 5' UTR of Mblac1. More work will be needed to characterize the functional impact of either of these mutations and validate these genetic mouse models. As Mblac1 is expressed in a number of peripheral

tissues and we believe it impacts the function of GLT-1, viral knockdown approaches using ICV or nuclei specific injection of adeno associated viruses containing Mblac1 siRNA may be an important tool to assay the function of this gene in a tissue and temporal specific with minimal cost and time associated with generating a knockout mouse model.

Appendix A

DEVELOPMENT OF A NOVEL, ANALYTICAL PLATFORM FOR KINETIC ANALYSIS OF *C. ELEGANS* SWIMMING INDUCED PARALYSIS[2]

INTRODUCTION

Since the completion of the human genome project and the growing annotation of several model organism genomes, neuroscientists have exploited these systems to identify novel conserved genes that directly impact behavior. In the nematode *Caenhorhabditis elegans*, there exist a repertoire of simple, reproducible behaviors that are easily implemented in the lab to link genotype to phenotype. In particular, modulation of these behaviors are highly conserved across families of signaling molecules that include fast-acting neurotransmitters such as acetylcholine, gamma-aminobutyric acid, and glutamate as well as slower acting neuromodulators including dopamine (DA), serotonin (5-HT), and neuropeptides (Jorgensen 2005; Brockie and Maricq 2006; Chase 2007). DA was among the first neurotransmitters demonstrated to modulate locomotion in the worm (Schafer and Kenyon 1995). Since that time, genes necessary for DA synthesis, packaging, release, reuptake, and signaling at pre- and postsynaptic receptors have been cloned and their impact on worm behavior studied (Mcdonald et al. 2006).

[2] Adapted from Hardaway and Wang *et al. Journal of Neuroscience Methods* (under review)

In our previous report, we demonstrated that worms lacking activity of the presynaptic dopamine transporter (DAT) demonstrate DA and *dop-3* dependent Swimming Induced Paralysis (Swip) (Mcdonald et al. 2007). These efforts and others have revealed a clear need for a simple, open source analytical platform to quantify *C. elegans* swimming behavior and paralysis. In this study, we describe the development and implementation of a system for quantification of Swip. We demonstrate the capabilities of our tools by analyzing the highly penetrant Swip behavior of *dat-1* animals and the Swip behavior observed after treatment of animals with the tricyclic antidepressant and *dat-1* antagonist imipramine (IMI). We demonstrate that SwimR can reveal novel kinetic alterations in swimming produced by these manipulations that can be of use in dissecting the differential control of swimming behavior by converging signaling pathways.

MATERIALS AND METHODS

C. elegans Strains and Husbandry

C. elegans strains were cultured on bacterial lawns of OP50 and maintained at 12 to 20°C using standard methods unless otherwise noted (Brenner 1974). The wild-type strain is N2 Bristol. The *dat-1(ok157)III* strain was obtained from J. Duerr and J. Rand (Oklahoma Medical Research Foundation, Oklahoma City), and is a complete loss of function mutation that eliminates the majority of the DAT-1 coding sequence. A strain producing a loss of function disruption of DOP-

3 (*dop-3(vs106)X*) was obtained from the *Caenorhabditis* Genetics Center (University of Minnesota, Minneapolis) and *cat-2(tm2261)* from Shohei Mitani at the National Bioresource Project at Tokyo Women's Medical University.

Assessment of Swip Behavior

In both batch and automated analyses, we generated synchronous populations of these strains by hypochlorite treatment and harvesting arrested L1 animals. L1s were plated at a moderate density on fresh NGM/OP50 plates and incubated at temperatures ranging from 12 to 20 degrees. On test days, middle stage L4 animals were identified by characteristic morphological features and used for behavior as N2 animals show some stochastic Swip and quiescence bouts prior to and during the last larval molt. We placed worm test plates at room temperature for 15 min to acclimate to room temperature before testing. A stock of IMI (Sigma – Cat No. I7379) was dissolved in water to 100 mM on test days and serially diluted in water to the desired concentrations. For batch analyses, 100 μL of water or drug were dispensed in multiple wells of a Pyrex Spot Plate (Fisher catalog number 13-748B) and 10-15 L4 animals were gently transferred using an eyelash pick. After 10 min., we recorded the number of paralyzed worms/total worms. Two independent observers performed assays over several weeks using multiple worm preparations, blind to genotype or drug manipulation. For automated video analysis, single L4 hermaphrodites were placed in 20 μL of water or drug in a single well of a Pyrex Spot Plate, and 10 min. movies (uncompressed AVI format) of their swimming behavior were captured as

described in the supplementary materials. Every worm line was recorded sequentially and in parallel over several days to ensure that strains were identical in age.

SwimR Tools

Individual worm videos were tracked in open source morphometric tracking program (Tracker 2.0), and output files were analyzed in SwimR according to the Supplementary Materials.

Statistical Analysis

SwimR generates several output images and text files of the raw data used to generate them (see Supplementary Materials). Raw data from SwimR was input into Prism 6.0a (Graphpad, La Jolla,CA) and subsequent analyses performed as described in the text or figure legends.

RESULTS AND DISCUSSION

Development of a Single Worm Swimming Tracker and an R-based Analytical Platform (SwimR)

In our initial efforts to quantify thrashing behavior, we developed a tool (Tracker) that can analyze the swimming frequency of individual nematodes (Matthies et al. 2006; Mcdonald et al. 2007). This software provides an output of the worm

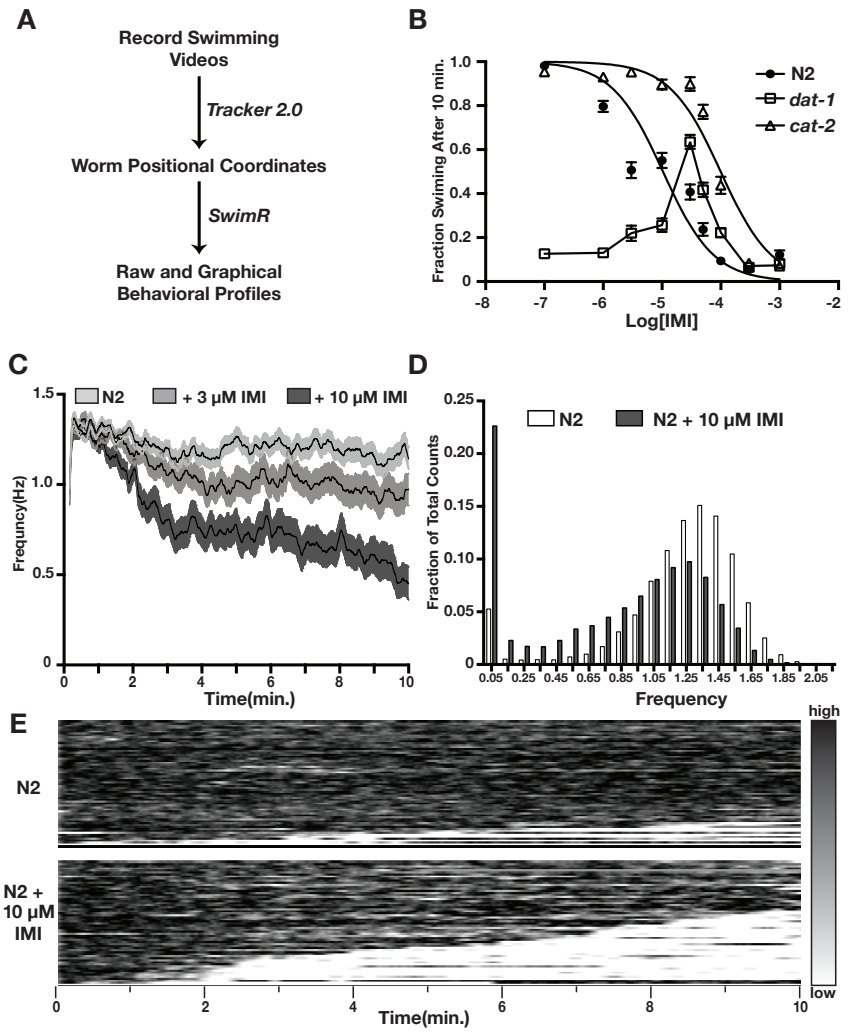

Figure 72 – Paralytic effects of IMI on *C. elegans* N2 animals as determined by manual and automated assays. **A)** Diagram of the workflow for *C. elegans* swimming analysis. **B)** Response of N2 (filled circles), *cat-2* (open triangles), and *dat-1* (open squares) to increasing concentrations of IMI. Dose Responses to IMI were fit using non-linear regression. Using these analyses we determined the IC_{50} of N2 and *cat-2* to be 10 µM (+/-1.5 µM) and 99 µM (+/-12 µM) respectively. Dose-response data points for *dat-1* were connected with a line between data points. **C)** Effect of IMI on N2 swimming frequency. Average frequency values were analyzed by 2-way ANOVA with with Dunnet's post tests of each time point in the drug condition to the corresponding basal time point. Shaded areas represent SEM. 3 µM IMI triggered a significant (P<.05) decrease in the average frequency beginning at the 4th minute (P<.05). 10 µM IMI induced a significant decrease in average frequency (P<.05) with individual time points reaching significance in the 2nd minute. **D)** Distribution of N2 swimming frequency values with and without IMI. IMI treatment induces a shift to lower frequency values. **E)** Heat map representations of N2 swimming frequency with or without 10 µM IMI.

positional coordinates during swimming (Figure 72A). Since *C. elegans* swim by the propagation of C-shaped bends on their dorsal and ventral sides, Tracker 2.0 uses a particle filter to assign a 3-point spine to a worm difference image. Within this program, parameters related to spine length, the number of particles, the maximum angle between two points along the spine, and the allowable displacement of the spine between frames can be altered to maximize tracking fidelity (See Supplementary Materials). To analyze subcomponents of worm swimming, we developed an open source analytical suite using R (http://www.r-project.org/). Our suite, SwimR, analyzes Tracker 2.0 files and uses several counting methods to determine the spine movement frequency. The frequency values, as determined using these methods, are provided in output directories to allow the user to tailor the counting method to the desired analysis. After the analysis of each worm track, SwimR constructs a matrix of frequency vs. time for each worm in the data set that is used for subsequent calculations and graphical output. SwimR analyzes the frequency matrix to extract kinetic parameters related to swimming frequency, paralysis probability and duration, and reversion characteristics.

Manual Analysis of IMI-Triggered Paralysis and Dose Selection

Previously we implemented Tracker and SwimR to demonstrate the power of our tools for characterizing and distinguishing the Swip behavior of multiple genetic models (Hardaway et al. 2012). Here, we analyze the paralysis of animals as

triggered by the *dat-1* antagonist IMI to understand whether SwimR is also capable of discerning patterns produced by pharmacological manipulations. IMI was first described as a potent inhibitor of *dat-1* mediated DA uptake following heterologous expression of the cloned transporter (Jayanthi et al. 1998). *In vivo* studies with IMI on behavior with the drug were not pursued as a null *dat-1* allele was not available at the time to test *for dat-1* specificity of IMI actions. With the null *dat-1(ok157)* allele now available, we returned to this question and utilized SwimR to determine the program's utility for dissection of acute, drug-induced Swip.

We first tested the effects of IMI using manual Swip assays, counting the number of animals that paralyze within a 10 minute time frame post application of IMI. We observed a robust loss of Swip *in cat-2* animals that lack expression of tyrosine hydroxylase, the rate limiting step in DA synthesis (Figure 72B), amounting to a 9-fold shift in the IMI IC_{50}. Thus, whereas at 50 μM IMI, N2 animals become nearly fully paralyzed, *cat-2* animals exhibit only modest (~20%) paralysis. Consistent with a DA dependence of IMI actions, we also observed a reduction in IMI potency with *dop-3* animals (Figure 74A), though the shift was more moderate (~5 fold). When IMI was tested on *dat-1* animals, we saw the expected inability of IMI to augment paralysis, consistent with the drug and mutation acting through a common pathway (Figure 74D). Interestingly, at 33 and 50 μM IMI, we observed a reversal of paralysis in *dat-1* animals, followed by a decline to

complete paralysis as the concentration was raised further. Although we have not explored the mechanism(s) for these effects, we note that IMI has been reported to inhibit the 5-HT transporter *mod-5* (Ranganathan et al. 2001), and may act at ion channels like *egl-2* (Weinshenker et al. 1999) to regulate egg-laying. Given the importance of 5HT's role in crawl-swim transitions (Vidal-Gadea et al. 2011), we hypothesize that *mod-5* plays a role in one or more of the components seen at concentrations above 33 μM. In order to explore the Swip of IMI with SwimR in relation to Swip of *dat-1*, we used 3 and 10 μM IMI in all further studies.

Automated Analysis of IMI-induced Swip Behavior

In the next set of studies, we generated single worm tracking files from videos using Tracker 2.0 and analyzed tracks by genotype and drug using SwimR. We compared individual frequency plots for each worm to its corresponding movie by eye to validate tracking fidelity. Some false tracking was observed, but this was usually due to a low-quality video containing poor contrast and/or debris in the well (See Supplementary Materials). Using SwimR, we generated data matrices for each genotype by drug combination containing properly tracked files for further analysis. We then used SwimR to analyze IMI's effects on each genotype.

IMI produced a robust, dose-dependent decrease in average thrashing frequency with the N2 strain. As shown in Figure 72C, 3 μM IMI produced a significant decrease in the N2 thrashing frequency that was more prominent with 10 μM IMI. In addition, IMI, irrespective of dose, reduced the average *maximal*

Table 2 – Swimming and Paralytic Measurements for IMI-induced Swip

	Maximal Frequency (Hz)	Latency to Paralyze (sec)	Reversion Incidence[A]	Reversion Frequency (events/ animal)	Reversion Probability[B]	Time to 1st Reversion (sec)	Average Reversion Event Length (sec)
N2(n=63)	1.82+/-0.141	305+/-165	0.455	3.80 +/-1.93	1070+/-693	93.9+/-132	17.5+/-24.0
N2 + 3 µM IMI(46)	1.60+/-0.262***	274+/-141	0.25	3.33+/-3.21	432+/-584	147+/-89.8	20.0+/-31.5
N2 + 10 µM IMI(38)	1.65+/-0.137***	297+/-169	0.2	1.25+/-0.50	42.7+/-52.3*	175+/-97.0	7.62+/-8.79
***dat-1(ok157)*(117)**	1.46+/-0.436	206+/-124	0.366	0.336+/-2.63	394+/-500	140+/-127	13.4+/-26.6
***dat-1* + 3 µM IMI(31)**	1.61+/-0.193	261+/-109	0.308	1.38+/-0.744	237+/-417	171+/-121	5.36+/-6.20
***dat-1* + 10 µM IMI(27)**	1.56+/-0.260	260+/-141	0.273	0.273+/-2.33	162+/-264	235+/-84.2	6.40+/-3.19
***cat-2(tm2261)*(38)**	1.75+/-0.091	N/A	N/A	N/A	N/A	N/A	N/A
***cat-2* + 3 µM IMI(23)**	1.82+/-0.097	438+/-138	0.333	0.333+/-3.5	0.333+/-3.50	177+/-44.3	1.15+/-0.54
***cat-2* + 10 µM IMI(27)**	1.53+/-0.183***	140+/68.3**[C]	0.25	9	715	98.2	5.87
***dop-3(vs106)*(22)**	1.88+/-0.034	223+/-206	1	2.67+/-1.15	1500+/-1550	157+/-139	15.89+/-10.0
***dop-3* + 3 µM IMI(27)**	1.81+/-0.050	379+/-165	0.333	0.333+/-2.00	986+/-1380	50.1+/-3.15	9.08+/-12.8
***dop-3* + 10 µM IMI(34)**	1.50+/-0.278***	188+/-144	0[D]*	N/A	N/A	N/A	N/A

A Reversion Probability = total time spent in reversion/ total time after paralysis onset

B Reversion Incidence = fraction of animals that reverse from paralysis

Asterisks(*) indicate a significant difference to control genotype as determined by one-way ANOVA with Dunnet's multiple comparision test where

* = $p < 0.05$, ** = $p < 0.01$, and *** = $p < 0.001$.

C – unpaired student's t test to *cat-2* + 3 µM IMI

D Chi-square test

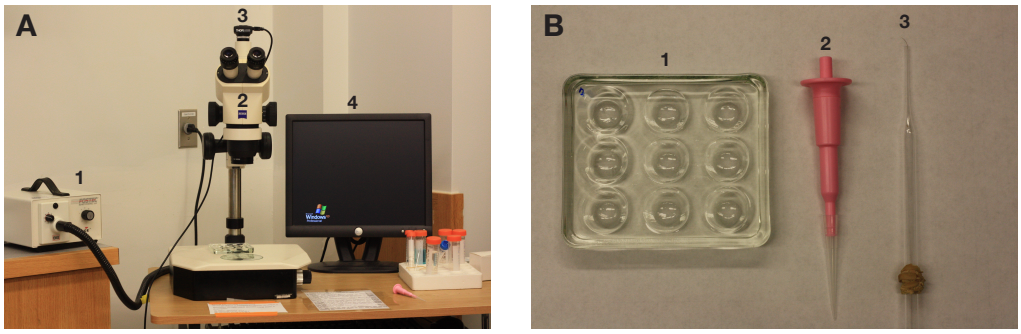

Figure 73 – Equipment setup for *C. elegans* swimming analyses and sample video recordings A) *C. elegans* swimming was assayed on a system containing stereo dissecting scope (2) on a mounted stage coupled to a ThorLabs DCC1545M camera (3) illuminated by a Fostec Fiber Optic Illuminator (1). Uncompressed .avi videos were acquired in VirtualDub (Avery Lee) on a PC WorkStation running either Windows XP or Windows 7 (4). **B)** Ancillary equipment necessary for swimming assays. Single worms were assay in 9-well Pyrex dishes (1) containing 20 µL of water or drug dissolved in water. Media was transferred using a fixed volume 20 µL pipette (2). A single worm was transferred from an NGM/OP50 plate into solution using an eyelash pick (3).

frequency of swimming across the entire recording (Figure 72D, Table 2, + Sup Fig 76A). As we observed a reduction in maximal swimming frequency in *dat-1* and DA-dependent Swip lines isolated in our forward genetic screen, we suspected that the reduction in maximal frequency after IMI treatment was due to the presence of paralyzers in this population limiting the time frame over which high swimming frequencies could be reached. To determine whether the decrease in average thrashing frequency was due to an increase in Swip latency or in penetrance, we used SwimR to plot a heat map of each worm's swimming frequency over time (Figure 72E and Figure 75A). In these plots, each track is placed in a single row, one above the other, and its thrashing frequency is scaled according to color where black/yellow represents its highest swimming frequency and white/blue represents paralysis. SwimR orders the maps so that the strongest paralyzers are placed at the bottom. As we observed a small amount paralysis in N2 animals without drug treatment, we could assess the properties of this paralysis for comparison with IMI treatment. Inspection of IMI treated animals revealed a higher incidence of Swip with 10 μM IMI relative to N2 animals without drug treatment with no change in Swip latency (Table 2). The increased penetrance of Swip was also evident in an increased density of low frequency values with 10 μM IMI treatment relative to no drug (Figure 72D and Figure 76A). Whereas N2 paralyzers without drug treatment displayed a high level of reversion from paralysis, paralysis triggered by IMI displayed a lower incidence of reversion, though this parameter did not reach statistical

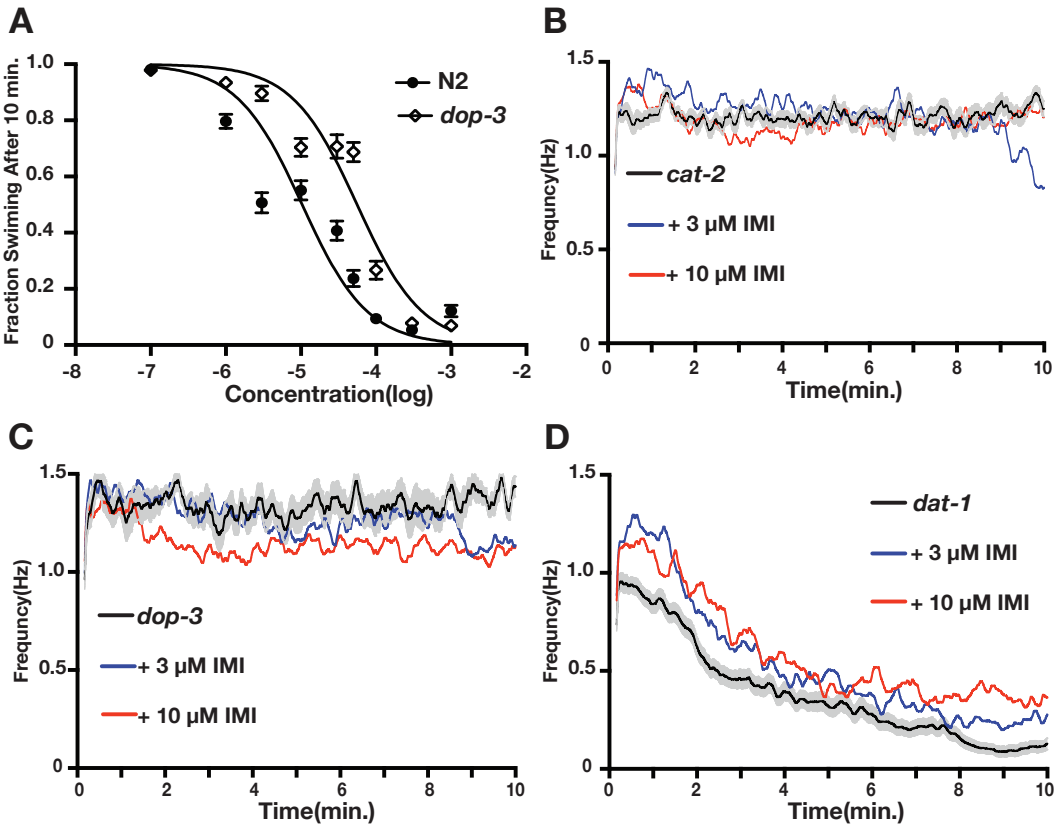

Figure 74 – IMI effects on swimming of *dat-1*, *cat-2* and *dop-3* animals A) Dose response effects of IMI on *dop-3(vs106)* as measured manually. Assays and statistical analyses were performed as described in Fig. 1 and in the methods. r^2 of fitted curves for N2 and *dop-3* were 0.9086 and 0.8265 and the IC_{50} values for N2 and *dop-3* were 10 µM (+/-1.5 µM) and 56 µM (+/- 7 µM) respectively. **B)** Automated recordings and analysis using Tracker 2.0. Average frequency of *cat-2(tm2261)* without drug, 3 µM IMI, and 10 µM IMI. Data were analyzed by 2-way ANOVA with Dunnet's post tests of each time point in the drug condition to the corresponding basal time point. Shaded area around the no drug condition represents the standard error. For illustrative purposes, the standard error is not shown for the drug conditions. Significant changes (P<.05) in average frequency for 3 µM IMI were observed, reaching significance at the 1st and 9th minute. The increase in frequency with 10 µM IMI during the 1st minute did not reach significance. **C)** Average frequency of *dop-3(vs106*) without drug, 3 µM IMI, and 10 µM IMI. Data were analyzed as above. We observed significant changes in average frequency for 3 µM IMI during the 9th minute. 10 µM IMI decreased the average frequency of *dop-3* during minutes 2-4 and 6-10. **D)** Average frequency of *dat-1(ok157)* without drug, 3 µM IMI, and 10 µM IMI. 3 µM IMI increased the average frequency of *dat-1* during several points in the first 4 minutes. 10 µM IMI increased the average frequency of *dat-1* during time points in the first four and last five minutes.

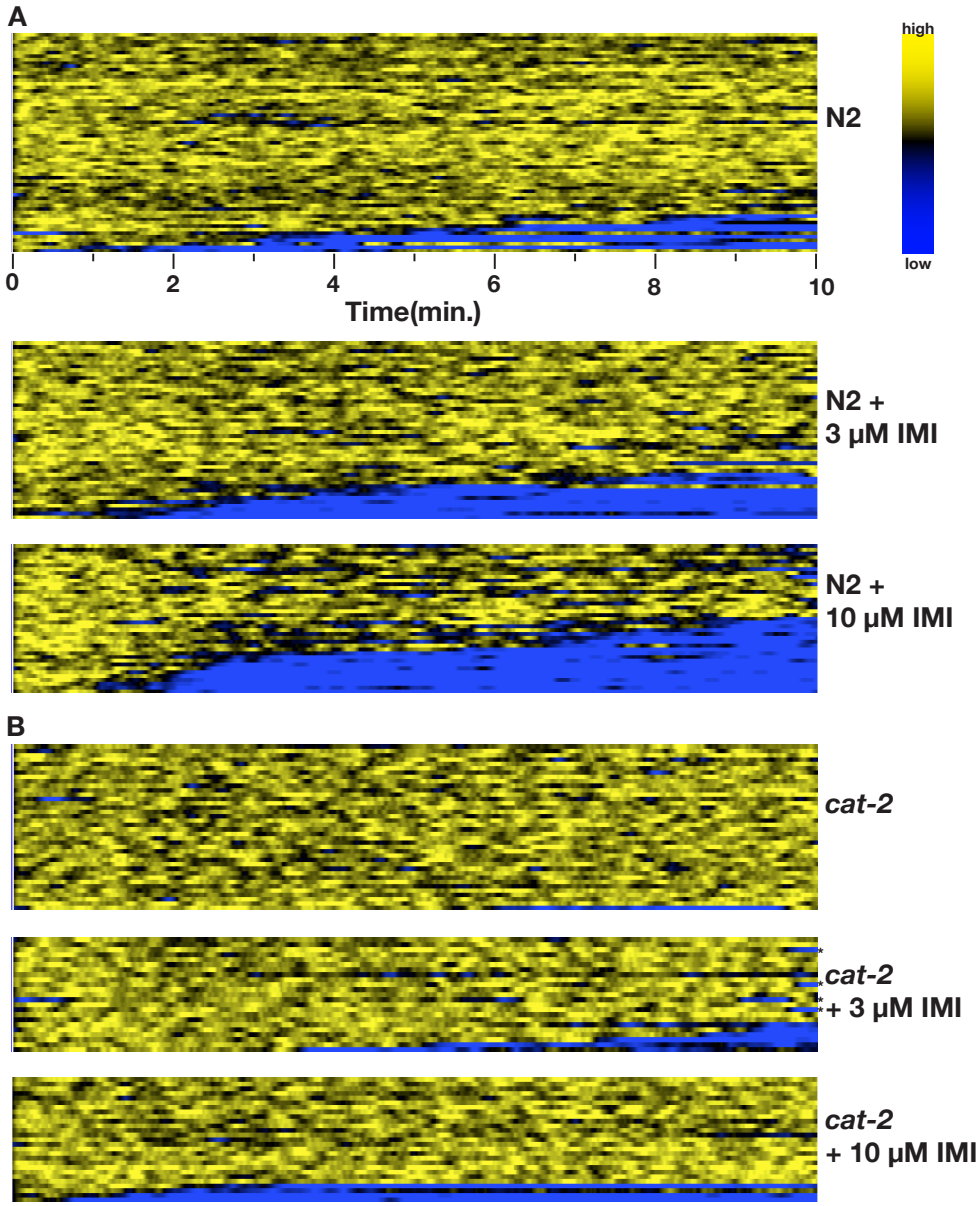

Figure 75 – Heat map representations of IMI effects on N2, *dat-1*, *cat-2,* and *dop-3* animals. Each row represents the frequency of swimming of an individual animal with thrashing frequency values represented as a color where yellow represents a high thrashing frequency and blue represents paralysis. We smoothed the raw frequency values in a 10 second moving window before plotting. For representative purposes, the top 5% of the thrashing frequency values are not used in this scale. Plots are ordered b ottom to top according to the latency to paralyze. **A)** IMI increases the incidence of paralysis of N2 animals in a dose dependent manner. **B)** IMI has limited, but detectable paralytic effects on *cat-2* worms at 3 µM and 10 µM. **C)** IMI has subtle immobilizing effects on *dop-3* worms at 3 µM and 10 µM. **D)** IMI alters the kinetic paralytic profile of *dat-1* worms.

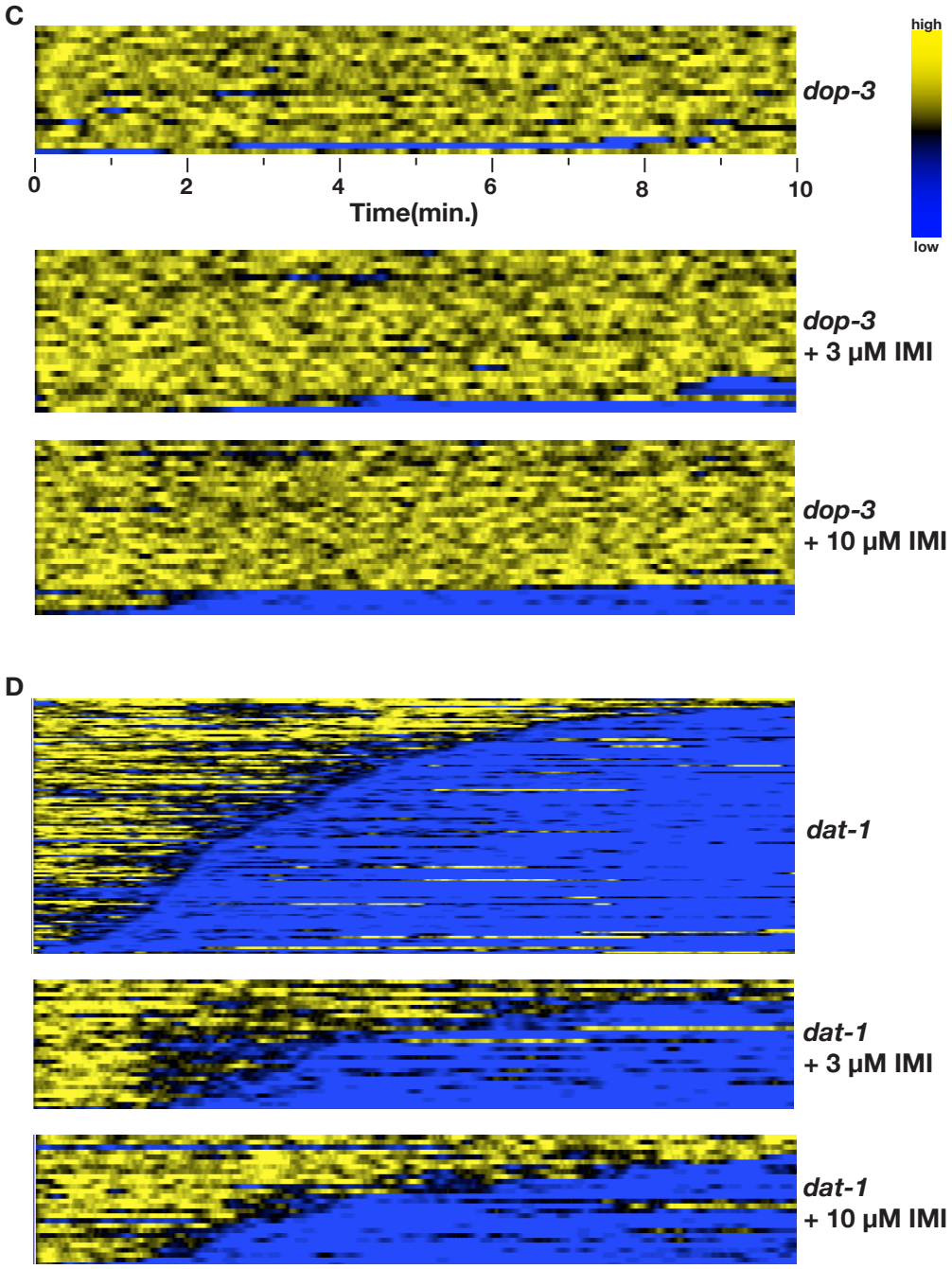

Figure 75(cont'd)

significance (Table 2). However, we observed that paralyzed worms treated with 10 μM IMI displayed a statistically significant reduction in reversion probability, with no change in the time to 1st reversion or reversion event length. Thus, IMI dose dependently increases the amount of paralysis evident in the population assayed and decreases the likelihood that the animals reverse.

Unlike our manual assays, using SwimR we detected *cat-2* and *dop-3* independent effects of IMI. Surprisingly, 3 μM IMI *increased* the average thrashing frequency of *cat-2* animals during the first two minutes and decreased thrashing frequency during the final minute. For *dop-3* animals, 3 μM IMI triggered a significant reduction in thrashing frequency in the final minute of recording whereas this behavior started in the third minute for 10 μM IMI. Unlike N2, only 10 μM had a significant effect on the maximal frequency reached by *cat-2* and *dop-3* worms. Inspection of the population plots for *cat-2* and *dop-3* revealed a higher incidence of paralytic worms at both doses and an increase in Swip latency for *cat-2* paralyzers treated with 10 μM IMI relative to 3 μM IMI (Figure 74B and Table 2). Consistent with the significant reduction in average thrashing frequency evident in the final minute, 3 μM IMI triggered paralysis at the end of several worm tracks (asterisks in Figure 75). Inspection of the frequency distribution for *cat*-2 and *dop*-3 treated with IMI revealed that the increase in average thrashing frequency during the first two minutes was reflected in a shift in the density of higher frequency value bins (Figure 76). As

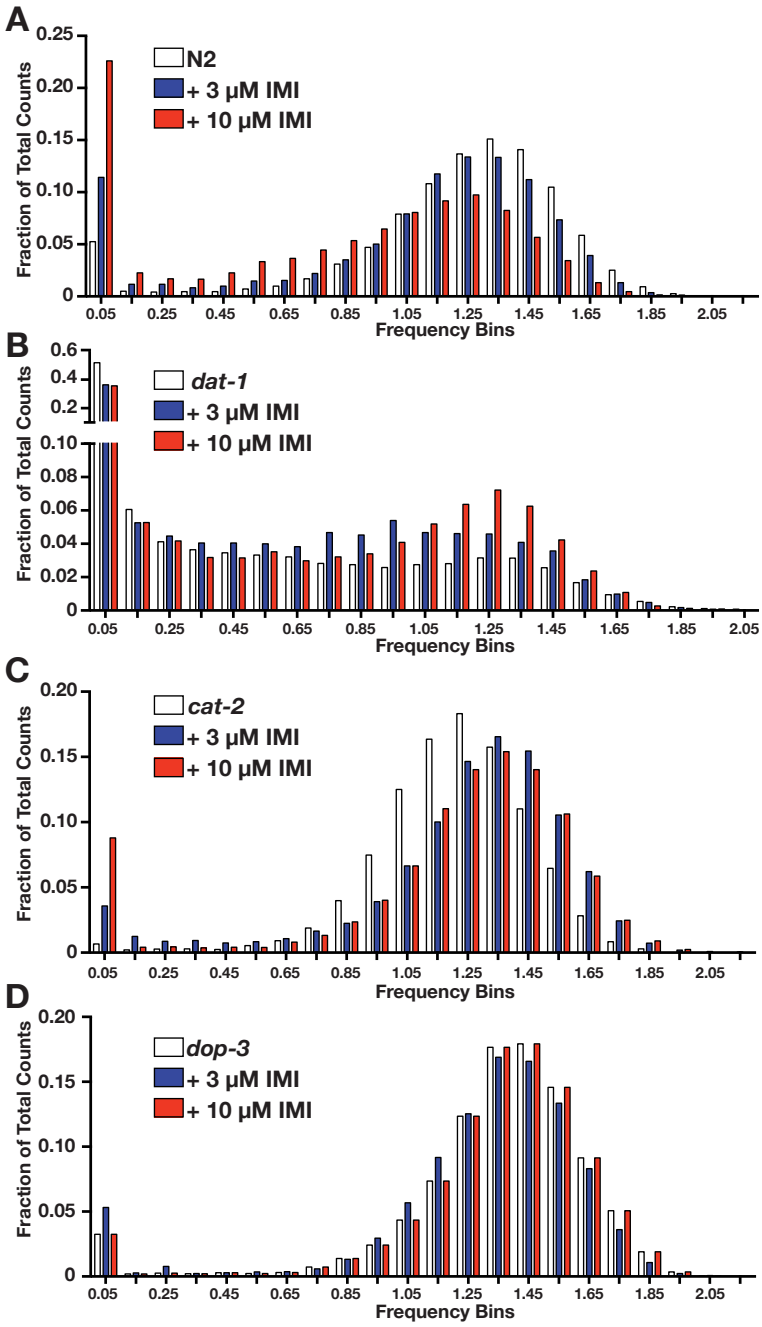

Figure 76 – Frequency distribution of IMI effects on N2, *dat-1*, *cat-2,* and *dop-3* animals. Frequency values were binned (0.1 Hz) and plotted as a fraction of the total # of values recorded. A) IMI increases the fraction of animals of low frequency bins and decreases the fraction of high frequency bins of N2 animals in a dose dependent manner. B) IMI dose dependently decreases the density of low frequency bins and increases the fraction of intermediate and high frequency bins in a *dat-1* strain. C) IMI increases the quotient of low frequency bins and increases the fraction of high frequency bins in *cat-2* animals. D) IMI causes only subtle alterations to low and high frequency bins in a *dop-3* strain.

we only detected a few paralyzers in either dose, we were underpowered to make any significant observations regarding IMI's effects on *cat-2* or *dop-3* paralytic reversion. Nonetheless, analysis with SwimR revealed that IMI alters swimming behavior in strains lacking *cat-2* or *dop-3*, though IMI effects on *cat-2* and *dop-3* are not as robust in reducing the average thrashing frequency.

IMI treatment of *dat-1* animals at 3 μM and 10 μM triggered a dose-dependent increase in average thrashing frequency across all time points, with 10 μM producing a more sustained significant increase across the recording time (Sup. Figure 74D). Unlike *cat-2* and *dop-3*, IMI did not alter the maximal frequency reached at either dose. Consistent with our manual assays, inspection of the heat maps (Figure 75), frequency distributions (Figure 76B), and analysis of Swip latency and reversion (Table 2) in *dat-1* animals treated with 3 μM and 10 μM IMI revealed that this increase in average thrashing frequency is due to a decrease in Swip penetrance. These observations represent the first identification of an acute pharmacological agent that rescues *dat-1* Swip. The apparent affinities of IMI for *dat-1* and *mod-5* suggest that IMI is more likely to act on *dat-1* (Jayanthi et al. 1998; Ranganathan et al. 2001). In *dat-1*'s absence however, IMI may have a higher bioavailability for targets like *mod-5* or *egl-2* (Weinshenker et al. 1995). Considering the classical antagonistic roles for DA and serotonin in behaviors like egg-laying and movement on plates, it seems plausible that *dat-1* and *mod-5* function in parallel to regulate the extrasynaptic tone of both neurotransmitters during worm swimming. Further

studies exploring these genetic interactions in context with IMI application may inform how these pathways converge to regulate swimming behavior.

These studies demonstrate the utility of SwimR for the analysis of both genetic and pharmacologically induced patterns of *C. elegans* swimming. In manual assays, we demonstrated that IMI induces paralysis consistent with DA and *dat-1* dependence. Analysis of IMI effects using SwimR revealed that whereas the behavioral effects of IMI clearly require endogenous DA signaling, additional pathways are likely to regulate responses even at low concentrations of the drug. Importantly, SwimR enabled us to depict and quantify subcomponents of IMI effects not detected with manual assays. For example, time-dependent changes in drug-modulated swimming behavior are missed in end-point, “yes-no” manual paralysis assays. We conclude that SwimR is a useful tool for exploring the differential impact of mutations and drugs on distinct signaling networks, one that, due to its freely available, open-platform nature, can be tailored to the specific interests of *C. elegans* researchers.

Appendix B

CANDIDATE-BASED ANALYSIS OF ION CHANNEL AND AUTORECEPTOR CONTRIBUTIONS TO *DAT-1* SWIMMING INDUCED PARALYSIS.

INTRODUCTION

Our previous studies of the identification of Swip in the *dat-1* strain established that this strain demonstrates a paralytic phenotype that requires the presence of DA and the *dop-3* receptor (P. W McDonald, et al., 2007). The identification of the Swip phenotype, the absence of *dat-1* mediate locomotory alterations on solid substrate, and the subsequent demonstration that Swip is osmosensitive suggest that there exist context-specific mechanisms that trigger excitation of DA neurons when worms are placed in water. In this study, we aim to describe the upstream mechanisms via a host of genetic and behavioral assays. We demonstrate that a network of presynaptic genes including the ion channels *trp-4* and *asic-1* and DA receptor *dop-2* function in DA neurons to control the penetrance of Swip in the *dat-1* mutant.

MATERIALS AND METHODS

C. elegans Strains and Husbandry

C. elegans strains were cultured on bacterial lawns of OP50 and maintained at 12 to 20°C using standard methods (Brenner, 1974) unless otherwise noted. The wild-type strain is N2 Bristol.

We used the following strains for this study:

dat-1(ok157)
dat-1(v21)
dat-1(vt22)
dop-2(vs105)
cat-2(tm2261)
asic-1(ok415)
trp-4(ok1605)
trp-4(sy695)
swip-10(vt29)
swip-10(vt33)

Genetic Crosses

Crosses were performed using publically available integrated fluorescent reporter strains to mark chromosomes *in trans*. Single worm PCR were performed to confirm the presence of the indicated mutation. For all deletions, we used a three primer multiplex strategy that produces PCR amplicons with 100-200 bp difference between N2 and mutant. This was highly effective in eliminating preferential amplification of a lower molecular weight species. In all cases, a synthetic heterozygous control was utilized to ensure that heterozygous clones could be identified within that experiment. All PCR reactions were performed with Platinum PCR Supermix (Life Technologies).

We generated the following strains by cross. Primers for genotyping are only listed once:

BY822 *trp-4(ok1605); dat-1(vt21)*

PCR genotyping of *trp-4(ok1605)* was performed using the following primers

5’ sense – AAGACTCCGGTACACGTTGC

3’ antisense – AGAAGCATCCGCACAAGACT

inner antisense – acagtaaccttggtcctggt

Genotyping of *dat-1(vt21)* was determined by sequencing of PCR products using the following primers:

5’ sense – tcctgcaaatctggaaaacc(sequencing primer)

3’ antisense – agctccagcaaaacttccaa

BY823 *trp-4(ok1605); dat-1(vt22)*

Genotyping of *dat-1(vt22)* was determined by sequencing of PCR products using the following primers:

5’ sense – acagcaatgtgtcgaagtgc(sequencing primer)

3’ antisense – ggttttccagatttgcagga

BY830 *dat-1(ok157); dop-2(vs105)*

PCR genotyping of *dat-1(ok157)* was performed using the following primers:

5’ sense – gcaatcacaacttggggaag

3’ antisense –aaagtggaagacacctatgttcatagc

inner antisense - ggttttccagatttgcagga

PCR genotyping of *dop-2(vs105)* was performed using the following primers

5’ sense – tttgtgcctcagttcgtctgac

3’ antisense – aacctcggtttcccttgttaggca

inner sense – cgagcactgcaatcagccatcaat

BY831 *trp-4(ok1605); dat-1(ok157)*

BY839 *asic-1(ok415) trp-4(sy695)*

asic-1(ok415) and *trp-4(sy695)* were crossed together to generate double heterozygote animals and recombinant progeny were identified by screening individual clones using the following primers:

asic-1(ok415):

5’ sense – gccgtgctctagccgtaatacag

3’ antisense – GCCCAGCTTCTGGCCATATGTA

inner antisense – gcctggatgcaaattagaattggctc

trp-4(sy695):

5’ sense – gtactgaaaaaaaactcgattccccc

3’ antisense – TGGTTCGCCCGTCTGTAAGCT

inner sense – CTACCAGCCTGTCGACGAGGAC

BY840 *asic-1(ok415) trp-4(sy695); dat-1(ok157)*

We crossed BY839 to *dat-1(ok157)*.

BY885 *asic-1(ok415) trp-4(sy695); swip-10(vt29)*

We crossed BY839 to *swip-10(vt29). swip-10(vt29)* genotype was determined by Sanger sequencing of PCR amplicons generated using the following primers:

Sense – ccagAACGATACGATGAACC(Sequencing primer)

Antisense – GCAACCATAGCGCCTTCTAG

BY886 *asic-1(ok415) trp-4(sy695); swip-10(vt33)*

We crossed BY839 to *swip-10(vt33)*. *swip-10(vt33)* genotype was determined by Sanger sequencing of PCR products using the same primers for *swip-10(vt29)*.

BY892 *asic-1(ok415); dat-1(ok157)*

C. elegans assay for Swip

In both batch and single worm analyses, we generated synchronous populations of these strains by hypochlorite treatment and harvesting arrested L1 animals. Early-mid stage L4 animals were identified by characteristic morphology and used for behavior as N2 animals show some stochastic Swip and quiescence bouts during the last larval molt. For automated analysis, single L4 hermaphrodites were placed in 20μL water or drug in a single well of a Pyrex Spot Plate (Fisher catalog number 13-748B), and 10 minute movies (uncompressed AVI format) of their swimming behavior were created and analyzed as described previously (Hardaway and Wang *et al.)*.

C. elegans assay for Basal Slowing Response

Assays were performed as described in Chase *et al.* with some modifications. We prepared food free 35 mm NGM plates and used them for 2-3 days of testing. For the food condition, we spread a thin layer of HB101 in a “donut” fashion around the edge of 35 mm plates with the bottom of a glass test tube. Bacteria were serially diluted, spread at several different dilutions, and incubated o/n at 37 degrees. The next day, food-containing plates were selected for BSR assay based on the density of bacterial growth which was complete (not spotty), but also textured and not overgrown. Overgrown bacterial lawns were capable of producing non-DA dependent slowing by virtue of imposing a thicker matrix for worm locomotion. We picked mid-stage L4 animals and placed them at 15 degrees o/n to generate young adult hermaphrodites. On the day of testing,

strains were blinded and experiments picked single young adults, rinsed them briefly in M9 (3-4 sec) to remove food, and placed them on either a food-free plate or directly adjacent to a bacterial source on a food-containing plate. After 30 seconds, we counted the number of body bends in a 20 second interval. On each day, 5 animals were scored in both conditions for each genotype. Data shown represents the cumulative average body bends over at least 3 days of experiments for two experimenters.

Isolation of mRNA

An asynchronous population of BY200 and *dat-1(vt22)* worms were harvested from a 10 cM 8p/NA22 plate by rinsing with M9. These worms were washed 5X with 15 mls of M9 and the pellet was frozen at -80° o/n. On the next day we ground up the pellet using a ceramic mortar and pestle that had been prefrozen with liquid nitrogen. RNA from 100 µl aliquots of the frozen powder was extracted in 1 ml of TRIzol (Life Technologies) according to the manufacturer's instructions. Precipitated RNA was suspended in RNAse and DNAse free water (Life Technologies). We purified mRNA from these total RNA preps using MicroPoly(A)Purist kit (Life Technologies) according to the manufacturers instructions. mRNA and Total RNA were run on an 1% agarose gel to confirm the purity and that rRNA was not present in our samples.

Whole Transcriptome Sequencing of BY200 and *dat-1(vt22)*

We used 100 ng of mRNA for cDNA library synthesis and used this library to construct a sequencing library for next-generation sequencing using single end 36mers on an Illumina Genome Analyzer Iia. The reads were trimmed to facilitate mapping and then mapped to a reference transcriptome (WS180). Average nucleotide coverage depth was ~5X. We normalized the # of reads at each particular gene by the number of total reads from that sample and the length of the gene (in Kb)(Mortazavi, Williams, McCue, Schaeffer, & Wold, 2008) and compared the fold enrichment of reads in BY200 and *dat-1(vt22)*. We then compared lists of genes that were either up or downregulated in *dat-1(vt22)* with a list of genes whose expression is known to be enriched in DA neurons to extract genes that are more likely to function presynaptically within DA neurons (Spencer, et al., 2011).

Transgenic rescue of *asic-1* and *trp-4*

To determine the cell autonomous role of *asic-1* and *trp-4*, we constructed vectors or used available vectors that drive their expression solely in DA neurons. We obtained a p_{dat-1}:*trp-4(*cDNA):SL2-YFP courtesy of the Schafer lab and a pore dead version of *trp-4* in the same backbone via the Xu lab (L. Kang, Gao, Schafer, Xie, & Xu, 2010; Kindt, et al., 2007). To express *asic-1* cell autonomously, we cloned an *asic-1* genomic fragment into a p_{dat-1} expression vector. The *asic-1* fragment was amplified from a p_{asic-1}:*asic-1*(genomic):GFP construct obtained from the Tavernarakis lab.

The following strains were generated by germline transformation:

BY1017-BY1019 – We injected p_{dat-1}: *asic-1* onto BY840(*asic-1(ok415) trp-4(sy695); dat-1(ok157)*) to generate *vtEx169-vtEx171*

BY1027-BY1029 – We injected p_{dat-1}: *trp-4* (EPK$^{1739\text{-}41}$KPK):SL2-YFP onto BY840 to generate *vtEx177-179*

BY1035-BY1036 – We injected p_{dat-1}: *trp-4*:SL2-YFP onto BY840 to generate *vtEx180-vtEx181*.

For Swip analyses, transgenic and non-transgenic progeny were picked onto separate plates, allowed to acclimate for at least three hours and then assay for Swip.

RESULTS

RNAseq of *dat-1* reveals compensatory changes in ion channels

We hypothesized that genes important for normal DA neuron physiology, DA biosynthesis, vesicular release, or postsynaptic signaling would be revealed by a loss of DA clearance through *dat-1*. To understand how *dat-1* functions in a network of DA neuron cell autonomous genes, we performed whole transcriptome sequencing on mRNA from wild type and *dat-1* strains and identified all of the genes whose expression was altered by at least 25% (Figure 77A). As we observed an inordinate number of genes whose expression was upregulated in *dat-1* (skewed right distribution in Fig. 77B), we focused on genes with downregulated expression in the *dat-1* mutant. Importantly, we compared our list of genes with altered expression levels to lists of genes

identified to be highly enriched in DA neurons identified by tiling arrays (Spencer, et al., 2011). Importantly, these analyses identified a number of genes whose expression is known to be enriched in DA neurons and are downregulated in the *dat-1* mutant, including *dat-1* itself (Figure 77C). These experiments revealed a high enrichment of genes associated with neuropeptide signaling including *egl-3*, the primary worm preprotein convertase, and a number of specific neuropeptide genes including *npsb–(7-11)*, *flp-(2,4,7,8,10, 25)* and *nlp-29* (Figure 77D). We also detected several ion channels including *trp-4, osm-9, lgc-49, lgc-53, aqp-6, unc-2, acr-5*, and *asic-1* and G-protein coupled receptors including *dop-2, dop-3, tyra-2*, and *tyra-3*. To validate the importance of DA neuron specific network, we focused our mechanistic analyses on genes whose actions have been studied and for which there are publically available alleles.

Loss of *asic-1* and *trp-4* mediates parallel suppression of *dat-1* Swip

Based on the downregulation of *trp-4* and *asic-1* and the literature describing their function, we hypothesized that these genes were required for normal *dat-1* Swip by evoking an increase in DA neuron excitability through swimming evoked mechanical stretch of *trp-4* containing DA neuron dendrites and enhancement of vesicular release through *asic-1* activity. We generated a series of strains

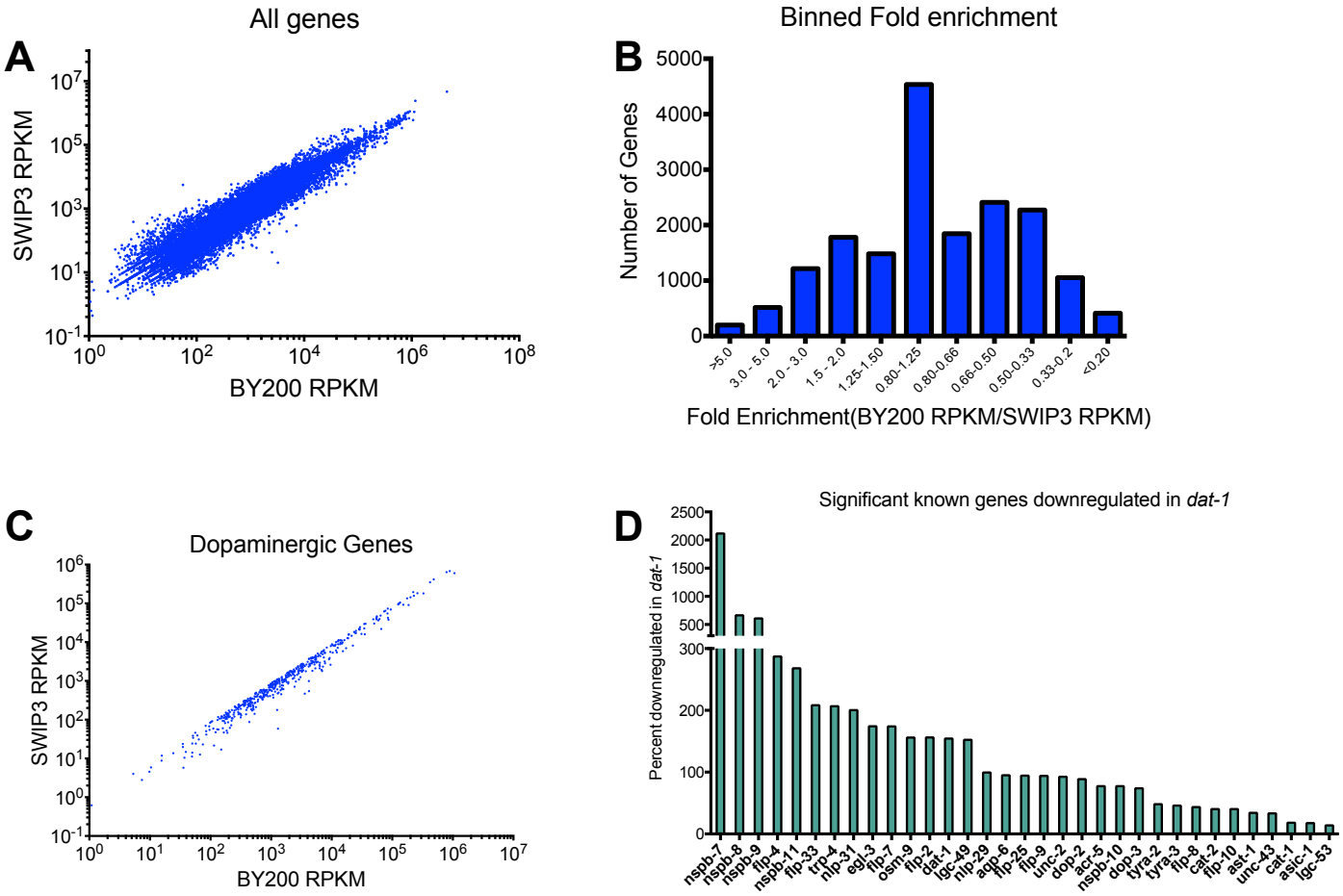

Figure 77 – Analysis of altered gene expression in the *dat-1* strain via RNAseq. A. Relative expression level plot for all genes in *dat-1*(SWIP3) vs the parental strain(BY200). **B.** Frequency distribution of ratio of expression in parental vs *dat-1*. We noted a large proportion of genes with elevated expression in *dat-1* (non Gaussian bump in genes with low parental/ *dat-1* RPKM ratio). **C.** Genes in **A** that are known to be enriched gene in DA neurons. **D.** Selected genes and the magnitude of their downregulation in the *dat-1* strain.

containing mutations in either or both of *asic-1* and *trp4* and *dat-1* and tested them for Swip. For *asic-1*, we did not observe any significant paralysis with its loss alone (Figure 78A), and in combination with *dat-1* we observed a significant incomplete suppression of *dat-1* that was most apparent at 100 mOsm (Figure 78B). For *trp-4*, we observed a highly significant basal paralysis that was not suppressed by an increase in osmolarity. We also observed more paralysis using the *trp-4(ok1605)* allele (data not shown) and they also have altered movement on plates. As we were concerned with this broader movement phenotype masking genetic interactions with *dat-1*, we pursued our analysis with the *sy695* allele in these studies. Surprisingly, loss of *trp-4(sy695)* did not suppress *dat-1* Swip (Figure 79). Rather, *trp-4* loss alone enhanced the penetrance of *dat-1* Swip and this enhancement was revealed only during basal Swip assays. To determine if *asic-1* and *trp-4* function redundantly to mediate *dat-1* Swip, we generated a triple mutant strain containing mutations in both *asic-1* and *trp-4* on the *dat-1* mutant background. We observed a highly significant suppression of *dat-1* Swip that restored their swimming levels to near that of the wildtype strain (Figure 80A).

Thrashing analysis of *asic-1* and *trp-4*'s contribution to *dat-1* Swip

To confirm *asic-1* and *trp-4* contributions to *dat-1* Swip, we analyzed the swimming behavior of the previously described lines using automated thrashing analysis (Hardaway and Wang, *under review*). Surprisingly, these analyses revealed a highly significant reduction in the thrashing frequency in the *asic-1*

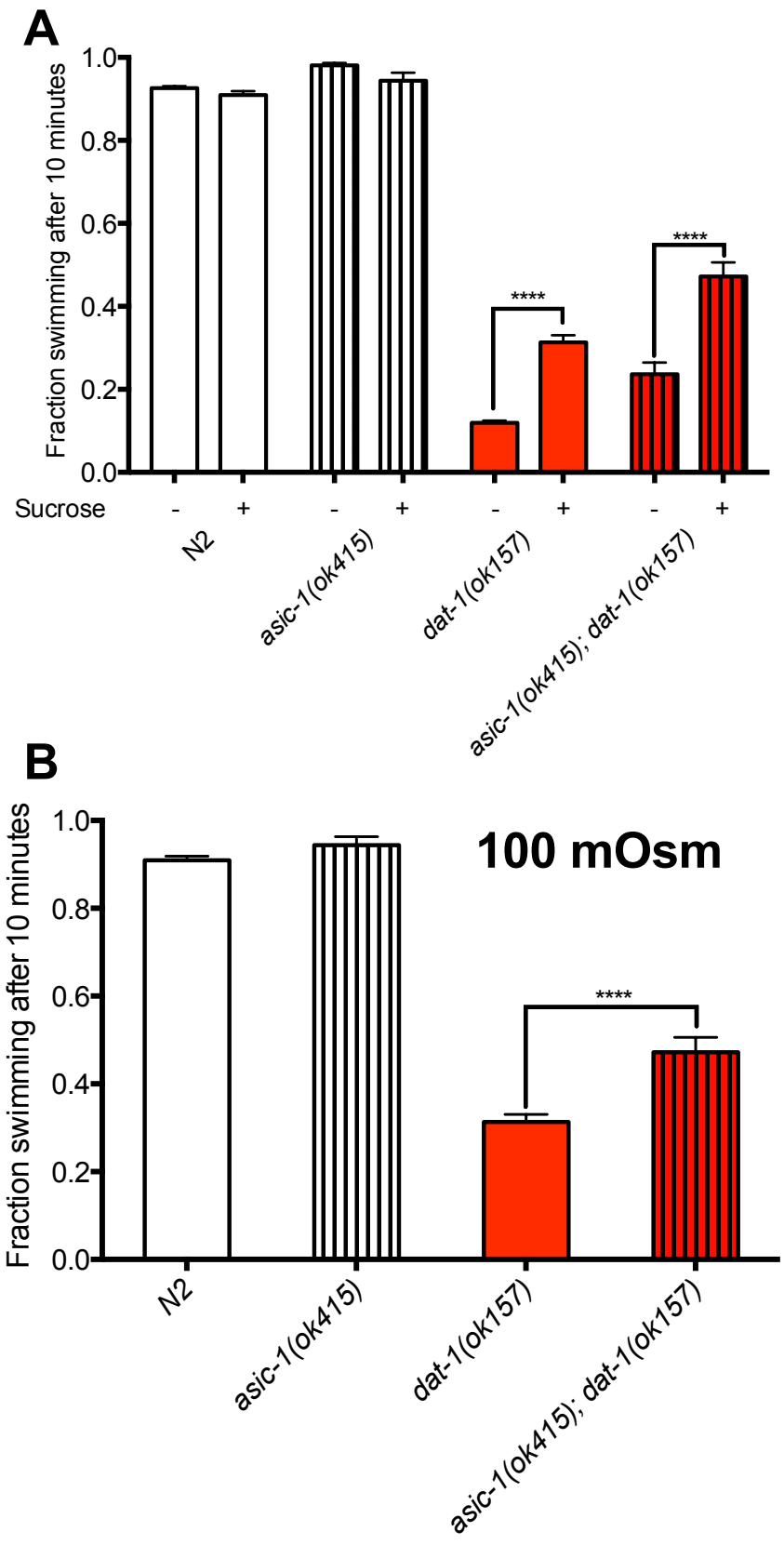

Figure 78 – *asic-1* incompletely suppresses Swip in the *dat-1* strain. A) Swip phenotype in water alone and in 100 mOsm-buffered water. Swip in either *dat-1* or *asic-1; dat-1* is significantly suppressed by elevated osmolarity. Data were analyzed by two-way ANOVA with Sidak's multiple comparison test comparing the osmolarity effect for each genotype and comparing genotypes at either osmolarity. **B)** Swip behavior at 100 mOsm only. *asic-1* incompletely suppresses Swip in *dat-1*. For both **A** and **B,** assays were performed and double mutant strains constructed as described in the methods. Two experimenters tested strains over the course of three weeks. Each column represents the average of at least 40 trials tested over this period.**** indicate $p<0.0001$ for the post tests.

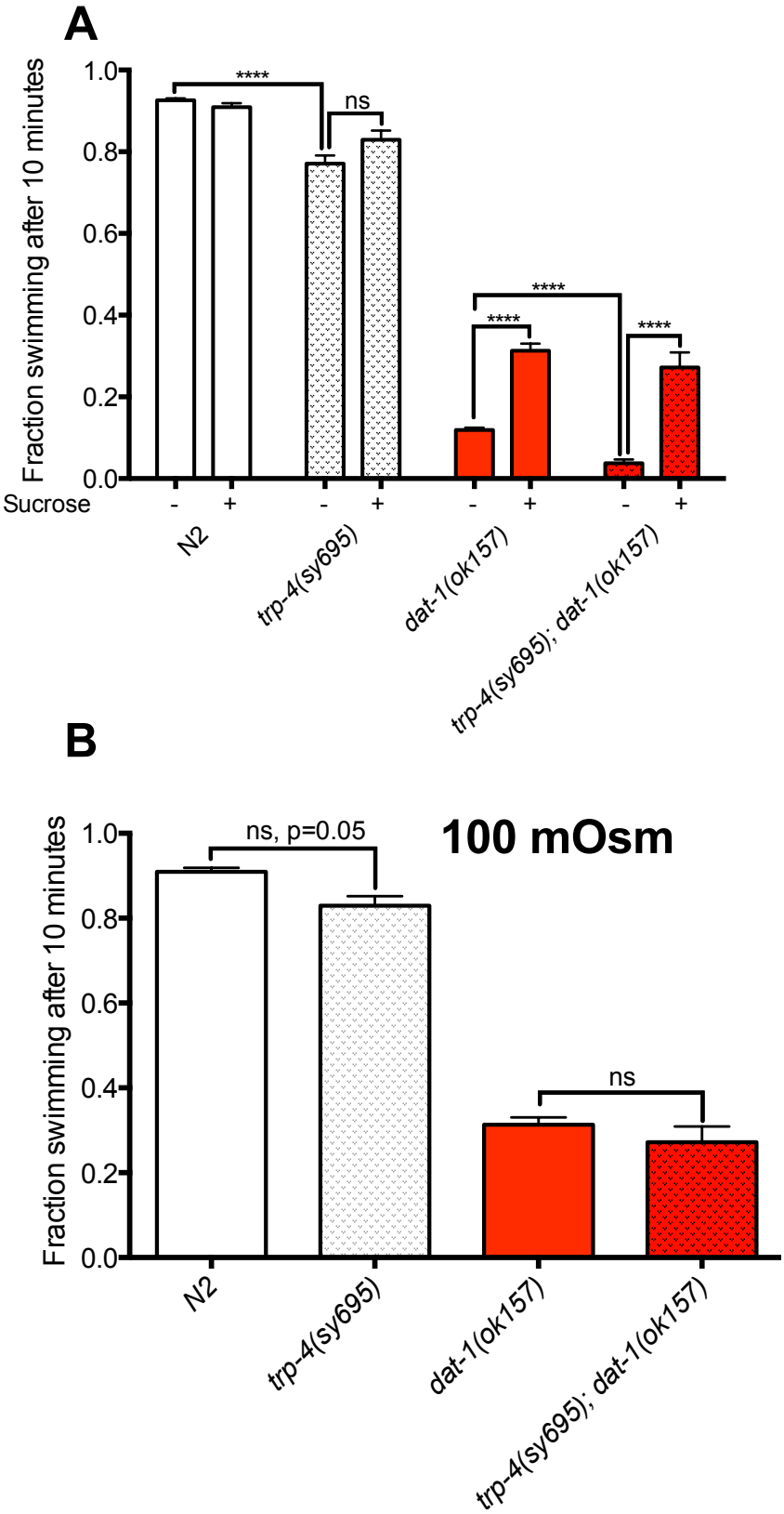

Figure 79 – *trp-4* demonstrates a basal paralysis that is not suppressed by elevated osmolarity and operates in parallel with *dat-1* at low osmolarity only. **A)** Swip phenotype in water alone and in 100 mOsm-buffered water. Swip in either *dat-1* or *trp-4; dat-1* is significantly suppressed by elevated osmolarity. Data were analyzed by two-way ANOVA with Sidak's multiple comparison test comparing the osmolarity effect for each genotype and comparing genotypes at either osmolarity. **B)** Swip behavior at 100 mOsm only. *trp*-4 demonstrates paralysis at 100 mOsm that did not reach statistical significance. *trp*-4 does not alter the penetrance of *dat-1* Swip at 100 mOsm. For both **A** and **B,** assays were performed and double mutant strains constructed as described in the methods. Two experimenters tested strains over the course of three weeks. Each column represents the average of at least 40 trials tested over this period.**** indicate $p<0.0001$ for the post tests.

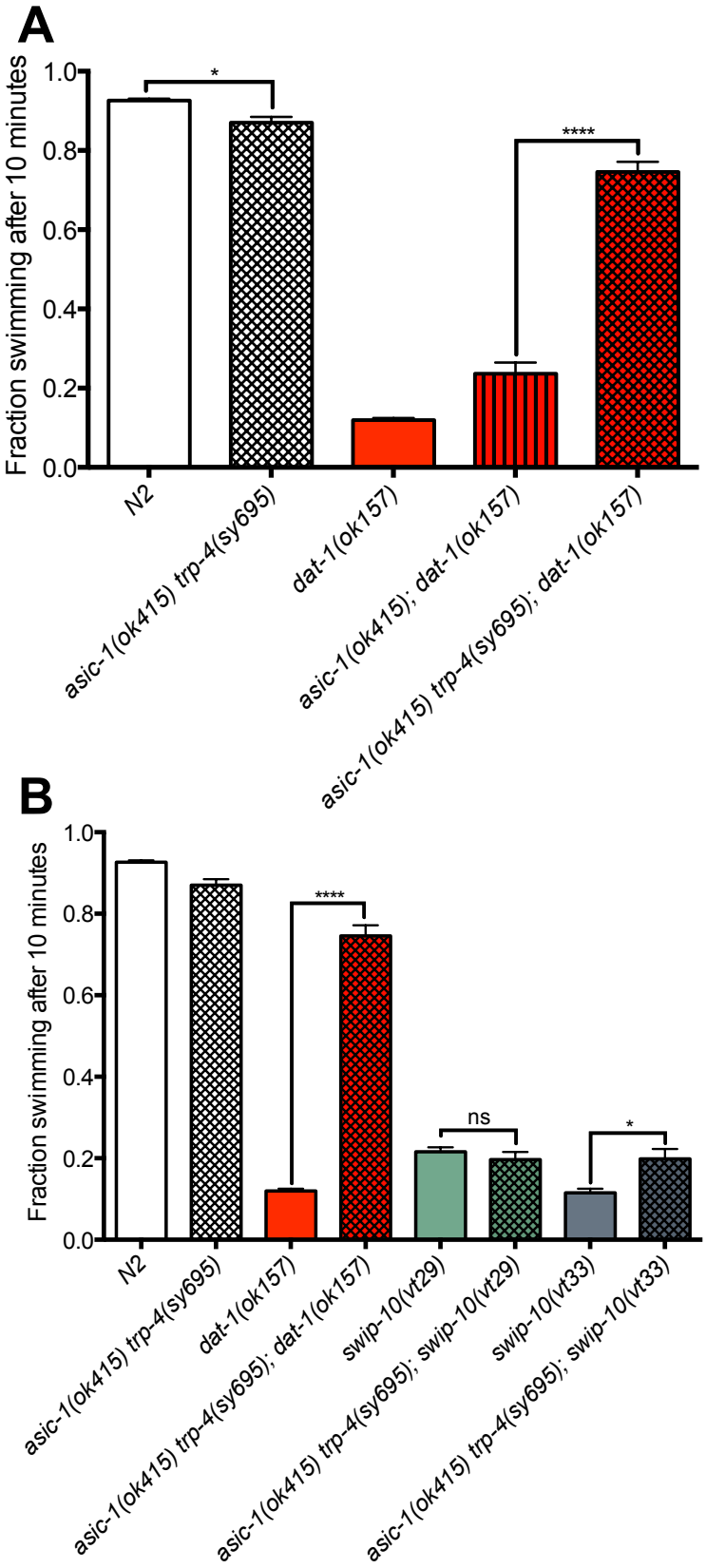

Figure 80 – *trp-4* loss enhances *asic-1* suppression of *dat-1* Swip. **A)** Swip phenotype in water alone. Loss of *trp-4* significantly enhances *asic*-1 suppression of *dat-1*. Data were analyzed by one-way ANOVA with multiple Bonferonni's post tests. **B)** Loss of *asic*-1 and *trp*-4 together has a reduced effect on Swip penetrance in the *swip-10(vt29)* or *swip-10(vt33)* mutant. For both **A** and **B,** assays were performed and double mutant strains constructed as described in the methods. Two experimenters tested strains over the course of three weeks. Each column represents the average of at least 40 trials tested over this period.* and **** indicate $p<0.05$ and 0.0001 for the post tests.

strain relative to the N2 (Figure 81A). Unlike our manual assays, we were not able to detect a significant suppression of *dat-1* Swip with loss of *asic-1* (Figure 81A). Therefore loss of *asic-1* results in a reduction in swimming frequency without causing paralysis(see Figure 78A) and the subtle suppression in *dat-1* Swip penetrance is only detectable in bulk population assays. Consistent with what we observed by hand, we detected a significant reduction in the average swimming frequency of *trp-4* (Figure 81B) or in the *asic-1 trp-4* strains (Figure 81C). We also observed a highly significant suppression of Swip in the *asic-1 trp-4; dat-1* strain with a significantly elevated thrashing frequency relative to *dat-1* throughout the 10 min. recording (Figure 81C). Thus our automated analyses confirm a more robust suppression of *dat-1* Swip with loss of both *asic-1* and *trp-4* than either alone.

asic-1 and *trp-4* function cell autonomously in DA neurons for Swip

To determine if *asic-1* and *trp-4* function cell autonomously in DA neurons to mediate *dat-1* Swip, we expressed these ion channels specifically in DA neurons on the *asic-1 trp-4; dat-1* background and tested transgenic and non-transgenic animals for Swip. Expression of wildtype *asic-1* or *trp-4* in DA neurons was sufficient to restore significant Swip in *asic-1 trp-4*; *dat-1* strain (Figure 82). To determine if channel activity was required in the *trp-4* gene, we expressed a previously validated pore dead version of *trp-4*(EPK$^{1739\text{-}41}$KPK). We did not observe significant restoration of Swip by expression of this version of *trp-4*.

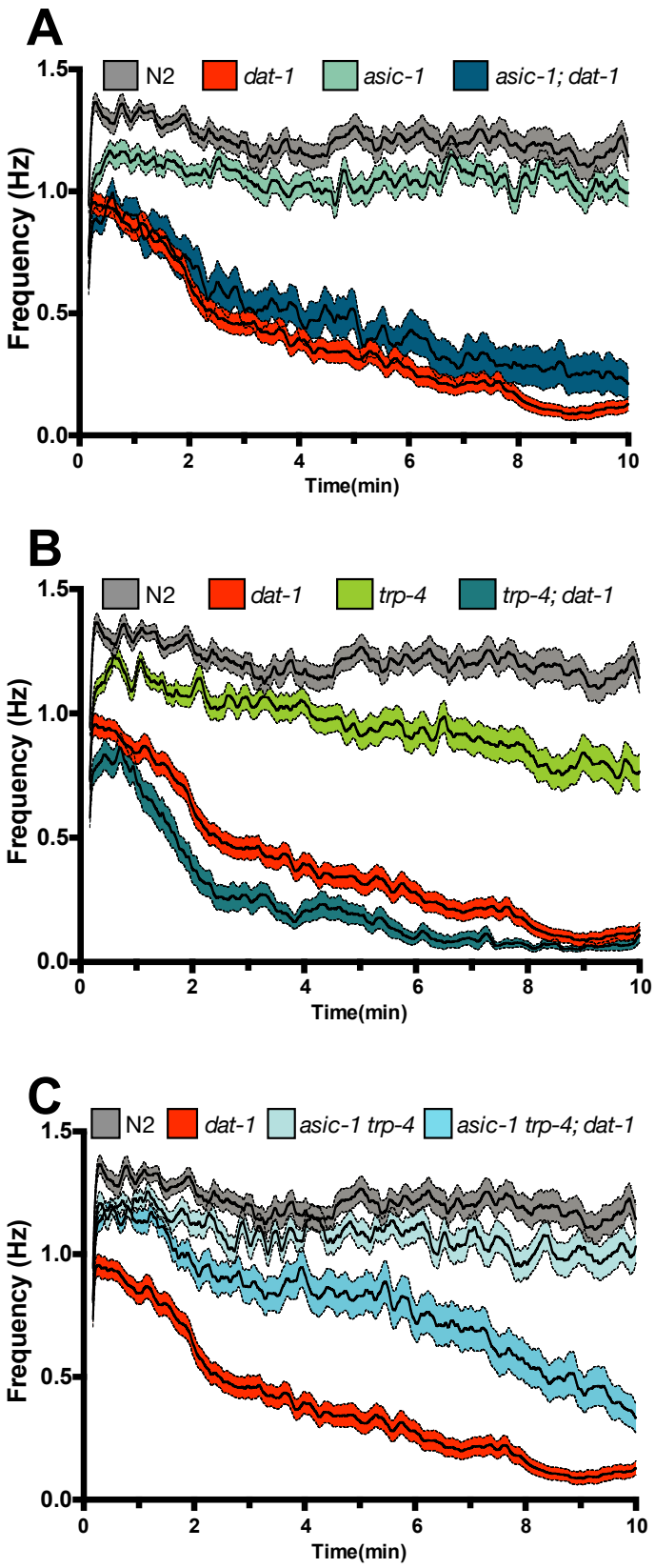

Figure 81 – Automated thrashing analysis of *asic-1, trp-4*, and *asic-1 trp-4* in context with *dat-1*. Recordings of individual L4 worms were performed as described in the methods and in Chapter VIII. **A)** *asic-1* average thrashing frequency is significantly reduced from N2(significant points in minutes 0-2, 4-5, 6, and 8-9). *asic-1; dat-1* does not show any significant difference from *dat-1* alone. **B)** *trp-4* is significantly reduced from N2(significant points in minutes 1-3 and 5-10). *trp-4; dat-1* is significantly reduced from *dat-1*(significant points in minutes 1-6). **C)** *asic-1 trp-4* thrashing frequency is significantly reduced from N2(minutes 7,8, + 10). *asic-1 trp-4; dat-1* thrashing frequency is significantly elevated over *dat-1*(minutes 1-10). For **A**, **B**, and **C**, data were analyzed by two-way ANOVA with multiple Bonferonni's post tests at each time point and the shaded areas represent the SEM of the average values.

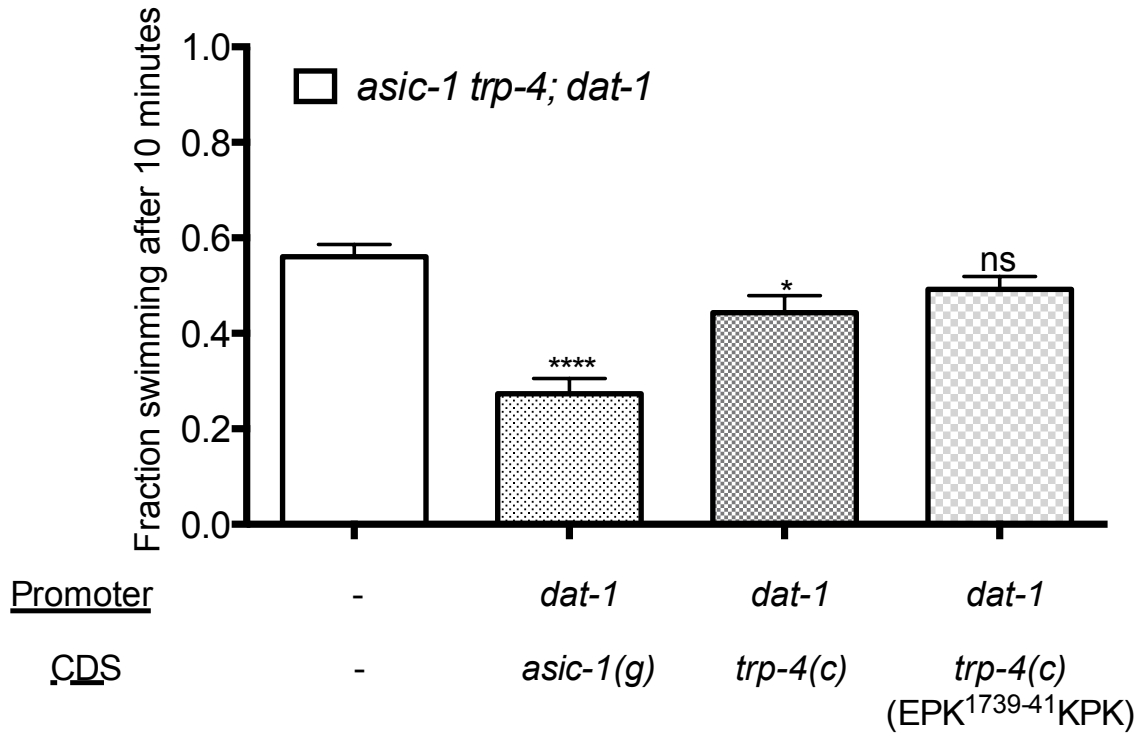

Figure 82 – *asic-1* and *trp-4* function cell autonomously in DA neurons to promote *dat-1* Swip and *trp-4* channel activity is required. Restoration of *asic-1* and *trp-4* specifically in DA neurons significantly restores Swip in the *asic-1 trp-4; dat-1* strain. Significant restoration is not seen when using a pore dead version of *trp-4*(right hand column). Transgenic strains were generated and tested as describe in the methods. Each transgene's effect was analyzed by an unpaired student's *t* test to non transgenic progeny assayed in parallel. The left hand empty column is representative of the penetrance of Swip that we observed in these experiments. * and **** indicate $p<0.05$ and 0.0001 respectively.

Therefore *asic-1* and *trp-4* function cell autonomously in DA neurons and channel activity of *trp-4* is required to promote Swip in the *dat-1* strain.

Loss of *asic-1* and *trp-4* disrupts BSR

Previous studies had indicated that *trp-4*, but not *asic-1*, were critical for promoting the excitability of DA neurons during BSR. Our studies with *dat-1* Swip were consistent with the hypothesis that *asic-1*, rather than *trp-4,* was the more important ion channel. Therefore we conducted our own assays of BSR in the *asic-1*, *trp-4*, and *asic-1 trp-4* strains. We independently validated that the *cat-2* and *dop-3* strains have a reduced magnitude of BSR relative to the N2 strain (Figure 83). Consistent with Li *et al.* and Kindt *et al*. and contrary to Voglis *et al*.; the *trp-4*, *asic-1*, and the *asic-1 trp-4* strains all demonstrated a reduced magnitude of BSR relative to the N2 strain (Kindt, et al., 2007; Li, et al., 2006; Voglis & Tavernarakis, 2008).

***asic-1* and *trp-4* are not fully required for *swip-10* Swip**

To determine if *asic-1* and *trp-4* activity are required more broadly for all hyperdopaminergic mutants, we crossed the *asic-1 trp-4* strain to a recently isolated strain that demonstrates Swip, but harbors normal *dat-1* activity(Hardaway, et al., 2012). Swip analyses of two *asic-1 trp-4; swip-10* strains revealed that *asic-1* and *trp-4* have a minimal contribution to this mutant (Figure 80B).

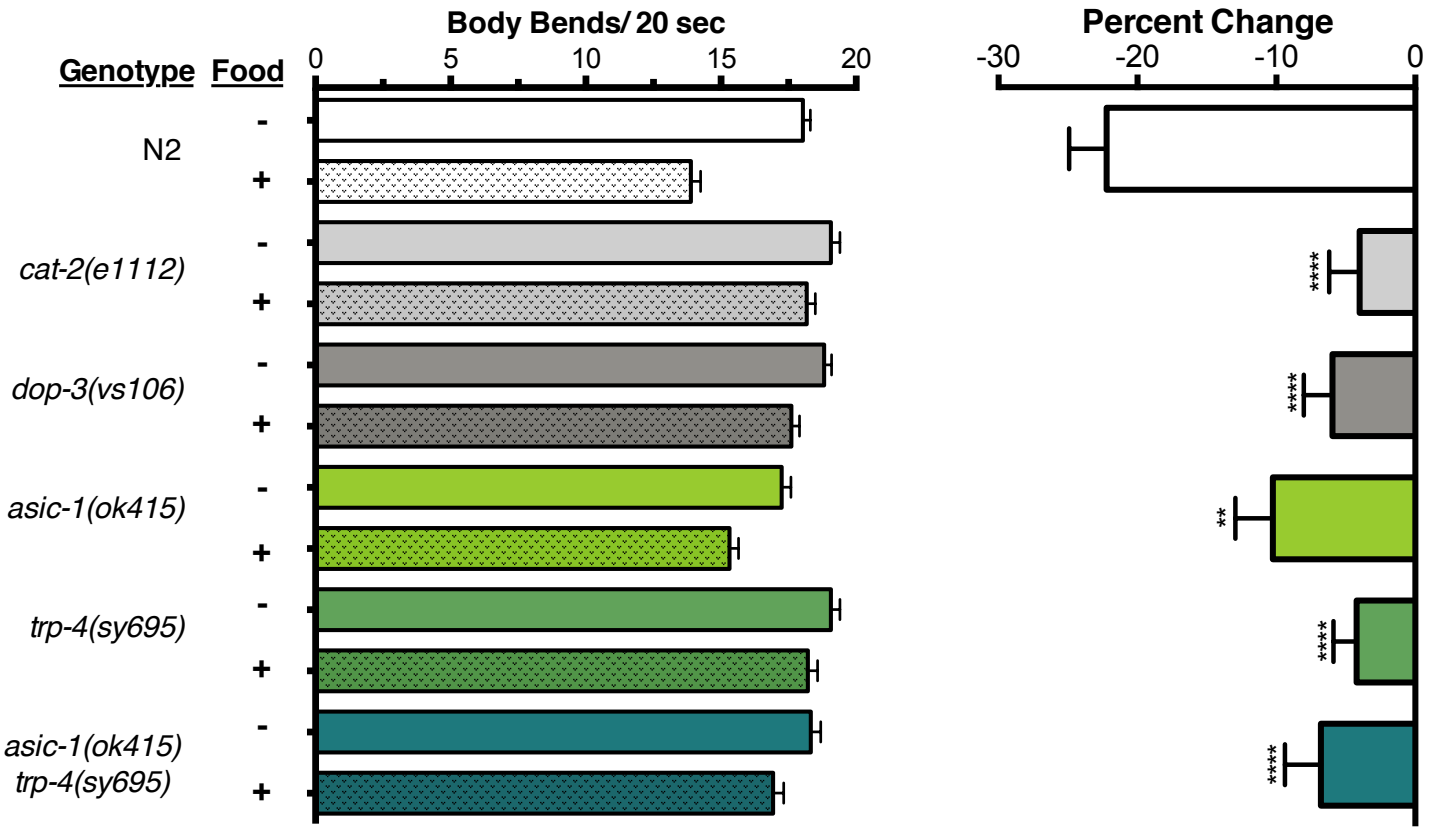

Figure 83 – Basal Slowing response of *asic-1* and *trp-4*. Loss of either *asic-1* or *trp-4* results in a reduction in the magnitude of BSR relative to the N2 strain. Assays were performed as described in the methods. Each column represents the average locomotory behavior of at least 28 animals tested over the course of three independent test days by two experimenters. Data is plotted as the raw counts over a 20 second interval on and off food and as the average percent change in body bends/20 sec for each animal tested over this period. Percent change data were analyzed by one way ANOVA with Dunnet's post tests to the N2 strain.

Loss of *dop-2* functions in parallel and enhances *dat-1* Swip

In our previous experiment of identifying genes downregulated in the *dat-1* mutant strain we identified the dopamine receptor *dop-2*. In the initial cloning of this receptor, the authors described robust expression in DA neurons and speculated in its role in presynaptic maintenance of DA signaling. To understand how *dop-2* interacts with *dat-1* in the regulation of extrasynaptic DAergic tone we crossed this mutant to the *dat-1* mutant and investigated its impact on *dat-1* Swip. We observed that the *dat-1; dop-2* strain exhibits Swip with elevated penetrance relative to the *dat-1* strain alone such that addition of 100 mOsm sucrose doesn't even trigger a significant suppression of Swip as it does in the *dat-1* strain (Figure 84A). Moreover, the penetrance of Swip at 100 mOsm was enhanced relative to the *dat-1* strain (Figure 84B).

Thrashing analysis of *dop-2* contribution to *dat-1* Swip

Our manual assays of *dop-2* and *dat-1; dop-2* in water and 100 mOsm buffer suggest that loss of *dop-2* enhances the penetrance of Swip in the *dat-1* strain. To determine if loss of *dop-2* alters the kinetic profile of *dat-1* Swip, we performed single worm thrashing analysis on *dop-2* and *dat-1; dop-2*. As we had observed in manual assays, the *dop-2* strain demonstrated a reduction in its average swimming frequency relative to N2 (Figure 85). In agreement with our previous data, we observed a significant reduction in the average swimming frequency of *dat-1; dop-2* relative to *dat-1*. These data are consistent with the hypothesis that the activity of *dop-2* promotes swimming in the *dat-1* strain.

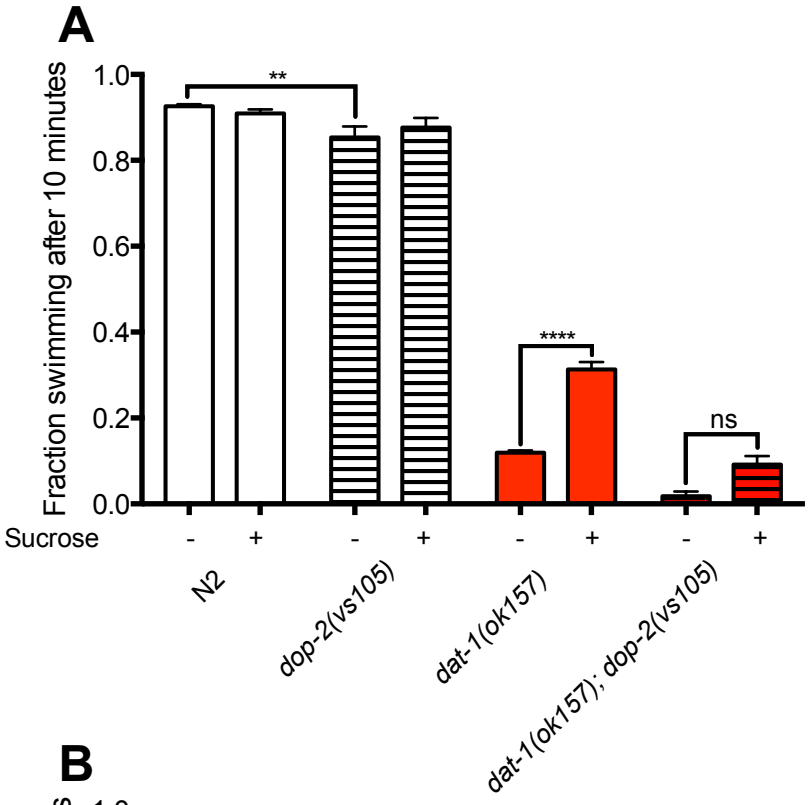

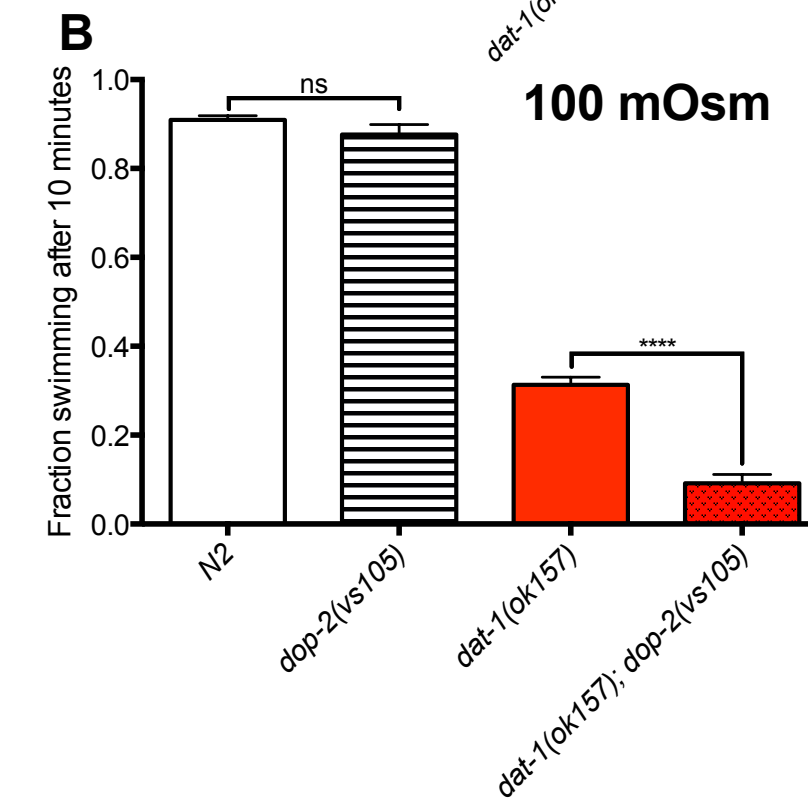

Figure 84 – *dop-2* demonstrates a basal paralysis that is not suppressed by elevated osmolarity and operates in parallel with *dat-1* A) Swip phenotype in water alone and in 100 mOsm-buffered water.*dop-2* exhibits significant basal Swip. Swip in *dat*-1, but not *dat-1; dop*-2 is significantly suppressed by elevated osmolarity. Data were analyzed by two-way ANOVA with Sidak's multiple comparison test comparing the osmolarity effect for each genotype and comparing genotypes at either osmolarity. **B)** Swip behavior at 100 mOsm only. Loss of *dop*-2 significantly enhances the penetrance of *dat*-1 at 100 mOsm. For both **A** and **B,** assays were performed and double mutant strains constructed as described in the methods. Two experimenters tested strains over the course of three weeks. Each column represents the average of at least 22 trials tested over this period.** and **** indicate $p<0.01$ and 0.0001 for the post tests

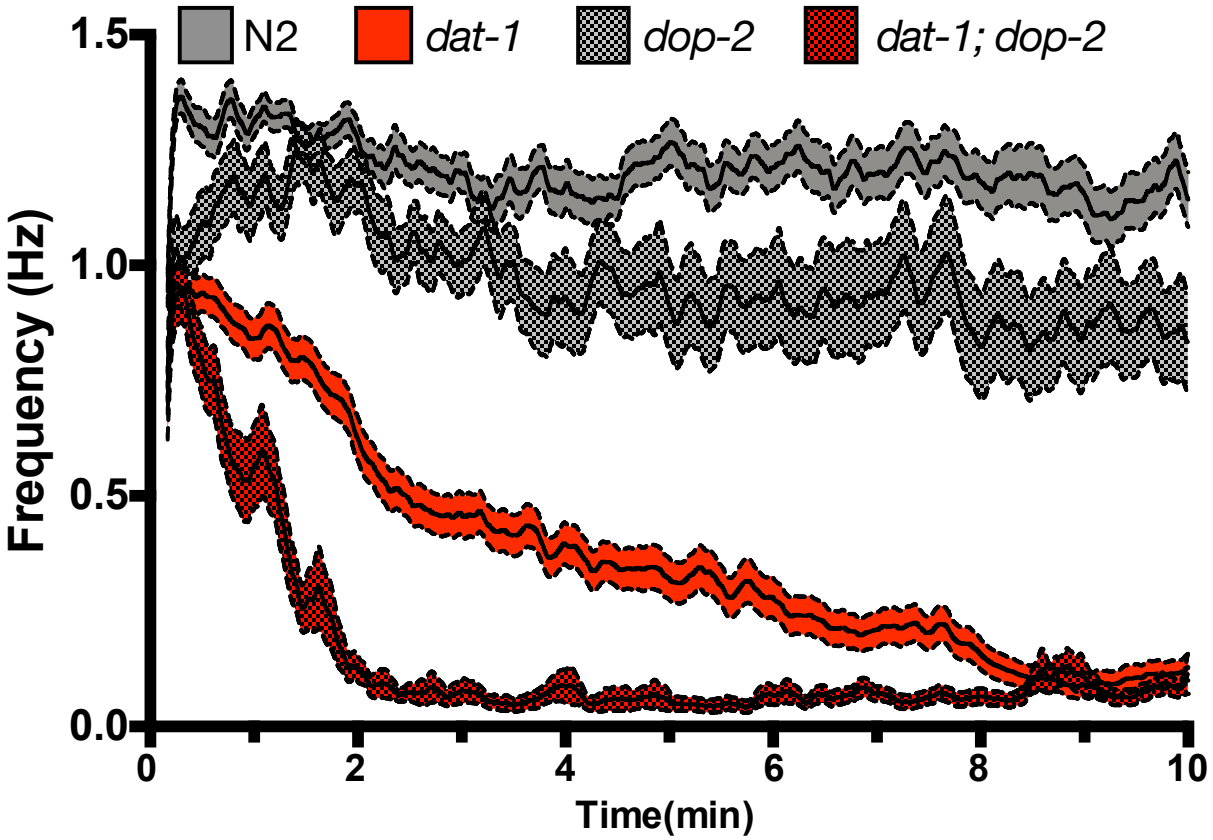

Figure 85 – Loss of *dop-2* triggers significant Swip and enhances the Swip in the *dat-1* strain. Single worm recordings were performed as described in the methods and videos were analyzed using SwimR. Data were analyzed by two way ANOVA with multiple Bonferroni post tests. *dop-2* was significantly reduced from N2 during point in minutes 1 and 4-10. *dat-1; dop-2* was significantly reduced from *dat-1* during points in minutes 1-6.

DISCUSSION

Reverse genetic approaches in multiple animal model systems have become an invaluable tool in understanding how genes contribute to complex behaviors. Unfortunately, genetic experiments using mouse and zebrafish models are require significant time and financial investment. Reverse genetic approaches using these models, therefore, are usually limited to understanding how one gene contributes to molecular, cellular, and behavioral phenotypes. Furthermore, gene expression changes associated with constitutive single gene mutations can help reveal candidate genetic network interactions for functional analysis. As multiple genes function within a cellular network to mediate complex behavioral phenotypes, we used the highly facile genetic system *Caenhorhabditis elegans* to identify genes that function within a DA neuron network to mediate a hyperdopaminergic phenotype known as Swip. We chose this phenotype as Swip is triggered by loss of single gene, *dat-1*, and is completely penetrant with nearly all of the animals with loss of *dat-1* demonstrating Swip.

To isolate candidates for analysis of the DA neuron Swip network, we performed RNAseq of wildtype and *dat-1* worms. As we have demonstrated that the *dat-1* strain demonstrates a phenotype associated with elevated extrasynaptic DA levels, we hypothesized that this strain may harbor transcriptional alterations in DA neuron enriched genes that might serve to normalize extrasynaptic DA levels. Following analysis of the RNAseq data and a comparison to a list of genes that are enriched in their DA neuron expression,

we identified a number of genes that were downregulated in the *dat-1* mutant. Most notable among these genes were several individual neuropeptide genes and the neuropeptide proprotein convertase *egl-3* (Kass, et al., 2001). Related work in the lab has demonstrated that *egl-3* is required for Swip in the *swip-10* mutant, but it is currently unknown if *egl-3*-mediated neuropeptide signaling is required for Swip in the *dat-1* mutant or other Swip-exhibiting mutants. Although these studies suggest that neuropeptide signaling in DA neurons may be a critical network contributor to Swip, neuropeptides like *nlp-12* are also known to function postsynaptically at the neuromuscular junction to mediate locomotion (Zhitao Hu, Pym, Babu, Murray, & Kaplan, 2011). Thus, future studies of *egl-3* and neuropeptides will need to distinguish between pre- and postsynaptic mechanism of DA effects. Amongst the set of downregulated genes, we identified a number that had already been characterized and with known expression in DA neurons. To understand how several presynaptic genes function in a network with *dat-1* to mediate Swip, we focused our genetic and behavioral analysis on three of them: *asic-1, trp-4*, and *dop-2*.

trp-4 was one of the first stretch-sensitive transient receptor potential (TRP) channels to be cloned and characterized in *C. elegans*. Li *et al*. found that a loss of *trp-4* led to more exaggerated body bends and an elevated worm centroid velocity (Li, et al., 2006). The former is mediated by its function in the DVA interneuron and the latter by its function in DA neurons. To determine if *trp-4* is required for stretch-mediated elevations in neuronal activity, they imaged changes in intracellular $Ca^{2=}$ in the DVA interneuron as a proxy for neural activity

via the fluorescent calcium sensor GCaMP. They found that mechanical bending of the worm was sufficient to evoke an increase in activity of the DVA interneuron and that *trp-4* was required for this effect. Kindt *et al*. further explored the physiological role of *trp-4* in DA neurons (Kindt, et al., 2007). The authors demonstrated that mechanical stimulation of DA neuron dendrites at the amphid sensilla was sufficient to evoke activity of DA neurons and that *trp-4* functions cell autonomously in DA neurons to mediate mechanical stretch-evoked changes in activity. In a technical tour *de force*, Kang *et al*. demonstrated that they could detect mechanoreceptive currents (MRCs) in DA neurons via whole cell patch clamp electrophysiology, that *trp-4* is required for MRCs, and that *trp-4* functions as a *bona fide* TRP channel to mediate changes in DA neuron physiology and during worm behavior (L. Kang, et al., 2010). As swimming produces exaggerated C-shaped body bends (Pierce-Shimomura, et al., 2008), we hypothesized that *trp-4* might mediate MRCs and elevated DA neuron excitability that promote the downstream release of vesicular DA. As we had already demonstrated that vesicular release of DA was required for *dat-1* Swip, we hypothesized that *trp-4* would be required for Swip.

asic-1 was cloned by Voglis *et al.* and demonstrated that it is required for dopamine and *dop-1* and *dop-2*-mediated associative learning in the worm (Voglis & Tavernarakis, 2008). They found that its expression is enriched at DA neuron synapses and that it functions to promote synaptic vesicle fusion and release of DA. Surprisingly, they did not observe that it was necessary for the dopamine-mediated BSR. As the *dat-1* Swip phenotype derives from elevated

extrasynaptic DA, we hypothesized that *asic-1*-mediated enhancement of vesicular release is required for *dat-1* Swip.

dop-2 was one of the first D2-like dopamine receptors to be cloned and its activity characterized (Suo, et al., 2003). The authors demonstrated that this receptor had a high affinity for dopamine relative to other biogenic amines and that its expression was enriched in the DA neurons. Surprisingly, to date, there has been no direct exploration of its functional role specifically in DA neurons. Genetic experiments of *dop-2* in behavioral conditioning led Voglis *et al*. to speculate that *dop-2* may function in a pathway with *asic-1* to **promote** synaptic velease release. Studies of somatodendritic D2 receptors in mice, however, have demonstrated that this receptor mediates hyperpolarization of DA neurons through activation of G-protein inwardly rectifying potassium (GIRK) channels (Beckstead, et al., 2004). Therefore, we hypothesized that *dop-2* may function to downregulate the release of DA in parallel with *dat-1* mediated DA clearance.

Our behavioral studies of *asic-1* and *trp-4* revealed that the *asic-1* strain exhibits normal swimming behavior and that loss of *trp-4* triggers a basal paralytic phenotype. More precise measurements of worm swimming frequency revealed that while loss of *asic-1* does not trigger paralysis, its loss reduces the average thrashing frequency. In these analyses, we confirmed that loss of *trp-4* does trigger a basal Swip phenotype as we had observed by hand. As the published work for *trp-4* suggests that its loss reduces DA signaling, we believe that the basal paralytic phenotype in the *trp-4* strain is not mediated by an

increase in DA. Cell specific restoration of *trp-4* in the DVA neuron and analysis of basal paralysis will be important to determine if this is indeed the case.

Our analysis of Swip in the *asic-1; dat-1* strain revealed that loss of *asic-1* significantly suppresses *dat-1* Swip and that its contribution is most easily revealed by a subtle increase in the osmolarity of the swimming media (Hardaway, et al., 2012). So while *asic-1* demonstrates a significant genetic interaction with the *dat-1* mutant, there exist redundant mechanisms to trigger Swip in the *dat-1* mutant. Similarly, our assays of the *trp-4; dat-1* mutant revealed that this strain revealed a surprising enhancement of Swip in the *dat-1* Swip phenotype which was revealed only at low osmolarity. Similar to the basal paralytic phenotype we observe in the *trp-4* mutant strain, we hypothesize that loss of *trp-4* alone only triggers additional paralysis through its function in a parallel pathway that may involve the activity of *trp-4* in the DVA neuron. To investigate whether *asic-1* and *trp-4* function redundantly to mediate *dat-1* Swip, we generated the *asic-1 trp-4* strain and crossed it to *dat-1*. Swip assays of the *asic-1 trp-4; dat-1* strain revealed that, though it does demonstrate significant Swip relative to the N2 strain, there is a highly significant suppression of Swip relative to *dat-1*. We therefore conclude that *asic-1* and *trp-4* can function redundantly to promote Swip in the *dat-1* strain, such that each of their individual contributions were only revealed when lost in combination. To determine if these ion channels contribute more broadly in all hyperdopaminergic strains, we crossed the *asic-1 trp-4* strain to another hyperdopaminergic strain, *swip-10*. Importantly, loss of *asic-1* and *trp-4* did not

mediate the same level of suppression as on the *dat-1*. As *asic-1 trp-4* did not completely restore *dat-1* Swip either, we hypothesize that there are additional pathway(s) that can promote either DA neuron excitation or vesicular release and these pathways may underlie Swip in other previously isolated Swip-harboring strains (Hardaway, et al., 2012).

To determine if *asic-1* and *trp-4* mediate these effects on *dat-1* Swip through their cell autonomous function in DA neurons, we transgenically restored these ion channels solely in DA neurons using the *asic-1 trp-4; dat-1* background. We found that DA neuron specific expression of either *asic-1* or *trp-4* could restore the penetrance of *dat-1* Swip. Using a previously validated pore dead version of *trp-4*, we determined that channel activity of *trp-4* is required to restore *dat-1* Swip. We conclude, therefore, that these ion channels function cell autonomously and redundantly in DA neurons to promote *dat-1* Swip. In the initial description of *asic-1*, the authors did not employ any techniques to measure *asic-1*'s contribution to excitability of DA neurons. Our studies suggest that *asic-1* may have a role in mediating depolarization of either the DA neuron cell bodies or through local excitation of the *dat-1* and *asic-1*-containing presynaptic terminals.

Our studies of *asic-1* and *trp-4* on *dat-1* Swip, suggested that these ion channels function redundantly, yet both perform vital functions to promote *dat-1* Swip. To understand if they function in more broad dopaminergic phenotypes, we assayed their requirement in the BSR. Consistent with published results, we determined that *trp-4* is required for BSR. Analysis of *asic-1* also revealed that it

is required for BSR. The difference between our studies and Voglis *et al.* is still unclear, but we speculate that there may be differences in our experimental protocol that are not mentioned in the published methods (Voglis & Tavernarakis, 2008).

To determine how *dop-2* functions within a *dat-1* network, we generated the *dat-1; dop-2* strains and tested it for Swip at low and intermediate osmolarities. The *dat-1; dop-2* strain demonstrated Swip with enhanced penetrance relative to the *dat-1* strain alone such that addition of 100 mM sucrose did not even generate significant suppression. As in the published *dat-1; vt29* strain, we conclude that *dop-2* functions in parallel to *dat-1* to promote Swip. Consistent with this model, we observed a significant basal Swip phenotype in strains with mutation of *dop-2* alone. DA neuron specific restoration of *dop-2* on the *dat-1; dop-2* background are necessary to determine if *dop-2* functions cell autonomously in DA neurons to suppress the penetrance of Swip in this strain. Nonetheless, our genetic experiments are consistent with a model whereby *dop-2* functions cell autonomously in DA neurons as a *bona fide* autoreceptor to inhibit 1) excitation of DA neuron cell bodies or presynaptic terminals, 2) activity of *cat-2* and biosynthesis of DA or 3) activity-coupled vesicular fusion of DA-containing vesicles.

We used the nematode *Caenhorhabditis* elegans to illustrate how a network of presynaptic genes in DA neurons interacts to coordinate the penetrance and kinetic profile of the hyperdopaminergic *dat-1* Swip phenotype. Our studies demonstrate that some of these genes, *asic-1* and *trp-4*, function

together and redundantly to promote Swip in the *dat-1* strain, whereas the dopamine autoreceptor, *dop-2*, functions in parallel to resist Swip.

FUTURE DIRECTIONS

The studies described above would likely benefit from replication of the RNA-seq experiment to validate the changes in gene expression that we observed. Independent replication of these findings might reveal new genes that were previously underappreciated and, more importantly, help filter out genes that are not independently replicated.

Our first RNAseq experiment indicated a high incidence of neuropeptide-related signaling genes. We have also observed that loss of *egl-3* fully restores Swip in another mutant, *swip-10*. These studies are consistent with a model whereby neuropeptides exert their influence somewhere within the Swip-generating neural circuitry. Future studies using pre- and post-synaptic related behavioral assays might reveal where in the circuit these neuropeptides are acting. Were we to determine that neuropeptides function upstream of the motor circuit to generate Swip, candidate based screening of *dat-1*-downregulated neuropeptides on the *dat-1* background using genetic or RNAi approaches may reveal which specific neuropeptides are critical for *dat-1* Swip.

In this study, we concentrated our efforts on understanding *trp-4*'s function in the DA neurons. To better understand how *trp-4* regulates the basal paralytic phenotype and Swip phenotype, we could restore *trp-4* in the DVA

neuron(via *twk-16* promoter) on the *trp-4* and *asic-1 trp-4; dat-1* backgrounds using the wildtype and pore dead versions.

Lastly, we observed a highly significant genetic interaction between *dat-1* and *dop-2*. To strengthen our model that *dop-2* functions presynaptically in DA neurons, we might use transgenic restoration of *dop-2* using DA neuron and non-DA neuron specific promoters on the *dat-1; dop-2* background and investigate how *dop-2* transgenic overexpression alters the penetrance and kinetic profile of Swip in this strain.

Appendix C

LIST OF EXPERIMENTS ATTEMPTED OR IN PROGRESS

General

1. *dat-1* Swip temporal window

2. Acute pharmacology on Swip – Haloperidol, Chlorpromazine, Olanzapine, AMPH, Nisoxetine (Bermingham)

3. Food Deprivation and Swip

4. Reagent subtractions and additions in plates: Effect on Swip (Whitaker)

swip-10 and other

5. Overexpression of dominant negative *glr-1(A/T)* in DA neurons

6. Swip with acute GLU in water (N2 and *cat-2*)

7. Rescue of *swip-10* with acute DNQX

8. Reversal Analysis of *swip-10*

9. Basal Swip characterization of putative xC^- homologs in worms

10. Swip with acute N-acetylcysteine treatment (N2 and *cat-2*)

11. Lines built and archived but not described here:

aqp-1; dat-1

aqp-2; dat-1

aqp-6; dat-1

aqp-7; dat-1

che-3; dat-1

ocr-2; dat-1

ocr-4; dat-1

ocr-4 ocr-2; dat-1

mod-5; dat-1

tph-1; dat-1

tbh-1; dat-1

12. Lines I attempted to build, but genetics didn't work:

osm-9; dat-1

dat-1; cat-1

DAT-1 C-Terminus

13. I made many C-terminal alanine substitutions in the p*dat-1*::GFP:*dat-1* cDNA expression vector to map out the residues required for function and trafficking. See Blakely Lab plasmid archive.

References

Alkema, Mark J, Hunter-Ensor, Melissa, Ringstad, Niels, & Horvitz, H Robert. (2005). Tyramine Functions independently of octopamine in the Caenorhabditis elegans nervous system. *Neuron, 46*(2), 247-260. doi: 10.1016/j.neuron.2005.02.024

Allen, Andrew T, Maher, Kathryn N, Wani, Khursheed A, Betts, Katherine E, & Chase, Daniel L. (2011). Coexpressed D1- and D2-Like Dopamine Receptors Antagonistically Modulate Acetylcholine Release in Caenorhabditis elegans. *Genetics, 188*(3), 579-590. doi: 10.1534/genetics.111.128512

Andén, N-E, Carlsson, A, Dahlström, A, Fuxe, K, Hillarp, N-Å, & Larsson, Ko. (1964). Demonstration and mapping out of nigro-neostriatal dopamine neurons. *Life sciences, 3*(6), 523-530.

Arenkiel, B. R., & Ehlers, M. D. (2009). Molecular genetics and imaging technologies for circuit-based neuroanatomy. [Research Support, N.I.H., Extramural
Research Support, Non-U.S. Gov't
Review]. *Nature, 461*(7266), 900-907. doi: 10.1038/nature08536

AXELROD, J. (1957). O-methylation of epinephrine and other catechols in vitro and in vivo. *Science, 126*(3270), 400-401.

Axelrod, Julius, & Laroche, Marie-Jeanne. (1959). Inhibitor of O-methylation of epinephrine and norepinephrine in vitro and in vivo. *Science, 130*(3378), 800-800.

Bacaj, Taulant, Tevlin, Maya, Lu, Yun, & Shaham, Shai. (2008). Glia are essential for sensory organ function in C. elegans. *Science, 322*(5902), 744-747. doi: 10.1126/science.1163074

Baker, David A, McFarland, Krista, Lake, Russell W, Shen, Hui, Tang, Xing-Chun, Toda, Shigenobu, & Kalivas, Peter W. (2003). Neuroadaptations in cystine-glutamate exchange underlie cocaine relapse. *Nat Neurosci, 6*(7), 743-749. doi: 10.1038/nn1069

Bamford, Nigel S, Zhang, Hui, Schmitz, Yvonne, Wu, Nan-Ping, Cepeda, Carlos, Levine, Michael S, . . . Sulzer, David. (2004). Heterosynaptic dopamine neurotransmission selects sets of corticostriatal terminals. *Neuron, 42*(4), 653-663.

Bebrone, C, Moali, C, Mahy, F, Rival, S, Docquier, J D, Rossolini, G M, . . . Galleni, M. (2001). CENTA as a Chromogenic Substrate for Studying -Lactamases. *Antimicrobial agents and chemotherapy, 45*(6), 1868-1871. doi: 10.1128/AAC.45.6.1868-1871.2001

Bebrone, Carine. (2007). Metallo- β -lactamases (classification, activity, genetic organization, structure, zinc coordination) and their superfamily. *Biochemical Pharmacology, 74*(12), 1686-1701. doi: 10.1016/j.bcp.2007.05.021

Beckstead, Michael J, Grandy, David K, Wickman, Kevin, & Williams, John T. (2004). Vesicular dopamine release elicits an inhibitory postsynaptic current in midbrain dopamine neurons. *Neuron, 42*(6), 939-946. doi: 10.1016/j.neuron.2004.05.019

Bellesi, Michele, & Conti, Fiorenzo. (2010). The mGluR2/3 Agonist LY379268 Blocks the Effects of GLT-1 Upregulation on Prepulse Inhibition of the Startle Reflex in Adult Rats. *Neuropsychopharmacology : official publication of the American College of Neuropsychopharmacology, 35*(6), 1253-1260. doi: 10.1038/npp.2009.225

Bello, E. P., Mateo, Y., Gelman, D. M., Noain, D., Shin, J. H., Low, M. J., . . . Rubinstein, M. (2011). Cocaine supersensitivity and enhanced motivation for reward in mice lacking dopamine D2 autoreceptors. [In Vitro
Research Support, N.I.H., Extramural
Research Support, N.I.H., Intramural
Research Support, Non-U.S. Gov't]. *Nature neuroscience, 14*(8), 1033-1038. doi: 10.1038/nn.2862

Benedetto, Alexandre, Au, Catherine, Avila, Daiana Silva, Milatovic, Dejan, & Aschner, Michael. (2010). Extracellular dopamine potentiates mn-induced oxidative stress, lifespan reduction, and dopaminergic neurodegeneration in a BLI-3-dependent manner in Caenorhabditis elegans. *PLoS Genet, 6*(8). doi: 10.1371/journal.pgen.1001084

Bennett, J P, Logan, W J, & Snyder, S H. (1972). Amino acid neurotransmitter candidates: sodium-dependent high-affinity uptake by unique synaptosomal fractions. *Science, 178*(4064), 997-999.

Bigelow, Henry, Doitsidou, Maria, Sarin, Sumeet, & Hobert, Oliver. (2009). MAQGene: software to facilitate C. elegans mutant genome sequence analysis. *Nat Meth, 6*(8), 549. doi: 10.1038/nmeth.f.260

Blakely, R D, Robinson, M B, & Amara, S G. (1988). Expression of neurotransmitter transport from rat brain mRNA in Xenopus laevis oocytes. *Proceedings of the National Academy of Sciences of the United States of America, 85*(24), 9846-9850.

Brenner, S. (1974). The genetics of Caenorhabditis elegans. *Genetics, 77*(1), 71-94.

Brockie, P J, Madsen, D M, Zheng, Y, Mellem, J, & Maricq, A V. (2001). Differential expression of glutamate receptor subunits in the nervous system of Caenorhabditis elegans and their regulation by the homeodomain protein UNC-42. *Journal of Neuroscience, 21*(5), 1510-1522.

Brockie, P J, Mellem, J E, Hills, T, Madsen, D M, & Maricq, A V. (2001). The C. elegans glutamate receptor subunit NMR-1 is required for slow NMDA-activated currents that regulate reversal frequency during locomotion. *Neuron, 31*(4), 617-630.

Brockie, P. J., & Maricq, A. V. (2006). Ionotropic glutamate receptors: genetics, behavior and electrophysiology. [Research Support, N.I.H., Extramural
Research Support, Non-U.S. Gov't
Research Support, U.S. Gov't, Non-P.H.S.
Review]. *WormBook : the online review of C. elegans biology*, 1-16. doi: 10.1895/wormbook.1.61.1

Brockie, Penelope J, & Maricq, Andres V. (2003). Ionotropic glutamate receptors in Caenorhabditis elegans. *Neurosignals, 12*(3), 108-125. doi: 10.1159/000072159

Brüss, M, Wieland, A, & Bönisch, H. (1999). Molecular cloning and functional expression of the mouse dopamine transporter. *J Neural Transm, 106*(7-8), 657-662.

Buckingham, Steven D, & Sattelle, David B. (2008). Strategies for automated analysis of C. elegans locomotion. *Invert Neurosci, 8*(3), 121-131. doi: 10.1007/s10158-008-0077-3

Bunney, B S, & Aghajanian, G K. (1976). The precise localization of nigral afferents in the rat as determined by a retrograde tracing technique. *Brain research, 117*(3), 423-435.

Bunzow, J R, Van Tol, H H, Grandy, D K, Albert, P, Salon, J, Christie, M, . . . Civelli, O. (1988). Cloning and expression of a rat D2 dopamine receptor cDNA. *Nature, 336*(6201), 783-787. doi: 10.1038/336783a0

Burt, D R, Enna, S J, Creese, I, & Snyder, S H. (1975). Dopamine receptor binding in the corpus striatum of mammalian brain. *Proceedings of the National Academy of Sciences of the United States of America, 72*(11), 4655-4659.

Caldwell, Guy A, & Caldwell, Kim A. (2008). Traversing a wormhole to combat Parkinson's disease. *Dis Model Mech, 1*(1), 32-36. doi: 10.1242/dmm.000257

Callebaut, Isabelle, Moshous, Despina, Mornon, Jean-Paul, & de Villartay, Jean-Pierre. (2002). Metallo-beta-lactamase fold within nucleic acids processing enzymes: the beta-CASP family. *Nucleic Acids Research, 30*(16), 3592-3601.

Cao, Songsong, Gelwix, Christopher C, Caldwell, Kim A, & Caldwell, Guy A. (2005). Torsin-mediated protection from cellular stress in the dopaminergic neurons of Caenorhabditis elegans. *J Neurosci, 25*(15), 3801-3812. doi: 10.1523/JNEUROSCI.5157-04.2005

Carlsson, A. (1959). Detection and assay of dopamine. *Pharmacological Reviews, 11*(2, Part 2), 300-304.

Carlsson, A, DAHLSTROEM, A, Fuxe, K, & LINDQVIST, M. (1965). HISTOCHEMICAL AND BIOCHEMICAL DETECTION OF MONOAMINE RELEASE FROM BRAIN NEURONS. *Life sciences, 4*, 809-816.

Carlsson, A, FALCK, B, Fuxe, K, & Hillarp, N-Å. (1964). CELLULAR LOCALIZATION OF MONOAMINES IN THE SPINAL CORD. *Acta physiologica Scandinavica, 60*, 112-119. doi: 10.1111/j.1748-1716.1964.tb02874.x

Carlsson, A, FALCK, B, Hillarp, N-Å, & TORP, A. (1962). Histochemical localization at the cellular level of hypothalamic noradrenaline. *Acta physiologica Scandinavica, 54*, 385-386. doi: 10.1111/j.1748-1716.1962.tb02364.x

Carlsson, A, LINDQVIST, M, MAGNUSSON, T, & WALDECK, B. (1958). On the presence of 3-hydroxytyramine in brain. *Science, 127*(3296), 471.

Carlsson, A. (1993). Thirty years of dopamine research. [Review]. *Advances in neurology, 60*, 1-10.

Carneiro, Ana M, Ingram, Susan L, Beaulieu, Jean-Martin, Sweeney, Ava, Amara, Susan G, Thomas, Sheila M, . . . Torres, Gonzalo E. (2002). The multiple LIM domain-containing adaptor protein Hic-5 synaptically colocalizes and interacts with the dopamine transporter. *J Neurosci, 22*(16), 7045-7054. doi: 20026740

Carvelli, Lucia, McDonald, Paul W, Blakely, Randy D, & DeFelice, Louis J. (2004). Dopamine transporters depolarize neurons by a channel mechanism. *Proc Natl Acad Sci USA, 101*(45), 16046-16051. doi: 10.1073/pnas.0403299101

Chalasani, Sreekanth H, Kato, Saul, Albrecht, Dirk R, Nakagawa, Takao, Abbott, L F, & Bargmann, Cornelia I. (2010). Neuropeptide feedback modifies odor-evoked dynamics in Caenorhabditis elegans olfactory neurons. *Nat Neurosci, 13*(5), 615-621. doi: 10.1038/nn.2526

Chalfie, M, Tu, Y, Euskirchen, G, Ward, W W, & Prasher, D C. (1994). Green fluorescent protein as a marker for gene expression. *Science, 263*(5148), 802-805.

Chase, Daniel L. (2007). Biogenic amine neurotransmitters in C. elegans. *WormBook*, 1-15. doi: 10.1895/wormbook.1.132.1

Chase, Daniel L, Pepper, Judy S, & Koelle, Michael R. (2004). Mechanism of extrasynaptic dopamine signaling in Caenorhabditis elegans. *Nat Neurosci, 7*(10), 1096-1103. doi: 10.1038/nn1316

Ciliax, B J, Heilman, C, Demchyshyn, L L, Pristupa, Z B, Ince, E, Hersch, S M, . . . Levey, A I. (1995). The dopamine transporter: immunochemical characterization and localization in brain. *J Neurosci, 15*(3 Pt 1), 1714-1723.

Clarke, Laura E, & Barres, Ben A. (2013). Emerging roles of astrocytes in neural circuit development. *Nature Reviews Neuroscience, 14*(5), 311-321. doi: 10.1038/nrn3484

Connor, John D. (1968). Caudate unit responses to nigral stimuli: evidence for a possible nigro-neostriatal pathway. *Science, 160*(3830), 899-900.

Connor, John D. (1970). Caudate nucleus neurones: correlation of the effects of substantia nigra stimulation with iontophoretic dopamine. *The Journal of physiology, 208*(3), 691.

Coyle, J T, & Snyder, S H. (1969a). Antiparkinsonian drugs: inhibition of dopamine uptake in the corpus striatum as a possible mechanism of action. [In Vitro]. *Science, 166*(3907), 899-901.

Coyle, J T, & Snyder, S H. (1969b). Catecholamine uptake by synaptosomes in homogenates of rat brain: stereospecificity in different areas. *The Journal of pharmacology and experimental therapeutics, 170*(2), 221-231.

Dahlström, Annica, & Fuxe, Kjell. (1964). A Method for the Demonstration of Monoamine‐Containing Nerve Fibres in the Central Nervous System. *Acta physiologica Scandinavica, 60*(3), 293-294.

Danjo, Rie, Kawasaki, Fumiko, & Ordway, Richard W. (2011). A Tripartite Synapse Model in Drosophila. *PLoS ONE, 6*(2), e17131. doi: 10.1371/journal.pone.0017131.s002

Davis, M Wayne, Hammarlund, Marc, Harrach, Tracey, Hullett, Patrick, Olsen, Shawn, & Jorgensen, Erik M. (2005). Rapid single nucleotide polymorphism mapping in C. elegans. *BMC Genomics, 6*, 118. doi: 10.1186/1471-2164-6-118

de Seny, Dominique, Prosperi-Meys, Christelle, Bebrone, Carine, Rossolini, Gian Maria, Page, Michael I, Noel, Philippe, . . . Galleni, Moreno. (2002). Mutational analysis of the two zinc-binding sites of the Bacillus cereus 569/H/9 metallo-beta-lactamase. *Biochem J, 363*(Pt 3), 687-696.

Deister, Christopher A, Teagarden, Mark A, Wilson, Charles J, & Paladini, Carlos A. (2009). An intrinsic neuronal oscillator underlies dopaminergic neuron bursting. *J Neurosci, 29*(50), 15888-15897. doi: 10.1523/JNEUROSCI.4053-09.2009

Dillon, J, Hopper, N A, Holden-Dye, L, & O'Connor, V. (2006). Molecular characterization of the metabotropic glutamate receptor family in Caenorhabditis elegans. *Biochem Soc Trans, 34*(Pt 5), 942-948. doi: 10.1042/BST0340942

Dominski, Zbigniew, Yang, Xiao-cui, & Marzluff, William F. (2005). The Polyadenylation Factor CPSF-73 Is Involved in Histone-Pre-mRNA Processing. *Cell, 123*(1), 37-48. doi: 10.1016/j.cell.2005.08.002

Duerr, J S, Frisby, D L, Gaskin, J, Duke, A, Asermely, K, Huddleston, D, . . . Rand, J. B. (1999). The cat-1 gene of Caenorhabditis elegans encodes a vesicular monoamine transporter required for specific monoamine-dependent behaviors. *J Neurosci, 19*(1), 72-84.

Egaña, Loreto A, Cuevas, Rolando A, Baust, Tracy B, Parra, Leonardo A, Leak, Rehana K, Hochendoner, Sarah, . . . Torres, Gonzalo E. (2009). Physical and functional interaction between the dopamine transporter and the synaptic vesicle protein synaptogyrin-3. *J Neurosci, 29*(14), 4592-4604. doi: 10.1523/JNEUROSCI.4559-08.2009

Erickson, J D, Eiden, L E, & Hoffman, B J. (1992). Expression cloning of a reserpine-sensitive vesicular monoamine transporter. *Proceedings of the National Academy of Sciences of the United States of America, 89*(22), 10993-10997.

Ewing, A G, Bigelow, J C, & Wightman, R M. (1983). Direct in vivo monitoring of dopamine released from two striatal compartments in the rat. *Science, 221*(4606), 169-171.

Fang-Yen, Christopher, Wyart, Matthieu, Xie, Julie, Kawai, Risa, Kodger, Tom, Chen, Sway, . . . Samuel, Aravinthan D T. (2010). Biomechanical analysis of gait adaptation in the nematode Caenorhabditis elegans. *Proc Natl Acad Sci USA, 107*(47), 20323-20328. doi: 10.1073/pnas.1003016107

Felton, Chaquettea M, & Johnson, Casonya M. (2011). Modulation of dopamine-dependent behaviors by the Caenorhabditis elegans Olig homolog HLH-17. *Journal of neuroscience research, 89*(10), 1627-1636. doi: 10.1002/jnr.22694

Flames, Nuria, & Hobert, Oliver. (2009). Gene regulatory logic of dopamine neuron differentiation. *Nature*, 1-6. doi: 10.1038/nature07929

Flibotte, Stephane, Edgley, Mark L, Chaudhry, Iasha, Taylor, Jon, Neil, Sarah E, Rogula, Aleksandra, . . . Moerman, Donald G. (2010). Whole-genome profiling of mutagenesis in Caenorhabditis elegans. *Genetics, 185*(2), 431-441. doi: 10.1534/genetics.110.116616

Freeman, Marc R, & Doherty, Johnna. (2006). Glial cell biology in Drosophila and vertebrates. *Trends in neurosciences, 29*(2), 82-90. doi: 10.1016/j.tins.2005.12.002

Gampe, Kristine, Hammer, Klaus, Kittel, Ágnes, & Zimmermann, Herbert. (2012). The medial habenula contains a specific nonstellate subtype of astrocyte expressing the ectonucleotidase NTPDase2. *Glia, 60*(12), 1860-1870. doi: 10.1002/glia.22402

Ghosh, R., & Emmons, S. W. (2008). Episodic swimming behavior in the nematode C. elegans. [Research Support, N.I.H., Extramural]. *The Journal of experimental biology, 211*(Pt 23), 3703-3711. doi: 10.1242/jeb.023606

Ghosh, R., & Emmons, S. W. (2010). Calcineurin and protein kinase G regulate C. elegans behavioral quiescence during locomotion in liquid. [Research Support, N.I.H., Extramural]. *BMC genetics, 11*, 7. doi: 10.1186/1471-2156-11-7

Giros, B, el Mestikawy, S, Godinot, N, Zheng, K, Han, H, Yang-Feng, T, & Caron, M G. (1992). Cloning, pharmacological characterization, and chromosome assignment of the human dopamine transporter. *Mol Pharmacol, 42*(3), 383-390.

Giros, B, Jaber, M, Jones, S R, Wightman, R M, & Caron, M G. (1996). Hyperlocomotion and indifference to cocaine and amphetamine in mice lacking the dopamine transporter. *Nature, 379*(6566), 606-612. doi: 10.1038/379606a0

Giros, B, Sokoloff, P, Martres, M P, Riou, J F, Emorine, L J, & Schwartz, J C. (1989). Alternative splicing directs the expression of two D2 dopamine receptor isoforms. *Nature, 342*(6252), 923-926. doi: 10.1038/342923a0

GOTO, Y, OTANI, S, & GRACE, A. (2007). The Yin and Yang of dopamine release: a new perspective. *Neuropharmacology, 53*(5), 583-587. doi: 10.1016/j.neuropharm.2007.07.007

Grosjean, Yael, Grillet, Micheline, Augustin, Hrvoje, Ferveur, Jean-François, & Featherstone, David E. (2007). A glial amino-acid transporter controls synapse strength and courtship in Drosophila. *Nature Neuroscience, 11*(1), 54-61. doi: 10.1038/nn2019

Haklai-Topper, Liat, Soutschek, Jürgen, Sabanay, Helena, Scheel, Jochen, Hobert, Oliver, & Peles, Elior. (2011). The neurexin superfamily of Caenorhabditis elegans. *Gene Expression Patterns, 11*(1-2), 144-150. doi: 10.1016/j.gep.2010.10.008

Hamamichi, Shusei, Rivas, Renee N, Knight, Adam L, Cao, Songsong, Caldwell, Kim A, & Caldwell, Guy A. (2008). Hypothesis-based RNAi screening identifies neuroprotective genes in a Parkinson's disease model. *Proc Natl Acad Sci USA, 105*(2), 728-733. doi: 10.1073/pnas.0711018105

Hardaway, J A, Hardie, S L, Whitaker, S M, Baas, Sarah, Zhang, Bing, Bermingham, Daniel P, . . . Blakely, Randy D. (2012). Forward Genetic Analysis to Identify Determinants of Dopamine Signaling in Caenorhabditis elegans Using Swimming-Induced Paralysis. *G3: Genes| Genomes| …*.

Hare, Emily E, & Loer, Curtis M. (2004). Function and evolution of the serotonin-synthetic bas-1 gene and other aromatic amino acid decarboxylase genes in Caenorhabditis. *BMC Evol Biol, 4*, 24. doi: 10.1186/1471-2148-4-24

Hasegawa, Sumitaka, Jackson, W Coyt, Tsien, Roger Y, & Rao, Jianghong. (2003). Imaging Tetrahymena ribozyme splicing activity in single live mammalian cells. *Proceedings of the National Academy of Sciences of the United States of America, 100*(25), 14892-14896. doi: 10.1073/pnas.2036553100

Haydon, P G. (2001). GLIA: listening and talking to the synapse. [Review]. *Nature Reviews Neuroscience, 2*(3), 185-193. doi: 10.1038/35058528

Herzog, E, Gilchrist, J, Gras, C, Muzerelle, A, Ravassard, P, Giros, B, . . . el Mestikawy, S. (2004). Localization of VGLUT3, the vesicular glutamate transporter type 3, in the rat brain. *Neuroscience, 123*(4), 983-1002. doi: 10.1016/j.neuroscience.2003.10.039

Herzog, Etienne, Takamori, Shigeo, Jahn, Reinhard, Brose, Nils, & Wojcik, Sonja M. (2006). Synaptic and vesicular co-localization of the glutamate transporters VGLUT1 and VGLUT2 in the mouse hippocampus. *Journal of Neurochemistry, 99*(3), 1011-1018. doi: 10.1111/j.1471-4159.2006.04144.x

Hills, Thomas, Brockie, Penelope J, & Maricq, Andres V. (2004). Dopamine and glutamate control area-restricted search behavior in Caenorhabditis elegans. *J Neurosci, 24*(5), 1217-1225. doi: 10.1523/JNEUROSCI.1569-03.2004

Hobert, Oliver. (2002). PCR fusion-based approach to create reporter gene constructs for expression analysis in transgenic C. elegans. *BioTechniques, 32*(4), 728-730.

Hodgkin, Jonathan. (2005). Introduction to genetics and genomics. *WormBook*, 1-3. doi: 10.1895/wormbook.1.17.1

Holden, P., & Horton, W. A. (2009). Crude subcellular fractionation of cultured mammalian cell lines. *BMC research notes, 2*, 243. doi: 10.1186/1756-0500-2-243

Hornykiewicz, Oleh. (1966). Dopamine (3-hydroxytyramine) and brain function. *Pharmacological Reviews, 18*(2), 925-964.

Horvitz, H R, Chalfie, M, Trent, C, Sulston, J E, & Evans, P D. (1982). Serotonin and octopamine in the nematode Caenorhabditis elegans. *Science, 216*(4549), 1012-1014.

Hu, Zhaoliang, Cooper, Margaret, Crockett, David P, & Zhou, Renping. (2004). Differentiation of the midbrain dopaminergic pathways during mouse development. *The Journal of comparative neurology, 476*(3), 301-311. doi: 10.1002/cne.20230

Hu, Zhitao, Pym, Edward C G, Babu, Kavita, Murray, Amy B Vashlishan, & Kaplan, Joshua M. (2011). A Neuropeptide-Mediated Stretch Response Links

Muscle Contraction to Changes in Neurotransmitter Release. *Neuron, 71*(1), 92-102. doi: 10.1016/j.neuron.2011.04.021

Hyman, S E, & Malenka, R C. (2001). Addiction and the brain: the neurobiology of compulsion and its persistence. *Nat Rev Neurosci, 2*(10), 695-703. doi: 10.1038/35094560

Hyman, Steven E, Malenka, Robert C, & Nestler, Eric J. (2006). Neural mechanisms of addiction: the role of reward-related learning and memory. [Review]. *Annual Review of Neuroscience, 29*, 565-598. doi: 10.1146/annurev.neuro.29.051605.113009

Iglewicz, Boris, & Hoaglin, David C. (1993). *How to detect and handle outliers*. Milwaukee, Wis.: ASQC Quality Press.

Ihrie, Rebecca A, Shah, Jugal K, Harwell, Corey C, Levine, Jacob H, Guinto, Cristina D, Lezameta, Melissa, . . . Álvarez-Buylla, Arturo. (2011). Persistent Sonic Hedgehog Signaling in Adult Brain Determines Neural Stem Cell Positional Identity. *Neuron, 71*(2), 250-262. doi: 10.1016/j.neuron.2011.05.018

Iwatsubo, Takeshi. (2007). Pathological biochemistry of alpha-synucleinopathy. *Neuropathology, 27*(5), 474-478.

Jayanthi, L D, Apparsundaram, S, Malone, M D, Ward, E, Miller, D M, Eppler, M, & Blakely, Randy D. (1998). The Caenorhabditis elegans gene T23G5.5 encodes an antidepressant- and cocaine-sensitive dopamine transporter. *Mol Pharmacol, 54*(4), 601-609.

Jin, Y, Jorgensen, E, Hartwieg, E, & Horvitz, H R. (1999). The Caenorhabditis elegans gene unc-25 encodes glutamic acid decarboxylase and is required for synaptic transmission but not synaptic development. *J Neurosci, 19*(2), 539-548.

Jonsson, G., Einarsson, P., Fuxe, K., & Hallman, H. (1975). Microspectrofluorimetric analysis of the formaldehyde induced fluorescence in midbrain raphe neurons. *Medical biology, 53*(1), 25-39.

Kalivas, Peter W. (2009). The glutamate homeostasis hypothesis of addiction. *Nat Rev Neurosci, 10*(8), 561-572. doi: 10.1038/nrn2515

Kang, Chanhee, & Avery, Leon. (2009). Systemic regulation of starvation response in Caenorhabditis elegans. *Genes & Development, 23*(1), 12-17. doi: 10.1101/gad.1723409

Kang, Lijun, Gao, Jingwei, Schafer, William R, Xie, Zhixiong, & Xu, X Z Shawn. (2010). C. elegans TRP Family Protein TRP-4 Is a Pore-Forming Subunit of a Native Mechanotransduction Channel. *Neuron, 67*(3), 381-391. doi: 10.1016/j.neuron.2010.06.032

Kass, J., Jacob, T. C., Kim, P., & Kaplan, J. M. (2001). The EGL-3 proprotein convertase regulates mechanosensory responses of Caenorhabditis elegans. [Research Support, Non-U.S. Gov't
Research Support, U.S. Gov't, P.H.S.]. *The Journal of neuroscience : the official journal of the Society for Neuroscience, 21*(23), 9265-9272.

Kilty, J. E., Lorang, D., & Amara, S. G. (1991). Cloning and expression of a cocaine-sensitive rat dopamine transporter. *Science, 254*(5031), 578-579.

Kindt, Katie S, Quast, Kathleen B, Giles, Andrew C, De, Subhajyoti, Hendrey, Dan, Nicastro, Ian, . . . Schafer, William R. (2007). Dopamine mediates context-dependent modulation of sensory plasticity in C. elegans. *Neuron, 55*(4), 662-676. doi: 10.1016/j.neuron.2007.07.023

KIRSHNER, N. (1962). Uptake of catecholamines by a particulate fraction of the adrenal medulla. *Science, 135*(3498), 107-108.

Kitahama, K, Geffard, M, Okamura, H, Nagatsu, I, Mons, N, & Jouvet, M. (1990). Dopamine- and dopa-immunoreactive neurons in the cat forebrain with reference to tyrosine hydroxylase-immunohistochemistry. *Brain research, 518*(1-2), 83-94.

Knackstedt, Lori A, Larowe, Steven, Mardikian, Pascale, Malcolm, Robert, Upadhyaya, Himanshu, Hedden, Sarra, . . . Kalivas, Peter W. (2009). The role of cystine-glutamate exchange in nicotine dependence in rats and humans. *Biol Psychiatry, 65*(10), 841-845. doi: 10.1016/j.biopsych.2008.10.040

Kopin, I J. (1985). Catecholamine metabolism: basic aspects and clinical significance. *Pharmacological Reviews, 37*(4), 333-364.

Kriegstein, Arnold, & Álvarez-Buylla, Arturo. (2009). The Glial Nature of Embryonic and Adult Neural Stem Cells. *Annual Review of Neuroscience, 32*(1), 149-184. doi: 10.1146/annurev.neuro.051508.135600

Kurian, Manju A, Li, Yan, Zhen, Juan, Meyer, Esther, Hai, Nebula, Christen, Hans-Jürgen, . . . Maher, Eamonn R. (2011). Clinical and molecular characterisation of hereditary dopamine transporter deficiency syndrome: an observational cohort and experimental study. *Lancet Neurol, 10*(1), 54-62. doi: 10.1016/S1474-4422(10)70269-6

Kurian, Manju A, Zhen, Juan, Cheng, Shu-Yuan, Li, Yan, Mordekar, Santosh R, Jardine, Philip, . . . Maher, Eamonn R. (2009). Homozygous loss-of-function mutations in the gene encoding the dopamine transporter are associated with infantile parkinsonism-dystonia. *J Clin Invest, 119*(6), 1595-1603. doi: 10.1172/JCI39060

Kuwahara, Tomoki, Koyama, Akihiko, Gengyo-Ando, Keiko, Masuda, Mayumi, Kowa, Hisatomo, Tsunoda, Makoto, . . . Iwatsubo, Takeshi. (2006). Familial Parkinson mutant alpha-synuclein causes dopamine neuron dysfunction in transgenic Caenorhabditis elegans. *J Biol Chem, 281*(1), 334-340. doi: 10.1074/jbc.M504860200

Lakso, Merja, Vartiainen, Suvi, Moilanen, Anu-Maarit, Sirviö, Jouni, Thomas, James H, Nass, Richard, . . . Wong, Garry. (2003). Dopaminergic neuronal loss and motor deficits in Caenorhabditis elegans overexpressing human alpha-synuclein. *J Neurochem, 86*(1), 165-172.

Lee, F J, Liu, F, Pristupa, Z B, & Niznik, H B. (2001). Direct binding and functional coupling of alpha-synuclein to the dopamine transporters accelerate dopamine-induced apoptosis. *FASEB J, 15*(6), 916-926.

Lee, Frank J S, Pei, Lin, Moszczynska, Anna, Vukusic, Brian, Fletcher, Paul J, & Liu, Fang. (2007). Dopamine transporter cell surface localization facilitated by a direct interaction with the dopamine D2 receptor. *EMBO J, 26*(8), 2127-2136. doi: 10.1038/sj.emboj.7601656

Lee, Ki-Hwan, Kim, Mi-Young, Kim, Dong-Hwan, & Lee, Yong-Sung. (2004). Syntaxin 1A and receptor for activated C kinase interact with the N-terminal region of human dopamine transporter. *Neurochem Res, 29*(7), 1405-1409.

Lee, R. Y., Sawin, E. R., Chalfie, M., Horvitz, H. R., & Avery, L. (1999). EAT-4, a homolog of a mammalian sodium-dependent inorganic phosphate cotransporter, is necessary for glutamatergic neurotransmission in caenorhabditis elegans. [Research Support, U.S. Gov't, P.H.S.]. *The Journal of neuroscience : the official journal of the Society for Neuroscience, 19*(1), 159-167.

Lemke, G. (2001). Glial control of neuronal development. [Review]. *Annual Review of Neuroscience, 24*, 87-105. doi: 10.1146/annurev.neuro.24.1.87

Leung, T C H, Lui, C N P, Chen, L W, Yung, W H, Chan, Y S, & Yung, K K L. (2011). Ceftriaxone Ameliorates Motor Deficits and Protects Dopaminergic Neurons in 6-Hydroxydopamine-Lesioned Rats. *ACS Chemical Neuroscience*, 111104091220006. doi: 10.1021/cn200072h

Li, Wei, Feng, Zhaoyang, Sternberg, Paul W, & Xu, X Z Shawn. (2006). A C. elegans stretch receptor neuron revealed by a mechanosensitive TRP channel homologue. *Nature, 440*(7084), 684-687. doi: 10.1038/nature04538

Lints, R, & Emmons, S. (1999). … dopaminergic neurotransmitter identity among Caenorhabditis elegans ray sensory neurons …. *Development*.

Lints, R., & Emmons, S. W. (1999). Patterning of dopaminergic neurotransmitter identity among Caenorhabditis elegans ray sensory neurons by a TGFbeta family signaling pathway and a Hox gene. [Research Support, U.S. Gov't, P.H.S.]. *Development, 126*(24), 5819-5831.

Lipski, J, Wan, C K, Bai, J Z, Pi, R, Li, D, & Donnelly, D. (2007). Neuroprotective potential of ceftriaxone in in vitro models of stroke. *Neuroscience, 146*(2), 617-629. doi: 10.1016/j.neuroscience.2007.02.003

Liu, Y, & Edwards, R H. (1997). The role of vesicular transport proteins in synaptic transmission and neural degeneration. [Review]. *Annual Review of Neuroscience, 20*, 125-156. doi: 10.1146/annurev.neuro.20.1.125

Liu, Y, Peter, D, Roghani, A, Schuldiner, S, Privé, G G, Eisenberg, D, . . . Edwards, R H. (1992). A cDNA that suppresses MPP+ toxicity encodes a vesicular amine transporter. *Cell, 70*(4), 539-551.

Loer, C M, & Kenyon, C J. (1993). Serotonin-deficient mutants and male mating behavior in the nematode Caenorhabditis elegans. *J Neurosci, 13*(12), 5407-5417.

Logan, W J, & Snyder, S H. (1971). Unique high affinity uptake systems for glycine, glutamic and aspartic acids in central nervous tissue of the rat. *Nature, 234*(5327), 297-299.

Ma, Yunmei, Pannicke, Ulrich, Schwarz, Klaus, & Lieber, Michael R. (2002). Hairpin opening and overhang processing by an Artemis/DNA-dependent protein kinase complex in nonhomologous end joining and V(D)J recombination. *Cell, 108*(6), 781-794.

Mandel, Corey R, Kaneko, Syuzo, Zhang, Hailong, Gebauer, Damara, Vethantham, Vasupradha, Manley, James L, & Tong, Liang. (2006). Polyadenylation factor CPSF-73 is the pre-mRNA 3'-end-processing endonuclease. *Nature, 444*(7121), 953-956. doi: 10.1038/nature05363

Mano, Itzhak, Straud, Sarah, & Driscoll, Monica. (2007). Caenorhabditis elegans glutamate transporters influence synaptic function and behavior at sites distant from the synapse. *J Biol Chem, 282*(47), 34412-34419. doi: 10.1074/jbc.M704134200

Marvin, Jonathan S, Borghuis, Bart G, Tian, Lin, Cichon, Joseph, Harnett, Mark T, Akerboom, Jasper, . . . Looger, Loren L. (2013). An optimized fluorescent probe for visualizing glutamate neurotransmission. *Nature Methods, 10*(2), 162-170. doi: 10.1038/nmeth.2333

Matthies, Dawn Signor, Fleming, Paul A, Wilkes, Don M, & Blakely, Randy D. (2006). The Caenorhabditis elegans choline transporter CHO-1 sustains acetylcholine synthesis and motor function in an activity-dependent manner. *J Neurosci, 26*(23), 6200-6212. doi: 10.1523/JNEUROSCI.5036-05.2006

Mazei-Robison, M. S, Bowton, E, Holy, M, Schmudermaier, M, Freissmuth, M, Sitte, H. H, . . . Blakely, Randy D. (2008). Anomalous Dopamine Release Associated with a Human Dopamine Transporter Coding Variant. *J Neurosci, 28*(28), 7040-7046. doi: 10.1523/JNEUROSCI.0473-08.2008

Mazei-Robison, Michelle S, Couch, R Steven, Shelton, Richard C, Stein, Mark A, & Blakely, Randy D. (2005). Sequence variation in the human dopamine transporter gene in children with attention deficit hyperactivity disorder. *Neuropharmacology, 49*(6), 724-736. doi: 10.1016/j.neuropharm.2005.08.003

McDonald, P. W, Hardie, S. L, Jessen, Tammy, Carvelli, Lucia, Matthies, D. S, & Blakely, Randy D. (2007). Vigorous Motor Activity in Caenorhabditis elegans Requires Efficient Clearance of Dopamine Mediated by Synaptic Localization of the Dopamine Transporter DAT-1. *J Neurosci, 27*(51), 14216-14227. doi: 10.1523/JNEUROSCI.2992-07.2007

McDonald, Paul W, Jessen, Tammy, Field, Julie R, & Blakely, Randy D. (2006). Dopamine Signaling Architecture in Caenorhabditis elegans. *Cell Mol Neurobiol, 26*(4-6), 591-616. doi: 10.1007/s10571-006-9003-6

Mellem, Jerry E, Brockie, Penelope J, Zheng, Yi, Madsen, David M, & Maricq, Andres V. (2002). Decoding of polymodal sensory stimuli by postsynaptic glutamate receptors in C. elegans. *Neuron, 36*(5), 933-944.

Mineur, Yann S, Picciotto, Marina R, & Sanacora, Gerard. (2007). Antidepressant-Like Effects of Ceftriaxone in Male C57BL/6J Mice. *Biological psychiatry, 61*(2), 250-252. doi: 10.1016/j.biopsych.2006.04.037

Mohn, Amy R, Yao, Wei-Dong, & Caron, Marc G. (2004). Genetic and genomic approaches to reward and addiction. *Neuropharmacology, 47 Suppl 1*, 101-110. doi: 10.1016/j.neuropharm.2004.07.025

Monsma, F J, McVittie, L D, Gerfen, C R, Mahan, L C, & Sibley, D R. (1989). Multiple D2 dopamine receptors produced by alternative RNA splicing. *Nature, 342*(6252), 926-929. doi: 10.1038/342926a0

Mortazavi, A., Williams, B. A., McCue, K., Schaeffer, L., & Wold, B. (2008). Mapping and quantifying mammalian transcriptomes by RNA-Seq. [Research Support, N.I.H., Extramural
Research Support, Non-U.S. Gov't]. *Nature Methods, 5*(7), 621-628. doi: 10.1038/nmeth.1226

Moshous, D, Callebaut, I, de Chasseval, R, Corneo, B, Cavazzana-Calvo, M, Le Deist, F, . . . de Villartay, J P. (2001). Artemis, a novel DNA double-strand break

repair/V(D)J recombination protein, is mutated in human severe combined immune deficiency. *Cell, 105*(2), 177-186.

Moussawi, Khaled, Pacchioni, Alejandra, Moran, Megan, Olive, M Foster, Gass, Justin T, Lavin, Antonieta, & Kalivas, Peter W. (2009). N-Acetylcysteine reverses cocaine-induced metaplasticity. *Nat Neurosci, 12*(2), 182-189. doi: 10.1038/nn.2250

Moussawi, Khaled, Zhou, Wenhua, Shen, Haowei, Reichel, Carmela M, See, Ronald E, Carr, David B, & Kalivas, Peter W. (2011). Reversing cocaine-induced synaptic potentiation provides enduring protection from relapse. *Proc Natl Acad Sci USA, 108*(1), 385-390. doi: 10.1073/pnas.1011265108

NAGATSU, T. (1991). Genes for human catecholamine-synthesizing enzymes. [Comparative Study]. *Neuroscience Research, 12*(2), 315-345.

NAGATSU, T, LEVITT, M, & UDENFRIEND, S. (1964). TYROSINE HYDROXYLASE. THE INITIAL STEP IN NOREPINEPHRINE BIOSYNTHESIS. *The Journal of biological chemistry, 239*, 2910-2917.

Nass, R, & Blakely, R. (2003). T HE C AENORHABDITIS ELEGANS D OPAMINERGIC S YSTEM: Opportunities for Insights …. *Annu. Rev. Pharmacol. Toxicol.*

Nass, Richard, Hahn, Maureen K, Jessen, Tammy, McDonald, Paul W, Carvelli, Lucia, & Blakely, Randy D. (2005). A genetic screen in Caenorhabditis elegans for dopamine neuron insensitivity to 6-hydroxydopamine identifies dopamine transporter mutants impacting transporter biosynthesis and trafficking. *J Neurochem, 94*(3), 774-785. doi: 10.1111/j.1471-4159.2005.03205.x

Nass, Richard, Hall, David H, Miller, David M, & Blakely, Randy D. (2002). Neurotoxin-induced degeneration of dopamine neurons in Caenorhabditis elegans. *Proc Natl Acad Sci USA, 99*(5), 3264-3269. doi: 10.1073/pnas.042497999

Nave, Klaus-Armin, & Trapp, Bruce D. (2008). Axon-glial signaling and the glial support of axon function. *Annu Rev Neurosci, 31*, 535-561. doi: 10.1146/annurev.neuro.30.051606.094309

Ng, K Y, Chase, T N, Colburn, R W, & Kopin, I J. (1971). Dopamine: stimulation-induced release from central neurons. [In Vitro]. *Science, 172*(3982), 487-489.

Nirenberg, M J, Liu, Y, Peter, D, Edwards, R H, & Pickel, V M. (1995). The vesicular monoamine transporter 2 is present in small synaptic vesicles and preferentially localizes to large dense core vesicles in rat solitary tract nuclei. *Proceedings of the National Academy of Sciences of the United States of America, 92*(19), 8773-8777.

O'Callaghan, C H, Morris, A, Kirby, S M, & Shingler, A H. (1972). Novel method for detection of beta-lactamases by using a chromogenic cephalosporin substrate. *Antimicrobial agents and chemotherapy, 1*(4), 283-288.

Oikonomou, Grigorios, & Shaham, Shai. (2010). The Glia of Caenorhabditis elegans. *Glia, 59*(9), 1253-1263. doi: 10.1002/glia.21084

Osakada, Fumitaka, Mori, Takuma, Cetin, Ali H, Marshel, James H, Virgen, Beatriz, & Callaway, Edward M. (2011). New Rabies Virus Variants for Monitoring and Manipulating Activity and Gene Expression in Defined Neural Circuits. *Neuron, 71*(4), 617-631. doi: 10.1016/j.neuron.2011.07.005

Paladini, Carlos A, Robinson, Siobhan, Morikawa, Hitoshi, Williams, John T, & Palmiter, Richard D. (2003). Dopamine controls the firing pattern of dopamine neurons via a network feedback mechanism. *Proc Natl Acad Sci USA, 100*(5), 2866-2871. doi: 10.1073/pnas.0138018100

Peter, D, Liu, Y, Sternini, C, de Giorgio, R, Brecha, N, & Edwards, R H. (1995). Differential expression of two vesicular monoamine transporters. *The Journal of neuroscience : the official journal of the Society for Neuroscience, 15*(9), 6179-6188.

Phillipson, O T. (1979). Afferent projections to the ventral tegmental area of Tsai and interfascicular nucleus: a horseradish peroxidase study in the rat. *The Journal of comparative neurology, 187*(1), 117-143. doi: 10.1002/cne.901870108

Pierce-Shimomura, Jonathan T, Chen, Beth L, Mun, James J, Ho, Raymond, Sarkis, Raman, & McIntire, Steven L. (2008). Genetic analysis of crawling and swimming locomotory patterns in C. elegans. *Proc Natl Acad Sci USA, 105*(52), 20982-20987. doi: 10.1073/pnas.0810359105

Piggott, Beverly J, Liu, Jie, Feng, Zhaoyang, Wescott, Seth A, & Xu, X Z Shawn. (2011). The Neural Circuits and Synaptic Mechanisms Underlying Motor Initiation in C. elegans. *Cell, 147*(4), 922-933. doi: 10.1016/j.cell.2011.08.053

Plotsky, P M, Wightman, R M, Chey, W, & Adams, R N. (1977). Liquid chromatographic analysis of endogenous catecholamine release from brain slices. [In Vitro]. *Science, 197*(4306), 904-906.

Portig, P J, Sharman, D F, & Vogt, M. (1968). Release by tubocurarine of dopamine and homovanillic acid from the superfused caudate nucleus. *The Journal of physiology, 194*(2), 565-572.

Portig, P J, & Vogt, Marthe. (1969). Release into the cerebral ventricles of substances with possible transmitter function in the caudate nucleus. *The Journal of physiology, 204*(3), 687-715.

Purves, Dale. (2008). *Neuroscience* (4th ed.). Sunderland, Mass.: Sinauer.

Qin, C, & Luo, M. (2009). Neurochemical phenotypes of the afferent and efferent projections of the mouse medial habenula. *Neuroscience, 161*(3), 827-837. doi: 10.1016/j.neuroscience.2009.03.085

Rasmussen, Bruce, Unterwald, Ellen M, & Rawls, Scott M. (2011). Glutamate transporter subtype 1 (GLT-1) activator ceftriaxone attenuates amphetamine-induced hyperactivity and behavioral sensitization in rats. *Drug and Alcohol Dependence, 118*(2-3), 484-488. doi: 10.1016/j.drugalcdep.2011.03.022

Roeper, Jochen. (2013). Dissecting the diversity of midbrain dopamine neurons. *Trends in neurosciences, 36*(6), 336-342. doi: 10.1016/j.tins.2013.03.003

Rothstein, J D, Dykes-Hoberg, M, Pardo, C A, Bristol, L A, Jin, L, Kuncl, R W, . . . Welty, D F. (1996). Knockout of glutamate transporters reveals a major role for astroglial transport in excitotoxicity and clearance of glutamate. *Neuron, 16*(3), 675-686.

Rothstein, J D, Martin, L J, & Kuncl, R W. (1992). Decreased glutamate transport by the brain and spinal cord in amyotrophic lateral sclerosis. [In Vitro]. *The New England journal of medicine, 326*(22), 1464-1468. doi: 10.1056/NEJM199205283262204

Rothstein, Jeffrey D, Jin, Lin, Dykes Hoberg, Margaret, & Kuncl, Ralph W. (1993). Chronic inhibition of glutamate uptake produces a model of slow neurotoxicity. *Proceedings of the National Academy of Sciences of the United States of America, 90*(14), 6591-6595.

Rothstein, Jeffrey D, Patel, Sarjubhai, Regan, Melissa R, Haenggeli, Christine, Huang, Yanhua H, Bergles, Dwight E, . . . Fisher, Paul B. (2005). Beta-lactam antibiotics offer neuroprotection by increasing glutamate transporter expression. *Nature, 433*(7021), 73-77. doi: 10.1038/nature03180

Rutledge, Charles O, & Jonason, Jan. (1967). Metabolic pathways of dopamine and norepinephrine in rabbit brain in vitro. *Journal of Pharmacology and Experimental Therapeutics, 157*(3), 493-502.

RYAN, K. (2004). Evidence that polyadenylation factor CPSF-73 is the mRNA 3' processing endonuclease. *RNA, 10*(4), 565-573. doi: 10.1261/rna.5214404

Salahpour, Ali, Ramsey, Amy J, Medvedev, Ivan O, Kile, Brian, Sotnikova, Tatyana D, Holmstrand, Ericka, . . . Caron, Marc G. (2008). Increased amphetamine-induced hyperactivity and reward in mice overexpressing the dopamine transporter. *Proc Natl Acad Sci USA, 105*(11), 4405-4410. doi: 10.1073/pnas.0707646105

Sari, Youssef, Smith, Kathryn D, Ali, Pir K, & Rebec, George V. (2009). Upregulation of GLT1 attenuates cue-induced reinstatement of cocaine-seeking behavior in rats. *Journal of Neuroscience, 29*(29), 9239-9243. doi: 10.1523/JNEUROSCI.1746-09.2009

Sarin, Sumeet, Prabhu, Snehit, O'meara, M Maggie, Pe'er, Itsik, & Hobert, Oliver. (2008). Caenorhabditis elegans mutant allele identification by whole-genome sequencing. *Nature Methods, 5*(10), 865-867. doi: 10.1038/nmeth.1249

Sawin, E R, Ranganathan, R, & Horvitz, H Robert. (2000). C. elegans locomotory rate is modulated by the environment through a dopaminergic pathway and by experience through a serotonergic pathway. *Neuron, 26*(3), 619-631.

Schafer, William R, & Kenyon, C J. (1995). A calcium-channel homologue required for adaptation to dopamine and serotonin in Caenorhabditis elegans. *Nature, 375*(6526), 73-78. doi: 10.1038/375073a0

Schmitt, Kyle C, & Reith, Maarten E A. (2010). Regulation of the dopamine transporter: aspects relevant to psychostimulant drugs of abuse. *Annals of the New York Academy of Sciences, 1187*, 316-340. doi: 10.1111/j.1749-6632.2009.05148.x

Schmitz, Y., Schmauss, C., & Sulzer, D. (2002). Altered dopamine release and uptake kinetics in mice lacking D2 receptors. [In Vitro
Research Support, Non-U.S. Gov't
Research Support, U.S. Gov't, Non-P.H.S.
Research Support, U.S. Gov't, P.H.S.]. *The Journal of neuroscience : the official journal of the Society for Neuroscience, 22*(18), 8002-8009.

Seeman, P, Chau-Wong, M, Tedesco, J, & Wong, K. (1975). Brain receptors for antipsychotic drugs and dopamine: direct binding assays. *Proceedings of the National Academy of Sciences of the United States of America, 72*(11), 4376-4380.

Seeman, P, Chau-Wong, M, Tedesco, J, & Wong, K. (1976). Dopamine receptors in human and calf brains, using [3H] apomorphine and an antipsychotic drug. *Proceedings of the National Academy of Sciences of the United States of America, 73*(12), 4354-4358.

Seeman, P. (2010). Dopamine D2 receptors as treatment targets in schizophrenia. [Comparative Study
Review]. *Clinical schizophrenia & related psychoses, 4*(1), 56-73. doi: 10.3371/CSRP.4.1.5

Seifert, Gerald, Schilling, Karl, & Steinhäuser, Christian. (2006). Astrocyte dysfunction in neurological disorders: a molecular perspective. *Nature Reviews Neuroscience, 7*(3), 194-206. doi: 10.1038/nrn1870

Seri, Bettina, Garc a-Verdugo, Jos Manuel, Collado-Morente, Lucia, McEwen, Bruce S, & Álvarez-Buylla, Arturo. (2004). Cell types, lineage, and architecture of the germinal zone in the adult dentate gyrus. *The Journal of comparative neurology, 478*(4), 359-378. doi: 10.1002/cne.20288

Shimada, S, Kitayama, S, Lin, C L, Patel, A, Nanthakumar, E, Gregor, P, . . . Uhl, G. (1991). Cloning and expression of a cocaine-sensitive dopamine transporter complementary DNA. *Science, 254*(5031), 576-578.

Smith, Cody J, Watson, Joseph D, Spencer, W Clay, O'brien, Tim, Cha, Byeong, Albeg, Adi, . . . Miller, David M. (2010). Time-lapse imaging and cell-specific expression profiling reveal dynamic branching and molecular determinants of a multi-dendritic nociceptor in C. elegans. *Developmental biology, 345*(1), 18-33. doi: 10.1016/j.ydbio.2010.05.502

Sokoloff, P, Giros, B, Martres, M P, Bouthenet, M L, & Schwartz, J C. (1990). Molecular cloning and characterization of a novel dopamine receptor (D3) as a target for neuroleptics. [Comparative Study]. *Nature, 347*(6289), 146-151. doi: 10.1038/347146a0

Sondheimer, Ilan, & Knackstedt, Lori A. (2011). Ceftriaxone prevents the induction of cocaine sensitization and produces enduring attenuation of cue- and cocaine-primed reinstatement of cocaine-seeking. *Behavioural Brain Research, 225*(1), 252-258. doi: 10.1016/j.bbr.2011.07.041

Spencer, W Clay, Zeller, Georg, Watson, Joseph D, Henz, Stefan R, Watkins, Kathie L, McWhirter, Rebecca D, . . . Miller, David M. (2011). A spatial and temporal map of C. elegans gene expression. *Genome Research, 21*(2), 325-341. doi: 10.1101/gr.114595.110

Stacey, S M, Muraro, N I, Peco, E, Labbe, A, Thomas, G B, Baines, R A, & van Meyel, D J. (2010). Drosophila Glial Glutamate Transporter Eaat1 Is Regulated by Fringe-Mediated Notch Signaling and Is Essential for Larval Locomotion. *Journal of Neuroscience, 30*(43), 14446-14457. doi: 10.1523/JNEUROSCI.1021-10.2010

Sugiura, Mai, Fuke, Satoshi, Suo, Satoshi, Sasagawa, Noboru, Van Tol, Hubert H M, & Ishiura, Shoichi. (2005). Characterization of a novel D2-like dopamine receptor with a truncated splice variant and a D1-like dopamine receptor unique to invertebrates from Caenorhabditis elegans. *J Neurochem, 94*(4), 1146-1157. doi: 10.1111/j.1471-4159.2005.03268.x

Sulston, J, Dew, M, & Brenner, S. (1975). Dopaminergic neurons in the nematode Caenorhabditis elegans. *J Comp Neurol, 163*(2), 215-226. doi: 10.1002/cne.901630207

Sunahara, R K, Guan, H C, O'Dowd, B F, Seeman, P, Laurier, L G, Ng, G, . . . Niznik, H B. (1991). Cloning of the gene for a human dopamine D5 receptor with higher affinity for dopamine than D1. [Comparative Study]. *Nature, 350*(6319), 614-619. doi: 10.1038/350614a0

Sunahara, R K, Niznik, H B, Weiner, D M, Stormann, T M, Brann, M R, Kennedy, J L, . . . Israel, Y. (1990). Human dopamine D1 receptor encoded by an intronless gene on chromosome 5. *Nature, 347*(6288), 80-83. doi: 10.1038/347080a0

Suo, Satoshi, Ishiura, Shoichi, & Van Tol, Hubert H M. (2004). Dopamine receptors in C. elegans. *Eur J Pharmacol, 500*(1-3), 159-166. doi: 10.1016/j.ejphar.2004.07.021

Suo, Satoshi, Sasagawa, Noboru, & Ishiura, Shoichi. (2002). Identification of a dopamine receptor from Caenorhabditis elegans. *Neuroscience letters, 319*(1), 13-16.

Suo, Satoshi, Sasagawa, Noboru, & Ishiura, Shoichi. (2003). Cloning and characterization of a Caenorhabditis elegans D2-like dopamine receptor. *J Neurochem, 86*(4), 869-878.

Torres, Gonzalo E, Gainetdinov, Raul R, & Caron, Marc G. (2003). Plasma membrane monoamine transporters: structure, regulation and function. *Nat Rev Neurosci, 4*(1), 13-25. doi: 10.1038/nrn1008

Torres, Gonzalo E, Yao, W D, Mohn, A R, Quan, H, Kim, K M, Levey, A I, . . . Caron, Marc G. (2001). Functional interaction between monoamine plasma membrane transporters and the synaptic PDZ domain-containing protein PICK1. *Neuron, 30*(1), 121-134.

Trantham-Davidson, H, LaLumiere, R T, Reissner, K J, Kalivas, P W, & Knackstedt, L A. (2012). Ceftriaxone Normalizes Nucleus Accumbens Synaptic Transmission, Glutamate Transport, and Export following Cocaine Self-Administration and Extinction Training. *Journal of Neuroscience, 32*(36), 12406-12410. doi: 10.1523/JNEUROSCI.1976-12.2012

Usiello, A., Baik, J. H., Rouge-Pont, F., Picetti, R., Dierich, A., LeMeur, M., . . . Borrelli, E. (2000). Distinct functions of the two isoforms of dopamine D2

receptors. [Research Support, Non-U.S. Gov't]. *Nature, 408*(6809), 199-203. doi: 10.1038/35041572

Van Tol, H H, Bunzow, J R, Guan, H C, Sunahara, R K, Seeman, P, Niznik, H B, & Civelli, O. (1991). Cloning of the gene for a human dopamine D4 receptor with high affinity for the antipsychotic clozapine. [Comparative Study]. *Nature, 350*(6319), 610-614. doi: 10.1038/350610a0

Vidal-Gadea, Andrés, Topper, Stephen, Young, Layla, Crisp, Ashley, Kressin, Leah, Elbel, Erin, . . . Pierce-Shimomura, Jonathan T. (2011). Caenorhabditis elegans selects distinct crawling and swimming gaits via dopamine and serotonin. *Proc Natl Acad Sci USA*. doi: 10.1073/pnas.1108673108

Voglis, G., & Tavernarakis, N. (2008). A synaptic DEG/ENaC ion channel mediates learning in C. elegans by facilitating dopamine signalling. *EMBO J, 27*(24), 3288-3299. doi: emboj2008252 [pii]
10.1038/emboj.2008.252

Wani, K. A., Catanese, M., Normantowicz, R., Herd, M., Maher, K. N., & Chase, D. L. (2012). D1 Dopamine Receptor Signaling Is Modulated by the R7 RGS Protein EAT-16 and the R7 Binding Protein RSBP-1 in Caenoerhabditis elegans Motor Neurons. *PLoS ONE, 7*(5), e37831. doi: 10.1371/journal.pone.0037831

Ward, Sara Jane, Rasmussen, Bruce A, Corley, Gladys, Henry, Craig, Kim, Jae K, Walker, Ellen A, & Rawls, Scott M. (2011). Beta-lactam antibiotic decreases acquisition of and motivation to respond for cocaine, but not sweet food, in C57Bl/6 mice. *Behavioural Pharmacology, 22*(4), 370-373. doi: 10.1097/FBP.0b013e3283473c10

Watabe-Uchida, Mitsuko, Zhu, Lisa, Ogawa, Sachie K, Vamanrao, Archana, & Uchida, Naoshige. (2012). Whole-Brain Mapping of Direct Inputs to Midbrain Dopamine Neurons. *Neuron, 74*(5), 858-873. doi: 10.1016/j.neuron.2012.03.017

Wightman, R M, Strope, E, Plotsky, P, & Adams, R N. (1978). In vivo voltammetry: monitoring of dopamine metabolites in CSF following release by electrical stimulation. *Brain research, 159*(1), 55-68.

Wightman, R M, Strope, E, Plotsky, P M, & Adams, R N. (2004). Monitoring of transmitter metabolites by voltammetry in cerebrospinal fluid following neural pathway stimulation. *Nature, 262*(5564), 145-146.

Wu, Hsiao-Huei, Bellmunt, Elena, Scheib, Jami L, Venegas, Victor, Burkert, Cornelia, Reichardt, Louis F, . . . Carter, Bruce D. (2009). Glial precursors clear sensory neuron corpses during development via Jedi-1, an engulfment receptor. *Nat Neurosci, 12*(12), 1534-1541. doi: 10.1038/nn.2446

Wu, Hsiao-Huei, & Levitt, Pat. (2013). Prenatal Expression of MET Receptor Tyrosine Kinase in the Fetal Mouse Dorsal Raphe Nuclei and the Visceral Motor/Sensory Brainstem. *Developmental Neuroscience*. doi: 10.1159/000346367

Yang, Yongjie, Gozen, Oguz, Watkins, Andrew, Lorenzini, Ileana, Lepore, Angelo, Gao, Yuanzheng, . . . Rothstein, Jeffrey D. (2009). Presynaptic Regulation of Astroglial Excitatory Neurotransmitter Transporter GLT1. *Neuron, 61*(6), 880-894. doi: 10.1016/j.neuron.2009.02.010

Yong, D, Toleman, M A, Giske, C G, Cho, H S, Sundman, K, Lee, K, & Walsh, T R. (2009). Characterization of a New Metallo- -Lactamase Gene, blaNDM-1, and a Novel Erythromycin Esterase Gene Carried on a Unique Genetic Structure in Klebsiella pneumoniae Sequence Type 14 from India. *Antimicrobial agents and chemotherapy, 53*(12), 5046-5054. doi: 10.1128/AAC.00774-09

Yoshimura, S, Murray, J I, Lu, Y, Waterston, R H, & Shaham, S. (2008). mls-2 and vab-3 control glia development, hlh-17/Olig expression and glia-dependent neurite extension in C. elegans. *Development, 135*(13), 2263-2275. doi: 10.1242/dev.019547

Zheng, Y, Brockie, P J, Mellem, J E, Madsen, D M, & Maricq, A V. (1999). Neuronal control of locomotion in C. elegans is modified by a dominant mutation in the GLR-1 ionotropic glutamate receptor. *Neuron, 24*(2), 347-361.

Zhou, Q Y, Grandy, D K, Thambi, L, Kushner, J A, Van Tol, H H, Cone, R, . . . Civelli, O. (1990). Cloning and expression of human and rat D1 dopamine receptors. [Comparative Study]. *Nature, 347*(6288), 76-80. doi: 10.1038/347076a0